Soils and Rocks Volume 34, N. 4 2011

ISSN 1980-9743

Soils and Rocks

Soils and Rocks

An International Journal of Geotechnical and Geoenvironmental Engineering

Special Issue: Construction on Soft Soils
Guest Editors: M.S.S. Almeida & B. Indraratna

Volume 34, N. 4
December 2011

Soils and Rocks is an International Journal of Geotechnical and Geoenvironmental Engineering published by

ABMS - Brazilian Association for Soil Mechanics and Geotechnical Engineering
Av. Prof. Almeida Prado, 532, – Prédio 11 – Térreo
Cidade Universitária, 05508-901 São Paulo, SP
Brazil

SPG – Portuguese Geotechnical Society
LNEC, Avenida do Brasil, 101
1700-066 Lisboa
Portugal

Issue Date: *December 2011*

Issue: *350 copies and 2150 online-distributed copies*

Manuscript Submission: *For review criteria and manuscript submission information, see Instructions for Authors at the end.*

SOILS and ROCKS

An International Journal of Geotechnical and Geoenvironmental Engineering

Editor André Pacheco de Assis - University of Brasilia, Brazil

Co-editor Ricardo Oliveira - COBA, Portugal

Special Issue: Construction on Soft Soils

Guest Editors: M.S.S. Almeida & B. Indraratna

Soils and Rocks publishes papers in English in the broad fields of Geotechnical Engineering, Engineering Geology and Geo-environmental Engineering. The Journal is published in April, August and December. Subscription price is US$ 90.00 per year. The journal, with the name "Solos e Rochas", was first published in 1978 by the Graduate School of Engineering, Federal University of Rio de Janeiro (COPPE-UFRJ). In 1980 it became the official magazine of the Brazilian Association for Soil Mechanics and Geotechnical Engineering (ABMS), acquiring the national character that had been the intention of its founders. In 1986 it also became the official Journal of the Brazilian Association for Engineering Geology and the Environment (ABGE) and in 1999 became the Latin American Geotechnical Journal, following the support of Latin-American representatives gathered for the Pan-American Conference of Guadalajara (1996). In 2007 the journal acquired the status of an international journal under the name of Soils and Rocks, published by the Brazilian Association for Soil Mechanics and Geotechnical Engineering (ABMS), Brazilian Association for Engineering Geology and the Environment (ABGE) and Portuguese Geotechnical Society (SPG). In 2010, ABGE decided to publish its own journal and left the partnership.

Soils and Rocks

1978,	1 (1, 2)
1979,	1 (3), 2 (1,2)
1980-1983,	3-6 (1, 2, 3)
1984,	7 (single number)
1985-1987,	8-10 (1, 2, 3)
1988-1990,	11-13 (single number)
1991-1992,	14-15 (1, 2)
1993,	16 (1, 2, 3, 4)
1994-2010,	17-33 (1, 2, 3)
2011,	**34 (1, 2, 3, 4)**

ISSN 1980-9743 CDU 624.131.1

ISSN 1980-9743

SOILS and ROCKS

An International Journal of Geotechnical and Geoenvironmental Engineering

Publication of

ABMS - Brazilian Association for Soil Mechanics and Geotechnical Engineering

SPG - Portuguese Geotechnical Society

Volume 34, N. 4, December 2011

Table of Contents

Articles

Soils and Rocks
v. 34, n. 4

Special Issue: Construction on Soft Soils

Guest Editors:
M.S.S. Almeida & B. Indraratna

The Interaction Between Reinforcement and Vertical Drains and Effect on the Performance of Embankments on Soft Ground

R.K. Rowe, C. Taechakumthorn

Abstract. This paper reviews the behaviour of reinforced embankments on soft ground. Case of the Almere test embankment is used as an example to demonstrate the key function of reinforcement in improving the performance of embankments on soft foundation. The effects of partial drainage are summarized for reinforced embankments and contrasted the results from undrained analyses to highlight the effect of partial consolidation during construction. Effects of the interaction between reinforcement and prefabricated vertical drains (PVDs) are presented. It is concluded that the combined effects of partial consolidation provided by PVDs and the tension mobilized in reinforcement can substantially increase the stability of an embankment on a given soft soil. This paper also provides brief explanation of a recent design approach for embankments on soft soil, considering the combined effect of reinforcement and PVDs. Effects of the creep/relaxation characteristics of geosynthetic reinforcement and rate-sensitive nature of soft cohesive foundation soil are discussed. It is shown that time-dependent nature of geosynthetics and foundation can decrease the failure height of a reinforced embankment. Also, the long-term performances of a reinforced embankment can vary significantly depending on the soil and reinforcement characteristics. The results suggest the need for care when the foundation soil is rate-sensitive.

Keywords: reinforced embankment, geosynthetics, PVDs, creep/relaxation, soft ground, design methods.

1. Introduction

Geosynthetic reinforcement and prefabricated vertical drains (PVDs) have revolutionized many aspects of the design and construction of embankments on soft ground. They have been shown to provide a cost effective alternative to more traditional techniques, when appropriately designed and installed. The behaviour of reinforced embankments on typical soft deposits is now well understood and many design procedures have been proposed (*e.g.* Fowler & Koerner, 1987; Humphrey & Holtz, 1987; Jewell, 1987; Rowe & Soderman, 1987; Rowe & Li, 1999; Bergado *et al.*, 2002; Varuso *et al.*, 2005; Kelln *et al.*, 2007; Bergado & Teerawattanasuk, 2008; Abusharar *et al.*, 2009; Tolooiyan *et al.*, 2009; and Huang & Han, 2009). However, while these design methods are conservative for conventional (rate-insensitive) soils, they may be quite unconservative for less conventional (rate-sensitive) soils (Rowe & Li, 2005; Li & Rowe, 2008 and Rowe & Taechakumthorn, 2008a). There has been limited research into the behaviour of embankments on rate-sensitive soils. One key case study was reported by Rowe *et al.* (1995).

The beneficial effects of PVDs for accelerating the gain in soil strength are well recognized (*e.g.* Li & Rowe, 1999; Indraratna & Redana, 2000; Bergado *et al.*, 2002; Bo, 2004; Zhu & Yin, 2004; Chai *et al.*, 2006; Taechakumthorn & Rowe, 2008; Sinha *et al.*, 2009; Saowapakpiboon *et al.*, 2010; Saowapakpiboon *et al.*, 2011; Karunaratne, 2011 and Indraratna *et al.*, 2011). For example, when PVDs are used in conjunction with basal reinforcement, the presence of PVDs can substantially reduce the long-term creep deformation while allowing more rapid construction than could be safely considered without the use of PVDs (Li & Rowe, 2001 and Rowe & Taechakumthorn, 2008a).

The objective of this paper is to summarize research on the effect of basal reinforcement and PVDs on the design and construction of embankments over soft ground. The short-term and long-term performances of reinforced embankments are discussed. The effect of partial drainage during the construction, stage construction, and the presence of PVDs is illustrated. This paper also summarizes a design approach (Li & Rowe, 2001) which considers the effects of the interaction between reinforcement and PVDs for embankments constructed on typical (rate-insensitive) soft clay deposits. The effect of creep/relaxation of geosynthetic reinforcement and foundation soil on the behaviour of reinforced embankments is demonstrated. Finally, a number of parametric studies are used to highlight some design considerations and potential problems that might be anticipated during construction. This paper is an extended version of the keynote lecture presented at the symposium of new techniques for design and construction in soft clays (Rowe & Taechakumthorn, 2010).

R.K. Rowe, Professor, Civil Engineering and GeoEngineering Centre at Queen's-RMC, Department of Civil Engineering, Queen's University, Canada. e-mail: kerry@civil.queensu.ca.
C. Taechakumthorn, Research Fellow, Faculty of Engineering, University of Wollongong, New South Wales, Australia. e-mail: ctaechak@uow.edu.au.
Submitted on October 18, 2010; Final Acceptance on December 15, 2011; Discussion open until July 31, 2012.

2. Reinforced Embankment on Soft Ground

When embankments are constructed on soft cohesive foundations, the lateral earth pressure within the embankment fill imposes shear stresses on the foundation soil, reducing the bearing capacity of the foundation and hence embankment stability (Jewell, 1987). The role of the basal reinforcement is to provide confining stress to counteract some or all of the earth pressure within the embankment and to resist the lateral deformation of the foundation, thereby increasing the bearing capacity and embankment stability. Typically, reinforced embankments are designed based on consideration of (a) bearing capacity, (b) global stability, (c) pullout/anchorage and (d) deformations (Rowe & Soderman, 1987; Leroueil & Rowe, 2001). Before going into the detailed design procedures it is, however, useful to understand when and how reinforcement contributes to the embankment stability. The role of reinforcement can be illustrated with respect to the Almere test embankments (Rowe & Soderman, 1984).

The Almere test embankment allows the comparison of the observed and calculated behaviour of both an unreinforced embankment and an embankment reinforced using a multi-filament woven geotextile (with tensile stiffness J = 2000 kN/m) constructed on a soft soil deposit. The deposit was comprised of approximately 3.3 m of very soft organic clay, with an undrained strength of 8 kPa, underlain by dense sand. A trench was excavated (see insert to Fig. 1) at the edge of the proposed embankment and the clayey soil was placed over the reinforcement to form a retaining bank (see insert to Fig. 1). The hydraulic fill was then placed until failure occurred. The reinforced section experienced a relatively ductile failure at a height of 2.75 m, after 25 h of sand filling. This was in contrast to the rapid failure of the unreinforced section at a height of 1.75 m. It seems likely that the geosynthetic reinforcement was the major reason for the differences in the observed behaviour. Figure 1 shows that for fill heights less than 1 m, the clay was largely elastic and the strains in the reinforcement remained essentially constant. As the fill thickness was increased from 1 m to 2 m, there was extensive plastic failure within the clay.

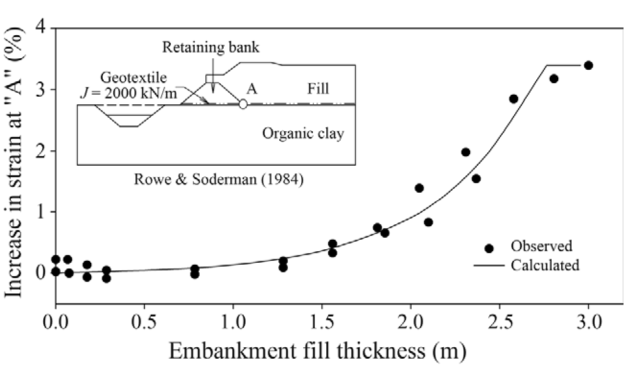

Figure 1 - Comparison of predicted and observed reinforcement strains at A (modifiedfrom Rowe & Jones 2000).

At a given embankment height, the reinforcement reduced the growth of the plastic region within the soil. For example, in the unreinforced case the analysis predicted failure at a fill height of 1.8 m (Rowe & Soderman, 1984). In contrast, at the same height in the reinforced embankment, the displacements were smaller and the plastic region was not contiguous. The analysis indicated that a contiguous plastic region had developed in the soil at a fill height of 2.05 m (approximately 15% higher than the corresponding height for the unreinforced embankment; Rowe & Soderman, 1984).

The development of a contiguous plastic region (at about 2.0 m in this case) represented the first stage of collapse for a reinforced embankment since, after that, the embankment was completely dependent upon the reinforcement for the support of any additional fill. As a result, while geosynthetic reinforcement was trying to maintain the integrity of the system, placing additional fill caused reinforcement strains to increase rapidly until either loading ceases or failure occurs (in this case at a predicted height of 2.66 m due to failure at the geosynthetic-soil interface).

3. Undrained Behaviour of Reinforced Embankments

In an undrained analysis of an unreinforced embankment, the collapse height of the embankment simply corresponds to the height at which the soil shear strength is fully mobilized along a potential failure surface (Rowe & Soderman, 1985 and Rowe & Mylleville, 1990). However, for most reinforced embankments, collapse also involves failure of soil-reinforcement system which may include (a) failure of reinforcement, (b) failure of the soil-reinforcement interfaces, or (c) failure because the reinforcement is not stiff enough to control deformations to an acceptable level. The concepts of net embankment height (defined as fill thickness minus maximum settlement) and allowable compatible reinforcement strain were introduced to account for failure due to excessive displacements before the reinforcement reaches its pullout capacity or its ultimate tensile strain (Rowe & Soderman, 1985).

For example, Fig. 2 shows net embankment height and the maximum reinforcement strain plotted against the fill thickness for an embankment constructed quickly on a soft clayey foundation. The failure of this reinforced embankment due to excessive subsidence occurred at a fill thickness equal to 2.4 m and a reinforcement strain of 5.2%, which is well below the tensile failure strain for most of geosynthetic products (Shinoda & Bathurst, 2004). Therefore, it is important to define an allowable 'compatible' reinforcement strain corresponding to the failure thickness of a reinforced embankment. A second allowable strain will be related to the reinforcement strength. The lower of these two strains would be used together with reinforcement stiffness to get the allowable reinforcement force used in a limit equilibrium calculation. Figure 3 shows the variation of allowable compatible strain, ε_a, (for the case of reinforced embankment on soft foundations having uniform undrained shear strength with depth) with the dimensionless parameter, Ω, (Rowe & Soderman, 1985) defined as:

$$\Omega = \left(\frac{\gamma_f H_c}{s_u}\right)\left(\frac{s_u}{E_u}\right)\left(\frac{D}{B}\right)_e^2 \qquad (1)$$

where; γ_f is a bulk unit weight of the embankment fill; H_c is the collapse height of the unreinforced embankment; s_u and E_u are undrained shear strength and modulus of the soft foundation, respectively; $(D/B)_e$ is the ratio of the effective depth of the deposit to the crest width, as defined in Fig. 3. It should be noted that when using Eq. (1) it is not conservative to underestimate the undrained modulus of the soft foundation, since a lower value of E_u corresponds to a high value of ε_a, which in turn gives a high reinforcement force, T_{rein}.

For the cases when embankments are constructed on a foundation whose strength increases with depth, the inclusion of reinforcement changes the collapse mechanism by forcing the failure surface to pass through stronger and stiffer soil. This case is not addressed by design chart proposed by Rowe & Soderman (1985) for the soil having constant shear strength with depth and so Hinchberger & Rowe (2003) developed a design chart for estimating the reinforcement strain at failure for the reinforced embankment on foundations having increasing shear strength with depth (Fig. 4). The strain presented in Fig. 4 represents an upper limit; the allowable strain may in some cases be controlled by the strain at rupture of the reinforcement (which in turn may be reduced by some appropriate partial factor). Also, for soft brittle soils which are susceptible to strain-softening, the limiting reinforcement strain may be as low as 0.5%-2.0% in order to reduce the maximum shear strain developed in foundation soils to an acceptable level (Rowe & Mylleville, 1990 and Mylleville & Rowe, 1991).

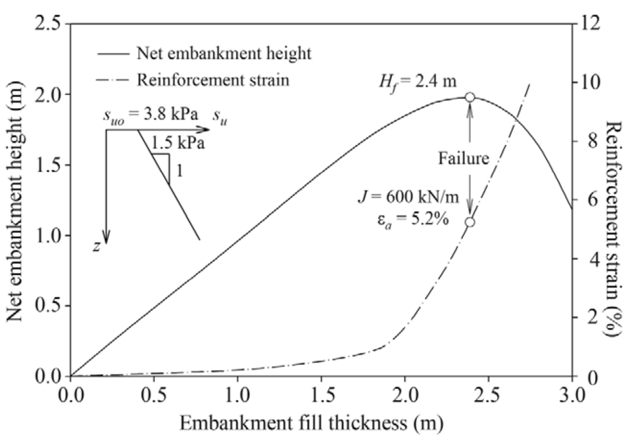

Figure 2 - Maximum net embankment height and allowable reinforcement strain (modified from Hinchberger & Rowe 2003).

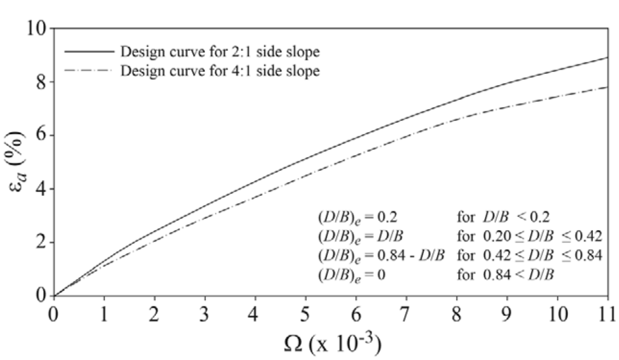

Figure 3 - Variation of allowable compatible strain ε_a with dimensionless parameter Ω (modified from Rowe & Soderman 1985).

4. Partially Drained Behaviour of Reinforced Embankments

The observed construction-induced excess pore water pressures from a large number of field cases suggest that significant partial consolidation of the foundation may occur during embankment construction at typical construction rates (Crooks *et al.*, 1984; Leroueil & Rowe, 2001). This applies to natural soft cohesive deposits that are typically slightly overconsolidated. It also has been reported that often there may be a significant strength gain due to partial consolidation during embankment construction (*e.g.* Bergado *et al.*, 2002; Bo, 2004; Chai *et al.*, 2006 and Saowapakpiboon *et al.*, 2010).

Although field cases suggest the importance of considering partial consolidation, they do not allow a direct comparison of cases where it is, or is not, considered. Finite element analyses, however, do provide a powerful tool for comparing the behaviour of reinforced embankments constructed under undrained and partially drained conditions (Rowe & Li, 1999). For example, Fig. 5 shows the variation in calculated embankment failure height with reinforce-

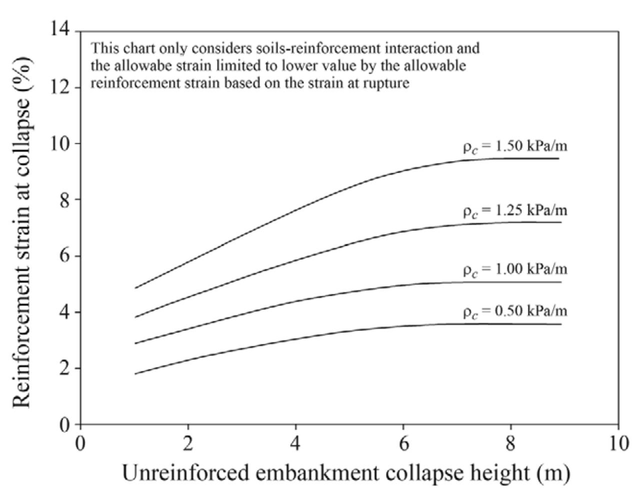

Figure 4 - Chart for estimating reinforcement strains at embankment failure for foundation soils with strength increase with depth (modified from Hinchberger & Rowe 2003).

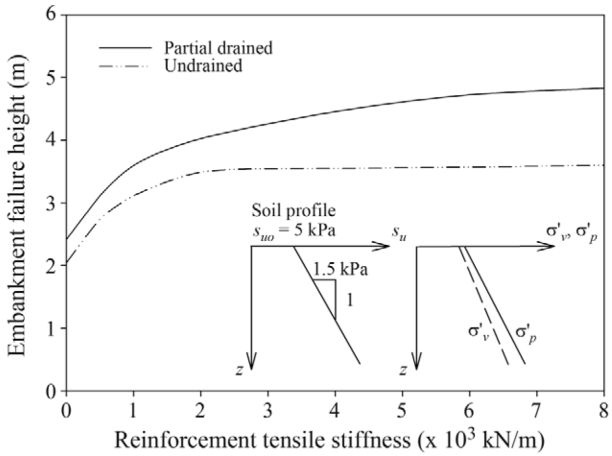

Figure 5 - Embankment failure height against reinforcement tensile stiffness (modified from Li & Rowe 2001).

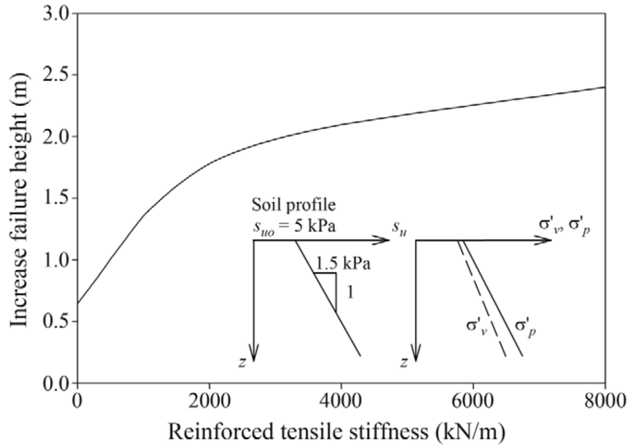

Figure 6 - Increase of failure height after 95% consolidation at end of first stage construction (modified from Li & Rowe 2001).

ment stiffness for undrained and partially drained conditions. The construction rate employed in the analysis was 1 m/month to allow partial dissipation of the excess pore water pressure during construction. The fully coupled analyses gave an increase in the unreinforced embankment failure height from 2.1 m (for undrained analysis) to 2.4 m. A change of reinforcement stiffness from 500 kN/m to 8000 kN/m also resulted in an increase in failure height by between 1.4 m and 3.8 m, compared with between 0.7 m to 1.4 m for the undrained analysis. This implies that the reinforcement had a greater effect for the partially drained cases than for undrained cases. However, for this particular soil profile (see insert to Fig. 5: s_u = undrained shear strength, σ'_v = vertical effective stress and σ'_p = maximum preconsolidation pressure), the increase in reinforcement stiffness had the most significant effect on the embankment failure height for stiffness values up to only J = 2000 kN/m and the benefit of increasing reinforcement stiffness diminishes for very stiff reinforcement.

When a soft foundation soil does not initially have the strength to safely support a given embankment, stage construction may be employed to allow sufficient consolidation and strength gain to occur to support the final embankment load. Li & Rowe (1999) showed that geosynthetic reinforcement may eliminate the need for stage construction or, in cases where staging was still needed; it reduced the number of stages required. The effect of reinforcement stiffness on multi-stage construction is illustrated in Fig. 6. To obtain this figure, embankments were first numerically constructed to the maximum height permitted with a factor of safety of 1.3 at the end of stage one and allowed to consolidate to 95% average degree of consolidation. Then additional fill was placed until failure. It can be seen that the stiffer the reinforcement, the greater the increase in embankment failure height due to foundation soil strength gain. These results are encouraging but the time to 95% consolidation was too long for most practical cases. This does, however, imply that there may be significant benefit arising from combining reinforcement with methods of accelerating consolidation, such as PVDs, as discussed in the following section.

5. Interaction Between Reinforcements and PVDs

Since the first prototype of a prefabricated drain made of cardboard (Kjellman, 1948), prefabricated vertical drains have been widely used in embankment construction projects, due to their advantages in terms of cost and ease of construction (*e.g.* Hansbo, 1981; Nicholson & Jardine, 1981; Jamiolkowski *et al.*, 1983; Holtz, 1987; Lockett & Mattox, 1987; Holtz *et al.*, 2001; Bergado *et al.*, 2002; Bo, 2004; Zhu & Yin, 2004; Chai *et al.*, 2006; Sinha *et al.*, 2007; Sinha *et al.* 2009 and Saowapakpiboon *et al.*, 2010). PVDs accelerate soil consolidation by shortening the drainage path and taking advantage of a naturally higher horizontal hydraulic conductivity of the foundation soil. This technique improves embankment stability by allowing strength gain in the foundation soil associated with the increase in effective stress due to consolidation.

The combined effects of reinforcement and PVDs have been investigated by Li & Rowe (1999, 2001) and Rowe & Taechakumthorn (2008a). It has been shown that the use of PVDs in conjunction with typical construction rates results in relatively rapid dissipation of excess pore pressures and when combined with geosynthetic reinforcement it enhances the stability of the embankment. Figure 7 shows the variation of net embankment height with fill thickness from finite element simulations, where S is the spacing of PVDs in a square pattern. For this particular foundation soil A (see insert in Fig. 7) and PVDs at a spacing of 2 m, the unreinforced embankment can be constructed to a height of 2.85 m. If reinforcement with tensile stiffness J = 250 kN/m is used, the failure height increases to 3.38 m. It is noted that, for these assumed soil properties

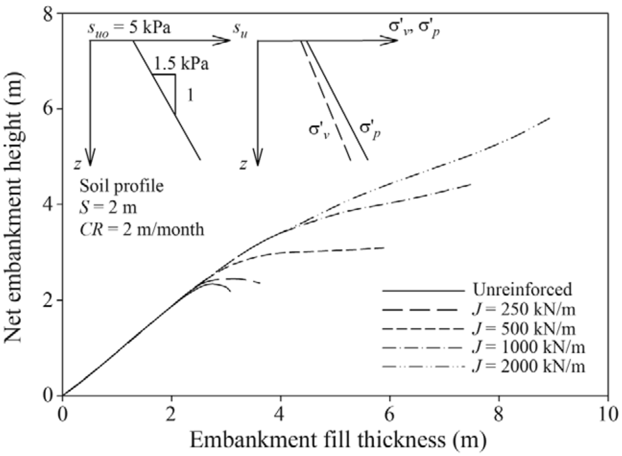

Figure 7 - The combined effect of reinforcement and PVDs on the short-term stability of the embankment (modified from Rowe & Li 2005).

and a construction rate of 2 m/month, the embankment will not fail due to bearing capacity failure of the foundation soil if the reinforcement stiffness is greater than 500 kN/m.

Reinforcement also reduces the shear stress and consequent shear deformations in the foundation soil. When the use of PVDs is combined with reinforcement, it can enhance the beneficial effect of the reinforcement in reducing horizontal deformations of the foundation soil below the embankment as illustrated in Fig. 8. With the use of PVDs, less stiff reinforcement can be employed while still providing about the same control on lateral deformation as the use of stiffer reinforcement without PVDs

6. Consolidation of the PVDs-Improved Soils Under Linear Loading Condition

Even though, the significant increase in degree of soil consolidation during embankment construction, owing to the presence of PVDs, has been reported (*e.g.* Lockett & Mattox, 1987; Fritzinger, 1990; Schimelfenyg *et al.*, 1990; Volk *et al.*, 1994; Holtz *et al.*, 2001; Bergado *et al.*, 2002; Bo, 2004; Zhu & Yin, 2004; Chai *et al.*, 2006; Sinha *et al.*, 2009 and Saowapakpiboon *et al.*, 2010), the magnitude and distribution of strength gain have received relatively little attention. Based on finite element analyses, Li & Rowe (2001) have shown that there is significant increase in undrained shear strength of foundation soils improved with PVDs. Figure 9 shows the contours of the increase in undrained shear strength of the foundation soil during construction for a reinforced (J = 2000 kN/m) embankment having height H = 4.4. For the sake of clarity, Fig. 9 does not include the increase in undrained shear strength near the top and bottom layers, where the gradient of shear strength increase is high because of the drainage boundary effects. Owing to the presence of the PVDs, the average increase in undrained shear strength was rather uniform throughout most of the thickness of the deposit (with some drainage boundary effects at the top and bottom of the foundation).

To analyze the consolidation of PVDs-improved soils during embankment construction, consideration should be given to vertical and radial drainage, construction rate, as well as the difference between consolidation coefficients of soils in the overconsolidated and normally consolidated stress ranges. Generally, a numerical analysis is required to consider these factors. Li & Rowe (2001) proposed an approximate method to calculate the consolidation of foundation soils allowing for the aforementioned factors. The proposed method can be performed by hand, or by using a spreadsheet calculation, without rigorous numerical analysis as outlined below.

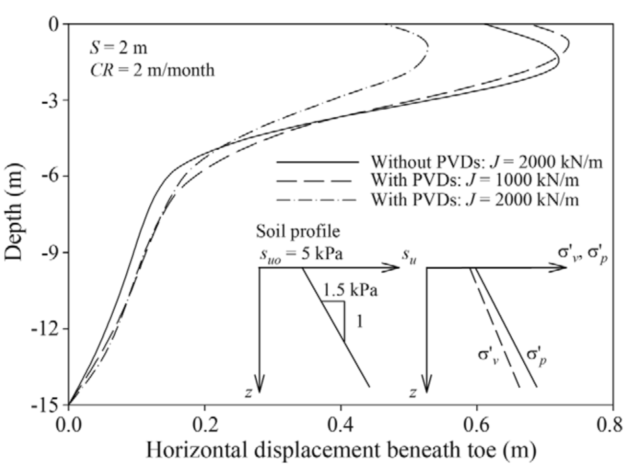

Figure 8 - The combined effect of reinforcement and PVDs on lateral deformation beneath the toe of the embankment (modified from Rowe & Li 2005).

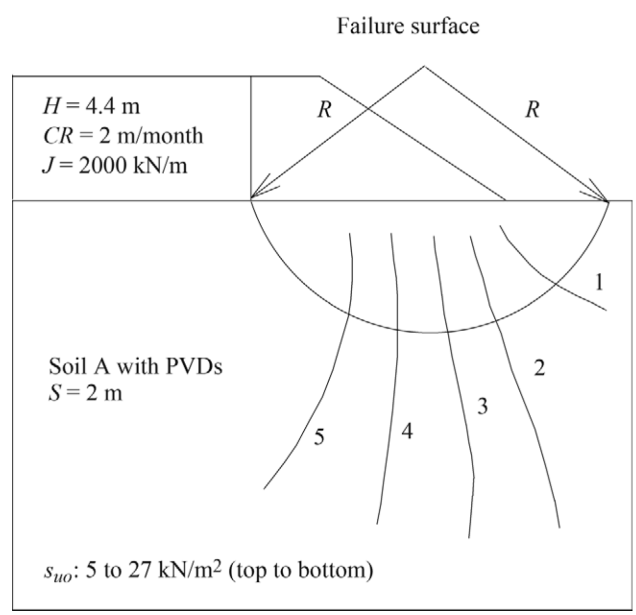

Figure 9 - Contours showing the increase in undrained shear strength, Δs_u in kPa, at end of construction, as calculated from FEM analyses (modified from Li & Rowe 2001).

The analysis is greatly simplified due to the fact that by including PVDs, the dissipation of pore pressure is essentially uniform with depth (except at the top and bottom boundaries) as implied by the strength gain contours shown in Fig. 9. The procedure, as described by Li & Rowe (2001) considers an embankment expected to apply a vertical stress of $\Delta\sigma$ over a period of time t_c as shown in Fig. 10. It is assumed that soil becomes normally consolidated when the average degree of consolidation at a particular time, $t_{O/C,}$ is such that the average vertical effective stress of the soil is equal to the preconsolidation pressure. At this time, the compressibility of the soil changes from the recompression index ($C_{O/C}$) to compression index ($C_{N/C}$). For a deposit with two-way drainage, the average degree of consolidation at any time is defined as:

$$\bar{U} = \frac{D\Delta\sigma(t) - \int_o^D u dz}{D\Delta\sigma} \tag{2}$$

where D is the thickness of the deposit; $\Delta\sigma(t)$ is the applied stress at time t; and u is excess pore pressure at time t. At time $t_{O/C}$ the average degree of consolidation is $\bar{U}_{O/C}$ (*i.e.* calculated using the coefficient of consolidation of soil in overconsolidated state, $c_{vO/C}$) for a total stress of $\Delta\sigma$, and the average change in effective stress at this time is $\Delta\sigma\bar{U}_{O/C}$. After the application of full stress $\Delta\sigma$, the average excess pore pressure that needs to dissipate is equal to $\Delta\sigma(1 - \bar{U}_{O/C})$. The remaining excess pore water pressure is assumed to be developed over a period of time due to a change in stress of $\Delta\sigma(1 - \bar{U}_{O/C})$. After $t_{O/C}$, the average degree of consolidation, $\bar{U}_{N/C}$, is calculated using coefficient of consolidation of soil in normally consolidated state ($c_{vN/C}$). Figure 10 shows that the linear load function, O-A, is replaced by two linear load functions: O-B and O'-A for soil in overconsolidated and normally consolidated states, respectively. It's assumed that average degree of consolidation under load O-A after time $t_{O/C}$ is equivalent to the average degree of consolidation under the load O'-A plus the average degree of consolidation under load O-B that occurred at time $t_{O/C}$. Therefore, the total average degree of consolidation at time $t \geq t_{O/C}$ is described as:

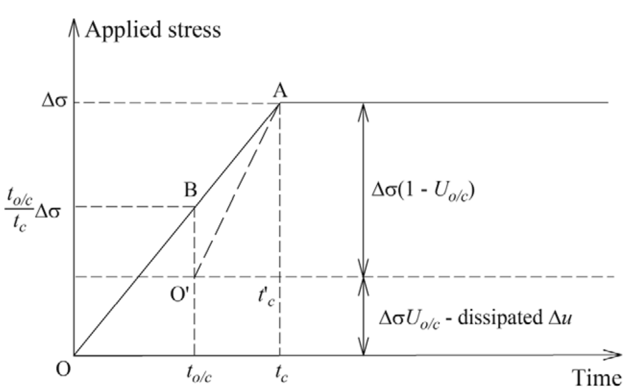

Figure 10 - Breakdown of linear ramp load function for consolidation analysis considering the soil in its overconsolidated and normally consolidated states (modified from Li & Rowe 2001).

$$\bar{U} = \bar{U}_{O/C} + (1 - \bar{U}_{O/C})\bar{U}_{N/C} \tag{3}$$

To consider the consolidation of soil under time-dependent loading, Olson (1977) derived relatively simple solutions considering both vertical and radial drainage for linear ramp loading problem. $\bar{U}_{O/C}$ and $\bar{U}_{N/C}$ can be calculated separately using Olson's (1977) solution as follows.

For vertical consolidation:

$$T \leq T_c : \bar{U}_v = \frac{T}{T_c}\left\{1 - \frac{2}{T}\sum\frac{1}{M^4}\left[1 - \exp(-M^2 T)\right]\right\} \tag{4}$$

$$T > T_c : \bar{U}_v = 1 - \frac{2}{T_c}\sum\frac{1}{M^4}\left[\exp(-M^2 T_c) - 1\right]\times \exp(-M^2 T) \tag{5}$$

where T is the time factor for vertical consolidation; T_c is the time factor at the end of construction and $M = \pi\ (2m + 1)/2$, $m = 0, 1, 2, 3$, until the sum of all remaining term is insignificant.

For horizontal (radial) consolidation:

$$T_h \leq T_{hc} : \bar{U}_h = \frac{1}{T_{hc}}\left\{T_h - \frac{1}{A}\left[1 - \exp(-AT_h)\right]\right\} \tag{6}$$

$$T_h > T_{hc} : \bar{U}_h = 1 - \frac{1}{AT_{hc}}\left[\exp(AT_{hc} - 1)\right]\exp(-AT_h) \tag{7}$$

where T_h is the time factor for horizontal consolidation; T_{hc} is the time factor at the end of construction and $A = 8/\mu$, μ is defined as:

$$\mu = \ln\left(\frac{n}{s}\right) + \left(\frac{k}{k_s}\right)\ln(s) - \frac{3}{4} + \pi z(2l - z)\frac{k}{q_w} \tag{8}$$

$$n = \frac{R}{r_w},\ s = \frac{r_s}{r_w} \quad \text{and} \quad q_w = \pi k_w r_w^2 \tag{9}$$

where: k, k_s and k_w are the hydraulic conductivity of soil in the horizontal direction, soil in the smear zone (the hydraulic conductivity of soil in smear zone was assumed to be isotropic and same as vertical hydraulic conductivity) and the vertical drain, respectively; q_w is the equivalent discharge capacity for the axisymmetric unit cell; r_w, r_s and R are the radius of the vertical drain, smear zone and influence zone, respectively. For the combined vertical and radial consolidation the method proposed by Carrillo (1942) can be employed as:

$$\bar{U} = 1 - (1 - \bar{U}_h)(1 - \bar{U}_v) \tag{10}$$

7. Design of Embankment of Soft Ground: Considering The Interaction Between Reinforcements and PVDs

Design of the reinforced embankment and PVDs are usually treated separately in current design methods even if both reinforcement and PVDs are used together. The design of reinforced embankments is usually based on undrained stability analyses without considering the effect of PVDs (*e.g.* Jewell, 1982; Mylleville & Rowe, 1988; Holtz *et al.*, 1997). Li & Rowe (2001) proposed a design method for reinforced embankment allowing the effect strength gain due to consolidation of the foundation soil. This design method is based on a limit state design philosophy and concepts proposed by Ladd (1991). The design procedure consists of four main steps, (a) select design criteria and parameters for both embankment fill and foundation soil, (b) establish the pattern and spacing of PVDs according to the required average degree of consolidation at the time to be considered, (c) estimate the average strength gain along the potential failure surface due to consolidation, and (d) select the required tensile stiffness of the reinforcement associated with the allowable compatible reinforcement strain (Rowe & Soderman, 1985 and Hinchberger & Rowe, 2003) using an undrained stability analysis (*i.e.* limit equilibrium method). The detailed design procedures, based on Li & Rowe (2001), are summarized as follows:

a) Select the design criteria and soil parameters including:

1. Embankment geometry: height (H), width (B), and side slope (n)

2. Required average degree of consolidation ($\overline{U}$) and available time (t) to achieve $\overline{U}$

3. Anticipated construction rate (CR)

4. Soil profile: undrained shear strength (s_u), preconsolidation pressure (σ'_p), vertical effective stress (σ'_v), coefficient of lateral earth pressure at rest (K'_o), coefficient of consolidation of soil in overconsolidated ($c_{vO/C}$) and normally consolidated ($c_{vN/C}$) state, vertical and horizontal hydraulic conductivity of the undisturbed soil (k_v and k_h), and hydraulic conductivity of the disturbed soil (k_s)

5. The longest vertical drainage path (H_d)

6. Embankment fill parameters: friction angle (ø) and bulk unit weight (γ_{fill})

b) Design of prefabricated vertical drains system:

1. Select the configuration of the PVDs system: installation pattern (*i.e.* triangular or square pattern), spacing of PVDs (S), and length of a single drain (L)

2. Estimate parameters used in radial consolidation analysis: effective diameter of drain influence zone (D_e), diameter of smear zone caused by installation (d_s), equivalent diameter (d_w) and equivalent discharge capacity (q_w)

3. Calculate the average degree of consolidation at available time, t, using Eqs. (2) and (3). If the calculated average degree of consolidation is less than the required $\overline{U}$, select the new PVDs configuration (*i.e.* spacing, S, and length, L) until $\overline{U}$ is met.

c) Estimate the average strength gain along the potential failure surface:

1. Estimate the average influence factor (I_q) for the increase in total stress along the potential failure surface using:

$$I_q = \frac{\Delta\sigma_m}{\Delta\sigma} \text{ where } \Delta\sigma = \gamma_{fill} H$$
$$\text{and } \Delta\sigma_m = \frac{1}{3}(\Delta\sigma_x + \Delta\sigma_y + \Delta\sigma_z) \tag{11}$$

where $\Delta\sigma_x$, $\Delta\sigma_y$ and $\Delta\sigma_z$ can be estimated using elastic solutions (*e.g.* Poulos & Davis, 1974).

2. Calculate the average degree of consolidation along the potential failure surface at the end of construction ($\overline{U}_f$).

3. Estimate the average strength increase (Δs_{uf}) of soil along the potential failure surface at the end of construction using the method proposed by Li & Rowe (2001) as:

$$\Delta s_{uf} = \left[\beta(\sigma'_{mi} + \gamma_{fill} H I_q \overline{U}_f)\right] - s_{uo}$$
$$\text{where } \beta = \frac{3}{1+2K'_o}\frac{s_u}{\sigma'_p} \tag{12}$$

where σ'_{mi} is the initial effective mean stress.

d) Selecting the required tensile stiffness of the reinforcement:

1. Apply partial factor to both load and resistance of the system as appropriate: f_c for the undrained shear strength of the foundation soil ($s^*_{uf} = s_{uf} / f_c$; $s_{uf} = s_{uo} + \Delta s_{uf}$), $f_ø$ for friction angle of fill material ($\tan^* \phi' = (\tan\phi')/f_\phi$), and f_γ for the unit weight of the fill material ($\gamma^*_{fill} = \gamma_{fill} f_\gamma$)

2. Use limit equilibrium method to calculate the equilibrium ratio (ERAT) of the restoring moment to overturning moment of the embankment without reinforcement using the factored soil parameters. If ERAT ≥ 1, the reinforcement is not needed. However, if ERAT < 1, reinforcement is required.

3. Use limit equilibrium program designed for the analysis of the reinforced embankment (*e.g.* REAP: Mylleville & Rowe, 1988) to calculate the required reinforcement tensile force, T_{req}, using the factored soil parameters (*i.e.* the tensile force that required to give ERAT = 1).

4. Choose an allowable reinforcement strain, ε_{all}, and then the required reinforcement stiffness can be selected as:

$$J \geq \frac{T_{req}}{\varepsilon_{all}} \tag{13}$$

This approach can be easily applied for a stage construction sequence by adding the consolidation during the stoppage between stages when calculating the average degree of consolidation, while keep the other steps the same. In order to ensure embankment stability during construction, it is important to monitor the development of reinforcement strains, excess pore water pressure, settlement, and horizontal deformation to confirm that the observed behaviour is consistent with the design assumptions (Rowe & Li, 2005).

8. Reinforced Embankment on Rate-Sensitive Soil

It has been recognized by many researchers (Lo & Morin, 1972; Vaid & Campanella, 1977; Vaid *et al.*, 1979; Graham *et al.*, 1983; Kabbaj *et al.*, 1988 and Leroueil, 1988) that natural soft deposits exhibit significant time-dependent behaviour and their undrained shear strength is strain-rate dependent (rate-sensitive). The performance of the reinforced embankment constructed on the rate-sensitive soil also has been investigated by both field studies and numerical analyses (Rowe *et al.*, 1996; Hinchberger & Rowe, 1998; Rowe & Hinchberger, 1998; Rowe & Li, 2002; and Rowe & Taechakumthorn, 2008a,b). For example, Rowe *et al.* (1996) showed that in order to accurately predict the responses of the Sackville embankment on a rate-sensitive soil, it is essential to consider the effect of soil viscosity. Rowe & Hinchberger (1998) proposed an elasto-viscoplastic constitutive model and demonstrated that the model could adequately describe the behaviour of the Sackville test embankment. The proposed model was also verified with another well documented field study, the Gloucester test embankment (Bozozuk & Leonards, 1972), and showed good prediction compared with the observed field data (Hinchberger & Rowe, 1998). Following subsections summarize the key finding from sensitivity analyses on the effect of soil viscosity using the aforementioned elasto-viscoplastic model (Rowe & Hinchberger, 1998).

8.1. Short-term stability of reinforced embankment

By definition, the undrained shear strength of rate-sensitive soils depends on the rate of loading (*i.e.* rate of embankment construction); the faster is the loading rate, the stronger the soil appears. For that reason, the loading rate is an important factor when conducting an analysis of embankment performance on a rate-sensitive soil. The effect of construction rate and geosynthetic reinforcement on the short-term stability of reinforced embankments is illustrated in Fig. 11. Series of reinforced embankments with axial stiffness of 0 (unreinforced), 500 and 1000 kN/m were constructed numerically at different construction rates until failure. It is evident (Fig. 11) that faster construction rate results in a higher short-term embankment failure height for all cases. The reinforcement also improved embankment stability. The stiffer the reinforcement, the higher the short-term failure height. However, this short-term benefit hides a long-term problem as will be discussed later.

8.2. Long-term mobilized reinforcement strains

To investigate the effect of the various parameters such as reinforcement stiffness, construction rate and the effect of PVDs on the long-term behaviour of a reinforced embankment on the rate-sensitive soil, a series of 5 m high reinforced embankments were numerically constructed on rate-sensitive foundation soil. The results from Case I and Case II (Fig. 12) show the effect of construction rate. The reinforcement strains at the end of the construction were 1.6% and 2.6% for Cases I and II, respectively. The reinforcement strain for the slower construction rate (Case II) was higher because the soil exhibited lower short-term strength and transferred more load to the reinforcement. However, this slower construction rate allowed a higher degree of partial consolidation and reduced the amount of overstress in the soil. Consequently, there was less creep and stress relaxation in the soil following construction. This resulted in smaller long-term reinforcement strains. The results from Case I and III (Fig. 12) show the effect of reinforcement stiffness and as expected the stiffer reinforcement (Case III) gave smaller strains at both the end of construction and also in the long-term. Designers usually aim to limit reinforcement strains to about 5%-6% (Rowe & Li, 2005). The results for Cases I and II correspond to

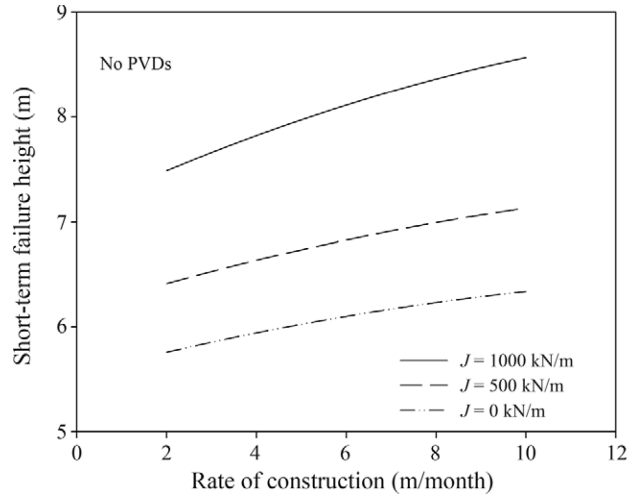

Figure 11 - The effect of construction rate and reinforcement stiffness on short-term stability of the embankment (modified from Rowe & Taechakumthorn 2008b).

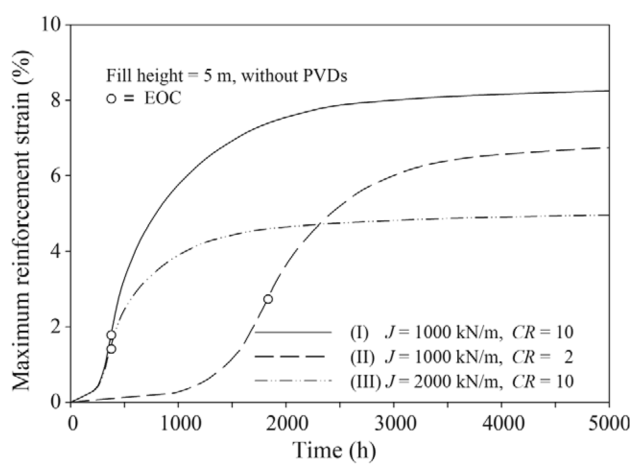

Figure 12 - The effect of construction rate and reinforcement stiffness on mobilized reinforcement strains (modified from Rowe & Taechakumthorn 2008a).

long-term reinforcement strains of 8.3% and 6.9%, respectively and hence exceed typical desirable limits. Stiffer geosynthetic reinforcement would be required to control the long-term reinforcement strain to within the allowable limit. For example with the stiffer reinforcement (Case III), the long-term reinforcement strain can be limited to 4.9%.

The rate of excess pore water dissipation and the consequent rate of shear strength gain in the soil can be increased using PVDs. Results given in Fig. 13 show that with the use of PVDs, the long-term mobilized reinforcement strain can be significantly reduced. For example the 5 m high reinforced embankment with the reinforcement stiffness J = 1000 kN/m, even a construction rate as low as 2 m/month, gave rise to a long-term reinforcement strains of 6.9% which exceeds the typical allowable limit of 5% (Fig. 12). In contrast, with PVDs at 3 m spacing and an even faster construction rate at 10 m/month, the construction still only gave a maximum long-term reinforcement strain of 4.6% (Case I, Fig. 13). With stiffer (J = 2000 kN/m) reinforcement, PVDs reduced the long-term reinforcement strain from 4.9% to 3.3% (Case III in Fig. 12 and Case II, Fig. 13). In fact, for reinforcement with a stiffness of 2000 kN/m, a reinforced embankment could be constructed up to 5.75 m without the long-term reinforcement strain exceeding about 5% (Case III, Fig. 13). For this same 5% long-term limit strain and PVDs at 3 m spacing, embankments could be constructed to 6.50 and 7.85 for J = 4000 and 8000 kN/m respectively (see insert to Fig. 13).

8.3. Excess pore water dissipation

In contrast to a rate-insensitive soft soil, for a rate-sensitive foundation there are two processes happen simultaneously during and following embankment construction: (a) excess pore water pressure dissipation due to consolidation, and (b) generation of excess pore water pressure due to the creep of the foundation soil. Figure 14 shows the contours of the change in excess pore water pressure between

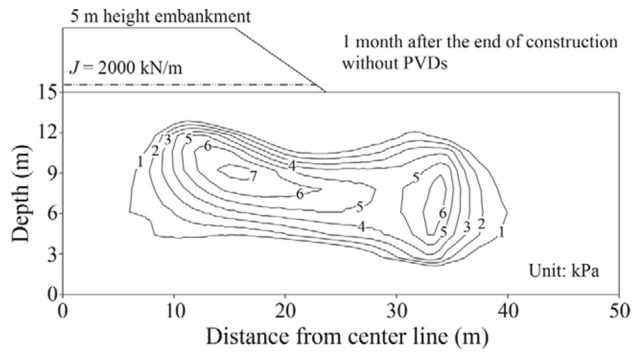

Figure 14 - Contours of the change in excess pore water pressure between immediately after and 1 month after the end of construction (modified from Taechakumthorn & Rowe 2008).

immediately after and 1 month after the end of construction for a 5 m high reinforced embankment (J = 2000 kN/m; no PVDs). The foundation soil has same basic soil properties as those of the rate-insensitive soil discussed earlier (*i.e.* insert drawing in Figs. 5 to 8) and the rate-sensitive characteristics similar to Sackville soil described by Rowe & Hinchberger (1998). The shear induced generation of pore pressures is evident in the areas of higher shear stress along the potential slip surface (Fig. 14). Thus, for rate-sensitive soil the maximum excess pore water pressure and hence the minimum factor of safety with respect to embankment stability, often occur after the end of construction.

The effect of reinforcement stiffness and PVDs on the excess pore water pressure is presented in Fig. 15. The excess pore water pressures were monitored at a point 6 m beneath the crest of the embankment where the maximum increase in excess pore water pressure was indicated (Fig. 14). The excess pore water pressures at the end of construction were approximately 80 kPa for all cases at the construction rate of 10 m/month and kept increasing post construction for all reinforcement stiffnesses considered until a peak was reached. This phenomenon is similar to

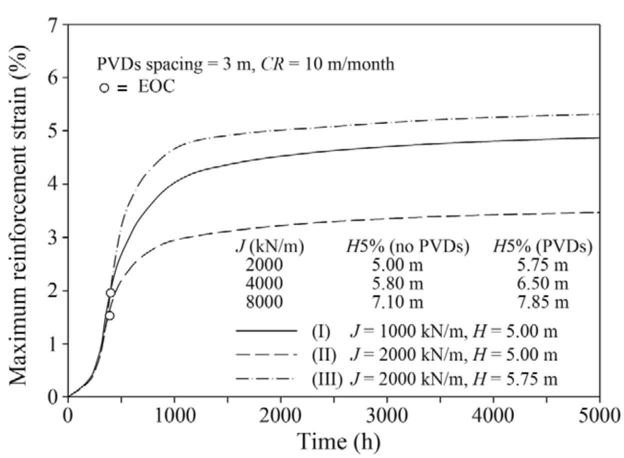

Figure 13 - The effect of PVDs and reinforcement stiffness on mobilized reinforcement strains (modified from Taechakumthorn & Rowe 2008).

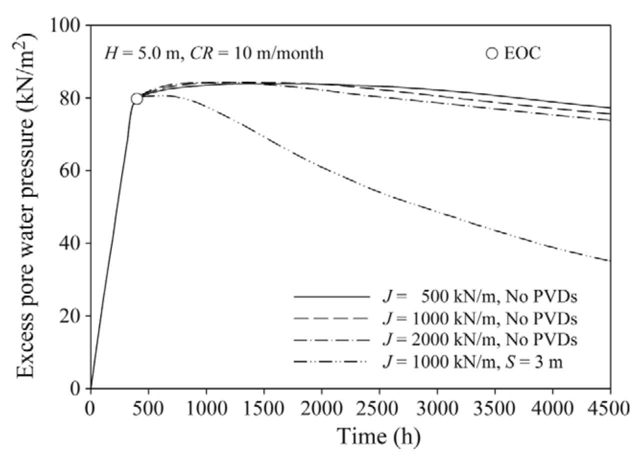

Figure 15 - The effect of reinforcement stiffness and PVDs on dissipation of excess pore pressures (modified from Taechakumthorn & Rowe 2008).

that observed at the Sackville test embankment (Rowe & Hinchberger, 1998). As noted above, the excess pore pressures decreased due to consolidation but also increased due to creep of the foundation soil. By providing greater confinement to the soil, the stiffer reinforcement reduced the effects of creep induced pore water pressure and resulted in faster dissipation of pore pressure as shown in Fig. 15. The installation of PVDs significantly minimized the effect of delayed excess pore water pressure on the rate-sensitive soil. As demonstrated in Fig. 15, with PVDs, the excess pore water pressure rapidly decreases following the end of construction.

8.4. Differential settlement and lateral deformation

Reinforcement has the potential to reduce differential settlement and heave of the foundation for embankments on rate-sensitive soil. Figures 16 and 17 show profiles of ground surface and lateral deformation beneath the toe for embankments with different reinforcement stiffnesses at 1 month after the end of construction. For the case of an unreinforced embankment (J = 0 kN/m), the differential settlement between center and crest of the embankment was 1.1 m but for the reinforced embankment, this was reduced to 0.5 and 0.3 m for reinforcement stiffness of 1000 and 2000 kN/m (Fig. 16). The maximum calculated heaves were 1.8, 0.8, and 0.6 m for the unreinforced embankment and for the reinforcement stiffnesses of 1000 and 2000 kN/m, respectively. The presence of PVDs considerably reduced the differential settlement of the foundation. The results from Case IV in Fig. 16 show that with the use of PVDs, even with the less stiff reinforcement (J = kN/m), the differential settlement was reduced to 0.2 m and the maximum heave was 0.5 m.

Reinforcement also had a beneficial effect on lateral deformation as demonstrated in Fig. 17. The maximum lateral deformation below the embankment toe was reduced from 2.4 m, for the unreinforced case, to 1.0 and 0.8 m for the reinforcement stiffness of 1000 and 2000 kN/m, respectively. With the use of lower reinforcement stiffness (J = 1000 kN/m) combined with PVDs, the maximum lateral deformation was reduced to only 0.7 m. This was smaller than that obtained from Case III using a reinforcement stiffness of 2000 kN/m, as a result of higher degree of partial consolidation and consequently higher soil strength increase as well as less overstress in the foundation occurs when the PVDs were employed.

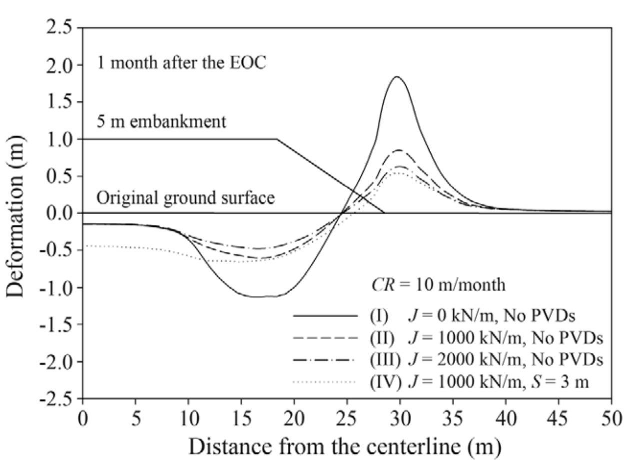

Figure 16 - The effect of reinforcement stiffness and PVDs on the differential settlement and heave of the foundation (modified from Taechakumthorn & Rowe 2008).

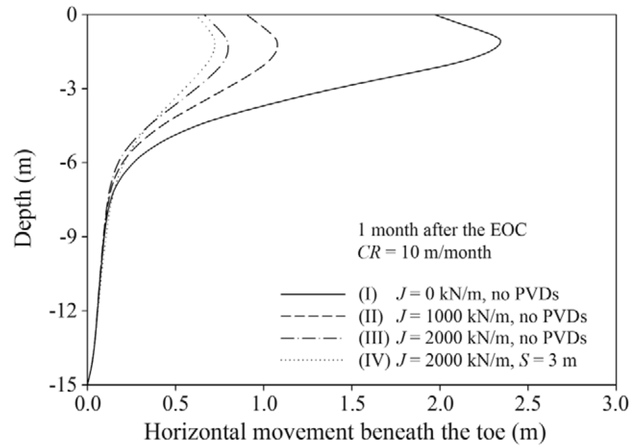

Figure 17 - The effect of reinforcement stiffness and PVDs on the differential and lateral deformation (modified from Taechakumthorn & Rowe 2008).

9. Effects of Creep/Relaxation of Geosynthetics Reinforcements

Experimental studies have shown that geosynthetics typically made of polyester (PET), polypropylene (PP) and polyethylene (PE) are susceptible to creep to some extent (Allen *et al.*, 1982; McGown *et al.*, 1982; Christopher *et al.*, 1986; Greenwood & Myles, 1986; Jewell & Greenwood, 1988; Bathurst & Cai, 1994; Leshchinsky *et al.*, 1997; Shinoda & Bathurst, 2004; Jones & Clarke, 2007; Kongkitkul & Tatsuoka, 2007 and Yeo & Hsuan, 2010). The importance of considering creep/relaxation of geosynthetics reinforcement, to understand the time-dependent behaviour of the reinforced embankment on soft ground has been highlighted in the literature (Li & Rowe, 2001; Li & Rowe 2008 and Rowe & Taechakumthorn, 2008b).

For creep-sensitive reinforcement, the reinforcement strain may significantly increase with time owing to creep of the reinforcement after embankment construction (Li & Rowe, 2001). Figure 18 shows (solid lines) the development of reinforcement strain with time up to 98% consolidation for embankments reinforced (on rate-insensitive soil) using HDPE (upper figure) and PET (lower figure) geosynthetics. Also shown (dashed lines) are the strains that would be developed if the reinforcement was assumed elastic with stiffness selected such that, at the end of construction, the reinforcement strain is the same as that developed in the viscous reinforcement. Thus, the difference

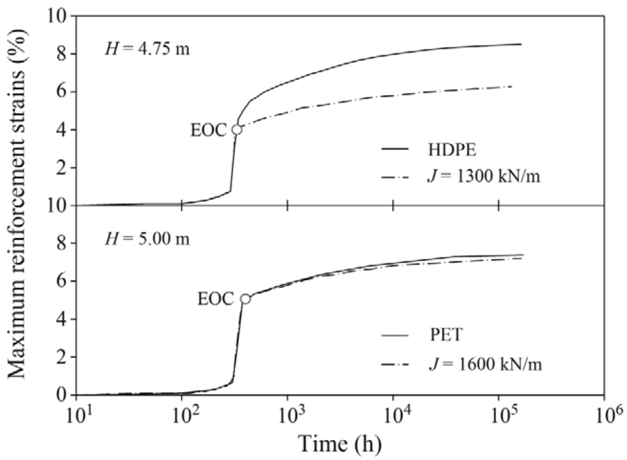

Figure 18 - Variation of reinforcement strain with time during and following embankment construction (modified from Rowe & Li 2005).

between the solid and dashed lines represents the creep strain due to the viscous nature of the reinforcement. For the PET reinforcement, creep is insignificant and the long-term reinforcement strains for both viscous and elastic reinforcement are practically the same. For the HDPE geogrid reinforcement, there is about 2% creep strain between the end of construction and the time of 98% consolidation.

Li & Rowe (2001) demonstrated that the isochronous stiffness deduced from standard creep test can reasonably represent the stiffness of geosynthetics reinforcement at the critical stage, for rate-insensitive foundation soils. The study also recommended that the isochronous stiffness should be used in design to estimate the mobilized reinforcing force at the end of embankment construction. Figure 19 compares the mobilized reinforcement stiffness with isochronous stiffness deduced from in-isolation creep test data during and after the construction of the HDPE geogrid and PET geosynthetic-reinforced embankments. It can be seen that the mobilized stiffness decreases with time and very

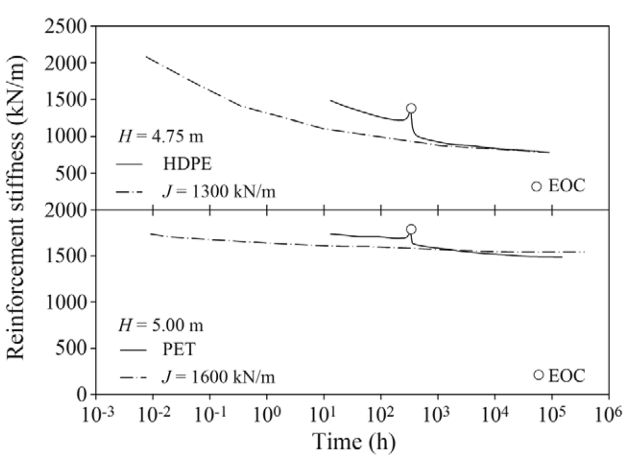

Figure 19 - Variation of reinforcement tensile stiffness with time during and following embankment construction (modified from Rowe & Li 2005).

closely approaches the isochronous stiffness in the long term. This also agrees with the finding of Li & Rowe (2008) and Rowe & Taechakumthorn (2008b) for the case of rate-sensitive foundation.

Time-dependence of the mobilized reinforcement stiffness shown in Fig. 19 also implies that the force in the reinforcement following the end of embankment construction may be significantly lower than expected in design owing to the viscous behaviour of geosynthetic reinforcement during embankment construction. This highlights the need for care when applying tensile stiffness from standard load-strain tests to deduce the design tensile force. In addition to creep effects, consideration should be given to potential construction damage of reinforcement (Allen & Bathurst, 1994, 1996).

10. Conclusions

The behaviour of reinforced embankments and the current design approaches have been examined for a number of different situations. The field case study of the Almere embankment shows that the use of geosynthetic reinforcement can substantially increase the failure height of the embankment over soft ground. The results demonstrated that the performance of the reinforced embankment can change significantly depending on the type of geosynthetic used and/or the nature of the foundation soil. Therefore, careful consideration must be given when selecting the type of constitutive relationship used to model each component of a reinforced embankment. Basal reinforcement can improve the stability of an embankment on both conventional (rate-insensitive) as well as rate-sensitive soil. Furthermore, the effect of partial consolidation during embankment construction can enhance the effect of reinforcement which encourages the combining of reinforcement with methods of accelerating consolidation, such as PVDs. When stage construction is required, the use of reinforcement can reduce the number of stages needed by increasing the height that can be safely attained in each stage. With the presence of PVDs, the assumption of total stress analysis is too conservative and the design method proposed by Li & Rowe (2001) can be employed to address the effect of strength gain, associated with the partial consolidation, during the construction.

For the reinforced embankment constructed over rate-sensitive soil, although the viscoplastic nature of the foundation can increase the short-term stability of the embankment, it significantly degrades the long-term embankment stability following the end of construction. The use of reinforcement provides a confining stress to the system and limits creep in the foundation. PVDs can provide a significant enhancement to the performance of reinforced embankments. For example, PVDs allow a higher degree of consolidation during and following the construction, which minimizes overstress and creep in the soil, and results in less differential settlement and lateral movement as well as long-term reinforcement strain.

Due to the time-dependent nature of the geosynthetic reinforcement, reinforcement stiffness at the end of construction is less than that provided by the standard tensile test. This implies that the reinforcement force used in the design may not represent what has been mobilized in the field. The isochronous stiffness measured from a standard creep tests appears reasonably, and conservatively, to represent the reinforcement stiffness in the field at the end of construction. The results also suggest that reinforcement creep and stress-relaxation allow an increase in the shear deformations of the foundation soil which will degrade the long-term performance of the reinforced embankment and may even lead to long-term failure, if the foundation soil exhibits strain-softening behaviour. Care must be taken in the design when dealing with creep-susceptible reinforcement and/or when the foundation soil is rate-sensitive.

Acknowledgments

All work reported in this paper was funded by the National Sciences and Engineering Research Council of Canada.

References

Abusharar, S.W.; Zheng, J.J.; Chen, B.G. & Yin, J.H. (2009) A simplified method for analysis of a piled embankment reinforced with geosynthetics. Geotextiles and Geomembranes, v. 27:1, p. 39-52.

Allen, T.M. & Bathurst, R.J. (1994) Characterization of geosynthetic load-strain behaviour after installation damage. Geosynthetics International, v. 1:2, p. 181-199.

Allen, T.M. & Bathurst, R.J. (1996) Combined allowable strength reduction factor for geosynthetic creep and installation damage. Geosynthetics International, v. 3:3, p. 407-439.

Allen, T.M.; Vinson, T.S. & Bell, J.R. (1982) Tensile strength and creep behaviour of geotextile in cold region applications. Proc. 2nd Int. Conf. on Geotextiles, Las Vegas, v. 3, pp. 775-780.

Bathurst, R.J. & Cai, Z. (1994) In-isolation cyclic load-extension behavior of two geogrids. Geosynthetics International, v. 1:1, p. 3-17.

Bergado, D.T. & Teerawattanasuk, C. (2008) 2D and 3D numerical simulations of reinforced embankments on soft ground, Geotextiles and Geomembranes, v. 26:1, p. 39-55.

Bergado, D.T.; Long, P.V. & Murthy, B.R. (2002) A case study of geotextile-reinforced embankment on soft ground. Geotextiles and Geomembranes, v. 20:6, p. 343-365.

Bo, M.W. (2004) Discharge capacity of prefabricated vertical drain and their field measurements, Geotextiles and Geomembranes, v. 22:1-2, Special Issue on Prefabricated Vertical Drains, p. 37-48.

Bozozuk, M. & Leonards, G.A. (1972) The Gloucester test fill. Proc. ASCE Special Conf. on Performance of Earth and Earth-Supported Structures, Purdue University, Lafayette, Ind., v. 1:1, pp. 299-317.

Carrillo, N. (1942) Simple two- and three-dimensional cases in theory of consolidation of soils. Journal of Mathematics and Physica, v. 21:1, p. 1-5.

Chai, J.C.; Carter, J.P. & Hayashi, S. (2006) Vacuum consolidation and its combination with embankment loading. Canadian Geotechnical Journal. v. 43:10, p. 985-996.

Christopher, B.R.; Holtz, R.D. & Bell, W.D. (1986) New tests for determining the in-soil stress-strain properties of geotextiles. Proc. 3rd Int. Conf. on Geotextiles, Vienna, v. 3, pp. 683-688.

Crawford, C.B.; Fannin, R.J.; deBoer, L.J. & Kern C.B. (1992) Experiences with prefabricated vertical (wick) drains at Vernon, B.C. Canadian Geotechnical Journal, v. 29:1, p. 67-79.

Crooks, J.H.; Becker, D.E.; Jeffries, M.G. & McKenzis, K. (1984) Yield behaviour and consolidation I: Pore pressure response. Proc. ASCE Sym. on Sedimentation Consolidation Models, Prediction and Validation, San Francisco, pp. 356-381.

Fowler, J. & Koerner, R.M. (1987) Stabilization of very soft soils using geosynthetics. Proc. of Geosynthetics '87 Conf., New Orleans, v. 1, pp. 289-299.

Fritzinger, S.A. (1990) Subaqueous use of high-strength geotextiles. Proc. 4th Int. Conf. on Geotextiles and Geomembranes and Related Products, The Hague, v. 1, pp. 143-148.

Graham, J.; Crooks, H.A. & Bell, A.L. (1983) Time effects on the stress-strain behaviour of natural soft clays. Geotechnique, v. 33:3, p. 327-340.

Greenwood, J.H. & Myles, B. (1986) Creep and stress relaxation of geotextiles. Proc. of 3rd Int. Conf. on Geotextiles, Vienna, v. 3, pp. 821-824.

Hansbo, S. (1981) Consolidation of fine-grained soils by prefabricated drains. Proc. 10th Int.Conf. on Soil Mech. and Found. Eng., Stockholm, v. 3, pp. 677-682.

Hinchberger, S.D. & Rowe, R.K. (1998) Modelling the rate-sensitive characteristics of the Gloucester foundation soil. Canadian Geotechnical Journal, v. 35:5, p. 769-789.

Hinchberger, S.D. & Rowe, R.K. (2003) Geosynthetic reinforced embankments on soft clay foundations: predicting reinforcement strains at failure. Geotextiles and Geomembranes, v. 21:3, p. 151-175.

Holtz, R.D.; Shang, J.Q. & Bergado, D.T. (2001) Soil improvement. R.K. Rowe (eds) Geotechnical and Geoenvironmental Engineering Handbook. Kluwer Academic, Norwell, pp. 429-462.

Holtz, R.D. (1987) Preloading with prefabricated vertical strip drains. Geotextiles and Geomembranes, v. 6:1-3, p. 109-131.

Holtz, R.D.; Christopher, B.R. & Berg, R.R. (1997) Geosynthetic Engineering. BiTech Publichers, Richmond, 452 pp.

Huang, J. & Han, J. (2009) 3D coupled mechanical and hydraulics modeling of a geosynthetics-reinforced deep mixed column-supported embankment. Geotextiles and Geomembranes, v.27:4, p. 272-280.

Humphrey, D.N. & Holtz, R.D. (1987) Reinforced embankments: A review of case histories. Geotextiles and Geomembranes, v. 6:4, p. 129-144.

Indraratna, B. & Redana, I.W. (2000) Numerical modeling of vertical drains with smear and well resistance installed in soft clay. Canadian Geotechnical Journal, v. 37:1, p. 132-145.

Indraratna, B.; Rujikiatkamjorn, C.; Balasubramaniam, A.S. & McIntosh, G. (2012) Soft ground improvement via vertical drains and vacuum assisted preloading, Geotextiles and Geomembranes, v. 30:Special Issue, p. 16-23.

Jamiolkowski, M.; Lancellotta, R. & Wolski, W. (1983) Precompression and speeding up consolidation: general report. Proc. 8th European Conf. on Soil Mech., Helsinki, v. 3, pp. 1201-1226.

Jewell, R.A (1982) A limit equilibrium design method for reinforced embankments on soft foundations. Proc. 2nd Int. Conf. on Geotextiles, Las Vegas, v. 4, pp. 671-676.

Jewell, R.A. (1987) Reinforced soil walls analysis and behaviour. Jarret, P.M. & McGown, A. (eds) NATO Advance Research Workshop on the Application of Polymeric Reinforcement in Soil Retaining Structure, Kluwer Academic Publishers, Boston, pp. 365-408.

Jewell, R.A. & Greenwood, J.H. (1988) Long-term strength and safety in steep soil slopes reinforced by polymer materials. Geotextiles and Geomembranes, v. 7:1, p. 81-118.

Jones, C.J.F.P. & Clarke, D. (2007) The residual strength of geosynthetic reinforcement subjected to accelerated creep testing and simulated seismic events, Geotextiles and Geomembranes, v. 25:3, p. 155-169.

Kabbaj, M.; Tavenas, F. & Leroueil, S. (1988) *In-situ* and laboratory stress-strain relationships. Geotechnique, v. 38:1, p. 83-100.

Karunaratne, G.P. (2011) Prefabricated and electrical vertical drains for consolidation of soft clay, Geotextiles and Geomembranes, v. 29:4, p. 391-401.

Kelln, C.; Sharma, J.; Hughes, D. & Gallagher, G. (2007) Deformation of a soft estuarine deposit under a geotextile reinforced embankment. Canadian Geotechnical Journal, v. 44:5, p. 603-617.

Kjellman, W. (1948) Accelerating consolidation of fine-grained soils by means of cardboard wicks. Proc. 2nd Int. Conf. on Soil Mech. and Found. Eng., Rotterdam, pp. 302-305.

Kongkitkul, W. & Tatsuoka, F. (2007) A theoretical framework to analyze the behaviour of polymer geosynthetic reinforcement in temperature-accelerated creep test. Geosynthetics International, v. 14:1, p. 23-38.

Ladd, C.C. (1991) Stability evaluation during staged construction. Journal of Geotechnical Engineering, v. 17:4, p. 540-615.

Leroueil, S. (1988) Tenth canadian geotechnical colloquium: Recent developments in consolidation of natural clays. Canadian Geotechnical Journal, v. 25:1, p. 85-107.

Leroueil, S. & Rowe, R. K. 2001. Embankments over soft soil and peat. R.K. Rowe (eds) Geotechnical and Geoenvironmental Engineering Handbook. Kluwer Academic Norwell, pp. 463-500.

Leshchinsky, D.; Dechasakulsom, M.; Kaliakin, V.N. & Ling, H.I. (1997) Creep and stress relaxation of geogrids. Geosynthetics International, v. 4:5, p. 463-479.

Li, A.L. & Rowe, R.K. (1999) Reinforced embankments constructed on foundations with prefabricated vertical drains. Proc. 52nd Canadian Geotechnical Conf., Regina, Sask, pp. 411-418.

Li, A.L. & Rowe, R.K. (2001) Combined effects of reinforcement and prefabricated vertical drains on embankment performance. Canadian Geotechnical Journal, v. 38:6, p. 1266-1282.

Li, A.L. & Rowe, R.K. (2008) Effects of viscous behaviour of geosynthetic reinforcement and foundation soils on the performance of reinforced embankments. Geotextiles and Geomembranes v. 26:4, p. 317-334.

Lo, K.Y. & Morin, J.P. (1972) Strength anisotropy and time effects of two sensitive clays. Canadian Geotechnical Journal, v. 9:3, p. 261-277.

Lockett, L. & Mattox, R.M. (1987) Difficult soil problems on Cochrane Bridge finessed with geosynthetics. Proc. Geosynthetic '87 Conf., New Orleans, v. 1, pp. 309-319.

McGown, A.; Andrawes, K.Z. & Kabir, M.H. (1982) Load-extension testing geotextiles confined in-soil. Proc. 2nd Int. Conf. on Geotextiles, Las Vegas, v. 3, pp. 793-798.

Mylleville, B.L.J. & Rowe, R.K. (1988) Simplified Undrained Stability Analysis for Use in the Design of Steel Reinforced Embankments on Soft Foundations. Faculty of Engineering Science, University of Western Ontario, GEOT-3-88, 73 pp.

Mylleville, B.L.J. & Rowe, R.K. (1991) On the design of reinforced embankments on soft brittle clays. Proc. Geosynthetics '91 Conf., Atlanta, v. 1, pp. 395-408.

Nicholson, D.P. & Jardine, R.J. (1981) Performance of vertical drains at Queenborough bypass. Geotechnique, v. 31:1, p. 67-90.

Olson, R.E. (1977) Consolidation under time dependent loading. Journal of the Geotechnical Engineering Division, v. 103:GT1, p. 55-60.

Poulos, H.G. & Davis, E.H. (1974) Elastic Solutions for Soil and Rock Mechanics. Wiley, New York, 424 pp.

Rowe, R.K. & Hinchberger, S.D. (1998) The significance of rate effects in modelling the Sackville test embankment. Canadian Geotechnical Journal, v. 35:3, p. 500-516.

Rowe, R.K. & Jones, C.J.F.P. (2000) Geosynthetics: Innovative materials and rational design. Keynote Lecture. Proc. Int. Conf. on Geotechnical and Geological Eng., Melbourne, pp. 1124-1156.

Rowe, R.K. & Li, A.L. (1999) Reinforced embankments over soft foundations under undrained and partially drained conditions. Geotextiles and Geomembranes, v. 17:3, p. 129-146.

Rowe, R.K. & Li, A.L. (2002) Behaviour of reinforced embankments on soft rate sensitive soils. Geotechnique, v. 52:1, p. 29-40.

Rowe, R.K. & Li, A.L. (2005) Geosynthetic-reinforced embankments over soft foundations. Geosynthetics International, v. 12:1, p. 50-85.

Rowe, R.K. & Mylleville, B.L.J. (1990) Implications of adopting an allowable geosynthetic strain in estimating stability. Proc. 4th Int. Conf. on Geotextiles, Geomembranes and Related Products, The Hague, v. 1, pp. 131-136.

Rowe, R.K. & Soderman, K.L. (1984) Comparison of predicted and observed behaviour of two test embankments. Geotextiles and Geomembranes, v. 1:2, p. 143-160.

Rowe, R.K. & Soderman, K.L. (1985) An approximate method for estimating the stability for geotextiles reinforced embankments. Canadian Geotechnical Journal, v. 22:3 p. 392-398.

Rowe, R.K. & Soderman, K.L. (1987) Reinforcement of the embankments on soils whose strength increase with depth. Proc. of Geosynthetics '87 Conf., New Orleans, v. 1, pp. 266-277.

Rowe R.K. & Taechakumthorn C. (2008a) Combined effect of PVDs and reinforcement on embankments over rate-sensitive soils. Geotextiles and Geomembranes, v. 26:3, p. 239-249.

Rowe, R.K. & Taechakumthorn C. (2008b) The effect of soil viscosity on the behaviour of reinforced embankment. Keynote Lecture. Proc. 1st Int. Conf. on Transportation Geotechnics, Nottingham, pp. 47-56.

Rowe, R.K. & Taechakumthorn, C. (2010) The interaction between reinforcement and drains and their effect on the performance of embankments on soft ground. Symposium on New Techniques for Design and Construction in Soft Clays, Guaruja, pp. 7-19.

Rowe, R.K.; Gnanendran, C.T.; Landva, A.O. & Valsangkar, A.J. (1995) Construction and performance of a full-scale geotextile reinforced test embankment, Sackville, New Brunswick. Canadian Geotechnical Journal, v. 32:3, p. 512-534.

Rowe, R.K.; Gnanendran, C.T.; Landva, A.O. & Valsangkar, A.J. (1996) Calculated and observed behaviour of a reinforced embankment over soft compressible soil. Canadian Geotechnical Journal, v. 33:2, p. 324-338.

Saowapakpiboon, J.; Bergado, D.T.; Youwai, S.; Chai, J.C.; Wanthong, P. & Voottipruex, P. (2010) Measured and predicted performance of prefabricated vertical drains (PVDs) with and without vacuum preloading. Geotextiles and Geomembranes, v. 28:1, p. 1-11.

Saowapakpiboon, J.; Bergado, D.T.; Voottipruex, P.; Lam, L.G. & Nakakuma, K. (2011) PVD improvement combined with surcharge and vacuum preloading including simulations, Geotextiles and Geomembranes, 29:1, p. 74-82.

Schimelfenyg, P.; Fowler, J. & Leshchinsky, D. (1990) Fabric reinforced containment dike, New Bedford superfund site. Proc. 4th Int. Conf. on Geotextiles and Geomembranes and Related Products, The Hague, v. 1, pp. 149-154.

Shinoda M. & Bathurst, R.J. (2004) Lateral and axial deformation of PP, HDPE and PET geogrids under tensile load. Geotextiles and Geomembranes, v. 22:4, p. 205-222.

Sinha, A.K.; Havanagi, V.G. & Mathur, S. (2009) An approach to shorten the construction period of high embankment on soft soil improved with PVD. Geotextiles and Geomembranes, v. 27:6, p. 488-492.

Taechakumthorn, C. & Rowe, R.K. (2008) Behaviour of reinforced embankments on rate-sensitive foundation installed with prefabrication vertical drains. Proc. 12th IACMAG Conf., Goa, pp. 3559-3566.

Tolooiyan, A.; Abustan, I.; Selamat, M.R. & Ghaffari, S. (2009) A comprehensive method for analyzing the effect of geotextile layers on embankment stability, Geotextiles and Geomembrane 27:5, p. 399-405.

Vaid, Y.P. & Campanella, G. (1977) Time-dependent behaviour of undisturbed clay. Journal of the Geotechnical Engineering, v. 103:GT7, p. 693-709.

Vaid, Y.P.; Robertson, P.K. & Campanella, R.G. (1979) Strain rate behaviour of Saint-Jean-Vianney clay. Canadian Geotechnical Journal, v. 16:1, p. 34-42.

Varuso, R.J.; Grieshaber, J.B. & Nataraj, M.S. (2005) Geosynthetic reinforced levee test section on soft normally consolidated clays. Geotextiles and Geomembranes, v. 23:4, p. 362-383.

Volk, J.C.; Hunt, R.E.; Leshchinsky, D.; Diloreto, R. & Collins, T.G. (1994) Reinforced embankment over very soft soil: Grassy Sound highway embankment. Proc. 5th Int. Conf. on Geotextiles, Geomembranes and Related Products, Singapore, v. 1, pp. 41-48.

Yeo, S.S. & Hsuan, Y.G. (2010) Evaluation of creep behavior of high density polyethylene and polyethylene-terephthalate geogrids. Geotextiles and Geomembranes, v. 28:5, p. 409-421.

Zhu, G. & Yin, J.H. (2004) Consolidation analysis of soil with vertical and horizontal drainage under ramp loading considering smear effects. Geotextiles and Geomembranes, v. 22:1-2, Special Issue on Prefabricated Vertical Drains, p. 63-74.

List of Symbols

J: tensile stiffness of reinforcement
ε_a: allowable compatible strain
ε_{all}: allowable reinforcement strain
T_{rein}: reinforcement tensile force
T_{req}: required reinforcement tensile force
Ω: dimensionless parameter
γ_f: bulk unit weight of the embankment fill
H_c: the collapse height of the unreinforced embankment
s_u: undrained shear strength of the soft foundation
E_u: modulus of the soft foundation
$(D/B)_e$: ratio of the effective depth of the deposit to the crest width
σ'_v: vertical effective stress
σ'_p: maximum preconsolidation pressure
S: spacing of PVDs
$\Delta\sigma$: apply vertical stress
$C_{N/C}$: compression index
$C_{O/C}$: recompression index
$\Delta\sigma(t)$: applied stress at time t
u: excess pore pressure at time t
$\overline{U}_{O/C}$: average degree of consolidation for the overconsolidated soil
$\overline{U}_{N/C}$: average degree of consolidation for the normally consolidated soil
T: time factor for vertical consolidation
T_c: time factor for vertical consolidation at the end of construction
T_h: time factor for horizontal consolidation
T_{hc}: time factor for horizontal consolidation at the end of construction
k_v: hydraulic conductivity of soil in the vertical direction
k_h: hydraulic conductivity of soil in the horizontal direction
k_s: hydraulic conductivity of soil in the smear zone
k_w: hydraulic conductivity of the vertical drain
q_w: equivalent discharge capacity for the axisymmetric unit cell
r_w: equivalent radius of the vertical drain
r_s: equivalent radius of the smear zone
R: equivalent radius of the influence zone
I_q: influence factor
fc: partial factor for the undrained shear strength of the foundation soil
fø: partial factor for friction angle of fill material
fγ: partial factor for the unit weight of the fill material

Working Hypothesis, Special Laboratory Tests, Working Tools, Analysis of the Monitoring of a Pilot Embankment Built on Soft Clay in Santos with Wick Drains and its Application to the Final Design

J.P.P. Rémy, I.S.M. Martins, P.E.L. Santa Maria, V.N. Aguiar, M.E.S. Andrade

Abstract. Routine in-situ and laboratory investigations carried out for the basic design failed to provide reliable values for compressibility and consolidation parameters of soft clay layers at the site of a terminal to be built in Santos. A pilot embankment was designed and built divided in three equal areas, two with wick drains in a square mesh at spacings of 1.2 m and 2.4 m respectively and one with no drain. The basic working hypothesis adopted by the authors was that, in the field, primary and secondary consolidation occur simultaneously. High quality standard and special (long term and relaxation) oedometer tests provided reliable values of C_c, C_r and σ'_p and the OCR value of 2.1 as equivalent to the end of secondary consolidation allowing to estimate the total primary and secondary compressions of one of the most compressible layers (layer 6). No of the shelf tool is available to backanalyze the measured compression of a soft clay layer based on the adopted hypothesis. The first tool tested, the ε *vs.* $\log(\sigma'_v)$ Bjerrum type abacus with lines of equal $\dot{\varepsilon}$ values built from the oedometer tests results, proved to be non applicable. The second tool tested, the same type of abacus extrapolated from the first one for the field conditions through Taylor and Merchant's theory also proved to be non applicable. Both the third tool tested, the fitting of a theoretical Taylor and Merchant type curve to the measured compression curve in the area with no drain and the fourth tool tested, the fitting of a theoretical curve obtained through a method tailored by the authors designated "Primary Barron + secondary pseudo Taylor and Merchant" to the measured compression curves in the areas with wickdrains proved to provide excellent conformity of the theoretical and measured curves. The c_v and c_h field values thus obtained are of the same order of magnitude as the laboratory values and show the same trend to decrease when the effective stress increases, contradicting the current creed based on backanalysis through Asaoka's method, *i.e.* considering that secondary consolidation only starts after primary consolidations ends, that field c_v and c_h values are commonly 10 to 100 times higher than laboratory values. Based on their results the authors conclude that the excellent conformity of the theoretical and the measured curves obtained with the working hypothesis they adopted, the results of the laboratory tests they performed and the tools they used for the back-analysis, leads to the conclusion that the working hypothesis, the laboratory tests and the tools proved to be very efficient and trustworthy in leading to reliable compressibility and consolidation parameters of the soft clay, and will be equally efficient and trustworthy when used for the final design of the improvement of the foundation soft clay layer.

Keywords: soft clay, pilot embankment, secondary consolidation, wick drains, soil improvement.

1. Introduction

A multipurpose terminal is to be built at Barnabé Island on the Santos Channel opposite Santos Harbour as shown in Fig. 1. The total area to be filled is 800 000 m^2. Area 3 will be used for containers storage and part of it will be reclaimed underwater.

The field investigations carried out for the basic design included:

• 176 2½" diameter percussion borings with SPT at every meter, 148 of them down to refusal, covering the whole area, including the quay and the vessels access channel areas, leading to an average distance between borings over the whole project area a little smaller than 100 m by 100 m, 220 "undisturbed" samples extracted from 4" and 6" diameter borings and

• 375 vane-tests in 31 borings and

• 15 cone penetration tests (CPT) with 78 pore pressure dissipation tests.

J.P.P. Rémy, Mecasolo Engenharia e Consultoria Ltda., Nova Friburgo, RJ, Brazil. e-mail: jpremy@mecasolo.com.br.
I.S.M. Martins, Grupo de Reologia, Área de Mecânica dos Solos, COPPE, Universidade Federal do Rio de Janeiro, Rio de Janeiro, RJ, Brazil. e-mail: ian@coc.ufrj.br.
P.E.L. Santa Maria, Grupo de Reologia, Área de Mecânica dos Solos, COPPE, Universidade Federal do Rio de Janeiro, Rio de Janeiro, RJ, Brazil. e-mail: paulo.santa-maria@acergy-group.com.
V.N. Aguiar, Mecasolo Engenharia e Consultoria Ltda., Nova Friburgo, RJ, Brazil. e-mail: vitor@mecasolo.com.br.
M.E.S. Andrade, Mecasolo Engenharia e Consultoria Ltda., Nova Friburgo, RJ, Brazil. e-mail: mauricioengdb@bol.com.br.
Submitted on October 29, 2010; Final Acceptance on December 15, 2011; Discussion open until July 31, 2012.

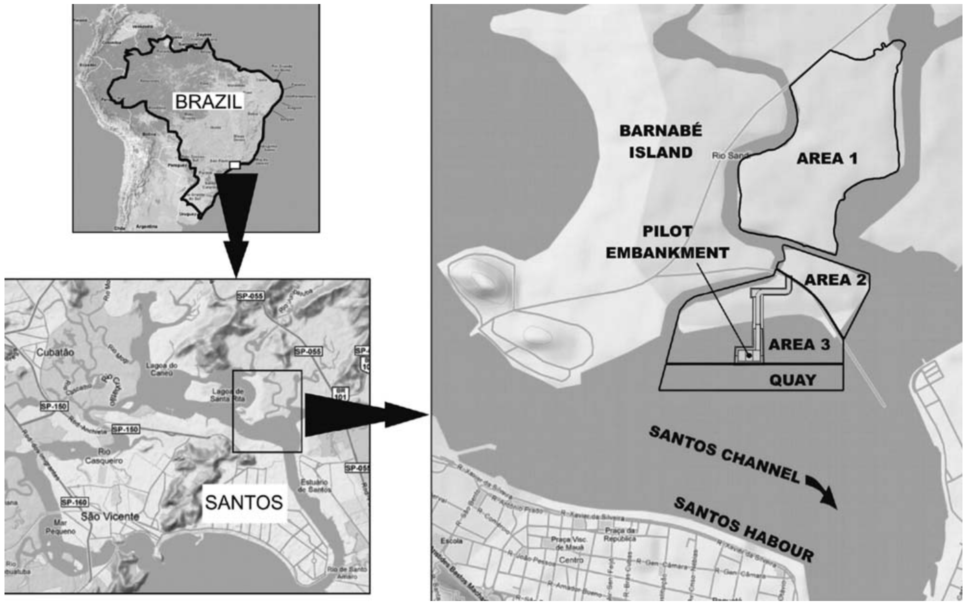

Figure 1 - Location of the container terminal.

The subsoil is rather heterogeneous and consists basically of very soft to soft clayey alluvium (SPT from 0 to 4) down to a total depth varying between 22.0 m and 43.1 m within which one or several sandy lenses or layers with SPT higher than 4 were found, mostly, with individual thicknesses of 1 to 3 m, in 83 of the 148 deep borings. The sum of these layers and lenses thicknesses is up to 2 meters in 34 borings, between 2 and 5 meters in 34 borings and between 5 and 11 meters in 15 borings.

The basic design geotechnical laboratory investigations consisted in:

• 220 grain-size distribution curves, Atterberg limits, unit weight, natural water content and specific gravity and

• 141 standard stage loading oedometer tests,

from which conservative clay layers parameters were obtained to be used for the basic design of soft soil treatment, earthworks (fills and dikes) and quay, tanks and building foundations.

2. Soil Parameters Critically Important for the Final Design and Construction of the Containers Terminal Still Not Reliably Known at the End of the Basic Design

All parameters listed in Table 1 are fairly reliable and local variations from the design values do not imply in drastic impacts on the three key points of the design which are (a) settlements values, (b) time necessary for these settlements (and the associated undrained shear strength increase) to occur and (c) fills and dikes slopes safety factors.

On the other hand, any variation of the compressibility, shear strength and consolidation parameters listed in Table 2 has a drastic impact on these key points, with special emphasis on the preconsolidation stress value which is the soil parameter with most influence on each and everyone of the three key points listed above.

A real field value of preconsolidation stress greater than the design value will lead to overestimated settlements and underestimated undrained shear strength of the soft clay. Hence, a safe design has to be based on a conservative design value of the preconsolidation stress chosen so that there be low probability of the real field value to be smaller than the design value.

On the other hand the choice of a preconsolidation stress design value on the low side may lead to a very antieconomical design due to the fact that it might require an unnecessary small spacing of wickdrains or an unnecessary thick preloading fill, or both, to meet the project deadline. This is mainly due to the fact that the value of the coefficient of consolidation in the recompression domain is usually between 30 and 100 times greater than in the virgin domain, as will be shown ahead.

The left side of Fig. 2 shows the preconsolidation stress values obtained from the 141 oedometer tests carried out for the basic design. The scattering is so high that these values could not be used to define the preconsolidation stress design profile. This is a typical example of "highly scattered lab data resulting from poor quality samples and inappropriate testing such as doubling the load in oedometer test (ill defined σ'_p)" as pointed out by Ladd (2008).

The only possible way of inferring the preconsolidation stress design profile was from the shear strength profiles given by the vane tests as shown by the two straight lines on the right side of Fig. 2. The equations of these two straight lines were used to obtain the design profile of σ'_p through the correlation between the in-situ undrained shear strength S_u, obtained from the vane test values, S_u(VT) (see

Table 1 - Physical properties of soft clay – Basic design values (*).

Depth	% < 5 μ (%)	w (%)	LL (%)	PI (%)	γ (kN/m³)	e_0
0 to 3 m						
3 to 6 m	36	73.5	78.2	47.1	15.6	2.08
6 to 9 m						
9 to 18 m	63	94.4	124.1	79.6	14.4	2.79
> 18 m	49	70.0	89.0	54.3	15.7	2.08

(*) % < 5 μ = percentage of particles smaller than 0.005 mm, w = natural water content, LL = liquid limit, PI = plasticity index, γ = unit weight, e_0 = initial void ratio (after sampling).

Table 2 - Compressibility, shear strength and consolidation parameters – Basic design values (**).

Depth	$C_c/(1 + e_0)$	C_e/C_c	σ'_p (kPa) (z in meters)	S_u (kPa) (z in meters)	S_u/σ'_p	c_h (m²/s)
0 to 3 m			1.6+4.7z	0.5+1.2z		
3 to 6 m	0.28	0.112	14+4.7z	4.0+1.2z		
6 to 9 m					0.26	2.5×10^{-7}
9 to 18 m	0.36	0.126	30+4.7z	9.0+1.2z		
> 18 m	0.29	0.146				

(**) C_c = compression index, C_e = expansion index, σ'_p = preconsolidation stress, S_u = undrained in-situ shear strength, c_h = horizontal coefficient of consolidation in the recompression range.

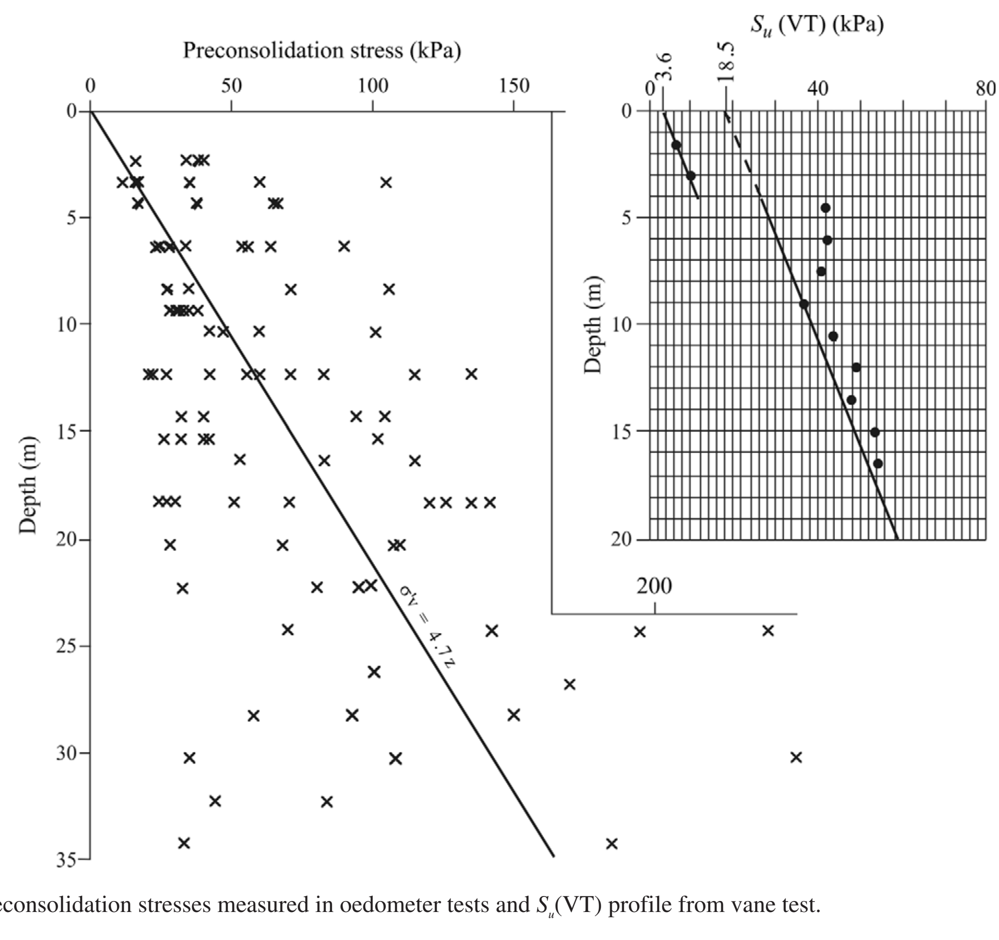

Figure 2 - Preconsolidation stresses measured in oedometer tests and S_u(VT) profile from vane test.

the right side of Fig. 2), by applying Bjerrum's reduction factor to obtain the field values S_u, and σ'_p.

3. Local Soil Profile and Soil Properties Under the Pilot Embankment

The main aim of the pilot embankment and its geotechnical investigations was to provide the best information about the consolidation characteristics of the soft clay. The embankment total length at elevation +3.00 m (which was the terminal pavement design elevation) is 150 m and its width at elevation +3.00 m is 70 m. It is divided in 3 areas as shown in Fig. 3. Area 1 is provided with a square mesh of wick drains spaced 1.20 m penetrating 30 m from elevation +1.80 m down to elevation -28.20 m. Area 2 is provided with a square mesh of wick drains spaced 2.40 m also penetrating from elevation +1.80 m down to elevation -28.20 m. Area 3 has no wick drain.

The geotechnical investigations under the pilot embankment consisted of 5 percussion borings with SPT at every meter down to refusal, three 6" borings to obtain 4" undisturbed samples for laboratory tests, 4 CPT with 28 pore pressure dissipation tests and 67 vane tests in 5 borings, as shown in Fig. 3. The water content of SPT samples was measured in the material collected close to the bottom of every sample and proved to be very helpful in defining the soil profile.

All undisturbed samples were extracted with stationary piston sampler with authors Martins and Aguiar present on the site to ensure that proper procedures were rigorously followed to provide the best possible samples quality. The 12 samples obtained in boring SRA-203 under area 3 were very carefully sealed with paraffin, wrapped, packed and transported into special manufactured wood boxes which allowed keeping them in their proper upside vertical position. These samples were transported to the soil mechanics laboratory of the Rheology Group at COPPE – UFRJ where they were tested. The test program consisted of unit weight, natural water content, specific gravity, grain size analysis, Atterberg limits and organic matter content for each sample. 42 standard and 32 special oedometer tests were performed under controlled temperature by Aguiar (2008) and Andrade (2009) on 70 mm diameter, 20 mm height specimens. The specimens were prepared according to Ladd and DeGroot (2003) recommendations. Figure 4 shows the results of 7 oedometer tests carried out on undisturbed specimens trimmed in sample number 6 and the result of one test carried out on a remoulded specimen prepared from the same sample.

In respect to Coutinho's (2007) samples quality classification criteria, all specimens from layer 6, save two specimens in sample SRA-203(10) and one in sample SRA-203(5), were classified as excellent to fair.

Figure 5 shows the soil profiles below the centers of areas 3, 2 and 1 as established based on the results of all field and laboratory soil investigations carried out in the subsoil under the pilot embankment. The figure shows the stratigraphy with each layer description, the SPT values, the positions of the undisturbed samples and the positions of the settlement measuring magnets. In area 3, it also shows the initial vertical effective stress profile (σ'_v) and the preconsolidation stress profile (σ'_p) obtained from the oedometer tests performed on SRA-203 samples as dis-

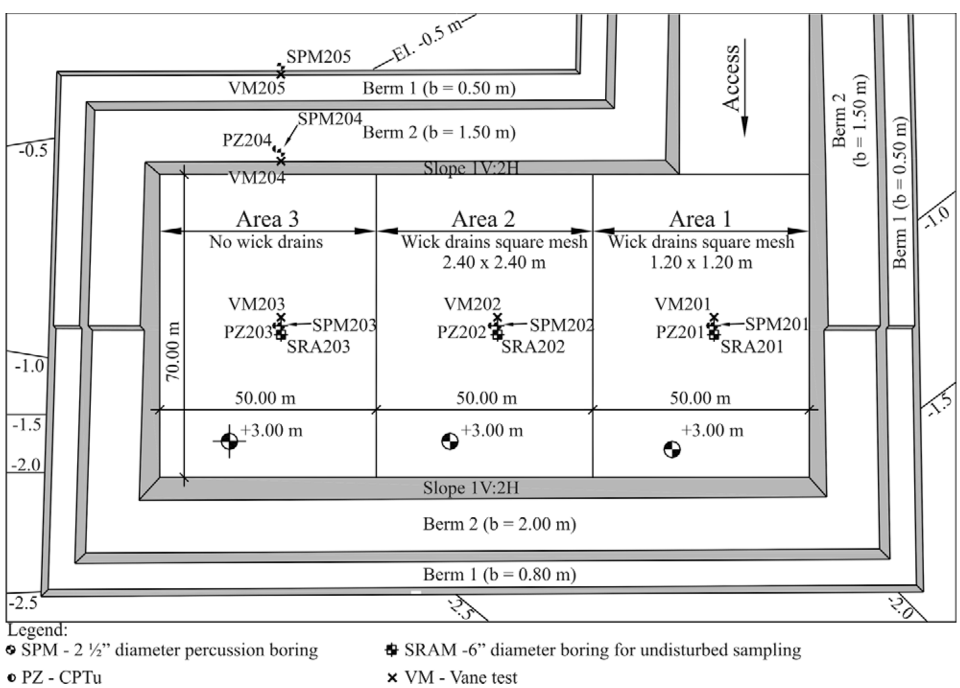

Figure 3 - Pilot embankment soil investigations location.

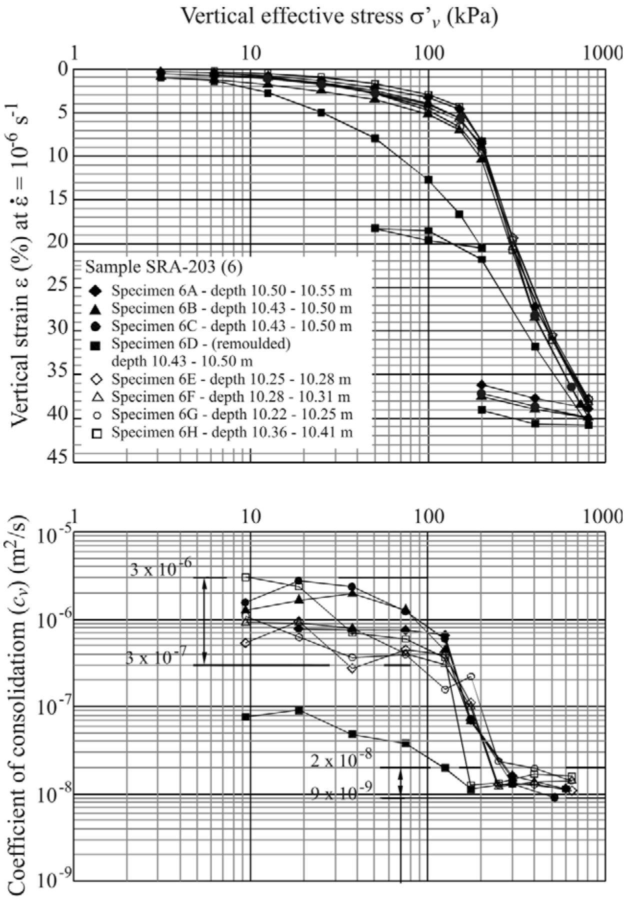

Figure 4 - Results of standard oedometer tests on sample number 6 of boring SRA-203.

cussed ahead. As shown in Fig. 6, the preconsolidation stresses obtained at strain rate $\dot{\varepsilon}_v = 10^{-6}$ s^{-1} from the good quality samples tested at COPPE were much higher than the adopted values for the basic design, the same being true for the $C_c/(1 + e_0)$ values. Andrade (2009) observed that the σ'_p values at $\dot{\varepsilon}_v = 10^{-6}$ s^{-1} are, in average, 8% higher than the σ'_p values determined for 24 h loading stages. The authors consider these COPPE values to be very reliable since the same high repeatability of the results shown in Fig. 4 was obtained on all the clayey samples of SRA-203, and very good repeatability, although not as high, was obtained on the more sandy samples. The samples taken from borings SRA-201 and SRA-202 were tested in another laboratory and their results which indicate that the specimen tested were of lower quality than the ones tested at COPPE are not included in the present analysis.

To define the σ'_p profile, a line passing through the highest σ'_p experimental values was chosen considering that these correspond to the highest quality specimens since any degree of remoulding of the samples lowers the value of σ'_p.

Table 3 shows the soils properties defined from the soils investigations carried out in the foundation of the pilot embankment, including the physical properties of samples from SRA-201 and SRA-202.

4. Pilot Embankment Construction History and Instrumentation

The pilot embankment construction was very carefully planned and carried out to avoid any local failure of the extremely soft clay layer (layer 1) which extends down to 1.5 to 2 meters depth. At first, nonwoven geotextile was laid on top of the soft clay layer, covering the whole area. Then a 15 to 30 cm thick layer of quarry dust was hydraulically carefully spread into place. This layer was covered with a geogrid with a strength of 800 kN/m and the fill material was slowly put into place, first being dumped under the water level and then as soon as access was possible at low tide, poured by trucks and bulldozers. When elevation + 1.80 m was reached, the wick drains were driven down to their design depth of 30 m below embankment level, requiring that holes be first drilled through the embankment and the geogrid. The embankment was then completed up to elevation +3.00 m as shown in Fig. 3.

Table 3 - Soils properties from the soils investigations of the pilot embankment (*).

Layer(**)	γ (kN/m^3)	$C_c/(1 + e_0)$	C_s/C_c	c_{v1} (m^2/s)	c_{v2} (m^2/s)	c_{h1} (m^2/s)
1	13.0	0.36	0.12	-	-	-
2	20.0	-	-	-	-	1.5 x 10^{-4}
3	16.5	0.28	0.19	1.7 x 10^{-6}	6.0 x 10^{-7}	1.0 x 10^{-6}
4	17.6	0.16	0.27	1.4 x 10^{-6}	1.5 x 10^{-6}	8.3 x 10^{-6}
5	16.5	0.28	0.19	1.7 x 10^{-6}	6.0 x 10^{-7}	1.0 x 10^{-6}
6	15.0	0.56	0.11	6.5 x 10^{-7}	1.5 x 10^{-8}	4.9 x 10^{-7}
7	18.1	0.16	0.27	1.5 x 10^{-6}	1.3 x 10^{-6}	2.1 x 10^{-5}
8	14.6	0.56	0.11	6.5 x 10^{-7}	1.5 x 10^{-8}	4.9 x 10^{-7}

(*) c_{v1} and c_{h1} are for $\sigma'_v \leq \sigma'_p$, and c_{v2} is for $\sigma'_v > \sigma'_p$ (c_{v1} and c_{v2} from oedometer tests, c_{h1} from CPT porepressure dissipation tests).
(**) for identification of each layer see Fig. 5.

After obtaining the first COPPE oedometer tests high preconsolidation stress values, it was decided to heighten the pilot embankment in order to apply a vertical stress higher than the preconsolidation stress. Figure 7 shows the highest embankment elevations in each area and the dates when they were reached as well as the locations of the set-

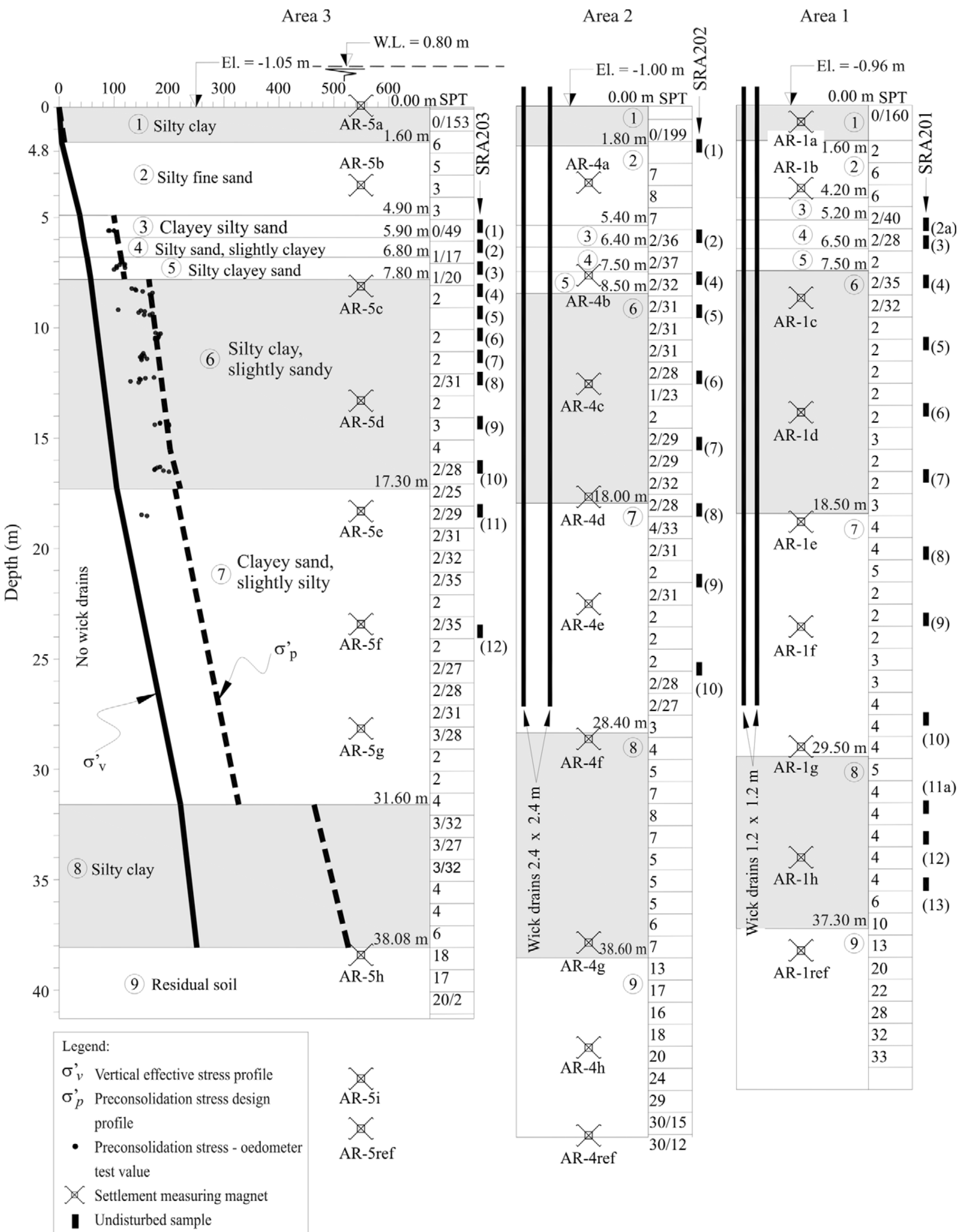

Figure 5 - Soil profiles under areas 3, 2 and 1 with positions of undisturbed samples and settlement measuring magnets.

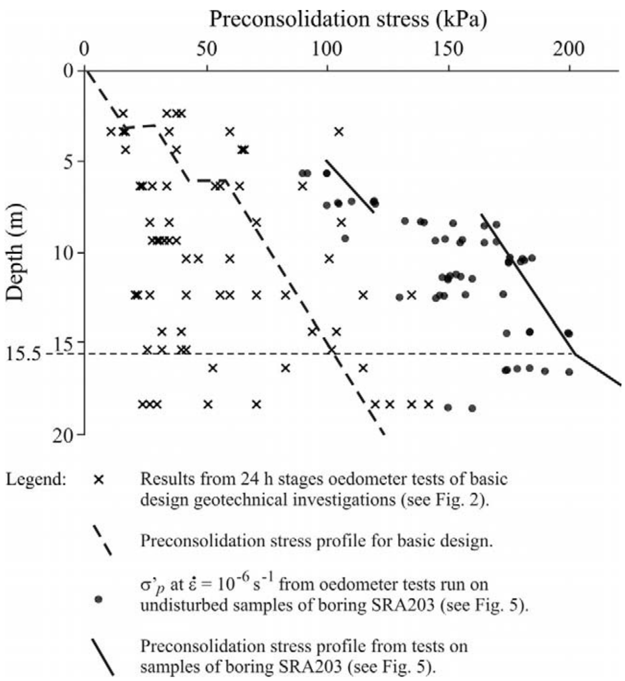

Figure 6 - Preconsolidation stress values and profiles.

tlement plates (PR), magnetic settlement gauges (MR) and inclinometers (IN) installed to monitor settlements, layers compressions and horizontal displacements, respectively.

When the decision to increase the embankment thickness was taken, the north half of area 3 had already been heightened to elevation +7.77 m, immediately after the embankment was completed to design elevation +3.00 m, with the aim to provoke a foundation failure towards inclinometers IN1, IN2 and IN3. While the heightening of the fill of the north half of area 3 was taking place, the stresses in the geogrid in the north south direction were measured with the installed strain gauges. The embankment did not show apparent deformations, almost no stress change was recorded in the strain gauges and very little lateral displacements were registered in the inclinometers. The analysis of this behaviour will not be discussed here because this subject is beyond the scope of the present work.

The pilot embankment was also instrumented with full profile hydraulic settlement gauges, electrical piezometers and open pipe piezometers, but these instruments, along with the inclinometers and the strain gauges of the geogrid were read for only a short period of time, too short to provide helpful data.

5. Special Laboratory Tests

26 long term oedometer tests were carried out. In some of them secondary consolidation was observed after unloading. Stress relaxation tests where the vertical displacements were restrained and the vertical stress measured were also carried out.

At the top of Fig. 8 are shown the results of oedometer tests run on 4 specimens trimmed in sample SRA-203(8), all consolidated under 800 kPa following the same procedure, and then unloaded to different stress values, generating different values of OCR. The specimens strains were then measured for 20 days under constant stress and constant temperature (20 °C ± 1°).

The results at the bottom of Fig. 8 show that after about 4000 min the specimen unloaded to OCR value of 1.60 stopped expanding and started to compress whereas

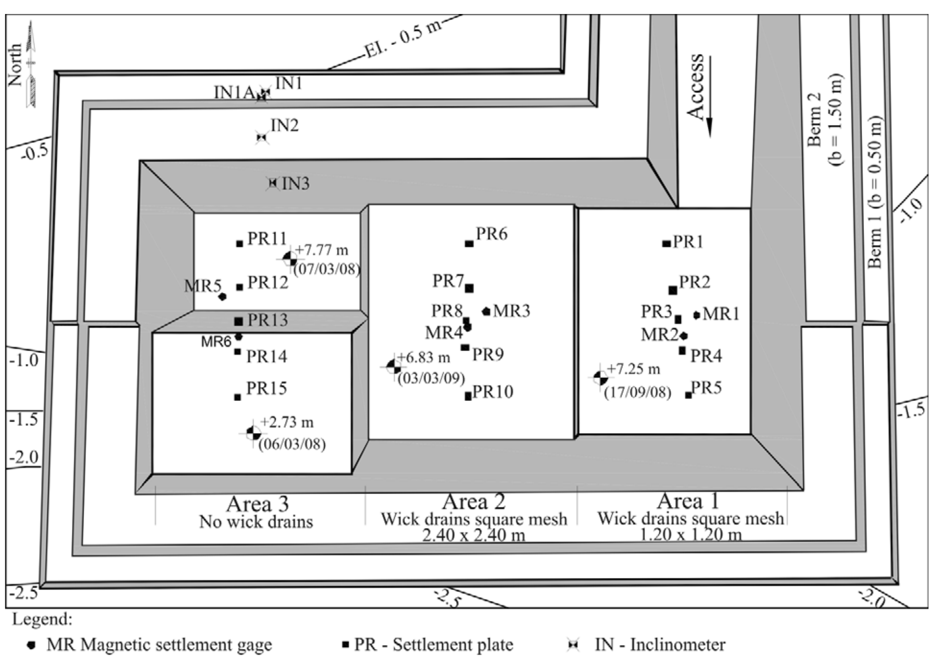

Figure 7 - Location of instruments for settlements, layer compressions and horizontal displacements measurements.

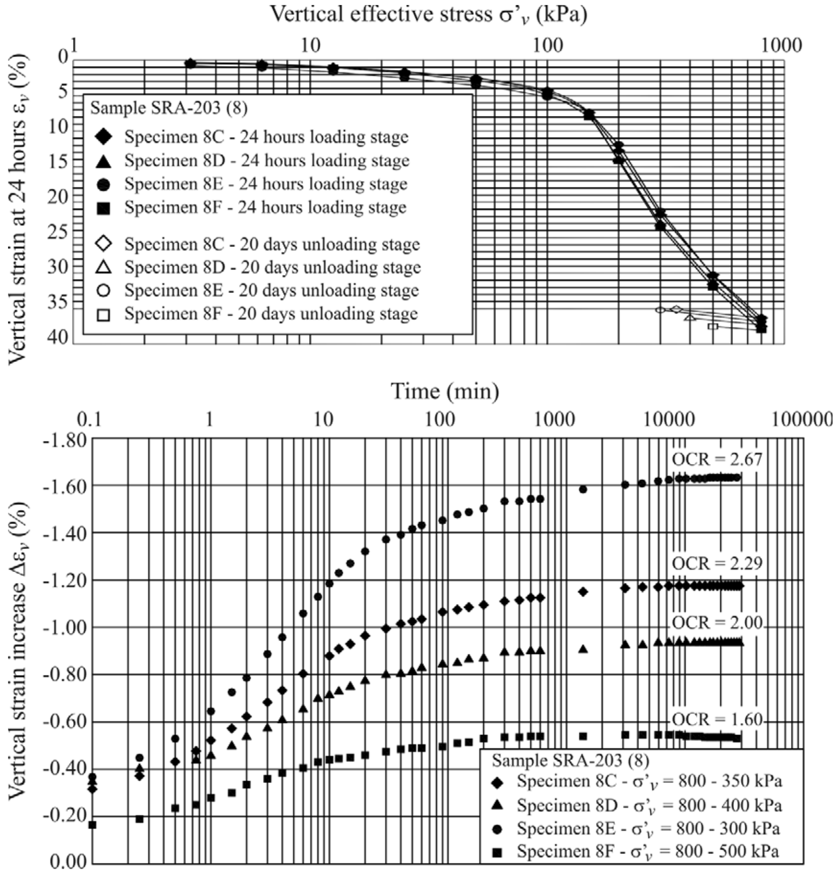

Figure 8 - Results of oedometer tests.

the specimens unloaded to OCR values of 2.00, 2.29 and 2.67 leveled off. Based on these and all other results from long term oedometer tests performed on other samples, Andrade (2009), following the procedure suggested by Feijó & Martins (1993), established that the end of secondary compression line could be drawn as being the line equivalent to an OCR value of 2.1 relative to the $\dot{\varepsilon} = 10^{-6}\ s^{-1}$ line. In their analysis the authors did not discriminate between the $\dot{\varepsilon} = 10^{-6}\ s^{-1}$ line and the end of primary compression line due to the proximity of these two lines observed in all oedometer tests results. This value can be compared to the equivalent OCR value close to 2.0 relative to E.O.P. found by Feijó (1991) for the end of secondary compression of Sarapuí clay in Rio de Janeiro, and to 1.7 relative to 24 h stages published by Martins *et al.* (2009) for various Rio de Janeiro soft clays.

The preconsolidation stresses σ'_p in layers 3, 4, 5, and 6 were established based on the oedometer tests results as seen on Fig. 6. It can be seen that, in layer 6, above 15.5 m depth the lab results show σ'_p values higher than 2.1 σ'_v leading to the conclusion that the preconsolidation is due to dune effect (Massad 1989). The same dune effect was considered to prevail in clayey sand layer 7 and the secondary compression preconsolidation effect was considered to be the predominant one in layer 1 and in layer 8 adopting $\sigma'_p = 2.1\ \sigma'_v$.

6. Pilot Embankment Monitoring Data

Due to the lack of readings of the other instruments, the monitoring data analyzed to assess the behaviour of the soft marine clay under the pilot embankment is limited to the settlement data provided by the settlement plates and the magnetic settlement gauges. Figure 9 shows the evolution of the elevation of the top of the embankment with time and the evolution of the total settlements in the center of area 1 measured through settlement plate PR3, in the center of area 2 measured through settlement plate PR8 and close to the center in area 3 measured through settlement magnet AR-5a of gauge MR5 for lack of readings of damaged settlement plate PR13.

The last points of the settlement curves above correspond to the values measured in october 5th of 2009 for settlements plates PR3 and PR8 and in october 2nd of 2009 for MR5, that is about 730 days (*i.e.* 2 years) after the beginning of construction. The values of the settlements and settlement rates measured in early october 2009 are shown in Table 4.

Figure 10 shows the evolution of the elevation of the top of the embankment with time and the evolution of the compression of layers 1, 2, 3, 4 and 5 altogether in the three areas. Figure 11 shows the evolution of the elevation of the top of the embankment with time and the evolution of layer 6 compression in the three areas. Figure 12 shows the evolution of the elevation of the top of the embankment with time and the evolution of the compression of layers 7 and 8 altogether in the three areas.

Table 5 shows the values of measured layers compressions and compression rates and of calculated strains and strain rates in october 2009.

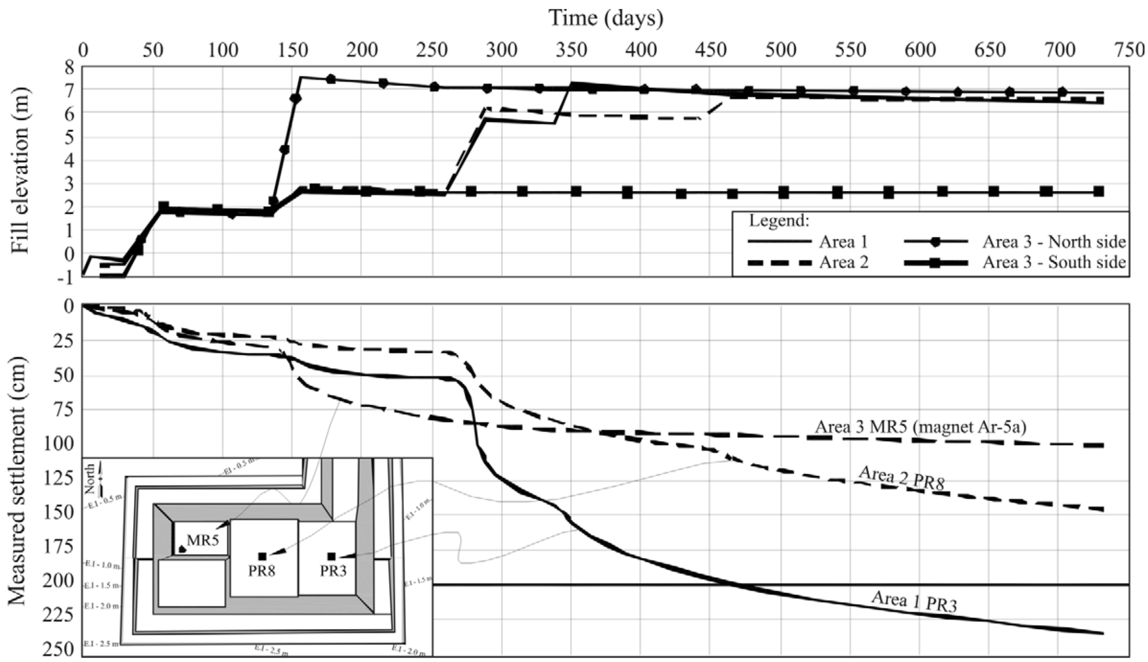

Figure 9 - Measured total settlements in the foundation.

Table 4 - Foundation settlements and settlement rates in early october 2009.

Area	Settlement	Strain	Settlement rate	Strain rate
1	236 cm	Not applicable	3.2 cm per month	Not applicable
2	146 cm	Not applicable	2.9 cm per month	Not applicable
3	101 cm	Not applicable	0.8 cm per month	Not applicable

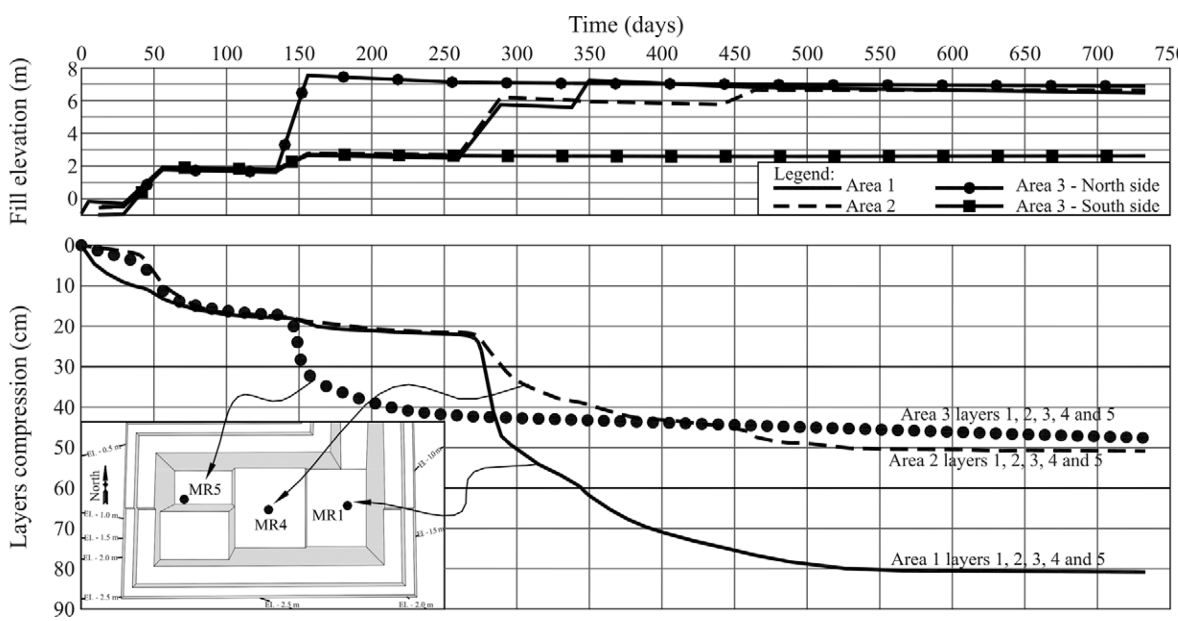

Figure 10 - Measured compression of layers 1, 2, 3, 4 and 5 altogether.

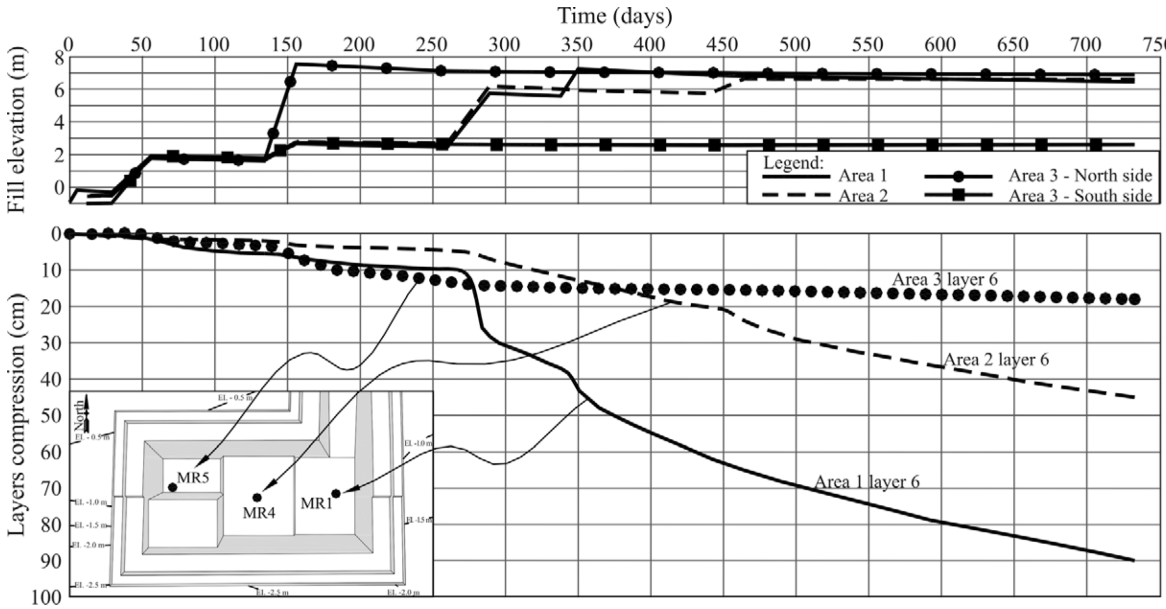

Figure 11 - Measured compression of layer 6.

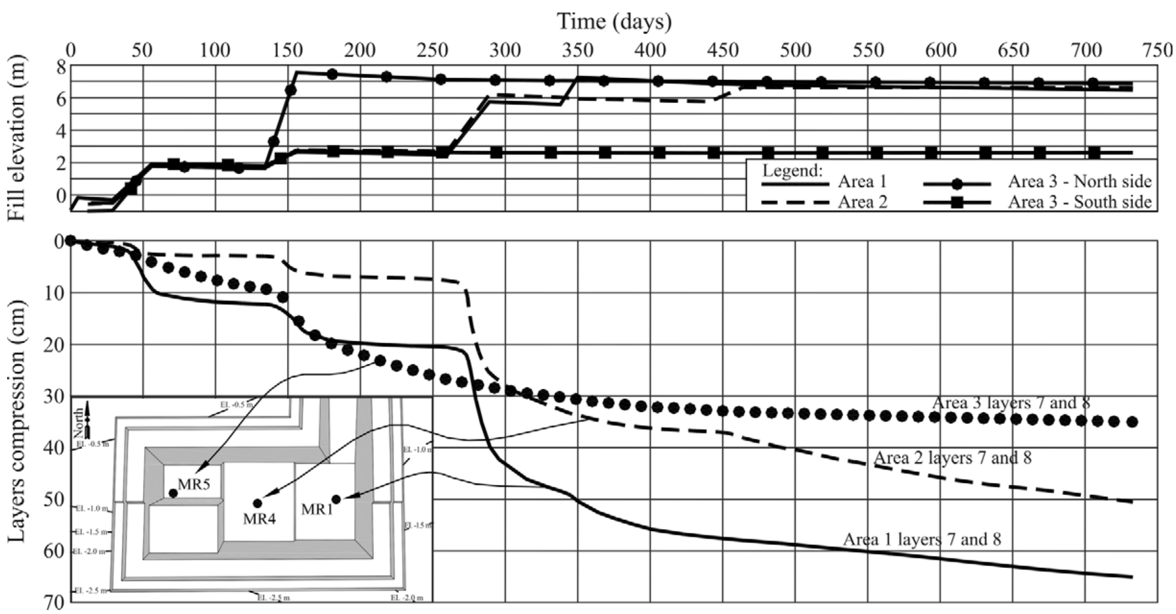

Figure 12 - Measured compression of layers 7 and 8 altogether.

7. Primary Compression and Secondary Compression

In order to analyze the settlement data presented in Figs. 9 to 12, the vertical stress increase and the final vertical effective stress (compared to the preconsolidation stress) have to be known. Figure 13 shows the profiles of final vertical stress increases calculated under the centers of areas 1, 2 and 3. The stress increase calculations were done considering the Holl (1940) formulas, apud Poulos & Davis (1974), to compute $\Delta\sigma$ at depth z under the corner of loaded rectangles. As can be seen, the stress increases are different under each area.

Figure 13 also shows the final effective vertical stresses under the centers of the three areas compared to the profiles of preconsolidation stresses. The term "final" used to characterize both vertical stresses and vertical stress increases means the values calculated for the final situation reached after full completion and stabilization of both primary and secondary consolidation settlements, taking into consideration the effect of the progressive partial submersion on the final stresses as the embankment settles. In order to obtain these "final" values, calculations had to be

Table 5 - Values of measured layers compressions and compression rates and of calculated strains and strain rates in early october 2009.

Layers	Compression (cm)			Compression rate (cm/month)		
	Area 1	Area 2	Area 3	Area 1	Area 2	Area 3
1, 2, 3, 4, 5(*)	80.8	50.9	47.6	0.1	0.1	0.3
6	90.0	45.0	18.0	2.5	1.7	0.3
7, 8(**)	65.1	50.5	35.0	0.6	1.1	0.2
Layers	**Strain (%)**			**Strain rate (s^{-1})**		
	Area 1	Area 2	Area 3	Area 1	Area 2	Area 3
1, 2, 3, 4, 5(*)	10.8	6.0	6.1	5.8×10^{-11}	4.8×10^{-11}	1.6×10^{-10}
6	8.2	4.7	1.9	9.5×10^{-10}	7.2×10^{-10}	1.2×10^{-10}
7, 8(**)	3.5	2.5	1.7	1.3×10^{-10}	2.1×10^{-10}	3.8×10^{-11}

(*) Most of the compression still in process is believed to occur predominantly in layer 1.
(**) Most of the compression still in process is believed to occur predominantly in layer 8.

done by successive iterations converging step by step to the final values.

In area 1, the final effective vertical stresses are clearly higher than the preconsolidation stresses σ'_p in layers 1, 3, 4 and 5, a little higher than σ'_p in layers 6 and 7 and much smaller than σ'_p in layer 8. In area 2, the final effective vertical stresses are clearly higher than σ'_p in layers 1, 3, 4 and 5, about equal to σ'_p in layers 6 and 7 and much smaller than σ'_p in layer 8. In the center of area 3, the final effective vertical stresses are higher than σ'_p in layers 1, 3, 4 and 5, smaller than σ'_p in layers 6 and 7 and much smaller than σ'_p in layer 8.

Figure 14 illustrates the way primary compression and secondary compression were computed. The case in which the final effective vertical stress is lower than the preconsolidation stress is shown at the top of the figure and the case in which the final effective vertical stress is higher than the preconsolidation stress is shown at the bottom.

The following terminology is used in Fig. 14: e_i = initial void ratio; σ'_{vi} = initial vertical effective stress; $\Delta\sigma_v$ = vertical stress increase; σ'_{vf} = final vertical effective stress; σ'_p = preconsolidation stress; e_p = final void ratio at the end of primary consolidation (without secondary); e_s = final ratio at the end of primary and secondary consolidation; Δe_p = variation of void ratio corresponding to primary compression and Δe_s = variation of void ratio corresponding to secondary compression.

Primary compression was computed through the common well known formulas using C_r and C_c in the recompression and virgin compression ranges respectively, and secondary compression was computed through the following formulas.

$$\Delta H_s = 0 \text{ when } \sigma'_{vf} \le \frac{\sigma'_p}{2.1} \quad (1)$$

$$\Delta H_s = H\frac{C_c}{1+e_0}\left(1-\frac{c_e}{c_c}\right)\log\left(2.1\frac{\sigma'_{vf}}{\sigma'_p}\right) \text{ when } \frac{\sigma'_p}{2.1} \le \sigma'_{vf} \le \sigma'_p \quad (2)$$

and

$$\Delta H_s = H\frac{C_c}{1+e_0}\left(1-\frac{c_e}{c_c}\right)\log(2.1) \text{ when } \sigma'_{vf} \ge \sigma'_p \quad (3)$$

For settlements evaluation purposes each layer was divided in 1 m thick sublayers.

The preconsolidation stresses and calculated final effective vertical stresses at mid-height of each whole layer, primary compressions and secondary compressions of layers 1 to 8 are shown in Tables 6, 7 and 8.

All the above compressions were computed considering all the soil mass between the drains in areas 1 and 2 to be perfectly undisturbed. It is the authors understanding that the existence of any remoulded zone around the drains would lead to higher settlements as clearly illustrated by Fig. 4. The discussion of this subject is beyond the scope of the present work.

As shown in Table 6, in area 1 the total compression of layer 6 equal to 2.20 m amounts to 52% of the total settlement equal to 4.20 m. As shown in Table 7, in area 2 the total compression of layer 6 equal to 1.78 m amounts to 46% of the total settlement equal to 3.89 m and as shown in Table 8, in area 3 the total compression of layer 6 equal to 1.38 m amounts to 48% of the total settlement equal to 2.89 m. Layer 1 comes second to layer 6 in the ranking of the layers which most contribute to the total settlement with 20%, 24% and 27% of the total settlement in areas 1, 2 and 3, respectively. In layer 1, no "undisturbed sample" could be retrieved in the very soft mud which constitutes this layer, as can be seen in Fig. 5, which means that no data about compressibility and consolidation properties could be obtained in the laboratory concerning layer 1. On the other hand, 7 "undisturbed samples" were retrieved in

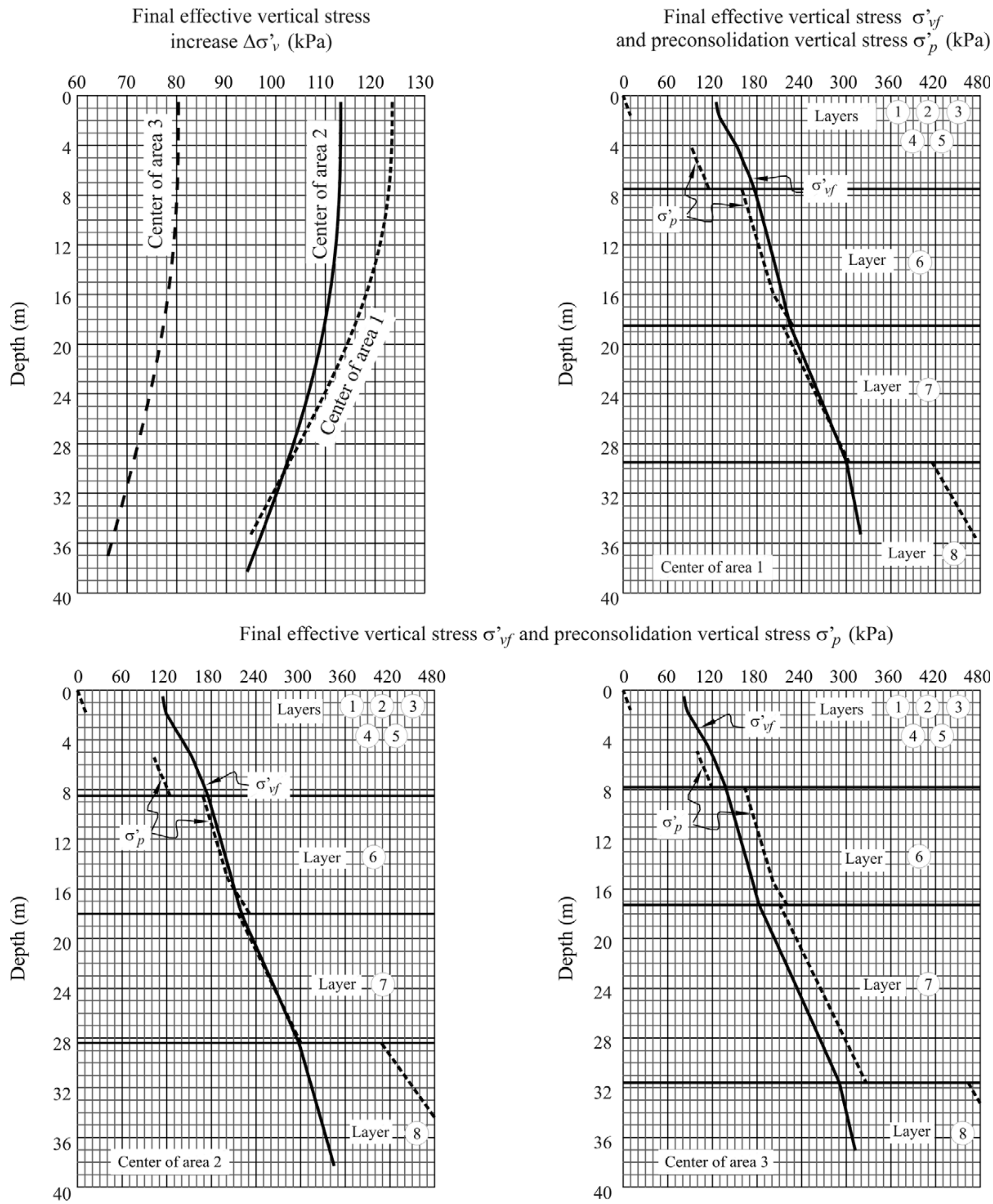

Figure 13 - Vertical stress increases and final effective vertical stresses under the centers of areas 1, 2 and 3.

layer 6 under area 3 and tested at COPPE which provided very good data for this layer. For these two reasons, the back-analysis presented in this paper is relative only to layer 6.

8. Drainage Conditions of Subsoil Layers

From the knowledge of the soil profiles and of the soil properties, the authors consider that the drainage conditions of the subsoil layers in areas 1, 2 and 3 are the ones described in Table 9.

9. Working Hypothesis

For the last 30 years or so, the main trend of thought of the most prolific brazilian researchers in the study of the behaviour of marine Santos soft clay has sustained that secondary consolidation only starts to take place at the end of

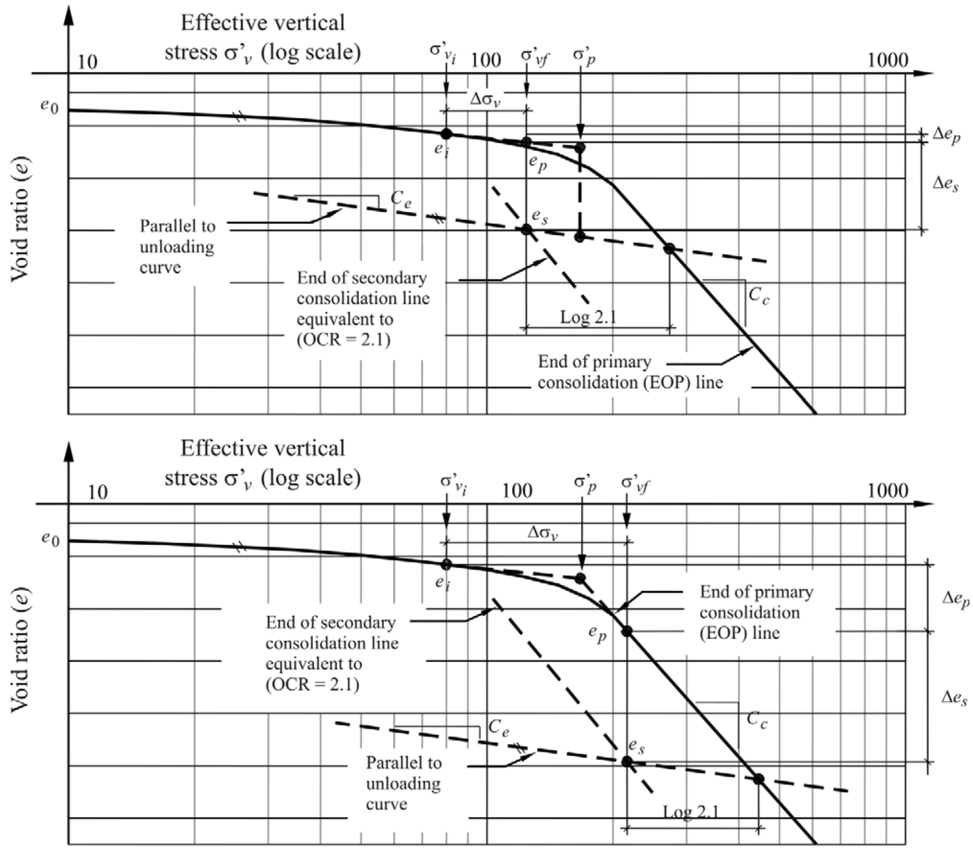

Figure 14 - Primary compression and secondary compression.

Table 6 - Preconsolidation stresses and calculated final effective vertical stresses at mid height of each layer and primary compressions and secondary compressions in area 1.

	Layer 1	Layer 2	Layer 3	Layer 4	Layer 5	Layer 6	Layer 7	Layer 8	Total
σ'_{vf}	125.9	141.3	157.4	165.4	173.4	201.6	263.1	310.5	
σ'_{p}	5.0		95.7	103.8	112.1	187.1	259.2	446.7	
ΔH_p	0.67			0.22 (*)		0.43	0.23	0.06	1.61
ΔH_s	0.16			0.15 (*)		1.77	0.00	0.51	2.59
ΔH_t	0.83			0.37 (*)		2.20	0.23	0.57	4.20
$\Delta H_m/\Delta H_t$	65%			71% (*)		41%	82% (**)	82% (**)	56%

Table 7 - Preconsolidation stresses and calculated final effective vertical stresses at mid height of each layer and primary compressions and secondary compressions in area 2.

	Layer 1	Layer 2	Layer 3	Layer 4	Layer 5	Layer 6	Layer 7	Layer 8	Total
σ'_{vf}	115.8	136.5	157.6	165.0	172.3	198.3	259.5	322.4	
σ'_{p}	5.7		106.3	113.4	121.2	192.5	258.4	470.8	
ΔH_p	0.76			0.17 (*)		0.26	0.21	0.06	1.46
ΔH_s	0.18			0.15 (*)		1.53	0.00	0.58	2.43
ΔH_t	0.94			0.32 (*)		1.79	0.21	0.64	3.89
$\Delta H_m/\Delta H_t$	31%			66% (*)		25%	60% (**)	60% (**)	38%

Table 8 - Preconsolidation stresses and calculated final effective vertical stresses at mid height of each layer and primary compressions and secondary compressions in area 3.

	Layer 1	Layer 2	Layer 3	Layer 4	Layer 5	Layer 6	Layer 7	Layer 8	Total
σ'_{vf}	82.8	101.7	121.3	127.9	134.5	160.6	237.4	301.6	
σ'_p	5.0		102.7	109.3	116.0	187.3	268.8	492.2	
ΔH_p	0.61			0.10 (*)		0.18	0.15	0.04	1.08
ΔH_s	0.16			0.15 (*)		1.20	0.00	0.30	1.81
ΔH_t	0.77			0.25 (*)		1.38	0.15	0.34	2.89
$\Delta H_m/\Delta H_t$	36%			77% (*)		13%	72% (**)	72% (**)	35%

(*) layers 3, 4 and 5 altogether.
(**) layers 7 and 8 altogether.
where: σ'_{vf} = final vertical effective stress at mid-height of whole layer (kPa), σ'_p = preconsolidation stress at mid-height of whole layer (kPa), ΔH_p = layer primary compression (m), ΔH_s = layer secondary compression (m), ΔH_t = layer total compression (m), ΔH_m = measured layer compression (m) in october 2009.

Table 9 - Drainage conditions of subsoil layers.

Layer(s)	Soil type	SPT	Areas 1 and 2 (Drains down to El. – 28.20 m)	Area 3 (No drain)
1	Silty clay	0	Double vertical + radial	Double vertical
2	Silty fine sand	2 to 8	Radial	Horizontal
3, 4, 5	Silty clayey sand to slightly clayey silty sand	0 to 2	Upwards vertical + radial	Upwards vertical
6	slightly sandy silty clay	1 to 4	Radial	Restricted double vertical
7	slightly silty clayey sand	2 to 5	Horizontal	Horizontal
8	Silty clay	3 to 10	Upwards vertical	Upwards vertical

primary consolidation. This working hypothesis has justified the fact that all settlements measured during the usual period of test embankments monitoring, i.e around a year more or less in most cases, have been considered by them to be entirely primary settlements. This was so since it was judged that primary consolidation had not yet reached its end and, consequently, secondary consolidation had not yet started to occur. The measured settlement curves, mainly the settlement plates curves, were then analyzed using Asaoka's method (Asaoka 1978).

Based on their consideration that for $\overline{U} \geq 33\%$ the series solution of Terzaghi's theory could be replaced by its first term which is:

$$\overline{U} = 1 - 0.811 e^{\frac{-\pi^2}{4}T} \tag{4}$$

it was then considered justifiable to use Asaoka's construction to obtain the total primary settlement and the consolidation coefficient, assuming that a few months after end of construction the average consolidation ratio under field test embankments could be considered to be higher than 33%.

In the case of radial drainage considering equal strain theory, the average consolidation ratio is given by an expression presented by Barron (1948) similar to the one above mentioned, but valid for any value of the consolidation ratio, so that Asaoka's construction could also be applied. In both cases, the consolidation coefficient and total primary settlement thus obtained have been considered sound and trustworthy.

This approach has led to the endlessly repeated conclusion that the back-analyzed field values of the consolidation coefficient are usually about 50 times higher than the laboratory consolidation coefficient and that this fact is totally explained and justified by the existence of providential very thin, obviously continuous, layers of pervious sand. It is worth mentioning that no lense of pervious sand was present in any of the the layer 6 samples.

The authors consider, first, that this explanation is too far-fetched to be acceptable at once and, second, that some basic points could not, and should not, have been overviewed for so many years, as has been the case, by the researchers in the process of reaching the above mentioned published conclusions and, then, of revalidating and republishing them year after year for so long. Some of these points are clearly pointed out by Gonçalves (1992).

The first point which has been systematically overviewed is the fact that the consolidation coefficient values are very different in the range of stresses up to the preconsolidation stress and in the range of stresses beyond the preconsolidation stress. This was very clearly illustrated in Fig. 4 and Bjerrum (1972), just as an example, can be quoted in this respect "The rate of pore pressure dissipation can in principle, be computed on a similar basis as the consolidation settlement, *i.e.* taking into account that the consolidation properties are different in the two ranges, the first one representing the increase in effective stresses in the range from p_0 to p_c and the second one representing the increase in effective stress beyond p_c". This point was clearly brought up by Gonçalves (1992) "It is well known that the c_v value of a preconsolidated soil can be 10 to 100 times higher than the c_v value of a normally consolidated soil. Some papers which compare the behaviours of the soils from Santos lowlands in the field and in the laboratory do not state how the c_v value was obtained and others admit to have used the c_v value corresponding to stresses $\sigma'_v > \sigma'_p$. If in these analysis the c_v value for the preconsolidated range had been used, the differences between field and laboratory behaviours would probably have been smaller".

The second point which has also been systematically overviewed is the fact that much evidence has been brought up in the last decades in the technical literature showing that secondary consolidation under embankments in the field occurs simultaneously with primary consolidation. The argument repeatedly used by the researchers to justify the working hypothesis of secondary consolidation only starting to occur after the end of primary consolidation is based on the fact that since long term settlements measured in the area of Santos vary rather linearly with the logarithm of time, then the formulation "$\Delta e = C\alpha \log \Delta t$" holds true and since $C\alpha$ is historically considered to express the evolution of secondary settlements after primary settlements have ended then the straight line obtained by plotting settlements *vs.* log of time has been taken as being the proof that the working hypothesis is true. Since to the authors it is clear that long field term settlements will vary, for a long period before coming close to stabilization, rather linearly with the logarithm of time, whether they are only primary, or only secondary or the sum of both, the above argument put forward by the researchers is no more than a sophism.

Figure 15 illustrates the traditional working hypothesis which is that the secondary consolidation starts after primary consolidation ends and the alternative working hypothesis which considers that the secondary consolidation and the primary consolidation occur simultaneously.

As clearly indicated on the left side of Fig. 15, with the tradional hypothesis until the end of the primary consolidation, the evolution of strain with time, up to ε_p, is expressed by Terzaghi's consolidation theory which is very familiar to all soils engineers. After the end of the primary consolidation takes place, then the evolution of vertical strain with time is expressed by the traditional formula $\Delta\varepsilon_v = C_{\alpha\varepsilon}\, \Delta \log(t)$ which is also very familiar to all soils engineers.

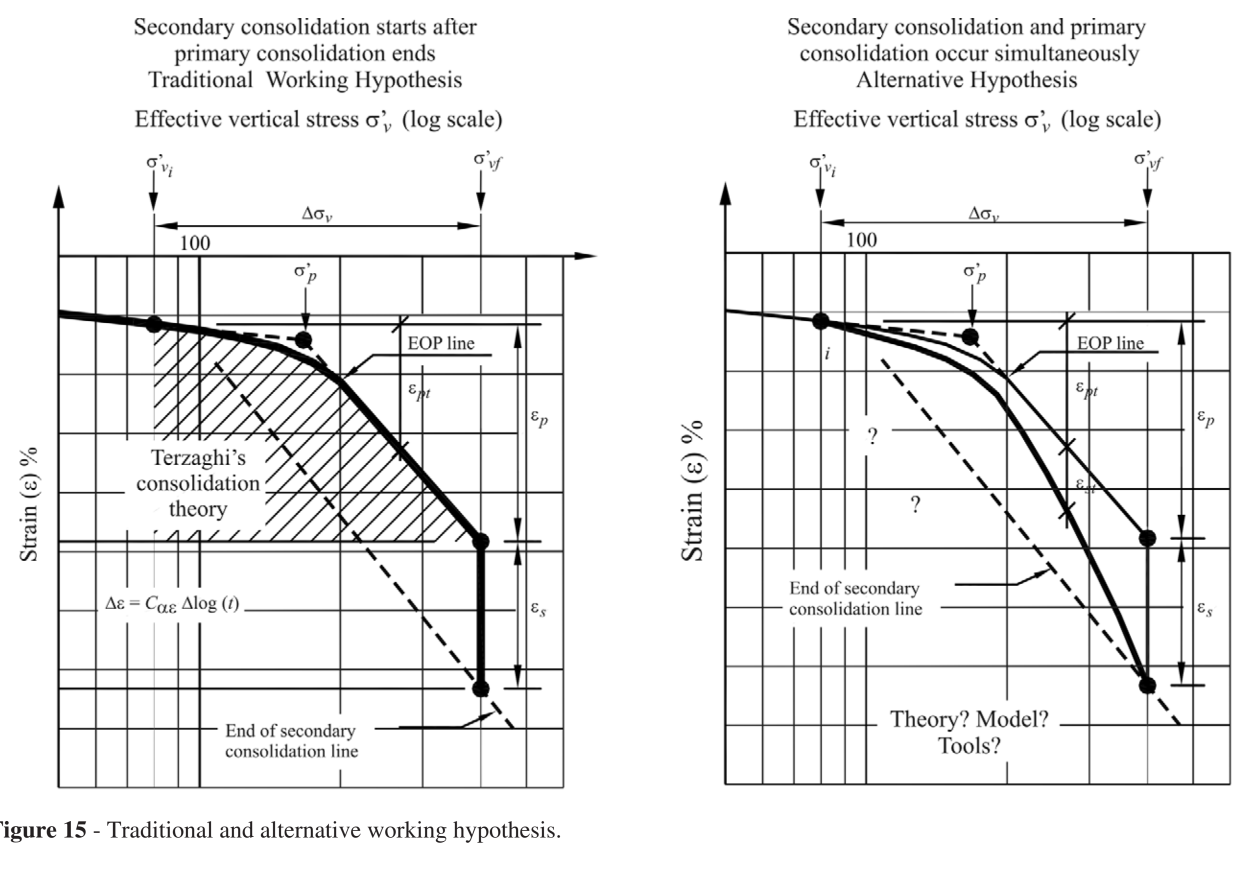

Figure 15 - Traditional and alternative working hypothesis.

The right side of Fig. 15 illustrates the alternative hypothesis which shows that with the primary and secondary consolidations occurring simultaneously, at any time, *t*, the strain is in part due to primary consolidation (ε_{pt}) and in part due to secondary consolidation (ε_{st}). In this case no "of the shelf" functional tool is readily available to calculate the evolution of strain with time, and even if such a tool existed it surely would not be familiar to almost all engineers. In spite of this main drawback of the alternative hypothesis the authors considered, based on the comments presented before, that the only acceptable working hypothesis is the one which considers that primary and secondary consolidations occur simultaneously and decided that this is the one which had to be adopted for their backanalysis, meaning, of course, that the first step to be taken would be to look for and to tailor, if necessary, the tools needed for this task.

10. Working Tool Number 1 to Analyze the Behaviour of the Thick SFL Clay Layer Under Area 3 with Vertical Drainage

A schematic path during field preloading was proposed by Bjerrum (1972) and a schematic path during a controlled gradient oedometer test and during a multiple-stage loading oedometer test were proposed by Leroueil *et al.* (1985). Both propositions are reproduced from the original papers in Fig. 16.

On the left side of Fig. 16, the authors added the values of the "Rate of secondary consolidation", ($\dot{\varepsilon}$) expressed in s^{-1}, calculated from the values per year indicated in Bjerrum's figure. The right side of Fig. 16 shows the figure of the paper by Leroueil *et al.* (1985) corresponding to the multiple stage loading test.

Leroueil *et al.* (1985) stated: "Taylor & Merchant (1940) were the first to suggest a model in which the rate of change in void ratio is a function of the effective stress, the void ratio and the rate of change in effective stress. This suggestion has been followed by numerous researchers. The rheological models proposed were seldom assessed experimentally or only on the basis of a few laboratory test results. Experimental studies, however, have been performed on natural clays and on resedimented clays but in each study only one type of test was used. It is thus difficult to obtain an overall view of the rheological behaviour of clays from these studies. As a result this abundant literature has modified neither the common practice based on the Terzaghi theory nor the way of thinking on clay behaviour". In the authors' knowledge not much has changed from 1985 to 2010, and for sure, practicing engineers continue not disposing of any practical tool to predict or to back-analyze the simultaneous evolution of primary and secondary settlements in soft clayey soils under embankments.

Based on the diagrams shown in Fig. 16 the authors went on to produce their first working tool consisting of an abacus, similar to Bjerrum's but specifically built for the soft clay of layer 6 tested at COPPE, from the laboratory test results. It was expected that this abacus would immediately yield the mean effective stress and mean primary con-

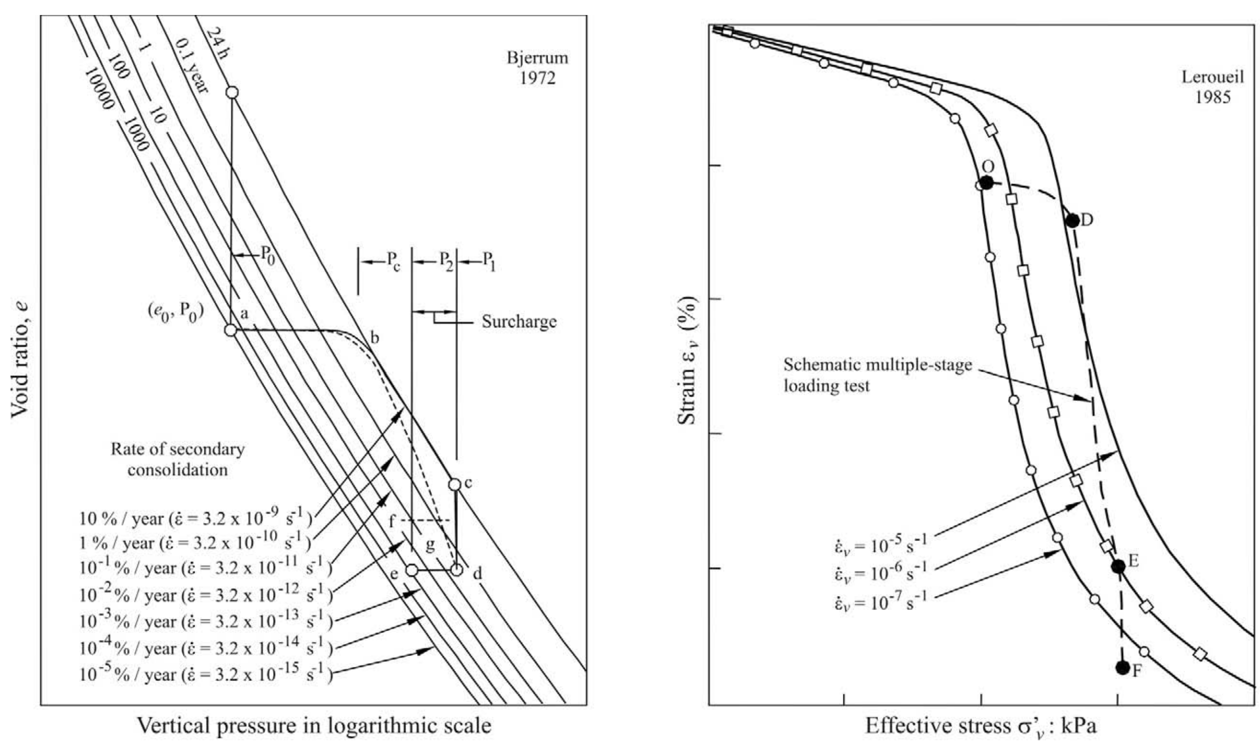

Figure 16 - Schematic path proposed by Bjerrum (1972) and Leroueil *et al.* (1985).

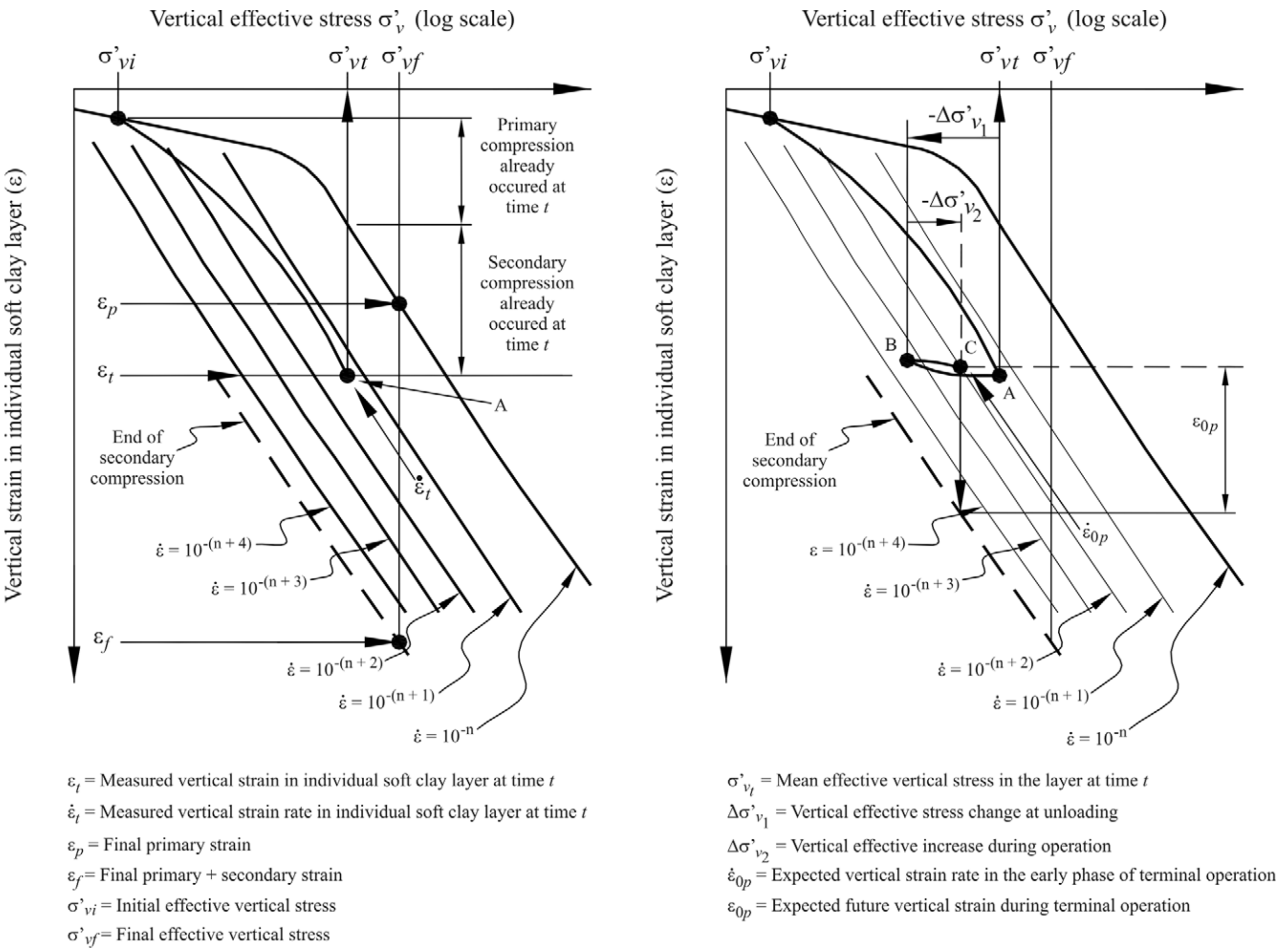

Figure 17 - Methodology expected to be used to analyze layer 6 compression under the pilot embankment.

solidation ratio of layer 6 from the known values of the strain (ε_t) and the strain rate ($\dot{\varepsilon}$) at time t. These two values which can be instantly calculated at any time t from the layer compression measurements under the pilot embankment would be plotted together on the abacus as illustrated on the left side of Fig. 17 with the strain at time t (ε_t) entered in ordinate as a horizontal line extended to the right until it meets the strain rate line representing the value of the strain rate ($\dot{\varepsilon}_t$) occurring in the layer at time t, at point A.

From point A, the value of σ'_{vt} = mean effective stress in the layer at time t would be directly read in the abacus giving the mean primary consolidation ratio (U_t) at time t calculated as

$$U_t = (\sigma'_{vt} - \sigma'_{vi}) / (\sigma'_{vf} - \sigma'_{vi}) \quad (5)$$

It was also expected that the abacus would provide the following informations concerning the future situation during the terminal operation phase that is, after removing the fill surcharge or after stopping applying vacuum in the drains, this resulting in a vertical unloading effective vertical stress change equal to $-\Delta\sigma'_{v1}$, and after terminal operation reaches its normal operation capacity with the application of an effective vertical stress increase $\Delta\sigma'_{v2}$, as illustrated respectively by point B and by point C on the right side of Fig. 17:

$\dot{\varepsilon}_{0p}$ = the expected vertical strain rate in the early phase of terminal operation and

ε_{0p} = the expected vertical strain left to occur during the terminal life.

From these two values, not only of layer 6, but also of all other layers, then the expected rate of settlement of the terminal pavement, in cm per month, at the beginning of normal operation and the total remaining settlement to occur and consequent expected frequency of maintenance operations and total volume of fill to be used to keep levelling the pavement to its nominal elevation during the life of the terminal could be quantified.

The special oedometer tests mentioned in item 5 were programmed to provide the necessary information to produce this type of abacus representative of the behaviour of layer 6. Figure 18 shows on the left side the results of all special oedometer tests which provided strain rates determination during secondary consolidation plotted as log of strain rate (log $\dot{\varepsilon}$ in s^{-1}) *vs.* overconsolidation ratio (OCR). The curve of the left side of Fig. 18 was used, together with the compressibility curve of sample SRA-203(4) to produce the abacus on the right side.

As shown in Table 5, in area 3, in October 2009, the measured strain in layer 6 was 1.9% and the strain rate was 1.2 x 10^{-10} s^{-1}. As can be seen on the right side of Fig. 18, the strain rate value plots very close to the line which represents the end of secondary compression on the abacus, obviously a nonsense since the consolidation ratio of layer 6 under area 3 is, without any doubt, very low as shown by its small measured compression equal to 18 cm when compared to the 90 cm of measured compression at the same time under area 1 as reported in Table 5.

This indicates that the abacus of Fig. 18 is only representative of the behaviour of a 2 cm thick sample of layer 6 soft clay and that for any given clay, there exists a different specific abacus which represents the behaviour of the clay, for each layer thickness.

The question which then arose is "can the abacus for layer 6 be obtained through some realistic model from the laboratory sample abacus of Fig. 18?"

11. Working Tool Number 2 to Analyze the Behaviour of the Thick SFL Clay Layer Under Area 3 with Vertical Drainage

Following this ill success with working tool number 1, the authors then decided to go for an abacus of the same type, but built specifically for the field conditions through extrapolating the abacus shown on the right side of Fig. 18 from the laboratory conditions to the field conditions by way of Taylor and Merchant's formulation as shown below.

As mentioned by Leroueil *et al.* (1985), many formulations have been put forward to try and model secondary consolidation occurring together with primary consolidation and Taylor and Merchant's theory (theory A) was the first one published in the technical literature stating a basic postulate to express the evolution of the soil void ratio with time during secondary consolidation. This postulate is illustrated at the top of Fig. 19 and its basic formulation is:

$$\frac{\partial e}{\partial t} = -\mu(\overline{cd}) \qquad (6)$$

which states "that the speed of occurrence of secondary compression is proportional to the undeveloped secondary compression" where μ is called the "coefficient of secondary compression". The mathematical solution to compute the "aggregate consolidation ratio" based on the above postulate was given by Taylor & Merchant (1940) in their paper and it shows that the evolution of this ratio depends on the two following parameters:

• *r* which is the ratio of the primary settlement over the total settlement, showing that Taylor and Merchant had a clear understanding that secondary compression was finite and could be estimated and

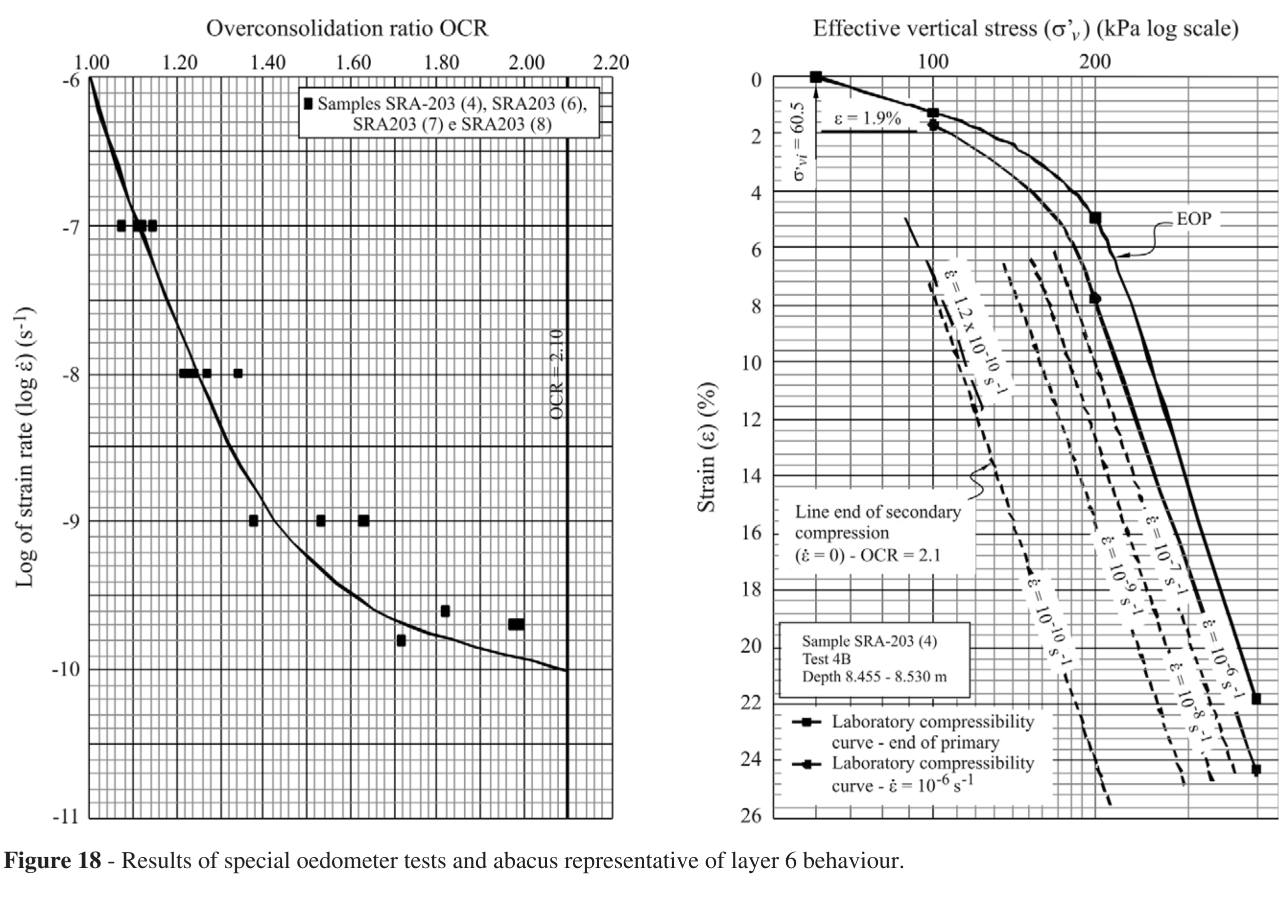

Figure 18 - Results of special oedometer tests and abacus representative of layer 6 behaviour.

- $F = \dfrac{\mu t}{rT} = \dfrac{\mu H_d^2}{rc_v}$ (7)

a dimensionless term called the "secondary compression factor".

The original paper includes a graph showing the aggregate consolidation ratio where it can be appreciated that this is the ratio of the settlement (or compression or strain) at time t over the total (primary plus secondary) settlement (or compression or strain) plotted as a function of the time factor T for the case of unidimensional vertical compression with only vertical drainage for an r value of 0.70 and for various values of the F factor which are reproduced as non dotted curves at the bottom of Fig. 19. The aggregate consolidation ratio will be referred to as U_{p+s}. In Taylor and Merchant's own words, this formulation is "based largely on physical intuition" and "the main value of this theory is not in the expression of a secondary compression time law, but in the rational explanation of the superimposed action of the two very different physical laws of time rate, allowing the prediction of the action in thick strata from the action in laboratory tests". This "prediction of the action in thick strata from the action in laboratory tests" is the way to extrapolate the abacus shown on the right side of Fig. 18 from the laboratory conditions to the field conditions by way of Taylor and Merchant's formulation as shown below which the authors decided to use to build their working tool number 2. Of course, the field abacus would be used in the same way as working tool number 1, that is determining the mean effective stress and mean primary consolidation ratio of layer 6 from the known values of strain and strain rate at time t.

It has been shown by Christie (1964) that the formulas published in Taylor and Merchant's paper are mistaken, but that their curves which are reproduced at the bottom of Fig. 19 are in accordance with the correct formulas reestablished by Christie (1964) in terms of excess pore pressure. Furthermore, Christie (1964) showed that Gibson & Lo's (1961) formulation is identical to Taylor and Merchant's although expressed in different terms. The mathematical formulation for Taylor and Merchant's theory has also been obtained by Carvalho (1997) in terms of void ratio. Carvalho's formulas were used by the authors to compute the aggregate consolidation ratio for $r = 0.70$ and F values of 0, 0.1 and 10 obtaining perfect agreement with Taylor and Merchant's curves as seen on Fig. 19. All further calculations performed using Taylor and Merchant's theory included ahead in this paper were done using Carvalho's formulas.

A number of long term oedometer tests has been performed in the laboratory of the Rheology Group of the Soil Mechanics Division at COPPE, Rio de Janeiro as shown in Figs. 20, 21 and 22.

Figures 20, 21 and 22 show the measured laboratory curves and the theoretical curves obtained from Taylor and

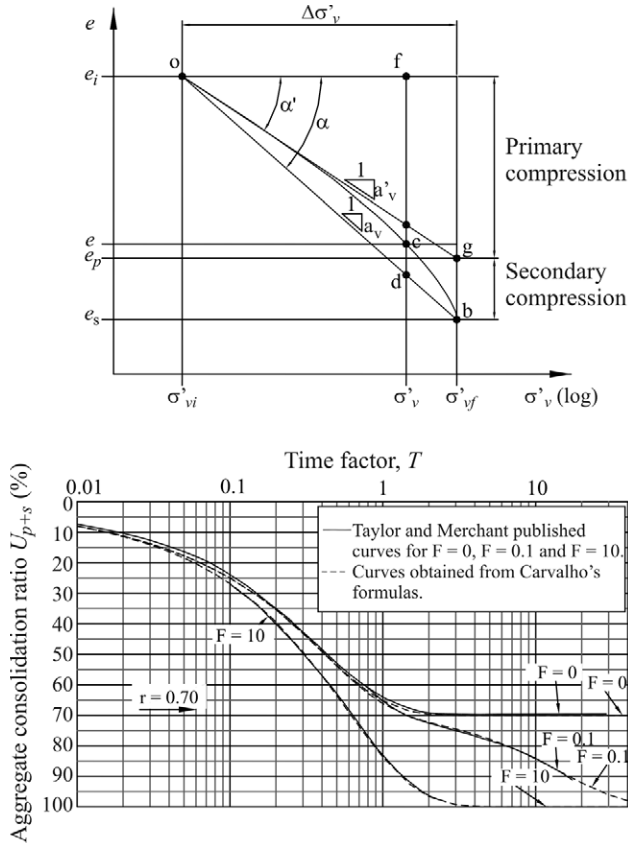

Figure 19 - Taylor and Merchant's theory (Theory A) basic postulate and aggregate consolidation curves.

Merchant's theory which best fit the experimental curves for two soft clay samples of the Rio de Janeiro area, Senac clay (Martins 2005) and Sarapuí clay (Vieira 1988) and for a specimen trimmed from a sample prepared through a mixture of kaolin (90%) and bentonite (10%) (Martins 2005), respectively. Line AB shows for each test the line from which the value of the coefficient of secondary consolidation $C\alpha$ would be normally determined from the oedometer test result. As can be seen this line only fits the test results up to $t = 10^5$ min, that is about 70 days, after that a much higher value of $C\alpha$ would be required to fit the test results.

The best fit is obtained by varying the three parameters: r, c_v and μ and each diagram on Figs. 20, 21 and 22 shows the values which provided the best fit in each case. The values, which are only valid for the given range of stresses applied on the tested samples and not for the clay deposit as a whole, are compared in Table 10.

The longest of the 3 tests is the one on the Senac clay, illustrated in Fig. 21, which lasted for 5 years and it can be seen that for the last 19 months, that is after 3.4 years up to 5 years, the compression was totally stabilized, confirming that the secondary compression is finite and that it completely stabilizes within a given time. As can be seen on all three diagrams, the Taylor and Merchant's theory agrees rather well with the experimental curves at the beginning

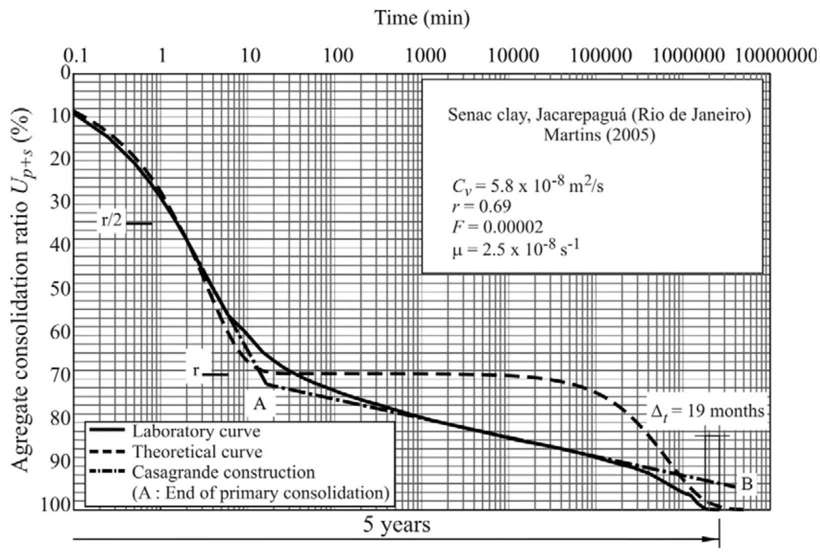

Figure 20 - Comparison of long term oedometer test in Senac clay with Taylor and Merchant's theory.

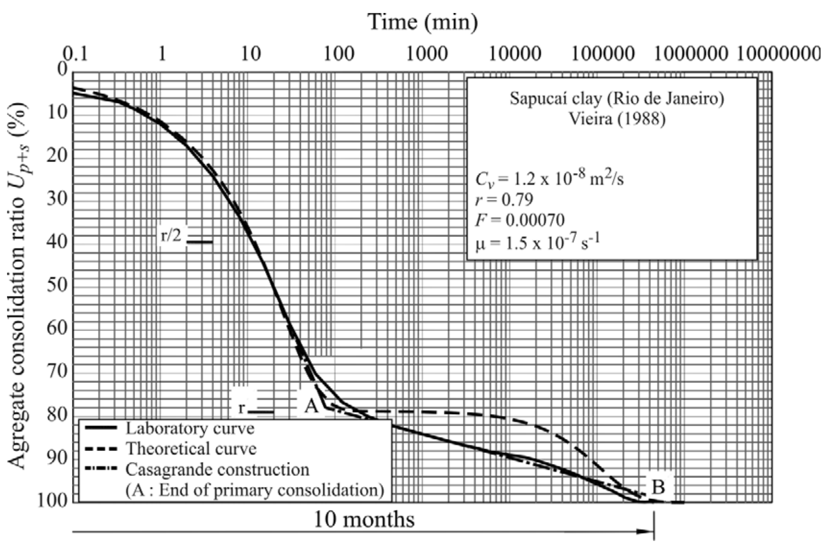

Figure 21 - Comparison of long term oedometer test in Sarapui clay with Taylor and Merchant's theory.

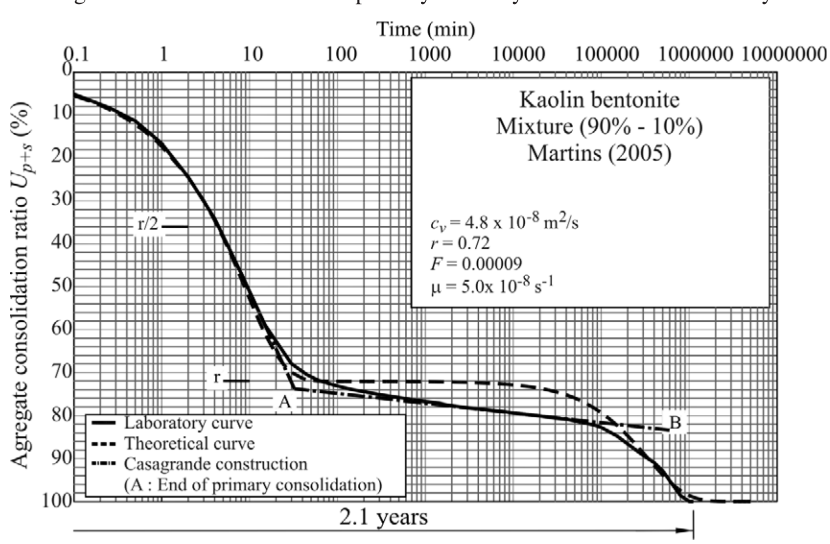

Figure 22 - Comparison of long term oedometer test in a kaolin-bentonite mixture with Taylor and Merchant's theory.

Table 10 - Values of r, c_v and μ for Senac clay, Sarapuí clay and kaolin-bentonite mixture.

	Senac clay	Sarapuí clay	Kaolin + bentonite
r	0.69	0.79	0.72
c_v (10^{-8} m^2/s)	5.8	1.2	4.8
μ (10^{-7} s^{-1})	0.25	1.5	0.5

and at the end of the consolidation process but fails to provide good agreement in between, where it can be seen that the measured secondary compression is consistently higher than the theoretically predicted one, which means, in other words, that the secondary consolidation on 2 cm thick samples proceeds faster than modeled by Taylor and Merchant's theory mainly in the middle of the process.

Figure 23 shows Taylor and Merchant's aggregate consolidation ratio U_{p+s} *vs.* time factor T for samples or clay layers, double drained (H_d = drainage distance = half the thickness) with thicknesses of 20 mm (lab sample), 40 mm, 80 mm, 200 mm, 1 m, 4 m and 20 m for a clay with $c_v = 1.0 \times 10^{-8}$ m^2/s, $\mu = 1.5 \times 10^{-7}$ s^{-1} and with $r = 0.30$.

Figure 24 shows Taylor and Merchant's aggregate consolidation ratio U_{p+s} *vs.* time t for samples or clay layers, double drained (H_d = drainage distance = half the thickness) with thicknesses of 20 mm (lab sample), 40 mm, 80 mm, 200 mm, 1 m, 4 m and 20 m for a clay with $c_v = 1 \times 10^{-8}$ m^2/s, $\mu = 1.5 \times 10^{-7}$ s^{-1} and with $r = 0.30$.

Line AB drawn on Fig. 24 for H_d = 10 mm, that is for the standard oedometer test, is the line from which the value of the coefficient of secondary consolidation $C\alpha$ would normally be determined from the laboratory consolidation curve plotted in terms of Δe *vs.* log (t). According to Taylor and Merchant's formulation, it can be seen that the inclinations of the lines drawn in Fig. 24 for clay thickesses up to

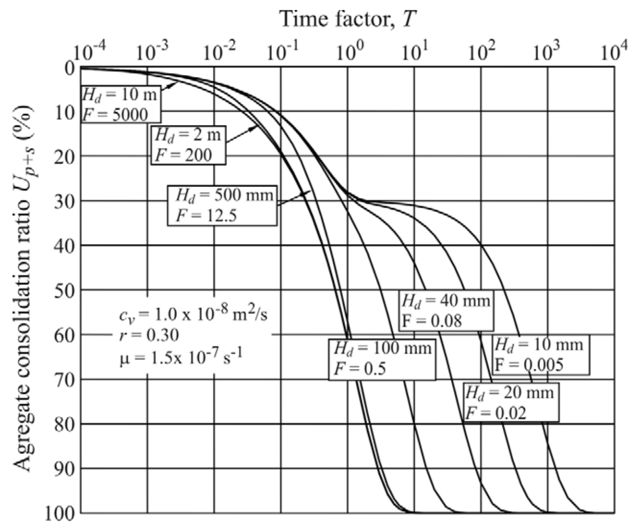

Figure 23 - Taylor and Merchant's curves: Aggregate consolidation ratio U_{p+s} *vs.* time factor T.

200 mm, that is for H_d up to 100 mm, in the range $U_{primary} >$ 90%, that is below the black point marked on each curve, would not be constant through time, as already observed on the actual laboratory tests curves shown in Figs. 20, 21 and 22. It can also be seen that the inclinations of all the curves in the range $U_{primary}$ > 90% are about the same for H_d between 500 mm and 10 m: 1:69 to 1:66, and it is clear that these inclinations are totally different from the laboratory $C\alpha$ line which is 1:1.1.

Table 11 shows the time to reach U_{p+s} equal to 99.9% from Taylor and Merchant's theory in a clay with $\mu = 1.5 \times 10^{-7}$ s^{-1} and $r = 0.3$.

It seems reasonable to expect that for any thickness, Taylor and Merchant's theoretical curves might be rather realistic at the beginning and at the end of the consolidation

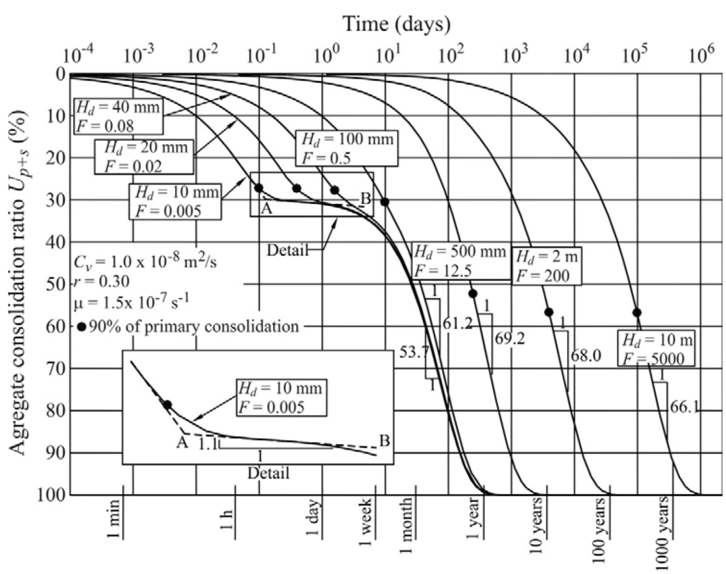

Figure 24 - Taylor and Merchant's curves: Aggregate consolidation ratio U_{p+s} *vs.* time t.

Table 11 - Time to reach U_{p+s} equal to 99.9% from Taylor and Merchant's theory in a clay with $\mu = 1.5 \times 10^{-7}$ s^{-1} and $r = 0.3$.

c_v (m^2/s)	Thickness (H) of double drained layer				
	2 cm	20 cm	2 m	10 m	20 m
4×10^{-7}	500 days 1.37 year	500 days 1.37 year	500 days 1.37 year	4000 days 11.0 years	15 000 days 41.1 years
10^{-8}	500 days 1.37 year	500 days 1.37 year	6000 days 16.4 years	150 000 days 411 years	600 000 days 1644 years

process and might underestimate the settlement (or strain) in the middle of the process as was observed on the 2 cm thick laboratory samples (see Figs. 20, 21 and 22). As a consequence, it might then be admitted that for all predictions based on Taylor and Merchant's theory with reliable soil parameters, with emphasis on a realistic value of c_v corresponding to the range of effective vertical stress (σ'_{vi} to σ'_{vf}) effectively applied, not a simple task when $\sigma'_{vi} < \sigma'_p < \sigma'_{vf}$, the real value of secondary compression will always be equal to or higher than the predicted one mainly in the middle of the process.

With this limitation in mind, the authors proceeded to build the abacus for the field conditions of layer 6 under the center of area 3 using Carvalho's formulas for the specific values of:

- Layer thickness = 9.50 m, vertically double drained with no restriction, although Table 9 indicates that drainage conditions of layer 6 is considered to be "Restricted double vertical",
- $C_c/(1 + e_0) = 0.56$ and $C_r/(1 + e_0) = 0.11 \times C_c/(1 + e_0) = 0.062$,
- $\sigma'_{vi} = 82$ kPa, $\Delta\sigma'_v = 78$ kPa and $\sigma'_{vf} = 160$ kPa,
- $\sigma'_p = 187$ kPa,
- $c_v = 1.5 \times 10^{-8}$ m^2/s and
- $\mu = 1.5 \times 10^{-7}$ s^{-1} (this value is the only one which has not been experimentally determined specifically for the clay of layer 6 since, to the authors' knowledge, the only way to determine the μ value is from long term oedometer tests run till the end of secondary consolidation, that is for at least 10 months as in the case of Sarapui clay shown in Fig. 21 to more than 41 months as in case of Senac clay shown in Fig. 20 through the adjustment of Taylor and Merchant's theoretical curves to the experimental curves. The value of μ which was used is the one of Sarapui clay.

The abacus thus obtained is shown on Fig. 25.

In this abacus, point P corresponds to the initial state of the middle of layer 6 before building the pilot embankment, that is with an initial vertical effective stress equal to 82 kPa and a strain ε' relative to its initial state obviously equal to zero. The preconsolidation stress in the middle of layer 6 is 187 kPa which corresponds to an OCR value a little higher than the value of 2.1 which would be equivalent to the end of secondary consolidation. This means that during consolidation under an applied load, layer 6 primary compression would plot on the primary recompression line PQ for σ'_v smaller than σ'_p. In october 2009, the measured mean strain in layer 6 was 1.9%, represented as ε' and the measured strain rate in layer 6 was $\dot{\varepsilon} = 1.2 \times 10^{-10}$ s^{-1} (as shown in Table 5) which would correspond to point Q in the abacus. As can be seen, point Q would correspond to an applied effective stress of 142 kPa which would mean an average primary consolidation ratio equal to (142-82)/(160-82) = 77%. This does not suit the experimental measured settlement data which, as already mentioned indicates that the consolidation ratio of layer 6 under area 3 is, without any doubt, very low as shown by its small measured compression equal to 18 cm when compared to the 90 cm of measured compression at the same time under area 1 as reported in Table 5. Point A is very close to the recompression line, in the heart of the recompression range. Since the c_v value which governs primary consolidation in the recompression range is roughly 50 times higher than the c_v value of 1.5×10^{-8} m^2/s of the virgin compression range used to build the abacus (see Fig. 4), it cannot be expected that the abacus shown in Fig. 25 yield worthy results.

The abacus was then rebuilt, using the same procedure but using the c_v value of the recompression range equal to 10^{-6} m^2/s but this also failed to lead to acceptable results. The authors had then to come to the conclusion that their second working tool consisting in an abacus tailored to represent the field conditions of layer 6 through extrapolation of the abacus built from the oedometer laboratory test results by way of Taylor and Merchant theory also failed to be usable, the main reason for this being that the c_v value in the field varies when the consolidation ratio increases, as will be seen in the conclusions, and that Taylor and Merchant's formulation used to built the abacus only allows the use of a constant c_v value.

12. Working Tool Number 3 to Back-Analyze the Behaviour of the Thick SFL Clay Layer Under Area 3 with Vertical Drainage

After coming to this conclusion, the authors found themselves left with only one alternative to back-analyze the measured compression in layer 6 under the center of area 3, and that was to try and adjust some Taylor and Merchant's curve to the measured curve of Fig. 11 determining the c_v value which would lead to a reasonable adjustment. As already mentioned, as settlement occurs, the total stress

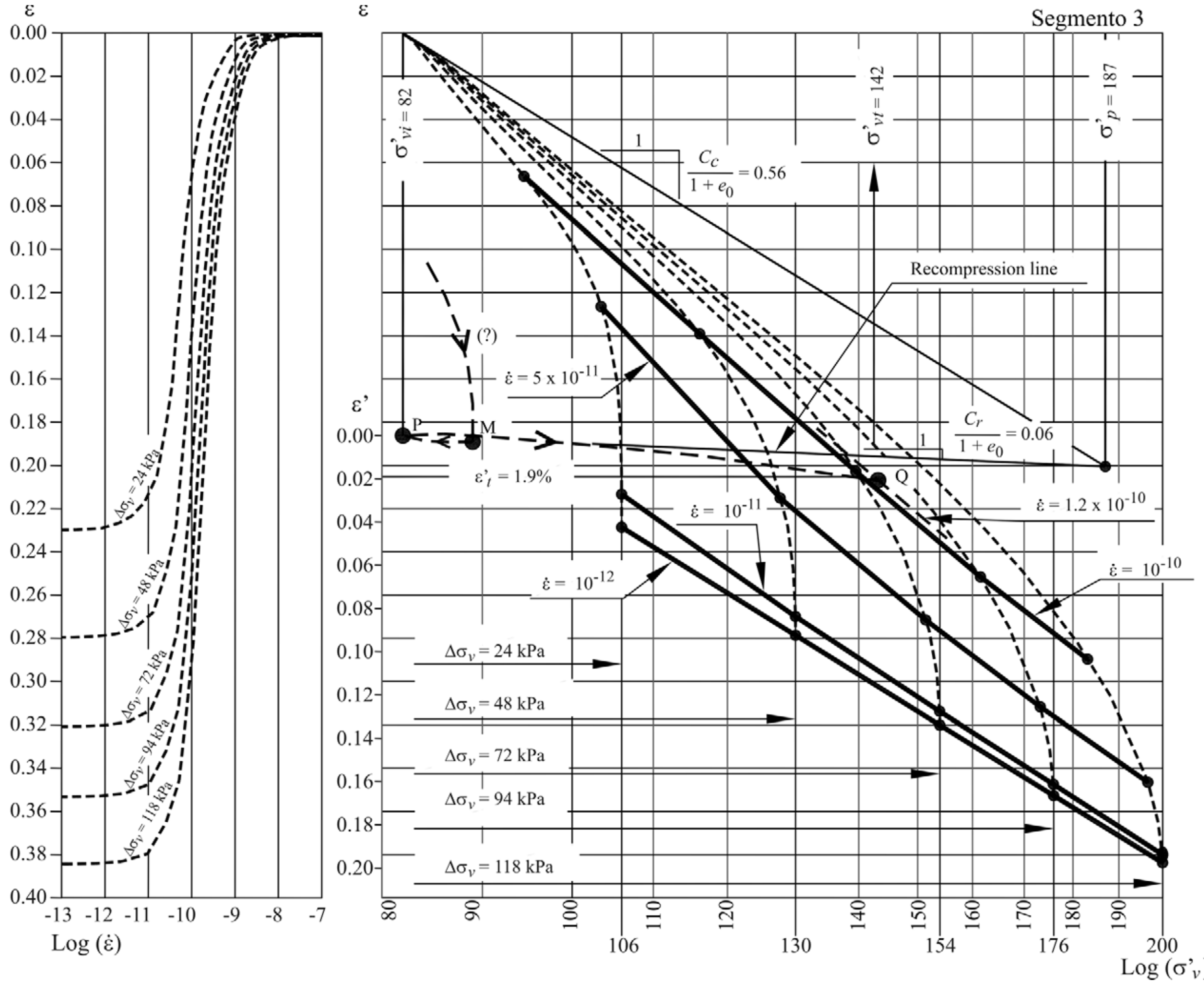

Figure 25 - Abacus built through Taylor and Merchant's theory for layer 6 of area 3 with $c_v = 1.5 \times 10^{-8}$ m^2/s.

σ_v in the middle of layer 6 decreases with time due to embankment submersion and the "pseudo final effective stress" which governs the consolidation process at any time, that is "σ_v - u_{hid}", also decreases as illustrated in Fig. 26. For their back-analysis, the authors took the decision to calculate the values of "σ_v - u_{hid}" acting in october 2009 in each of the 1 m thick sublayers considered for settlement calculations.

The "pseudo final effective stress" at mid-height of layer 6, "σ_v - u_{hid}" is equal to 179.2 kPa compared to σ'_{vi} = 81.4 kPa and σ'_p (lab) = 187.3 kPa and is, in fact, higher than the (real) final effective stress, equal to 160.6 kPa, to be reached after full primary and full secondary consolidations when the total settlement will be 2.89 m wheras the total settlement at the end of october 2009 was 1.01 m.

The primary and secondary compressions were then calculated considering that this "pseudo final effective stress" would be maintained constant thereafter, obtaining:

• "pseudo final primary compression" (ΔH_p)': 20 cm which is, in fact, higher than the (real) final primary compression to be reached after full primary consolidation which is equal to 18 cm as indicated in Table 8.

• "pseudo final secondary compression" (ΔH_s)': 142 cm which is, in fact, higher than the (real) final secondary compression to be reached after full secondary consolidation which is equal to 120 cm as indicated in Table 8 and their sum:

• the "pseudo final total compression" (ΔH_t)': 162 cm which is, in fact, higher than the (real) final total compression to be reached after full primary and full secondary consolidations which is equal to 138 cm.

It was immediately found out that no satisfying adjustment was to be obtained with only one constant value of c_v over the whole period. Figure 27 shows a theoretical Taylor and Merchant's curve reasonably well fitted to the measured compression curve of layer 6 under the center of area 3.

This adjustment was achieved by dividing the total measurement period into three periods. As can be seen on Fig. 27, the values of c_v which led to the adjustment of the theoretical curve to the measured one are:

• for the first period: $c_v = 2 \times 10^{-7}$ m^2/s,

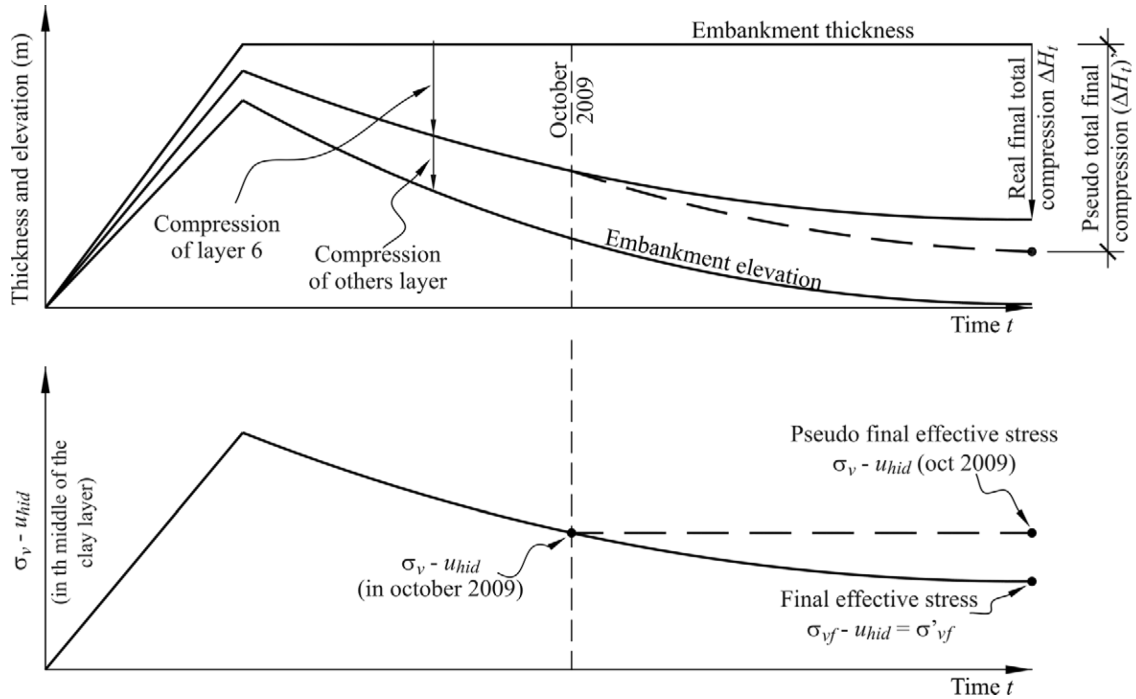

Figure 26 - Evolution of the "pseudo final effective stress" in the middle of layer 6 and of the "pseudo total final compression".

• for the second period: $c_v = 5 \times 10^{-8}$ m^2/s,

• for the third period: $c_v = 1 \times 10^{-8}$ m^2/s

Table 12 summarizes the results of the back-analysis of layer 6 compression with vertical drainage under the center of area 3 through Taylor and Merchant's theory, indicating:

• the equivalent time of the end of each period,

• the coefficient of consolidation for which the best fit was obtained between the theoretical curve and the measured compression curve, in each period: c_v during period 1, c_v during period 2, c_v during period 3,

• the total compression ΔH_{tj} measured at the end of each period,

• the calculated primary compression, ΔH_{pj}, and secondary compression, ΔH_{sj}, at the end of period 1, period 2 and period 3,

• the calculated ratio of the primary compression at the end of each period ΔH_{pj} to the "pseudo final primary compression" (ΔH_p)' called the "primary consolidation index",

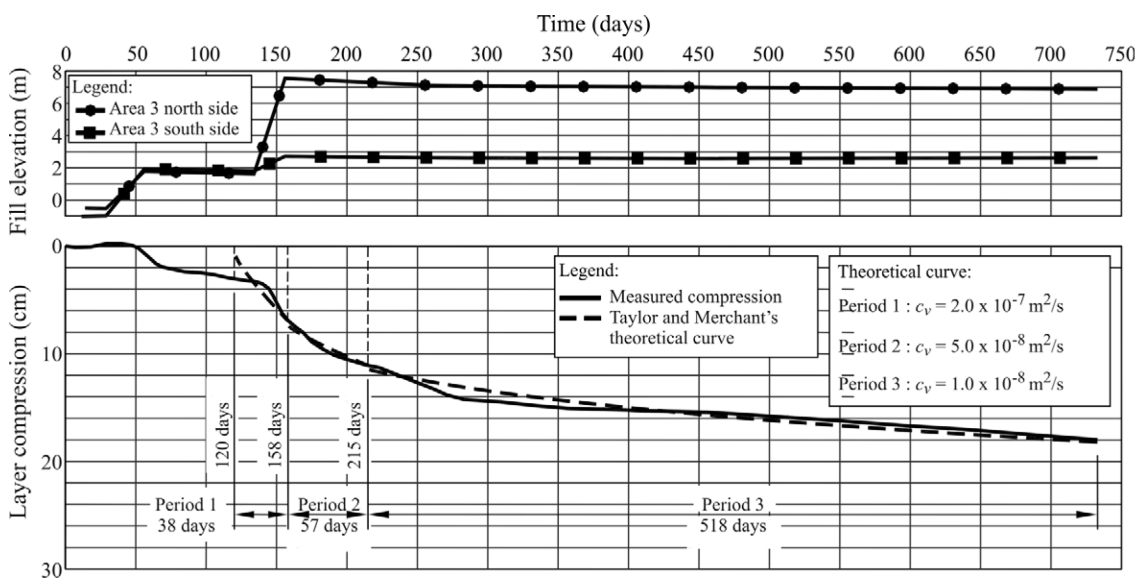

Figure 27 - Theoretical Taylor and Merchant's curve reasonably well fitted to the measured compression curve of layer 6 under the center of area 3.

Table 12 - Results of the back analysis of layer 6 compression under the center of area 3.

	Period 1	Period 2	Period 3
Time *t* (equivalent) at the end of each period	38 days	95 days	613 days
Back analyzed c_v value for each period	20 x 10^{-8} m^2/s	5.0 x 10^{-8} m^2/s	1.0 x 10^{-8} m^2/s
ΔH_{tj}: Total compression of layer 6 measured at the end of each period	7 cm	11 cm	18 cm
ΔH_{pj} compression at the end of each period obtained from Taylor and Merchant calculations	4 cm	6 cm	8 cm
$\Delta H_{pj}/(\Delta H_p)$' Primary consolidation index at the end of each period	4/20 = 20%	6/20 = 30%	8/20 = 40%
ΔH_{sj} compression at the end of each period obtained from Taylor and Merchant calculations	3 cm	5 cm	10 cm
$\Delta H_{sj}/(\Delta H_s)$' Secondary consolidation index at the end of each period	3/142 = 2.1%	5/142 = 3.5%	10/142 = 7.0%
$\Delta H_{tj}/(\Delta H_t)$' Aggregate consolidation index at the end of each period	7/162 = 4.3%	11/162 = 6.8%	18/162 = 11.1%

• the calculated ratio of the secondary compression at the end of each period ΔH_{sj} to the "pseudo final secondary compression" (ΔH_s)' called the "secondary consolidation index",

• the calculated ratio of the total compression at the end of each period ΔH_{tj} to the "pseudo final total compression" (ΔH_t)' called the "aggregate consolidation index".

It has to be emphasized that when secondary compression and primary compression occur simultaneously, the volume of water expelled in this situation is larger than the volume of water which would be expelled if only primary consolidation took place. Since the initial pore pressure and the initial gradient are not affected by the phenomenon of secondary consolidation, then the pore pressure dissipation has to be slower when secondary consolidation occurs simultaneously with primary consolidation than if it did not as illustrated in Fig. 28.

This fact has been pointed out by Garlanger (1971) among others. Larsson *et al.* (1997) can be quoted: "At compression, the time dependence leads to a larger compression than that calculated from the compression moduli alone. A condition for this extra compression to occur is that the corresponding amount of water flows out of the soil. In turn, a condition for this to occur within the same period of time as the compression corresponding to the moduli alone is that a higher gradient exists in the pore water. The immediate effect of the creep tendency (or time effects) during a short time step is therefore an increase in pore pressure, whose size is determined by the pontential creep deformation and the compression modulus". This is illustrated on the left side of Fig. 28. The right side of Fig. 28, shows the comparison of the measured settlement of an embankment on soft clay with Larsson *et al.*'s prediction. Taylor and Merchant's theory, although only stated in terms of void ratio, does not take into account the influence of the occurrence of secondary compression simultaneously with primary compression on the pore pressure, as clearly shown by Carvalho's formulas, but this influence will necessarily lead to a field c_v value lower than the laboratory pure primary consolidation c_v value as clearly illustrated at the top of the left side of Fig. 28.

It can be assumed that the value of the average primary consolidation ratio $\overline{U}_p$ is equal to the primary consolidation index $[\Delta H_{pj}/(\Delta H_p)']$, so that the average vertical effective stress in layer 6 at the end of each period can be computed from the following formula:

$$\sigma'_v = \sigma'_{vi} + [(\sigma_v - u_{hid}) - \sigma'_{vi}] \text{ x } \overline{U}_p = \sigma'_{vi} + [(\sigma_v - u_{hid}) - \sigma'_{vi}] \text{ x } [\Delta H_{pj} / (\Delta H_p)'] \qquad (8)$$

allowing then, to plot the back-analyzed values of c_v against the mean effective vertical stress σ'_v in layer 6 in area 3, as shown in Fig. 29.

It is well known that the yielding stress decreases when the strain rate decreases as illustrated in Fig. 16. It has, therefore, to be expected that the vertical effective stress at which the field c_v value passes from its higher value, between 3 x 10^{-6} m^2/s and 3 x 10^{-7} m^2/s (see Fig. 4) in the recompression range, to its lower value, between 9 x 10^{-9} m^2/s and 2 x 10^{-8} m^2/s (see Fig. 4) in the virgin compression range, is to be smaller than the σ'_p value determined in the oedometer tests.

It can be seen in Fig. 29 that the obtained results are in good agreement with the above observation and that the back-analyzed c_v field values are also in good agreement with the laboratory values in the transition range between the recompression range and the virgin compression range.

13. Working Tool Number 4 to Extrapolate the Use of the Taylor & Merchant Model to Back-Analyze the Behaviour of the Thick SFL Clay Layer Under Areas 1 and 2 with Radial Drainage

13.1. Methodology

For the back-analysis of the embankment settlement data for layer 6 under the centers of areas 1 and 2 the same approach is not applicable due to the fact that the mathe-

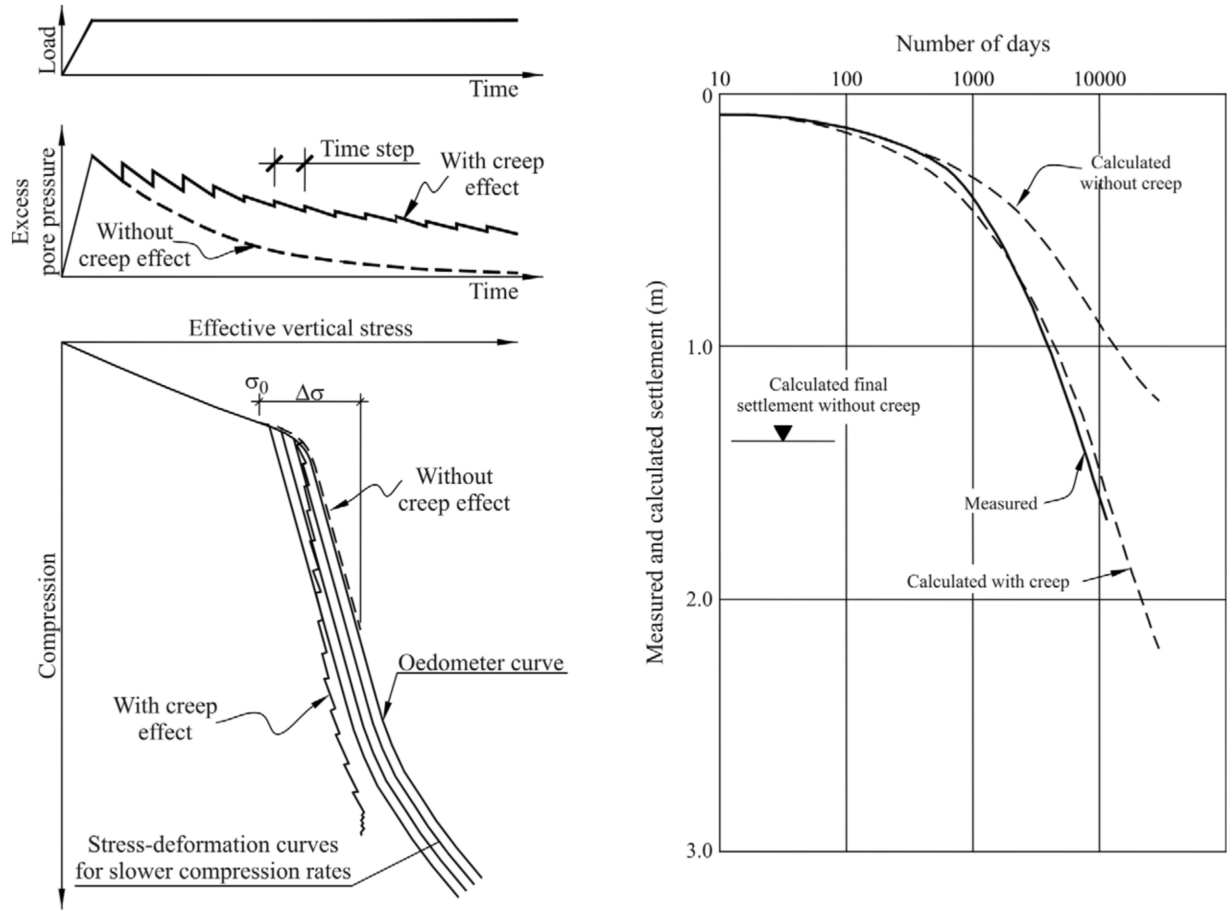

Figure 28 - Influence of the occurrence of secondary compression simultaneously with primary compression apud Larsson *et al.* (1997).

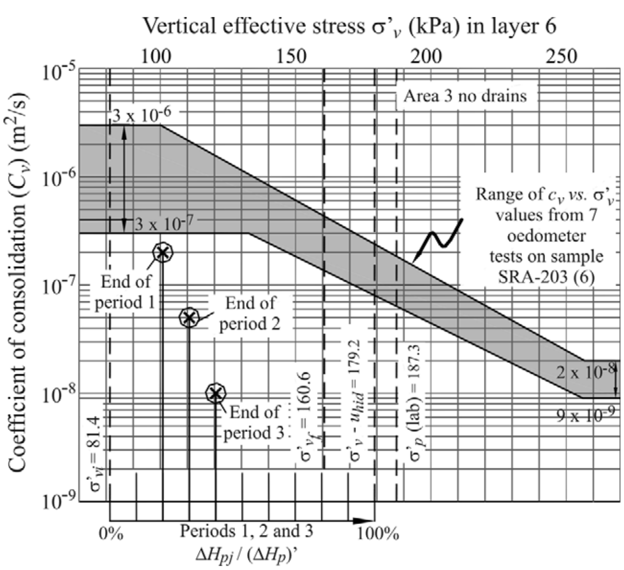

Figure 29 - Back-analyzed values of c_v *vs.* mean effective vertical stress in layer 6 under area 3.

matical formulation presently available based on Taylor and Merchant's theory only encompasses the case of vertical drainage. In this respect, the authors are not aware of any published analytical formulation of secondary consolidation associated with radial drainage.

It was then decided to compare the primary consolidation process of layer 6 undergoing vertical compression through pure radial drainage with a mean radial drainage distance R equal to 0.68 m which corresponds to the drain spacing of 1.2 m of the square wick drains mesh under area 1, to the primary consolidation process of a hypothetical layer undergoing vertical compression with pure vertical drainage to see if a layer such that both processes would follow approximately the same course could be found.

As can be seen in Table 3, for layer 6 the value of c_{h1} determined from CPT porepressure dissipation tests, which corresponds to the recompression range according to Teh and Houlsby (1991), is equal to 4.9 x 10^{-7} m^2/s and the oedometer test c_{v1} value in the recompression range is 6.5 x 10^{-7} m^2/s, that is $c_{h1} = 0.75\ c_{v1}$. Some oedometer tests with radial drainage were performed in the laboratory which yielded c_h values of the order of 3 times the c_v values in the normal compression range. For this reason, all further calculations were done for $c_h = c_v$ as well as for $c_h = 3\ c_v$.

For this comparison, the radial primary consolidation process of layer 6 was calculated using Barron (1948) formulas considering an equivalent radius r_w of 3.25 cm for the

0.5 cm x 10 cm wick drain and a smear zone around each drain with a radius r_s equal to twice the drain equivalent radius, and a permeability coefficient equal to a fifth of the undisturbed clay permeability coefficient. Figure 30 shows the dotted curve which expresses the (primary) consolidation ratio of layer 6 under area 1 *vs.* the logarithm of time calculated for a horizontal/radial coefficient of consolidation $c_h = 1.5 \times 10^{-8}$ m^2/s.

Figure 30 also shows the plain curve which corresponds to a hypothetical layer with vertical drainage, with the primary consolidation ratio calculated using Terzaghi (1936) formulation considering $c_v = 1.5 \times 10^{-8}$ m^2/s and the drainage distance *D* equal to 2.03 m for which the two curves reach *U* = 50% at the same time. Considering the closeness of the two curves, it can be concluded that this layer undergoing vertical compression with pure vertical drainage follows a primary consolidation process equivalent to the one of layer 6 under area 1 undergoing vertical compression through pure radial drainage and the *D* value of 2.03 m can be called the equivalent drainage distance: D_{eq}.

The equivalent drainage distance value is influenced by the ratio of the value of c_h of layer 6 to the assumed value of c_v of the equivalent layer with vertical drainage. It is also influenced by the assumed values of the radius and the coefficient of permeability of the smear zone. For this reason, the D_{eq} value was also determined for c_h/c_v equal to 3 and for a smear zone three times larger than the one considered before, that is with r_s = 19.5 cm.

The D_{eq} value was also determined following exactly the same methodology explained above for layer 6 undergoing vertical compression through pure radial drainage with a mean radial drainage distance *R* equal to 1.35 m which corresponds to the drain spacing of 2.4 m of the square wick drains mesh under area 2. Table 13 synthesizes all the calculated D_{eq} values.

It was then decided to use the following procedure to theoretically predict the course of compression of layer 6 under area 1 and under area 2:

• the course of the primary compression was calculated using Barron (1948) formulation considering the "pseudo final primary compression" (ΔH_p)' calculated as already mentioned, under the "pseudo final effective stresses",

• the course of the secondary compression was calculated using the formulas of Carvalho, isolating the secondary compression from primary compression, considering it to occur in a layer drained vertically with a drainage distance equal to D_{eq} with the "pseudo final secondary compression" value (ΔH_s)' and,

• sum the two above compressions to get the course of the total compression.

It was decided to call this method: "Primary Barron + secondary pseudo Taylor and Merchant".

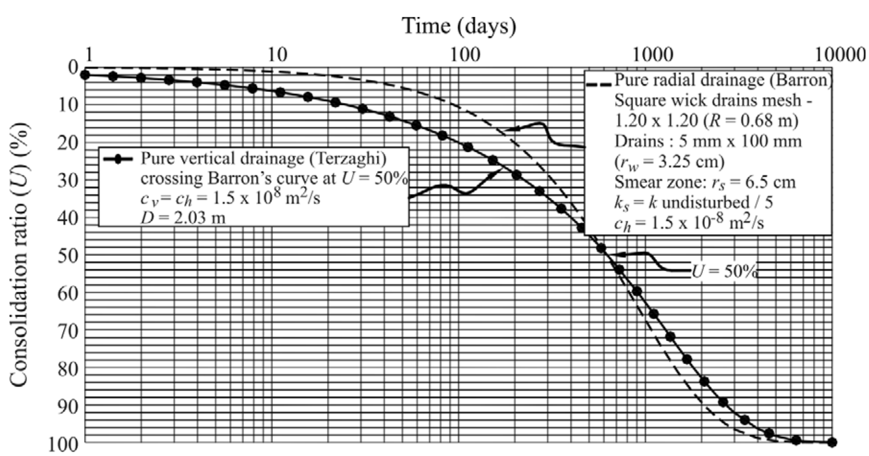

Figure 30 - Comparison of primary consolidation ratio between a clay layer with pure vertical drainage with $c_v = 1.5 \times 10^{-8}$ m^2/s and a clay layer with a 1.2 m x 1.2 m square mesh of wick drains (pure radial drainage) with $c_h = c_v = 1.5 \times 10^{-8}$ m^2/s .

Table 13 - D_{eq} values.

Area	c_h/c_v (*)	r_s	D_{eq}	Area	c_h/c_v (*)	r_s	D_{eq}
	1	6.5 cm	2.03 m		1	6.5 cm	4.33 m
1	3	6.5 cm	1.16 m	2	3	6.5 cm	2.49 m
	1	19.5 cm	2.67 m		1	19.5 cm	5.89 m

(*) ratio of c_h of layer 6 to the assumed value of c_v of the equivalent layer with vertical drainage.

13.2. Backanalysis of layer 6 compression under area 1

Under area 1, the "pseudo final effective stress" at mid-height of layer 6, "σ_v - u_{hid}" is equal to 221.3 kPa compared to σ'_{vi} = 81.2 kPa and σ'_p (lab) = 187.1 kPa and is, in fact, higher than the (real) final effective stress, equal to 201.6 kPa, to be reached after full primary and full secondary consolidations when the total settlement will be 4.20 m whereas the total settlement at the end of october 2009 was 2.36 m.

The primary and secondary compressions were then calculated considering that this "pseudo final effective stress" would be maintained constant thereafter, obtaining:

• "pseudo final primary compression" (ΔH_p)': 68 cm which is, in fact, higher than the (real) final primary compression to be reached after full primary consolidation which is equal to 43 cm as indicated in Table 6.

• "pseudo final secondary compression" (ΔH_s)': 177 cm which is, in fact, equal to the (real) final secondary compression to be reached after full secondary consolidation as indicated in Table 6 and their sum:

• the "pseudo final total compression" (ΔH_t)': 245 cm which is, in fact, higher than the (real) final total compression to be reached after full primary and full secondary consolidations which is equal to 220 cm.

It was immediately found out that no satisfying adjustment was to be obtained with only one constant value of c_h over the whole period. Figure 31 shows the theoretical curve obtained following the above described "Primary Barron + secondary pseudo Taylor and Merchant" procedure reasonably well fitted to the measured compression curve of layer 6 under the center of area 1 for the value of c_h of layer 6 equal to the value of c_v of the equivalent layer with vertical drainage and r_s = 6.5 cm.

This adjustment was achieved by dividing the total measurement period into two periods. As can be seen on Fig. 31, the values of c_h which led to the adjustment of the theoretical curve to the measured one are:

• for the first period: c_h = 5 x 10^{-8} m^2/s,

• for the second period: c_h = 2.3 x 10^{-8} m^2/s.

It has to be pointed out that in the above analysis, the vertical drainage in layer 6 has not been taken into account for considering that it would not affect significantly the results of the back-analysis.

Table 14 summarizes the results of the back-analysis of layer 6 compression with vertical drainage under the center of area 1 through the "Primary Barron + secondary pseudo Taylor and Merchant" procedure indicating:

• the equivalent time at the end of each period,

• the coefficient of consolidation for which the best fit was obtained between the theoretical curve and the measured compression curve, in each period: c_h during period 1, c_h during period 2,

• the total compression ΔH_{tj} measured at the end of each period,

• the calculated primary compression, ΔH_{pj} and secondary compression, ΔH_{sj} at the end of period 1 and period 2,

• the calculated ratio of the primary compression at the end of each period ΔH_{pj} to the "pseudo final primary compression" (ΔH_p)' called the "primary consolidation index",

• the calculated ratio of the secondary compression at the end of each period ΔH_{sj} to the "pseudo final secondary

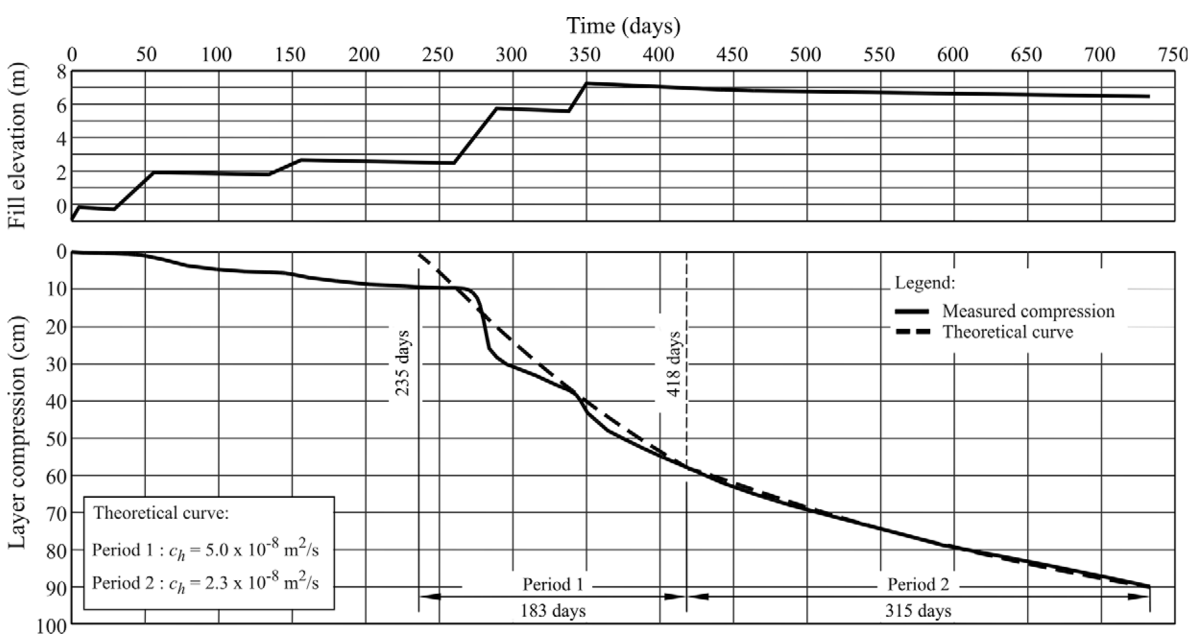

Figure 31 - Theoretical curve reasonably well fitted to the measured compression curve of layer 6 under the center of area 1.

compression" (ΔH_s)' called the "secondary consolidation index",

• the calculated ratio of the total compression at the end of each period ΔH_{tj} to the "pseudo final total compression" (ΔH_t)' called the "aggregate consolidation index".

Repeating the adjustment of a theoretical curve to the measured compression curve for the value of c_h of layer 6 equal to three times the value of c_v of the equivalent layer with vertical drainage and r_s = 6.5 cm, and for r_s = 19.5 cm, for the same two periods as above, the same good adjustments were obtained for the values of c_h shown in Table 15, with all other values identical to the ones shown in Table 14.

An can be seen the ratio of the c_h value in layer 6 to the c_v value admitted to determine the drainage distance of the equivalent layer with vertical drainage has no effect on the backanalyzed value of c_h.

As already mentioned in the backanalysis of layer 6 under area 3, it can be assumed that the value of the average primary consolidation ratio $\overline{U}_p$ is equal to the primary consolidation index $[\Delta H_{pj}/(\Delta H_p)']$, so that the average vertical effective stress in layer 6 at the end of each period can be computed from the following formula:

$$\sigma'_v = \sigma'_{vi} + [(\sigma_v - u_{hid}) - \sigma'_{vi}] \text{ x } \overline{U}_p = \sigma'_{vi} + [(\sigma_v - u_{hid}) - \sigma'_{vi}] \text{ x } [\Delta H_{pj}/(\Delta H_p)'] \quad (9)$$

allowing then, to plot the back-analyzed values of c_h against the mean effective vertical stress σ'_v in layer 6 in area 1, as shown in Fig. 32.

It can be seen in Fig. 32 that the obtained results are in good agreement with the observation that it has to be expected that the vertical effective stress at which the coefficient of consolidation field value passes from its higher value in the recompression range, to its lower value in the virgin compression range, is to be smaller than the σ'_p value determined in the oedometer tests. It can also be observed that the back-analyzed c_h field values are also in good agreement with the c_v laboratory values in the transition range between the recompression range and the virgin compression range.

13.3. Backanalysis of layer 6 compression under area 2

In area 2, the last phase of heightening the fill was postponed due to lack of fill material. For this reason, one set of values of "pseudo final effective stress", "pseudo final primary compression" and "pseudo final secondary compression" had to be used for t up to 450 days and another set of values had to be used for t > 450 days.

Under area 2, the "pseudo final effective stress" at mid-height of layer 6, "$\sigma_v - u_{hid}$" is equal to 205.9 kPa up to t = 450 days and equal to 221.9 kPa for t > 450 days, compared to σ'_{vi} = 86.6 kPa and σ'_p (lab) = 192.5 kPa and is, in fact, higher than the (real) final effective stress, equal to 198.3 kPa, to be reached after full primary and full secondary consolidations when the total settlement will be 3.89 m whereas the total settlement at the end of october 2009 was 1.46 m.

The primary and secondary compressions were then calculated considering that this "pseudo final effective stress" would be maintained constant thereafter, obtaining:

Table 15 - Values of c_h yielded by the back analysis.

c_h/c_v (*)	r_s	D_{eq}	c_h for Period 1	c_h for Period 2
1	6.5 cm	2.03 m	5.0 x 10^{-8} m^2/s	2.3 x 10^{-8} m^2/s
3	6.5 cm	1.16 m	5.0 x 10^{-8} m^2/s	2.3 x 10^{-8} m^2/s
1	19.5 cm	2.67 m	8.6 x 10^{-8} m^2/s	4.2 x 10^{-8} m^2/s

(*) ratio of c_h of layer 6 to the assumed value of c_v of the equivalent layer with vertical drainage.

Table 14 - Results of the back analysis of layer 6 compression under the center of area 1 for the value of c_h of layer 6 equal to the value of c_v of the equivalent layer with vertical drainage and r_s = 6.5 cm.

	Period 1	Period 2
Time t (equivalent) at the end of each period	183 days	498 days
Back analyzed c_h value for each period	5.0 x 10^{-8} m^2/s	2.3 x 10^{-8} m^2/s
ΔH_{tj}: Total compression of layer 6 measured at the end of each period	58 cm	90 cm
ΔH_{pj} compression at the end of each period obtained from "Primary Barron + secondary pseudo Taylor and Merchant" calculations	34 cm	49 cm
$\Delta H_{pj}/(\Delta H_p)'$ Primary consolidation index at the end of each period	34/68 = 50%	49/68 = 72%
ΔH_{sj} compression at the end of each period obtained from "Primary Barron + secondary pseudo Taylor and Merchant" calculations	24 cm	41 cm
$\Delta H_{sj}/(\Delta H_s)'$ Secondary consolidation index at the end of each period	24/177 = 14%	41/177 = 23%
$\Delta H_{tj}/(\Delta H_t)'$ Total consolidation index at the end of each period	58/245 = 24%	90/245 = 37%

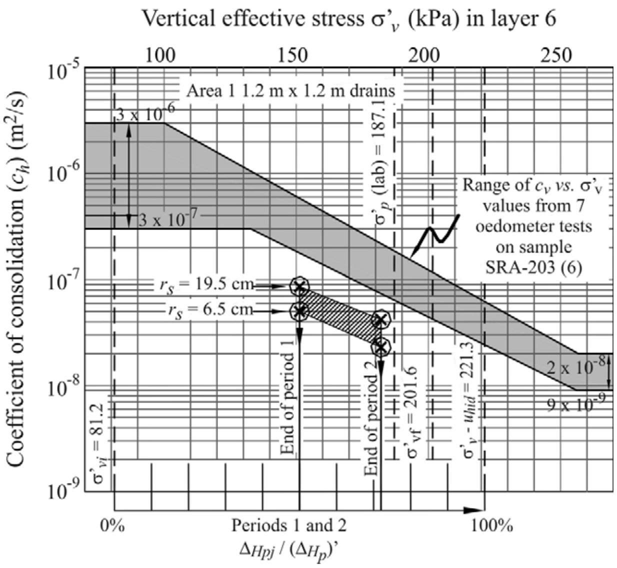

Figure 32 - Back-analyzed values of c_h *vs.* mean effective vertical stress in layer 6 under area 1.

• "pseudo final primary compression" (ΔH_p)': 34 cm for t up to 450 days and 51 cm for $t > 450$ days for which is, in fact, higher than the (real) final primary compression to be reached after full primary consolidation which is equal to 26 cm as indicated in Table 7.

• "pseudo final secondary compression" (ΔH_s)': 153 cm for t up to 450 days and 153 cm for $t > 450$ days which is, in fact, equal to the (real) final secondary compression to be reached after full secondary consolidation as indicated in Table 7 and their sum:

• the "pseudo final total compression" (ΔH_t)': 187 cm for t up to 450 days and 204 cm for $t > 450$ days which is, in fact, higher than the (real) final total compression to be reached after full primary and full secondary consolidations which is equal to 179 cm.

It was immediately found out that no satisfying adjustment was to be obtained with a constant value of c_h (and c_v) over the whole period. Figure 33 shows the theoretical curve obtained following the above described "Primary Barron + secondary pseudo Taylor and Merchant" procedure reasonably well fitted to the measured compression curve of layer 6 under the center of area 2 for the value of c_h of layer 6 equal to the value of c_v of the equivalent layer with vertical drainage and r_s = 6.5 cm.

This adjustment was achieved by dividing the total measurement period into three periods with period 1 up to t = 450 days and periods 2 and 3 for $t > 450$ days. As can be seen on Fig. 33, the values of c_h which led to the adjustment of the theoretical curve to the measured one are:

• for the first period: $c_h = 9 \times 10^{-8}$ m²/s,

• for the second period: $c_h = 9 \times 10^{-8}$ m²/s,

• for the third period: $c_h = 4.5 \times 10^{-8}$ m²/s.

Table 16 summarizes the results of the back-analysis of layer 6 compression with vertical drainage under the center of area 2 through the "Primary Barron + secondary pseudo Taylor and Merchant" procedure indicating:

• the equivalent time at the end of each period,

• the coefficient of consolidation for which the best fit was obtained between the theoretical curve and the measured compression curve, in each period: c_h during period 1, c_h during period 2, c_h during period 3,

• the total compression ΔH_{tj} measured at the end of each period,

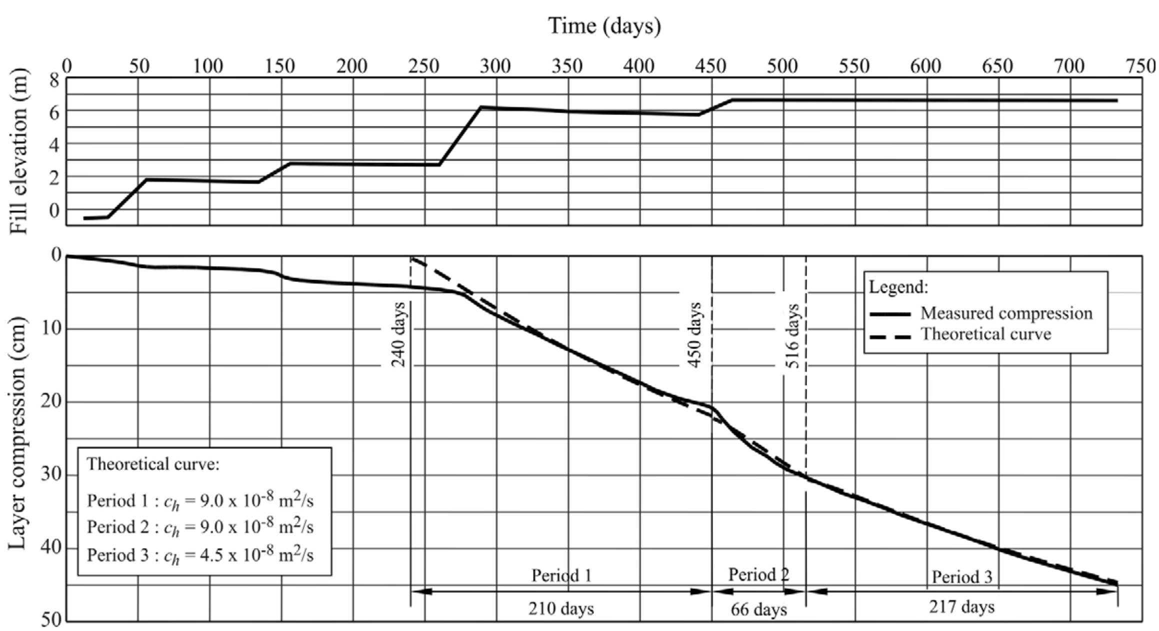

Figure 33 - Theoretical curve reasonably well fitted to the measured compression curve of layer 6 under the center of area 2.

• the calculated primary compression, ΔH_{pj} and secondary compression, ΔH_{sj} at the end of period 1, period 2 and period 3,

• the calculated ratio of the primary compression at the end of each period ΔH_{pj} to the "pseudo final primary compression" (ΔH_p)' called the "primary consolidation index",

• the calculated ratio of the secondary compression at the end of each period ΔH_{sj} to the "pseudo final secondary compression" (ΔH_s)' called the "secondary consolidation index",

• the calculated ratio of the total compression at the end of each period ΔH_{tj} to the "pseudo final total compression" (ΔH_t)' called the "aggregate consolidation index".

Repeating the adjustment of a theoretical curve to the measured compression curve for $c_h = 3\ c_v$ and for r_s = 19.5 cm, for the same three periods as above, the same good adjustments were obtained for the values of c_h shown in Table 17, with all other values identical to the ones shown in Table 16.

As already mentioned in the backanalysis of layer 6 under areas 3 and 1, the back-analyzed values of c_h can be plotted against the mean effective vertical stress σ'_v in layer 6 as shown in Fig. 34.

It can be seen in Fig. 34 that the obtained results are in good agreement with the observation that it has to be expected that the vertical effective stress at which the coefficient of consolidation field value passes from its higher value in the recompression range, to its lower value in the virgin compression range, is to be smaller than the σ'_p value determined in the oedometer tests. It can also be observed that the back-analyzed c_h field values are also in good

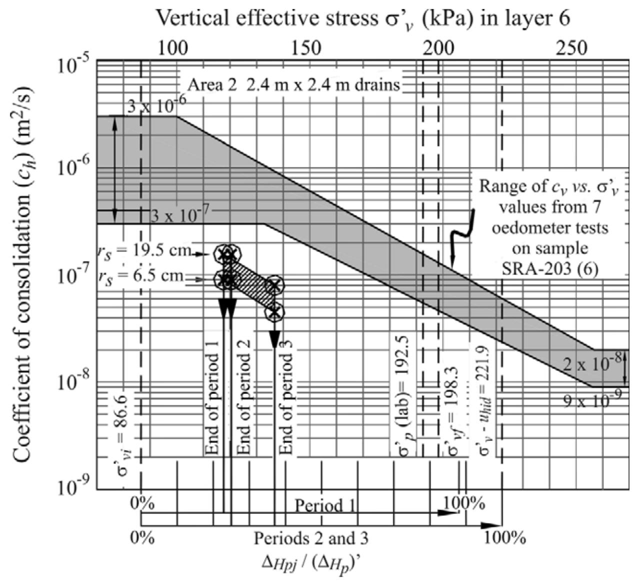

Figure 34 - Back-analyzed values of c_h *vs.* mean effective vertical stress in layer 6 under area 2.

Table 16 - Results of the back analysis of layer 6 compression under the center of area 2 for the value of c_h of layer 6 equal to the value of c_v of the equivalent layer with vertical drainage and r_s = 6.5 cm.

	Period 1	Period 2	Period 3
Time *t* (equivalent) at the end of each period	210 days	276 days	493 days
Back analyzed c_h value for each period	9.0×10^{-8} m²/s	9.0×10^{-8} m²/s	4.5×10^{-8} m²/s
ΔH_{tj}: Total compression of layer 6 measured at the end of each period	22 cm	30 cm	45 cm
ΔH_{pj} compression at the end of each period obtained from "Primary Barron + secondary pseudo Taylor and Merchant" calculations	9 cm	13 cm	19 cm
$\Delta H_{pj}/(\Delta H_p)$' Primary consolidation index at the end of each period	9/34 = 26%	13/51 = 25%	19/51 = 37%
ΔH_{sj} compression at the end of each period obtained from "Primary Barron + secondary pseudo Taylor and Merchant" calculations	13 cm	17 cm	26 cm
$\Delta H_{sj}/(\Delta H_s)$' Secondary consolidation index at the end of each period	13/153 = 9%	17/153 = 11%	26/153 = 17%
$\Delta H_{tj}/(\Delta H_t)$' Total consolidation index at the end of each period	22/187 = 12%	30/204 = 15%	45/204 = 22%

Table 17 - Values of c_h yielded by the back analysis.

c_h/c_v	r_s	D_{eq}	c_h for Period 1	c_h for Period 2	c_h for Period 3
1	6.5 cm	4.33 m	9.0×10^{-8} m²/s	9.0×10^{-8} m²/s	4.5×10^{-8} m²/s
3	6.5 cm	2.49 m	9.0×10^{-8} m²/s	9.0×10^{-8} m²/s	4.5×10^{-8} m²/s
1	19.5 cm	5.69 m	15.5×10^{-8} m²/s	15.5×10^{-8} m²/s	8.0×10^{-8} m²/s

(*) ratio of c_h of layer 6 to the assumed value of c_v of the equivalent layer with vertical drainage.

agreement with the laboratory c_v values in the transition range between the recompression range and the virgin compression range.

It has to be pointed out that in the above analysis, the vertical drainage in layer 6 has not been taken into account, although in the case of area 2, the Deq value is of the same order of magnitude as the vertical drainage distance equal to 4.75 m, as shown in Table 13. Taking the contribution of the vertical drainage into account would certainly have some influence on the obtained results and would, lead in this case to somewhat smaller values of c_h.

14. Comments on the Current Method Used to Analyze Embankments Settlements

As mentioned in item 9, the current method used to back-analyze embankments settlements is Asaoka's method which, as already discussed, is applied considering that the secondary settlement only starts occurring after the end of the primary settlement.

Now what happens when Asaoka's method is applied to a compression curve which reflects the simultaneous occurrence of primary and secondary compressions as modeled by a Taylor and Merchant curve?

Figure 35 shows a theoretical Taylor and Merchant's curve where 50% of the total compression is due to primary consolidation and the other 50% is due to secondary consolidation (r = 0.5). All input parameters are shown in Fig. 35.

The plain dotted line represents the known part of the total compression (primary + secondary) curve which is the one that is known from settlement monitoring up to t = 220 days. It is this part of the curve, between t = 40 days and t = 220 days after the end of construction, to which Asaoka's method is commonly applied, considering that:

• the secondary consolidation has not started yet and

• the primary consolidation ratio is higher than 33% (Massad, 2009), since, according to Massad: "The formula $U = 1\text{-}0.811\ e^{ct}$ where $c = 2.5\ c_v/(H_d)^2$ yields the value of the vertical consolidation ratio of Terzaghi's theory for $U \geq 60\%$ (Taylor, 1948)" and "Asaoka's method applicable range can be extended to $U \geq 33\%$ through the use of another exponential function which gives the value of the consolidation ratio in function of the time factor (Schofield & Wroth 1968, p. 79)."

Figure 36 shows Asaoka's construction applied to the measured values of the "supposed" primary compression varying from 12 cm at t = 40 days to 18 cm at t = 220 days.

As can be seen, the total primary compression thus obtained is 44 cm. From this value the primary consolidation ratio which is obtained at the end of the period is 1 8 cm: 44 cm = 41%.

Moreover, the c_v value obtained from Asaoka's construction equal to 5.7 x 10^{-7} m^2/s is 57 times higher than the real c_v value equal to 1.0 x 10^{-8} m^2/s.

At this point, most Asaoka's method users observe that all compression values higher than 14.5 cm satisfy the condition U > 33% which is then invoked to vouch for the validity of the results thus obtained.

Figure 37 compares the real compression curves (as represented by input Taylor and Merchant primary and total compression curves) with the predicted primary compression curve obtained using Asaoka's method and the predicted total compression curve predicted through Asaoka's method + $C\alpha$ (secondary). The Asaoka (primary) + $C\alpha$

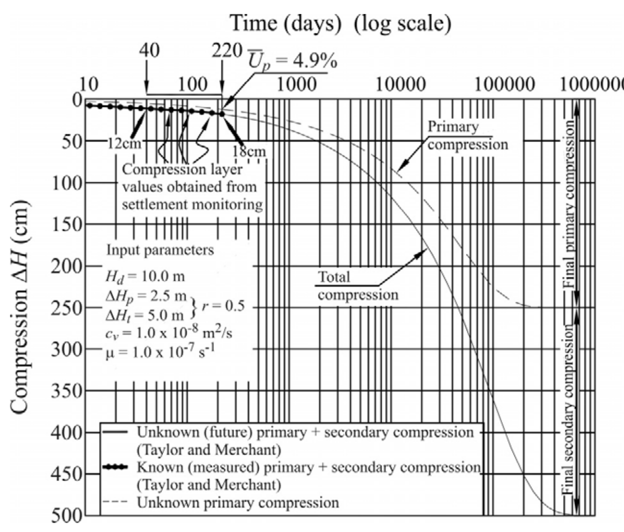

Figure 35 - Taylor and Merchant theoretical curve for r = 0.5.

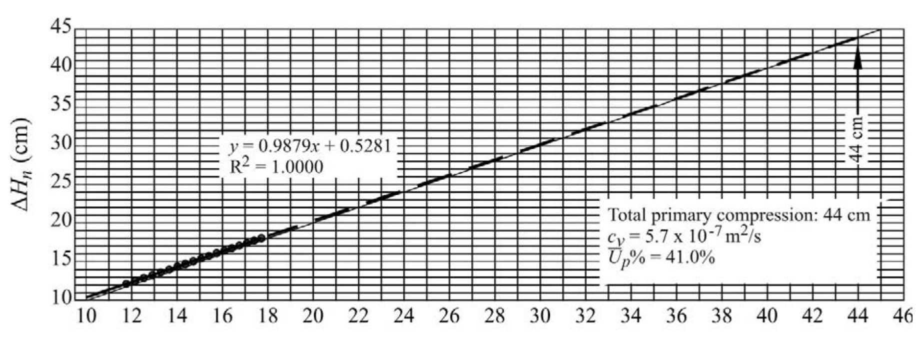

Figure 36 - Asaoka's construction applied to the part of the dotted curve of Fig. 35 between t = 40 days and t = 220 days.

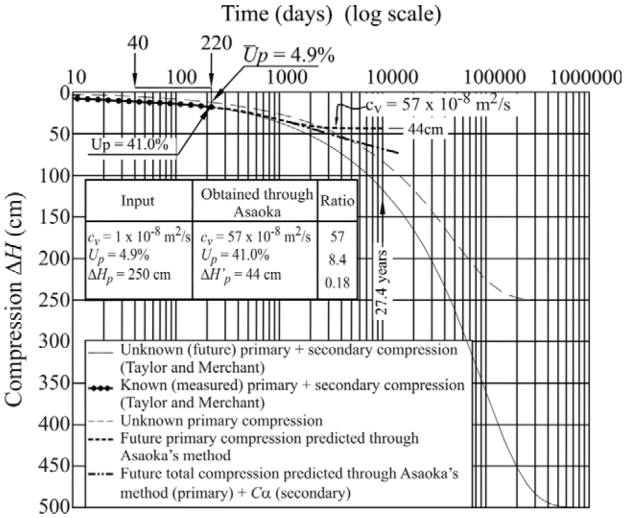

Figure 37 - Comparison of the real compression curves (as represented by input Taylor and Merchant primary and total compression curves) with the predicted primary compression curve obtained using Asaoka's method and the predicted total compression curve predicted through Asaoka's method + $C\alpha$ (secondary).

(secondary) curve illustrates the type of total compression curve which would be commonly considered in the design by drawing a straight line based on the laboratory value of $C\alpha$ tangent to the primary compression obtained through Asaoka's method.

As can be seen, the results obtained through Asaoka's method in this situation, a rather realistic situation in the authors' eyes, are totally mistaken, leading to overestimate by a factor of 57 the value of c_v. At the same time the final primary settlement is grossly underestimated as being only 18% of the real final primary settlement and the consolidation ratio at the end of the reading period is grossly overestimated, *i.e.* 41.0% against 4.9%.

Table 18 shows the results of Asaoka's method applied during the period from 40 to 220 days using $\Delta t = 10$ days to a number of known layer compression (primary plus secondary) *vs.* time curves of the Taylor and Merchant's type including the case presented above.

As can be seen in Table 18, the degree of discrepancy between the real values and the back analyzed values varies widely depending on the importance of the secondary compression (r value), the thickness of the layer (H_d) and the value of the coefficient of consolidation (c_v).

All back analyzed values, that is total primary settlement, consolidation ratio at the end of the monitoring period and c_v values, may be grossly underestimated in some cases and grossly overestimated in others. And it can be noted that the largest discrepancies concern the c_v value

Table 18 - Results of Asaoka's method applied to known layer compression (primary + secondary) *vs.* time curves of the Taylor and Merchant's type(*).

Input values							Back analyzed values through Asaoka's method			Ratio of back analyzed values over input values		
r	H_d (m)	ΔH_t (m)	ΔH_p (m)	C_v (m^2/s)	ΔH^* (cm)	U_p^* (%)	$\Delta H'_p$ (m)	$U_p^{*\prime}$ (%)	C'_v (m^2/s)	$\frac{\Delta H'_p}{\Delta H'_p}$	$\frac{U_p^{*\prime}}{U_p^*}$	$\frac{c'_v}{c_v}$
0.2	1.0	0.50	0.10	2 x 10^{-7}	34.7	100	0.48	72	2.5 x 10^{-8}	4.80	0.72	0.1
	4.0	2.00	0.40	2 x 10^{-7}	43.2	55	0.85	51	2.1 x 10^{-7}	2.13	0.92	1.1
	10.0	5.00	1.00	2 x 10^{-7}	44.1	22	0.94	47	1.1 x 10^{-6}	0.94	2.13	5.5
0.5	1.0	0.50	0.25	1 x 10^{-8}	16.0	49	0.28	57	1.6 x 10^{-8}	1.12	1.16	1.6
	1.0	0.50	0.25	5 x 10^{-8}	33.0	92	0.45	73	2.5 x 10^{-8}	1.80	0.80	0.5
	4.0	2.00	1.00	1 x 10^{-8}	15.9	12	0.29	55	2.2 x 10^{-7}	0.29	4.56	22
	4.0	2.00	1.00	5 x 10^{-8}	35.9	28	0.62	58	2.5 x 10^{-7}	0.62	2.11	5.0
	10.0	5.00	2.50	1 x 10^{-8}	18.0	4.9	0.44	41	5.7 x 10^{-7}	0.18	8.33	57
	10.0	5.00	2.50	5 x 10^{-8}	36.3	11	0.67	54	1.3 x 10^{-6}	0.27	4.93	26
0.8	1.0	0.50	0.40	1 x 10^{-8}	21.3	49.2	0.32	67	2.0 x 10^{-8}	0.80	1.35	2.0
	4.0	2.00	1.60	1 x 10^{-8}	21.4	12.3	0.33	65	3.0 x 10^{-7}	0.21	5.27	30
	10.0	5.00	4.00	1 x 10^{-8}	29.8	6.9	0.47	64	8.5 x 10^{-7}	0.12	9.23	85

(*) r = ratio of the primary settlement over the total settlement, H_d = drainage distance (= half the layer thickness), ΔH_t = layer total final compression, ΔH_p = layer primary final compression, c_v = vertical coefficient of consolidation, ΔH^* = layer total compression at t = 220 days, U_p^* = primary consolidation ratio at t = 220 days, $\Delta H'_p$ = layer primary final compression obtained through Asaoka's method, $U_p^{*\prime}$ = primary consolidation ratio at t = 220 days obtained through Asaoka's method, c'_v = vertical coefficient of consolidation obtained through Asaoka's method.

which varies from being underestimated by a factor of 10 to being overestimated by a factor of 85.

All these discrepancies are provoked by, and only by, the facts that the settlements occurring due to secondary compression are wrongly taken as part of the primary compression by Asaoka's method and that analyzed settlement values correspond to ratio consolidation values outside the proper range for which the method was devised.

As already mentioned, "when secondary compression and primary compression occur simultaneously, the volume of water expelled is larger than the volume of water which would be expelled if only primary consolidation took place. Since the initial pore pressure and gradient are not affected by the phenomenon of secondary consolidation, then the pore pressure dissipation has to be slower when secondary consolidation occurs simultaneously with primary consolidation than if it did not", which means that in this case the course of pore pressure dissipation departs from Terzaghi's theory and that the Asaoka procedure applied to the pore pressure measurements as proposed by Orleach (1983) might also lead to erroneous results.

15. Conclusions

The results obtained from the back-analysis of the SFL layer compression under area 3, with vertical drainage, performed making use of Taylor and Merchant's theory as presented in item 12 and of the results obtained from the back-analysis of the SFL layer compressions under areas 1 and 2, with radial drainage, making use of the so called "Primary Barron + secondary pseudo Taylor and Merchant" procedure as presented in item 13 in conjunction with the results of the good quality laboratory oedometer tests are synthesized in Fig. 38.

These results are presented in terms of coefficient of consolidation, in log scale, plotted *vs.* the mean vertical effective stress in the soft clay layer, in natural scale, relative to preconsolidation stresses values.

The darker shaded zone delimits the range of all c_v values determined from 7 standard oedometer tests run on an excellent quality undisturbed sample extracted close to the middle of the soft clay layer. The lighter grey hatched vertical zones indicate the range of preconsolidation stress (σ'_p) values obtained in the oedometer tests and the ranges of initial vertical effective stresses (σ'_{vi}) and of preconsolidation stresses (σ'_p) at mid height of the soft clay layer under the three embankment areas.

The observation of Fig. 38 leads to some very interesting conclusions which are presented hereafter.

• Conclusions regarding the variation of the value of c_v measured in the laboratory oedometer test with the effective stress

It can be seen in Fig. 38 that the c_v value measured in the laboratory is constant for σ'_v values up to σ'_p - 80 kPa, then decreases by a factor of almost 100 when σ'_v increases from σ'_p - 80 kPa up to σ'_p + 80 kPa, and is then constant for σ'_v values higher than σ'_p + 80 kPa up to the maximum stress presented in the graph.

As shown on Fig. 4 the c_v value for the totally remolded sample is much smaller than the c_v value for the undisturbed sample for effective stresses up to σ'_p + 80 kPa, but it

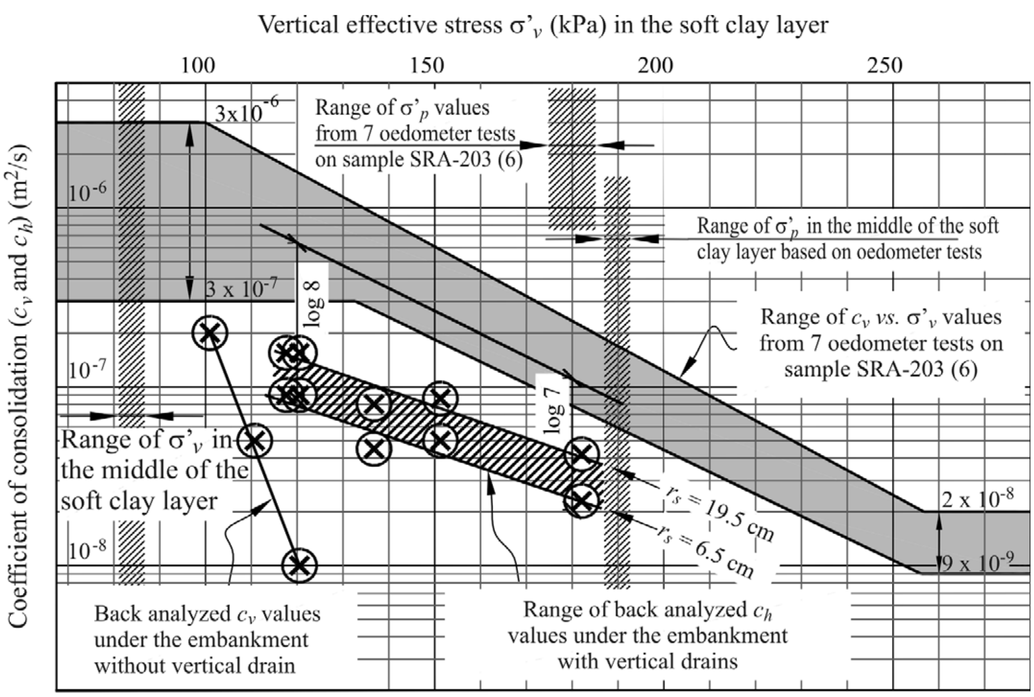

Figure 38 - Back analyzed values of field c_v and c_h *vs.* mean effective vertical stress in the soft clay layer.

is equal to the c_v value of the undisturbed clay for effective stress values above σ'_p + 80 kPa.

• Conclusions regarding the coefficient of consolidation values, c_v and c_h in the field obtained through the back-analysis of the SFL clay layer measured compressions

1. It is rather remarkable that the c_h values obtained from two totally distinct compression curve segments of layer 6, for period 1 and period 2 under area 2 for about the same value of σ'_v, are identical.

The two lines which delimit the hatched range of back analyzed c_h values under the embankment with vertical drains, that is with radial drainage, defined by ten points, show the tendency of the values of c_h to decrease when the applied effective stress increases. This decrease is very similar to the decrease of the c_v value measured in the oedometer test. This decrease is very significant even for values of σ'_v much smaller than the laboratory preconsolidation stress σ'_p and the decrease of the c_h value in the field takes place for smaller values of σ'_v than the decrease of c_v in the laboratory as should be expected, as already mentioned, due to the fact that the apparent consolidation stress (or the "yielding stress") decreases when the strain rate (which is much smaller in the field than in the laboratory) decreases.

2. In the case of vertical drainage, the values of c_v measured in the field under area 3 with no wick drain decrease much more sharply than in the case of radial drainage as shown by the plain line which goes through the points of the back analyzed c_v values under the embankment without vertical drain. The very fast decrease of the c_v value under area 3 is attributed to the fact that close to the top and to the bottom of the clay layer, the local consolidation ratio reaches values above 80% right at the beginning of the consolidation, with σ'_v close to the "pseudo final effective stress" "σ_v - u_{hid}" and since at this stress level the c_v value is close to the small virgin compression range value, then the top and bottom sublayers have a "sealing" effect on the vertical drainage of the sublayers in the middle of layer 6.

Figure 39 shows the primary consolidation ratio profile with depth within layer 6 under area 3 with no wick drain for the situation at the end of period 3 when the average primary consolidation ratio in the layer is equal to 40% as indicated in Table 12.

Of course, in the two areas with vertical drains the same high consolidation ratio and small c_v value also exist close to the top and to the bottom of the layer, but since the radial drainage is the predominant one, in this case these "sealing sublayers" have little effect on the consolidation of the layer.

3. For a given value of vertical effective stress, the value of c_v and of c_h measured in the field is quite smaller than the value of c_v measured in the laboratory oedometer test at least within the backanalyzed range and rather probably up to σ'_p + 80 kPa. In fact for the SFL Santos clay, it can be seen that the back analyzed c_h values under the embankment with vertical drains within the stress range shown in Fig. 38 are somewhere around 7 to 8 times smaller than the values of c_v in the oedometer tests up to σ'_p, with this difference decreasing as σ'_v increases. This is believed to be partly due to the already mentioned fact that the apparent "yielding stress" is smaller in the field than in the laboratory and partly due to the effect of the smeared zone around the drains.

• Conclusions regarding the efficiency of preloading with wick drains

If, as advocated by various authors like Saye (2001) the driving of the wick drains had the effect of remoulding a large volume of soil around the drains up to the point of remoulding the whole soft clay volume in the case of closely spaced drains as is the case under area 1, then the back-analyzed c_h values would not behave as shown in Fig. 37, in fact c_h values under area 1 would be much

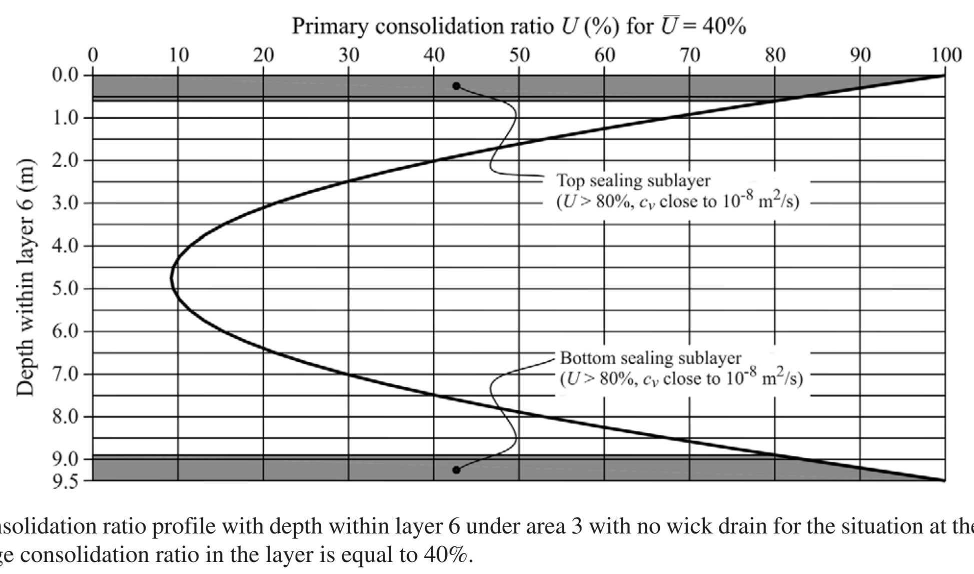

Figure 39 - Consolidation ratio profile with depth within layer 6 under area 3 with no wick drain for the situation at the end of period 3 when the average consolidation ratio in the layer is equal to 40%.

smaller than the c_h values under area 2 even for lower consolidation ratios. This is, obviously, not the case and since the coefficient of consolidation of the soil mass between the 1.2 m spaced drains is identical to the coefficient of consolidation of the soil mass between the 2.4 m spaced drains, then it can be concluded that the 1.2 m spaced drains are totally efficient in reducing the time for the primary settlement to occur by the factor of 4 ($2.4^2/1.2^2$) which is really expected from them showing, thus, their perfect efficacy. As can be clearly observed in Figs. 32, 34 and 38, this holds true whether the smeared zone radius is only 6.5 cm or 19.5 cm for the permeability ratio ks/k = 1/5. It has to be mentioned that this permeability ratio must come close to 1 for $\sigma'_v > \sigma'_p + 80$ kPa since c_v of the remolded soil comes close to c_v of the undisturbed soil in this stress range.

This result, which is contrary to many alleged published statements based on disputable results obtained through back-analysis not taking into account the simultaneous occurrence of secondary and primary consolidations, corroborates the asian and european practice where 1 meter spaced drains are most commonly used and where even smaller spacings are also used as in the case of the 0.5 m and 0.6 m spacings used in the Airbus A-380 factory site in Hamburg (Varaksin 2010).

• Conclusions regarding the working hypothesis

As mentioned in item 9, the conclusion that the c_v value measured in the field is discrepant from the c_v value measured in the laboratory, with the c_v field value typically 10 to 100 times higher than the c_v lab value, which has been repeatedly reached based on the working hypothesis that secondary consolidation would only start after the end of primary consolidation, needs, for its justification, to invoke the presence of providential very thin, continuous, layers of pervious sand, which is considered by the authors to be very far-fetched.

In many cases, this discrepancy might be due to the fact that the c_v value of the field conditions has been obtained for stress levels within the recompression or transition range since the $\Delta\sigma_v$ applied by field embankments to the foundations are normally quite small whereas the c_v value of the lab conditions has been taken as the value which corresponds to higher stress levels, within the virgin compression range, since no mention is made in most published papers about the stress levels at which these c_v values were determined.

As mentioned in item 14, in the cases when c_v values in the field and in the laboratory are compared for the same stress level, this discrepancy is provoked by, and only by, the facts that the settlements occurring due to secondary compression have been wrongly taken as part of the primary compression by Asaoka's method and all other methods based on the working hypothesis that secondary consolidation only starts after the end of primary consolidation and that analyzed settlement values correspond to ratio consolidation values outside the proper range for which the method was devised.

The conclusions reached by the authors regarding the coefficient of consolidation values c_v and c_h in the field obtained through the back-analysis of the SFL clay layer measured compressions are, on the contrary, in perfect agreement with what should be expected from common sense and from soil mechanics basic understanding of soil behavior.

This leads the authors to conclude that the working hypothesis which consists in considering that, in the field, primary consolidation and secondary consolidation occur simultaneously is the only realistic hypothesis which should be adopted. This conclusion has also been reached by most soil mechanics institutes around the world and is quickly being incorporated in engineering standards mainly in european countries.

• Conclusions regarding the high quality standard and special oedometer tests

As shown in item 3 the high quality standard oedometer tests provided reliable values of the compressibility parameters C_c and C_r and of the preconsolidation stress σ'_p which are critically important for the final design and construction of the terminal but which were not reliably known at the end of the basic design due to typical "highly scattered lab data resulting from poor quality samples" as pointed out by Ladd (2008). As shown in item 5, the high quality special oedometer tests provided the OCR value equivalent to the end of secondary consolidation, a value which is not normally called for by the designers who take for granted that secondary consolidation never finishes. The preconsolidation stresses measured in the high quality oedometer tests are much higher than the ones obtained from the large quantity of tests run during the basic design. Furthermore their values agree quite well with the OCR value equivalent to the end of secondary consolidation, defined as being equal to 2.1 in item 5, since the lab results show σ'_p values higher than 2.1 σ'_v above 15.5 m and close to 2.1 σ'_v below 15.5 m within the SFL layer. This agreement validates theses values. As has to be expected, the C_c values of the high quality oedometer tests are also quite higher than the ones obtained from the large quantity of tests run during the basic design. It also has to be mentioned that both the C_c and σ'_p values obtained from the high quality tests are quite higher than the C_c and σ'_p values which can be found in the technical litterature about Santos clay.

• Conclusions regarding the working tools

The fact is that there is no "off the shelf" practical tool available to back-analyze the monitoring data of embankment on soft soils with the working hypothesis which consists in considering that, in the field, primary consolidation and secondary consolidation occur simultaneously. This means that one still has to build his own tool before being able to start any such back-analysis.

As shown in item 10, the first tool which the authors built was the Bjerrum type abacus, plotting the strain, ε, *vs.* the vertical effective stress, σ'_v, in log scale, with the lines of equal values of strain rate, $\dot{\varepsilon}$, from the results of the special oedometer tests. But it was readily found that this tool was not usable for drainage distances different of the oedometer test one. Leroueil *et al.* (1985) had already warned about the *"Use and limitations"* of abacus built from oedometer tests results: "The rheological model proposed described by the two curves $\sigma'_p = f(\dot{\varepsilon}_v)$ and $\sigma'_v/\sigma'_p = g(\varepsilon_v)$ can be combined with a strain (or void ratio) permeability relation (ε_v - k or e - k), such as those described by Tavenas *et al.* (1983), to resolve problems of consolidation. It should be kept in mind, however, that the model has been established on small specimens and for strain rates usually encountered in the laboratory, and thus, for the moment, it must be used only under such conditions to interpret and understand clay behavior in the laboratory. It will probably be the basis for a reanalysis of the current practice for estimating settlements and settlement rates. However, before using this model for field applications where the strain rates are much lower and the clay layer much thicker, it is necessary to verify its validity under these conditions and in particular to determine how the σ'_p - $\dot{\varepsilon}_v$ curve extrapolates at low strain rates. A research programme on this problem is in progress at Laval University, Quebec."

As shown in item 11, the second tool which the authors built was the same type of abacus, but specifically built for the field conditions through extrapolating the laboratory abacus making use of Taylor and Merchant's theory. This second tool also failed to be usable.

The third tool which was tried did not really have to be built by the authors because it is already available, for the case of vertical drainage, although in the authors' knowledge it has never been used for this application before. The application of this tool needs that the final primary compression and the final secondary compression be known which, of course, asks for the reliable knowledge of the parameters provided by the high quality standard and special oedometer tests discussed above, that is C_c, C_r, σ'_p and the OCR value equivalent to the end of secondary consolidation.

Since the third tool is not applicable to the case of radial drainage and since, to the authors' knowledge, no analytical formulation of the evolution of secondary consolidation with time in the case of radial drainage can be found in the literature, then the authors built their fourth tool which is the "Pimary Barron + secondary pseudo Taylor and Merchant" as described in item 13.

In the light of all the above conclusions and considering the very good fit of the theoretical Taylor and Merchant curves with the measured compression curves under area 3 with vertical drainage and the very good fit of the theoretical "Primary Barron + secondary pseudo Taylor and Merchant" curves with the measured compression curves under areas 1 and 2 with radial drainage, it can be concluded that tool number 3 (Taylor and Merchant's theory for vertical drainage) and tool number 4 ("Primary Barron + secondary pseudo Taylor and Merchant" for radial drainage) did fulfill very satisfactorily their purpose to provide a trustworthy back-analysis of the measured compression curves of the SFL clay layers under the pilot embankment.

It is worth saying that in cases such as the one analyzed in this work, in which the stress increment is so that $\sigma'_{v0} < \sigma'_p < \sigma'_{vf}$, it is indispensable to take into consideration the variation of c_v and c_h values in the backanalysis in order to obtain a reasonable fitting between the theoretical and measured curves.

• Conclusions regarding the application of the results to the design of the improvement of the soft layer

It can be concluded, then, that the Taylor and Merchant theory can be used to predict the consolidation of the SFL clay layer with vertical drainage and the "Primary Barron + secondary pseudo Taylor and Merchant" procedure can be used to predict the consolidation of the SFL clay layer with radial drainage in any area of the Terminal, taking into account the proper local geometry and drainage conditions of the layer, as long as this prediction is done for various succeeding periods of time, using for each period the proper c_v (or c_h) value, estimated in function of the value of σ'_v applied during each period in the light of Fig. 38, although it might be expected that "the real value of the secondary compression might always be equal to or higher than the predicted one mainly in the middle of the process".

16. Final Comments

Based on the experience acquired during the five years which elapsed between the first soils report written in 2005 for the beginning of the basic design to the final interpretation of the pilot embankment data in 2010, the following comments come to the authors' minds:

• the soft marine Santos clay layer with SPT blow count from 0 to 4 named SFL (River lagoon sediments) is constituted of distinct layers, each with its specific compression and consolidation parameters, and has to be described and modeled as a number of layers as shown in Fig. 5,

• most routine oedometer tests which are performed on so called "undisturbed samples" fail to provide trustworthy values of compression and consolidation parameters and their only contributions to the knowledge of the subsoil conditions are the unit weight, the water content and the void ratio values,

• only high quality oedometer tests on good quality "undisturbed" samples provide trustworthy compressibility and consolidation parameters, and only oedometer tests with the highest achievable quality should be performed which implies that only proven first class soils investigation firms and laboratories should be contracted with their services closely supervised by the design engineer,

• special oedometer tests to determine the OCR value equivalent to the end of secondary consolidation should be performed for every design of embankments on soft clayey foundation,

• field c_v and c_h values are found to be smaller than or equal to (depending on the stress level) lab c_v values for the same effective stress level, and not the contrary,

• aging is the cause of overconsolidation which prevails on the dune action and sea level lowering for depths higher than 10 to 15 m in Barnabé Island area in the Santos harbour channel,

• all soft clay parameters obtained through Asaoka's method should be discarded and all data of embankment monitoring should be re-visited with the working hypothesis that primary consolidation and secondary consolidation occur simultaneously,

• practicing engineers are badly in need of reliable realistic working tools which they can use to back-analyze embankment monitoring and also to predict the behavior of the embankments which they design and build taking into account the simultaneous occurrence of primary and secondary consolidations,

• the literature versing on the field behavior of soft clay taking into account the simultaneous occurrence of primary and secondary compressions is very abundant and this is much more so than when Leroueil *et al.* (1985) wrote that "this abundant literature has modified neither the common practice based on the Terzaghi theory nor the way of thinking on clay behavior", however no practical tool has emerged from all this literature which can readily be used in common practice,

• in the lack of better practical available methods, the Taylor and Merchant's formulation and the "Primary Barron + secondary pseudo Taylor and Merchant" procedure used by the authors allow for reasonably reliable modeling of the soft clay field behavior, taking into account the simultaneous occurrence of primary and secondary consolidations, but since in Taylor and Merchant's own words, this formulation is "based largely on physical intuition" and "the main value of this theory is not in the expression of a secondary compression time law" it is to be hoped that, in the near future, some progress will be made in the understanding of the mechanism and in the expression of the evolution either of secondary consolidation or of total consolidation (without the need of a distinction between primary and secondary) with time,

• the lack of practical tools to take into account the simultaneous occurrence of primary and secondary consolidations has been, in the authors' understanding, the main hindrance to changes in common practice and this situation has much to do with the very little communication and lack of joint endeavour between practicing engineers and researchers.

Acknowledgments

The authors are grateful to EMBRAPORT in the person of Mr. Juvêncio Terra, for authorizing the use of the pilot embankment monitoring data to produce and publish this paper, and to Construtora Norberto Odebrecht in the person of Mr. Gilberto Gomes, who was always available to the authors to provide the instruments readings and all other relevant informations.

References

Aguiar, V.N. (2008) Características de Adensamento da Argila do Canal do Porto de Santos na Região da Ilha Barnabé. M.Sc. Thesis, COPPE/UFRJ, Rio de Janeiro, 223 pp.

Andrade, M.E.S. (2009) Contribuição ao Estudo das Argilas Moles da Cidade de Santos. M.Sc. Thesis, COPPE/UFRJ, Rio de Janeiro, 397 pp.

Asaoka, A. (1978) Observational Procedure of Settlement Prediction, Soils and Foundations, Japanese Society of Soil Mechanics Foundation Engineering, v.18:4, pp. 87-101.

Barron, R.A. (1948) Consolidation of fine-grained soils by drain wells. Transactions, ASCE, SM6, v. 113:2346, pp. 718-742.

Bjerrum, L. (1972) Embankments on Soft Ground, Proceedings of the Specialty Conference on Performance of Earth and Earth – Supported Structures, ASCE Soil Mechanics and Foundations Division, Purdue University, Lafayette, Indiana, USA, volume II, pp. 1-54.

Carvalho, S.R.L. (1997) Uma Teoria de Adensamento com Compressão Secundária. PhD Thesis, COPPE-UFRJ, Rio de Janeiro, 265 pp.

Christie, I.F. (1964) A Re-appraisal of Merchant's Contribution to The Theory of Consolidation, Géotechnique, v. 14:4, pp. 309-320.

Coutinho, R.Q. (2007) Characterization and Engineering Properties of Recife Soft Clays – Brazil, Characterization and Engineering Properties of Natural Soils, Proceedings of the Second International Workshop on Characterisation and Engineering Properties of Natural Soils, Singapore, 29 November-1 December 2006, K.K. Phoon, D.W. Hight, S. Leroueil, and T.S. Tan, Taylor & Francis Group, London, Chapter 12, pp. 2049-2100.

Feijó, R.L. (1991) Relação entre a Compressão Secundária, Razão de Sobreadensamento e Coeficiente de Empuxo no Repouso. M.Sc. Thesis, COPPE/UFRJ, Rio de Janeiro, 167 pp.

Feijó, R.L. & Martins, I.S.M. (1993) Relação entre a Compressão Secundária, OCR e K0. Proc. Simpósio Geotécnico Comemorativo dos 30 Anos da COPPE/UFRJ, COPPEGEO 93, COPPE/Federal University of Rio de Janeiro, Rio de Janeiro, pp. 27-40.

Garlanger, J.E. (1971) The Consolidation of Clays Exhibiting Creep Under Constant Effective Stress, Norwegian Geotechnical Institute, Internal Report, n. 50302, Oslo, pp.71-78.

Gibson, R.E. & Lo, K.Y. (1961) A Theory of Consolidation for Soils Exhibiting Secondary Compression, Publication Nº. 41, Norwegian Geotechnical Institute, Oslo, pp. 1-16.

Gonçalves, H.H.S. (1992) Análise Crítica Através de Modelos Visco-Elásticos dos Resultados de Ensaios de Laboratório para Previsão de Recalques dos Solos da Baixada Santista. PhD Thesis, USP, São Paulo, 184 pp.

Holl, D.L. (1940) Stress Transmission in Earth, Proc. High Res. Board, v. 20, pp. 709-721.

Ladd, C.C. & De Groot, D.J. (2003) Recommended Practice for Soft Ground Characterization, Arthur Casagrande Lecture, Proceedings of the 12th Panamerican Conference on Soil Mechanics and Geotechnical Engineering, Massachusetts Institute of Tecnology, Cambridge, June 22-25, pp. 1-55.

Ladd, C.C. (2008) Commentary: Soft Ground Geotechnics. Geo-Strata – Geo Institute of ASCE, v. 9:2, March/April 2008, pp. 10-11.

Larsson, R.; Bengtsson, P.E. & Eriksson, L. (1997) Prediction of Settlements of Embankments on Soft, Fine-Grained Soils – Calculation of Settlements and Their Course with Time, Information 13E, Swedish Geotechnical Institute, Linköping, 52 pp.

Leroueil, S.; Kabbaj, M.; Tavenas, F. & Bouchard, R. (1985) Stress-Strain Rate Relation for the Compressibility of Sensitive Natural Clays, Geotechnique, v. 35:2, pp. 159-180.

Martins, I.S.M. (2005) Algumas Considerações Sobre Adensamento Secundário. Conference given at Clube de Engenharia, Rio de Janeiro, 47 pp.

Martins, I.S.M.; Santa Maria, P.E.L. & Santa Maria, F.C.M. (2009) Laboratory Behaviour of Rio de Janeiro Soft Clays, Part 1: Index and Compression Properties, Soils and Rocks, v. 32:2, pp. 100-103.

Massad, F. (1989) Settlements of Earthworks Construction on Brazilian Marine Soft Clays in the Light of their Geological History, Proc. XII International Conference on Soils Mechanics and Foundation Engineering, Rio de Janeiro, v. 3. pp. 1749-52.

Massad, F. (2009) Solos Marinhos da Baixada Santista, Características e Propriedades Geotécnicas. Oficina de Textos, São Paulo, 247 pp.

Orleach, P. (1983) Techniques to Evaluate the Field Performance of Vertical Drains, Master Thesis, Massachusetts Institute of Technology, 159 pp.

Poulos, H.G. & Davis, E.H. (1974) Elastic Solutions for Soil and Rock Mechanics, John Wiley and Sons, New York, 411 pp.

Saye, S.R. (2001) Assessment of Soil Disturbance by The Installation of Displacement Sand Drains and Prefabricated Vertical Drains, GSP n. 119, pp. 325-362.

Schofield, A. & Wroth, P. (1968) Critical State Soil Mechanics, McGraw-Hill, London, 310 pp.

Tavenas, F.; Jean, P.; Leblond, P. & Leroueil, S. (1983) The Permeability of Natural Soft Clays: Part II, Permeability Characteristics. Can. Geotech. J. v. 20:4, pp. 645-660.

Taylor, D.W. & Merchant, W. (1940) A Theory of Clay Consolidation Accounting for Secondary Compression, Journal of Mathematics and Physics, v. 19:3, pp. 167-185.

Taylor, D.W. (1948) Fundamentals of Soils Mechanics, Wiley International Edition. J. Wiley & Sons, Cambridge, Massachusetts, pp. 700.

Teh, C.I. & Houlsby, G.T. (1991) An Analytical Study of The Cone Penetration Test in Clay, Géotechnique, v. 41:1, pp. 17-34.

Terzaghi, K. & Frohlich, O.K. (1936) Theorie der setzung von tonschichten. Franz Deuticke, Vienna (translated into French: Théorie des Tassements des Couches Argileuses. Dunod, Paris, 1939), 166 pp.

Varaksin, S. (2010) Vacuum Consolidation, Vertical Drains for the Environment Friendly Consolidation of Very Soft Polluted Mud at the Airbus A-380 Factory Site, Symposium on New Techniques for Design and Construction in Soft Clays, Guaruja, Oficina de Textos, São Paulo, pp. 87-102.

Vieira, L.O.M. (1988) Contribuição ao Estudo de Adensamento Secundário. M.Sc. Thesis, COPPE/UFRJ, Rio de Janeiro, 137 pp.

List of Symbols

w: Natural water content

z: Depth

γ: Unit weight

H: Layer thickness

H_d: Drainage distance

LL: Liquid limit

PI: Plasticity index

a_v: Coefficient of compressibility (primary + secondary) (Taylor & Merchant)

a'_v: Coefficient of primary compressibility (Taylor & Merchant)

b: Berm thickness

C_c: Compression index

C_e: Expansion index

C_r: Recompression index

$C\alpha$, $C_{\alpha\varepsilon}$: Coefficient of secondary consolidation (according to the theory which considers secondary consolidation to occur at the end of primary consolidation)

c_v: Vertical coefficient of consolidation

c_{v1}: Vertical coefficient of consolidation in the recompression domain

c_{v2}: Vertical coefficient of consolidation in the normally consolidation domain

c'_v: Vertical coefficient of consolidation obtained through Asaoka's method
c_h: Horizontal coefficient of consolidation
c_{h1}: Horizontal coefficient of consolidation in the recompression domain
D, Hd: Vertical drainage distance
D_{eq}: Equivalent vertical drainage distance
e_0: Initial void ratio (after sampling)
e: Void ratio
e_i: Initial void ratio corresponding to initial (*in situ*) vertical effective stress
e_p: Final void ratio at end of primary consolidation (without secondary)
e_s: Final void ratio at end of primary and secondary consolidation
El.: Elevation
F: Secondary compression factor
k: Horizontal permeability coefficient of undisturbed soil
k_s: Horizontal permeability coefficient of smear zone
r: Ratio of the primary settlement over the total settlement
r_s: Radius of the smear zone
r_w: Radius of the drain
R: Mean radial drainage distance
S_u: Undrained in-situ shear strength
S_u(VT): Undrained shear strength obtained from the vane test
T: Time factor
t: Time
U (or U_p or $U_{primary}$): Primary consolidation ratio
U_p*: Primary consolidation ratio at t = 220 days
U_p*': Primary consolidation ratio at t = 220 days obtained through Asaoka's method
U_t (or $\overline{B}$): Mean primary consolidation ratio at time t
U_{p+s}: Aggregate consolidation ratio (apud Taylor and Merchant)
u_{hid}: Hydrostatic water pressure
$\overline{U}_p$: Average primary consolidation ratio
μ: Coefficient of secondary compression (apud Taylor & Merchant)
W.L.: Water level
ε (or ε' or ε_v): Vertical strain
$\dot{\varepsilon}$ (or $\dot{\varepsilon}_v$): Vertical strain rate
$\dot{\varepsilon}_{0p}$: Expected vertical strain rate in the early phase of terminal operation
ε_{0p}: Expected future vertical strain during terminal operation
$\dot{\varepsilon}_t$: Measured vertical strain rate in individual soft clay layer at time t
ε_t (or ε'_t): Measured vertical strain in individual soft clay layer at time t
ε_f: Final vertical strain corresponding to primary + secondary consolidation
ε_p: Final vertical strain corresponding to primary consolidation
ε_{pt}: Vertical strain due to primary consolidation at time t
ε_s: Final vertical strain corresponding to secondary consolidation
ε_{st}: Vertical strain due to secondary consolidation at time t
σ_v: Total stress
σ_v - u_{hid}: Pseudo final effective stress
σ'_p: Preconsolidation stress
σ'_v (or P): Vertical effective stress
σ'_{vi}: Initial vertical effective stress
σ'_{vf}: Final effective vertical stress
σ'_{vt}: Mean effective stress in the layer at time t
$\Delta\sigma_v$ (or Δσ): Vertical stress increase
$\Delta\sigma'_v$: Effective vertical stress increase
$\Delta\sigma'_{v1}$: Vertical effective stress change at removing of surcharge
$\Delta\sigma'_{v2}$: Vertical effective stress increase during operation
ΔH: Layer compression
ΔH_n, ΔH_{n-1}: Layer compression of orders n and n-1 in Asaoka's construction
ΔH*: Layer compression at t = 220 days
ΔH_p: Layer primary compression
$\Delta H'_p$: Layer primary compression obtained through Asaoka's method
ΔH_{pj}: Primary compression at end of period j
ΔH_s: Layer secondary compression
ΔH_{sj}: Secondary compression at end of period j
ΔH_t: Layer total compression
ΔH_{tj}: Total (primary + secondary) compression at end of period j
ΔH_m: Measured layer compression in October 2009
$(\Delta H_p)'$: Pseudo final primary compression
$(\Delta H_s)'$: Pseudo final secondary compression
$(\Delta H_t)'$: Pseudo final total compression
Δe: Variation of void ratio
Δe_p: Variation of void ratio corresponding to primary compression
Δe_s: Variation of void ratio corresponding to secondary compression
$\Delta\varepsilon_v$: Vertical strain increase
Δt: Time increment
∂e: Infinitesimal void ratio increment
∂t: Infinitesimal time increment
α: Slope of stress *vs.* void ratio (primary + secondary compression) curve (Taylor & Merchant)
α': Slope of stress *vs.* void ratio (primary compression curve Taylor & Merchant)

Numerical Simulations and Full Scale Behavior of SDCM and DCM Piles on Soft Bangkok Clay

P. Voottipruex, D.T. Bergado, T. Suksawat, P. Jamsawang

Abstract. A new kind of reinforced Deep Cement Mixing (DCM) pile, namely: Stiffened Deep Cement Mixing (SDCM) pile is introduced to mitigate the problems due to the low flexural resistance, lack of quality control in the field and unexpected failure of DCM pile. The SDCM pile consists of DCM pile reinforced with precast concrete core pile. Previously, the full scale embankment loading test on soft Bangkok clay improved by SDCM and DCM piles was successfully conducted and monitored. The parameters were also derived from an earlier full scale load tests to failures and subsequent simulations. To continue the study on the behavior of SDCM and DCM piles, the 3D finite element simulations and parametric study have been done. The simulation results of the full scale embankment loading test indicated that the surface settlements decreased with increasing lengths of the concrete core piles from 4 to 6 m but slightly reduced from 6 to 7 m as well as slightly decreased with increasing sectional areas in the SDCM piles. In addition, the lateral movements of the embankment decreased by increasing the lengths (longer than 4 m) and, to a lesser degree, the sectional areas of the concrete core piles in the SDCM piles. The results of the numerical simulations closely agreed with the observed data from full scale field tests and successfully verified the parameters affecting the performances and behavior of both SDCM and DCM piles.

Keywords: SDCM piles, DCM piles, bearing capacity, lateral load, settlement, lateral movement, piled embankment.

1. Introduction

Although DCM pile has many advantages with various applications, failure caused by pile failure can occur especially when subjected to the lateral loads. Moreover, the unexpected lower strength than the design commonly occurs due to lack of quality control during construction. Thus, DCM pile still fails by pile failure mode which is lower than the soil failure mode particularly at the top of DCM pile due to low strength and stiffness as shown in Fig. 1 (a). In addition, Fig. 1 (b) shows the testing results of DCM pile on the soft Bangkok clay by Petchgate *et al.* (2003). About half of DCM piles failed by pile failure instead of soil failure. Consequently, the bearing capacity of DCM pile can be lower than the design load of 10 tons due to pile failure. Both pile and soil failures are illustrated in Fig. 1a.

To mitigate the above-mentioned problem, a new kind of composite pile named Stiffened DCM (SDCM) pile is introduced. This composite pile is composed of an inner precast concrete pile hereinafter called concrete core pile and an external DCM pile socket, where the high strength concrete pile is designed to bear the load, and DCM pile socket acts to transfer the axial force into the surrounding soil by skin friction.

The acceptance of numerical simulations in geotechnical problems is growing and finite element methods are increasingly used in the design of pile foundations. In this study, the full scale tests results were further simulated in order to study the parameters that affect the behavior of both the SDCM and DCM piles under the axial compression and lateral pile load as well as embankment load tests. Subsequently, the confirmed and verified parameters were used in the numerical experiments. Previously, the results of laboratory investigations of SDCM and their numerical simulations by Jamsawang *et al.* (2008) yielded useful parameters. The previous results served as the basis for the full scale pile load and embankment tests. Subsequently, numerical simulations were performed by Suksawat (2009) to back-calculate the strength parameters as well as to perform parametric study. Consequently, the results are presented in this paper.

2. Stiffened Deep Cement Mixed (SDCM) Piles

Stiffened Deep Cement Mixed (SDCM) piles are a composite structure of concrete piles and deep cement mixed piles combining the advantages of both components as shown in Fig. 2a,b. A pre-stressed concrete stiffer core is installed by inserting into the center of a DCM pile immedi-

P. Voottipruex, Lecturer, Department of Civil Engineering, King Mongkut's University of Technology North Bangkok, Thailand. e-mail: pnv@kmutnb.ac.th.
D.T. Bergado, Professor in Geotechnical and Earth Resources Engineering, School of Engineering and Technology, Asian Institute of Technology, Klongluang, Pathumthani, 12120 Thailand. e-mail: bergado@ait.ac.th.
T. Suksawat, Center Manager, GCOE-KU Project, Geotechnical and Earth Resources Engineering, School of Engineering and Technology, Asian Institute of Technology, Klongluang, Pathumthani, 12120 Thailand. e-mail: taweephong@ait.ac.th.
P. Jamsawang, Lecturer, Department of Teacher Training in Civil Engineering, King Mongkut's University of Technology North Bangkok, Bangkok 10800, Thailand. e-mail: pitthaya_nont@hotmail.com.
Submitted on November 3, 2010; Final Acceptance on December 15, 2011; Discussion open until July 31, 2012.

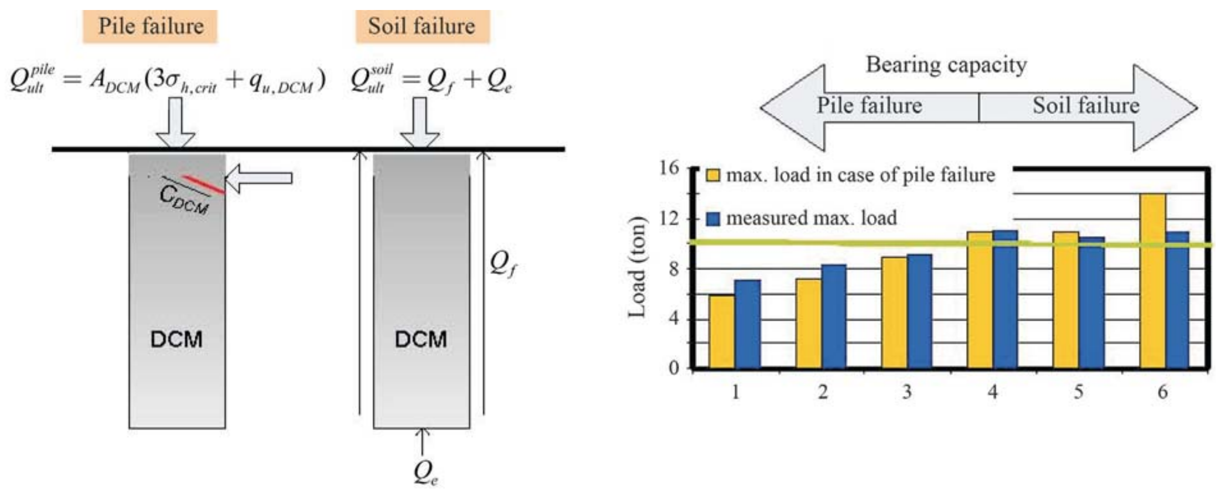

Figure 1 - Low quality of DCM piles on Soft Bangkok Clay (Petchgate *et al.*, 2003).

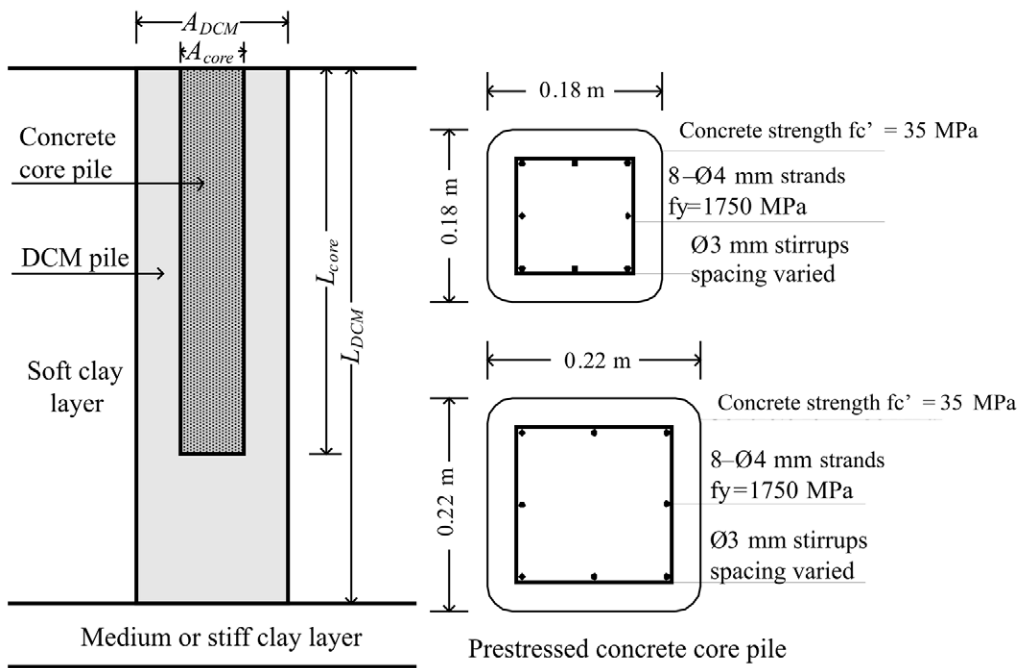

Figure 2 - (a) Schematic of SDCM pile, (b) Details of prestressed concrete core piles.

ately after the construction of wet mixing DCM pile. The two parts of the composite piles work together by supporting and transferring the vertical load effectively to the DCM pile and to the surrounding soil. In the SDCM pile, the DCM pile forms the surrounding outer layer supporting the concrete core pile increasing its stiffness and resisting compressive stress along the pile shaft. The dimensions of the two units should be such that both work together effectively and mobilize the full strength of the surrounding clayey soil. This novel method of improving the strength of DCM pile has been given different names by different researchers such as concrete cored DCM pile (Dong *et al.*, 2004), composite DMM column (Zheng & Gu, 2005) and stiffened deep cement mixed (SDCM) column method (Wu *et al.*, 2005).

2.1. DCM pile

The DCM pile is used as the socket pile in order to carry and transfer the load from concrete core pile to the surrounding soil. In this study, the DCM pile was constructed by wet mixing with 0.60 m diameter and 7.00 m length.

2.2. Concrete core pile

The Stiffened Deep Cement Mixing (SDCM) pile need some material to enhance its stiffness like steel pile, timber and concrete pile etc. The prestressed concrete pile is more suitable than the other materials because it is cheaper than the steel pile and easier to manufacture. Moreover, the quality of prestressed concrete is better when comparing to the timber piles. Thus, the prestressed concrete core pile was proposed to bear the axial load in compression pile load test and resist lateral loads when subjected to the horizontal loads in SDCM pile.

2.3. Interface friction

The interface friction or adhesion means the ratio of the adhesive strength, τ_u, to the unconfined compression strength, q_u, of the clay cement. This value represents the frictional or adhesion resistance per unit cement soil strength provided on per unit side area of the concrete core pile. It is denoted by R_{inter} and calculated by following equation:

$$R_{inter} = \frac{\tau_u}{q_u} \tag{1}$$

where τ_u is the adhesive strength that can be calculated from the ultimate frictional strength P_u divided by surface area of the stiffer core using the following equation:

$$\tau_u = \frac{P_u}{AL} \tag{2}$$

where A is the cylindrical surface area and L is the length of concrete core pile.

Many researchers have reported that the R_{inter} varies from 0.348 to 0.426 with an average value of 0.4 (Wu *et al.*, 2005 and Bhandari, 2006).

3. Project Site and Subsoil Profile

The full scale axial and lateral pile load tests were performed by Shinwuttiwong (2007) and Jamsawang (2008) and the full scale embankment load test was conducted by Jamsawang (2008) within the campus of Asian Institute of Technology (AIT). The site is situated in the central plains of Thailand famous for its thick layer deposit of soft Bangkok clay. The foundation soils and their properties at the site are shown in Fig. 3. The uppermost 2.0 m thick layer is the weathered crust, which is underlain by 6.0 m thick soft to medium stiff clay layer. A stiff clay layer is found at the depth of 8.0 m from the surface. The undrained shear strength of the soft clay obtained the from field vane test was 20 kPa and the strength of the stiff clay layer below the depth of 8.0 m from the surface is more than 40 kPa (Bergado *et al.*, 1990). Other parameters are shown in Table 1.

The strength of the concrete piles was found to be 35 MPa. Two lengths of concrete core piles were used in the field test, namely: 4.0 m and 6.0 m. However, for the numerical simulation the length of the concrete pile was varied from 1.00 m to 7.00 m with 1.0 m increase to evaluate the effect of the lengths of the core pile on the capacity of the SDCM pile. The Mohr-Coulomb model was recommended to simulate for mass concrete core pile instead of linear elastic model because its stiffness can be overesti-

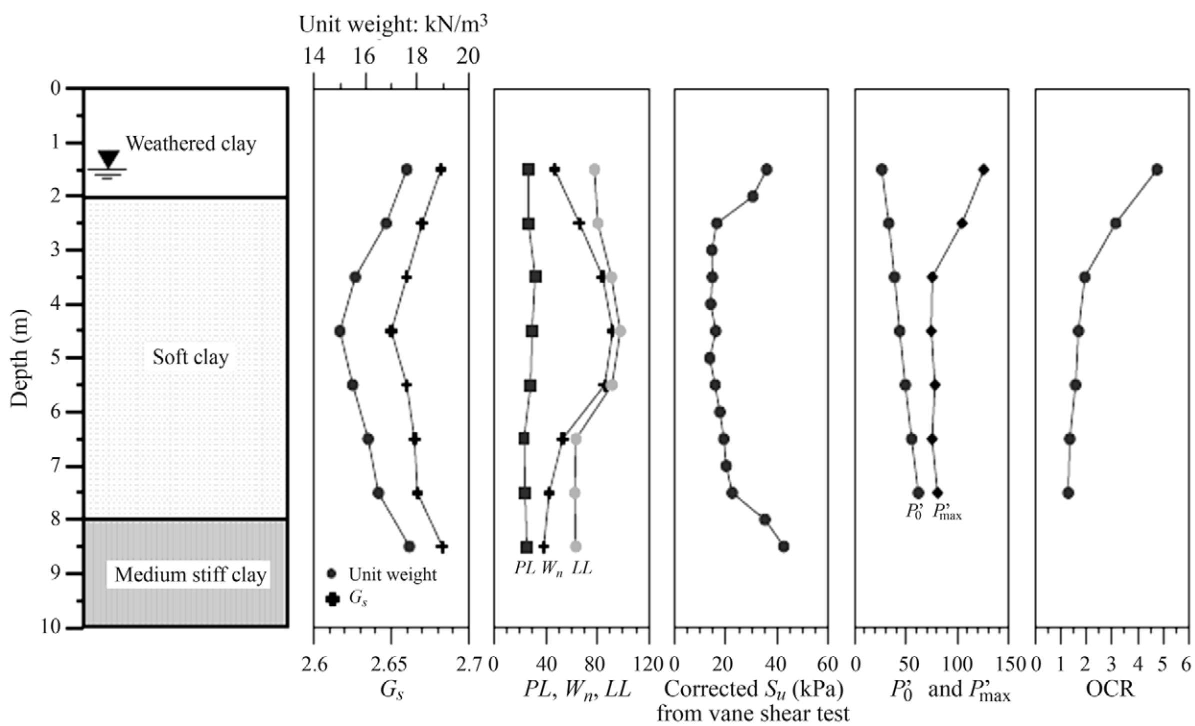

Figure 3 - Subsoil profile within the campus of AIT.

Table 1 - Soil models and parameters used in 3D FEM simulation.

Materials	Depth (m)	Model	γ (kN/m^3)	Material behavior	E'_{ref} (kPa)	ν	λ^*	κ^*	C' (kPa)	ϕ' (°)	k_x (m/day)	OCR	Tensile strength (kPa)
Subsoil													
Weathered crust	0-2.0	MCM	17	Undrained	2500	0.25			10	23	$1\text{x}10^{-3}$		
Soft clay	2.0-8.0	SSM	15	Undrained			0.10	0.02	2	23	$4\text{x}10^{-4}$	1.5	
Medium stiff clay	8.0-10.0	MCM	18	Undrained	5000	0.25			10	25	$2\text{x}10^{-4}$		
Stiff Clay	10.0-30.0	MCM	19	Undrained	9000	0.25			30	26	$4\text{x}10^{-4}$		
Foundation													
Concrete core pile		MCM	24	Drained	$2.8\text{x}10^7$	0.15			8000	40			5000
DCM pile (with interface elements)		MCM	15	Undrained	30000-60000	0.33			100-300	30	0.012	0-100	
Steel plate		LEM	-	Non-porous	$2.1\text{x}10^8$	0.15							

Note: SSM = Soft Soil Model, MCM = Mohr-Coulomb Model, LEM = Linear Elastic Model.

mated if the tensile strain is large enough to crack the concrete (Tand *et al.*, 2008).

4. Full Scale Axial and Lateral Pile Load as Well as Embankment Load Tests

The DCM pile was constructed by jet grouting method employing a jet pressure of 22 kPa and cement of 150 kg/m^3 of soil. The values of unconfined compressive strength of DCM obtained from field specimens ranged from 500 kPa to 1,500 kPa with average value of 900 kPa while the modulus of elasticity ranged from 50,000 kPa to 150,000 kPa with average value of 90,000 kPa indicating the empirical relation of $E_{50} = 100\,q_u$. The full scale pile load test piles consisted of 16 SDCM and 4 DCM piles. For the DCM pile 0.60 m. in diameter and 7.00 m length was used and SDCM with lengths ranging from of 4 and 6 m was utilized. The layout of full scale DCM and SDCM piles shown in Fig. 4 which indicates axial compressive (C), lateral (L) and pullout (P) pile load tests.

4.1. Axial compression pile load test

The axial compression pile tests were conducted on both the DCM and SDCM piles. As shown in Fig. 2b, the concrete core piles consisted of 0.18 m and 0.22 m. square piles. The DCM piles has 0.60 m. diameter. The load was applied increasing at 10 kN interval until pile failure. The bearing capacities of the 0.18 m square core pile with 4.00 m and 6.00 m were 265 kN and 300 kN, respectively, while the corresponding value for 0.22 m. square core pile with 4.00 m and 6.00 m were 275 kN and 315 kN, respectively. The bearing capacities of DCM piles were found to be 200 and 140 kN. The result from full scale pile load tests indicated that both the length and section area of concrete core piles increased the bearing capacities and reduced the settlement of SDCM piles. However, it was demonstrated that length was more dominant than the section area of the concrete core pile. Finally, the bearing capacity of SDCM pile is higher than the DCM pile. The ultimate bearing capacities of all piles were determined according to the failure criterion of Butler &Hoy (1977).

4.2 Lateral pile load test

The full scale lateral pile load tests were also conducted on designated SDCM piles. The 0.18 m and 0.22 m square core piles with 0.60 m DCM diameter were used. The horizontal load was applied depth at -0.30 m at the top of pile with increasing lateral load until pile failure. The maximum lateral load of the 0.18 m square core pile with length of 3.50 m and 5.50 m were 33 kN and 34.5 kN, respectively, while the maximum lateral load of the 0.22 m square core pile with length of 3.50 m and 5.50 m were 44.5 kN and 45.5 kN, respectively. By contrast, the maximum lateral load of DCM piles were only 3.5 and 2.5 kN for DCM L-1 and DCM L-2, respectively. The result indicated that the length of concrete core pile did not affect

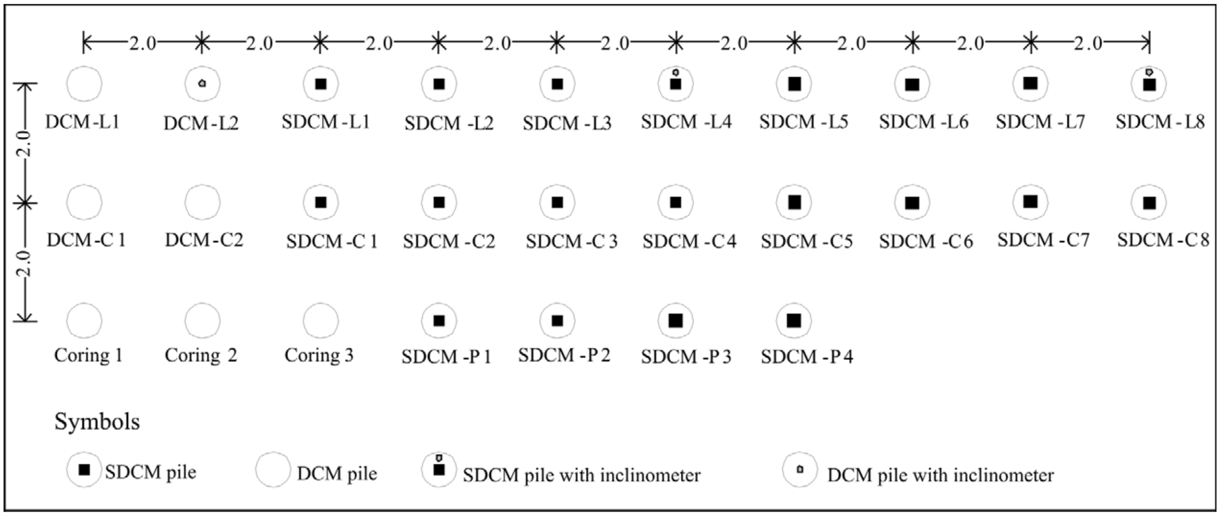

Figure 4 - Pile load test layout.

much the lateral capacity. However, the section area of the concrete core affects much the lateral capacity of the SDCM pile. Both the length and section area were significant factors in reducing the pile displacement when the concrete core pile length was increased from 3.50 m to 5.50 m. Finally, the lateral bearing capacity of SDCM pile was found to be higher than the DCM pile.

4.3. Embankment load test

Jamsawang (2008) and Jamsawang *et al.* (2008, 2009a,b) constructed the full scale test embankment on improved soft Bangkok clay using two different methods namely: stiffened deep cement mixing (SDCM) pile and deep cement mixing (DCM) pile. The DCM pile consisted of 7 m long and 0.6 m in diameter. The objectives of this research work were to investigate ground improvement performances under embankment loading and to verify the related design parameters. Surface settlements and lateral movements were monitored during and after the embankment construction for two years. Figure 5a,b shows the plan layout and side view of the embankment, respectively, together with the DCM and SDCM piles.

5. Procedure of Simulation

5.1. Procedure of numerical simulation of the axial compression and lateral pile load tests

Both axial compression pile load test and lateral pile load test were simulated by PLAXIS 3D Foundation software. The soft soil model (SSM) was used for the soft clay layer and the Mohr-Coulomb model (MCM) was used for the other elements including DCM and SDCM piles. Almost all of element used 15 node wedge element except plate and interface elements used the structural elements. The plate elements are based on the 8 node quadrilateral elements. The interface elements are different from the 8 node quadrilaterals that they have pairs of node with zero thickness instead of single node. The simulation model is indicated in Fig. 6. The soil models together with parameters are tabulated in Table 1.

The initial stage was setup as the in-situ state to generate the initial in-situ stresses. The DCM pile and concrete core pile were then added to the simulation. The excavation stage was simulated by removing 1.00 m of soil around the pile for the axial compression pile load test and 1.5 m of the soil for the lateral pile load test. In the subsequent stages, a plate was used to distribute the load in the axial pile test and the pile cap was added to distribute the load in the lateral pile test.

After the addition of plate in case of axial load test and the pile cap in the lateral load case, the loading of the piles was commenced. For axial compression pile load test, the vertical load was increased in interval of 10 kPa until failure. For the lateral pile load test, the horizontal load was increased in interval of 5 kPa until failure. The programming of stage loading is illustrated in Fig. 7.

5.2. Procedure of numerical simulation for the full embankment load test

The embankment is supported by two types of piles consisting of the 16-SDCM piles and 16-DCM piles (Figs. 5a,b). For the purpose of simulation, the length of concrete core piles in SDCM piles were varied from 3.00 to 7.00 m with varied sectional dimensions from 0.22 x 0.22 to 0.30 x 0.30 m. The embankment discretization model using Plaxis Foundation 3D software (Brinkgreve & Broere, 2006) is illustrated in Fig. 8a,b. The soil parameters and models used in the numerical simulations are tabulated in Table 1. The soft soil model (SSM) was used for the soft clay layer and the Mohr-Coulomb model (MCM) was used for other elements including DCM and SDCM piles. The basic soil elements were represented by 15 node wedge element except the plate and interface elements. The DCM pile was modeled by volume elements that can simulate deformation stresses. The prestressed concrete core pile was modeled as "massive pile" composed of volume elements. The interface elements were modeled as pairs of corresponding nodes with zero distance between each pair as stated in the previous section. Interface elements required strength reduction factor, R_{inter}, for soil strengths mobilized at the interface (see Table 1). The first phase was the initial

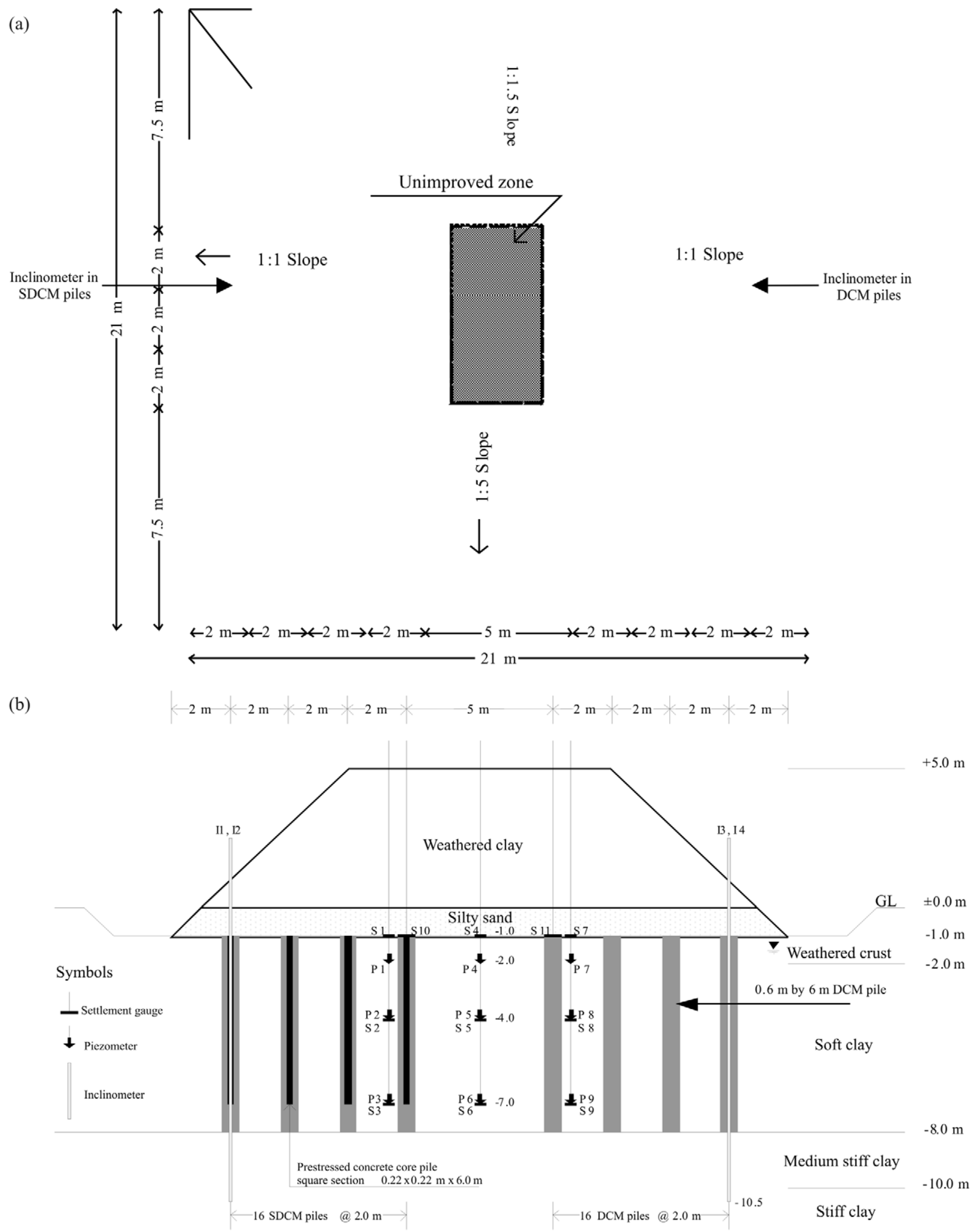

Figure 5 - (a) Top view of the test embankment. (b) Side view and location of instrument of the embankment.

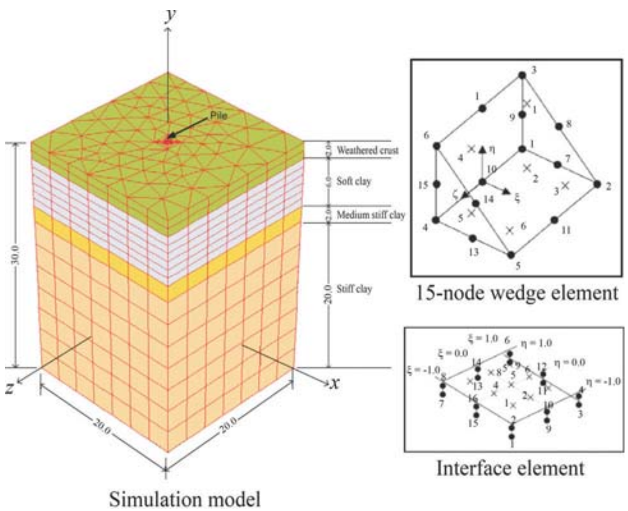

Figure 6 - Axial and lateral pile load test simulation model.

stage that was setup as the in-situ state (k_0 procedure) to generate the initial in-situ stresses. In the second phase, the DCM pile and concrete core pile were installed. Next step was the excavation stage of the uppermost 1.00 m of soil. The subsequent steps consisted of filling the silty sand at the first phase at the base and, subsequently, filled by weathered clay. Afterwards, the surface settlement at the top of SDCM, DCM and surrounding soil were checked after 60, 90, 120, 150, 180, 240, 300, 360, 420, 510 and 600 days, respectively. The details of the stage calculations are illustrated in Fig. 9.

6. Results

6.1. Axial compression pile simulation

As shown in Fig. 4, DCM C-1 and DCM C-2 were constructed for full scale load tests. The appropriate parameters from back analysis for mixture of cement-clay cohe-

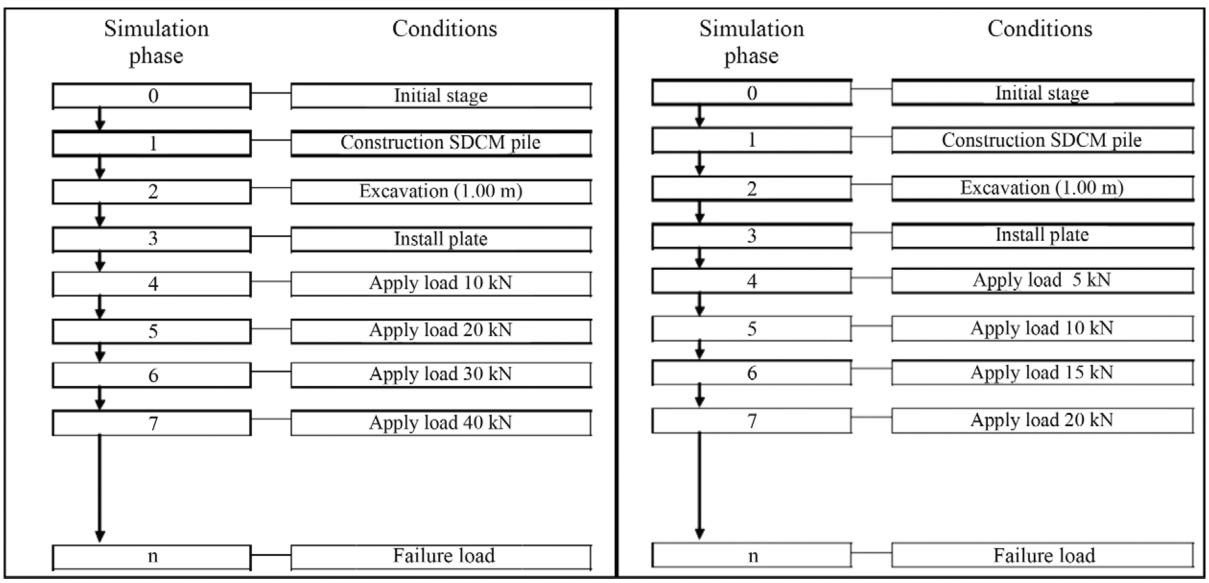

Figure 7 - Finite Element simulation for axial compression and lateral pile load test.

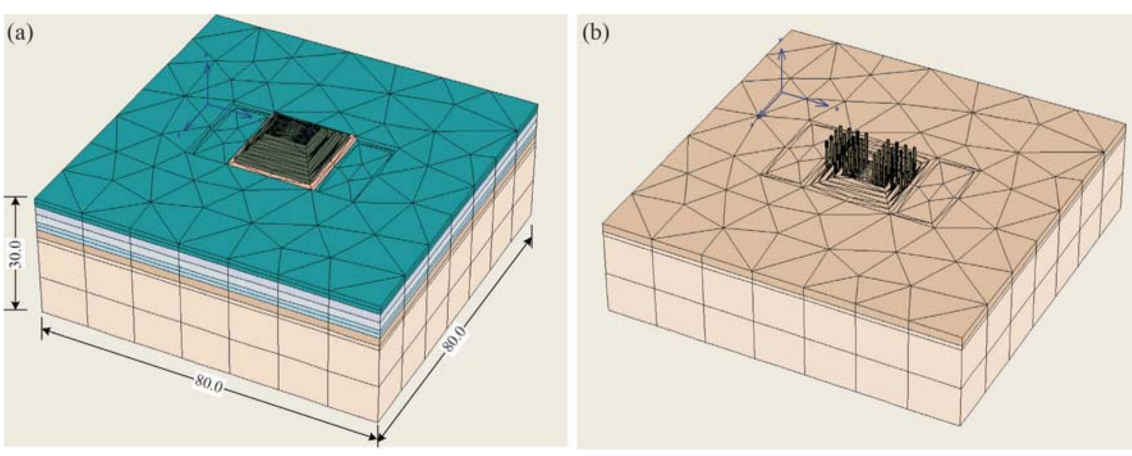

Figure 8 - Embankment simulation model used in 3D FEM simulation.

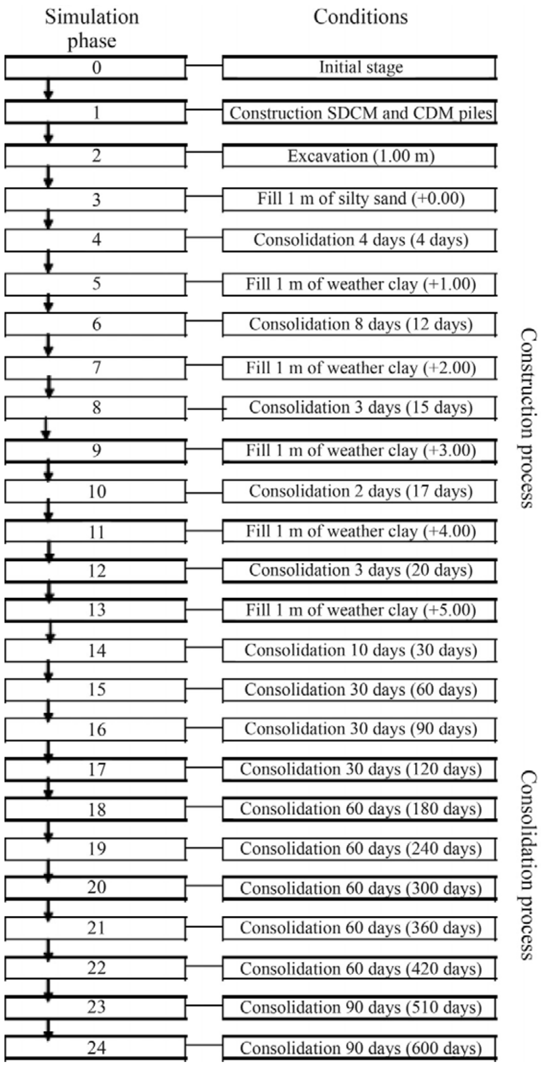

Figure 9 - Finite element simulation for full scale embankment load test.

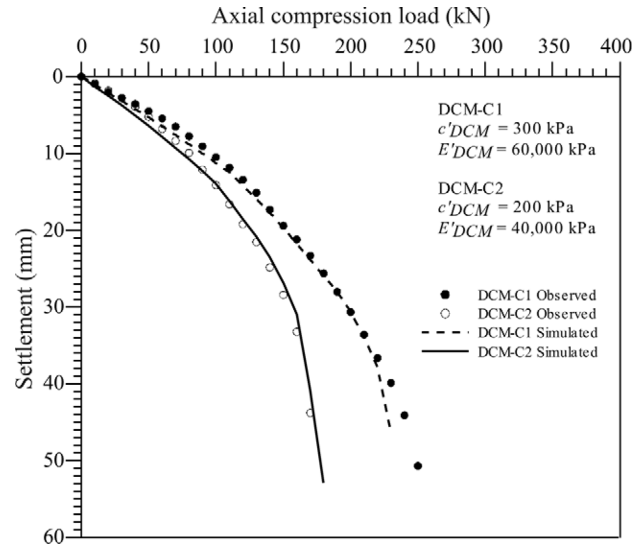

Figure 10 - Comparisons between observed and simulated axial compression load – settlement curves for DCM-C1 and DCM-C2.

sion in the DCM pile, C_{DCM}, obtained from the 3D finite element simulations were 300 kPa and 200 kPa, respectively, as illustrated in Fig. 10. However, the cement-clay modulus, E_{DCM}, were obtained as 60,000 kPa and 40,000 kPa for DCM C-1 and DCM C-2, respectively. Furthermore, for the SDCM pile, the corresponding value for C_{DCM} and E_{DCM} were 200 kPa and 30,000 kPa, respectively, as illustrated in Fig. 11. The slightly different results reflect the construction quality control in the field tests.

Figure 12 shows the summary of the ultimate bearing capacity of SDCM pile which proportionally increased linearly with the increased lengths of concrete core pile while the sectional areas of the concrete core pile only slightly increased the bearing capacity. Consequently, increasing the length ratio, L_{core}/L_{DCM}, has dominant effect than increasing the se

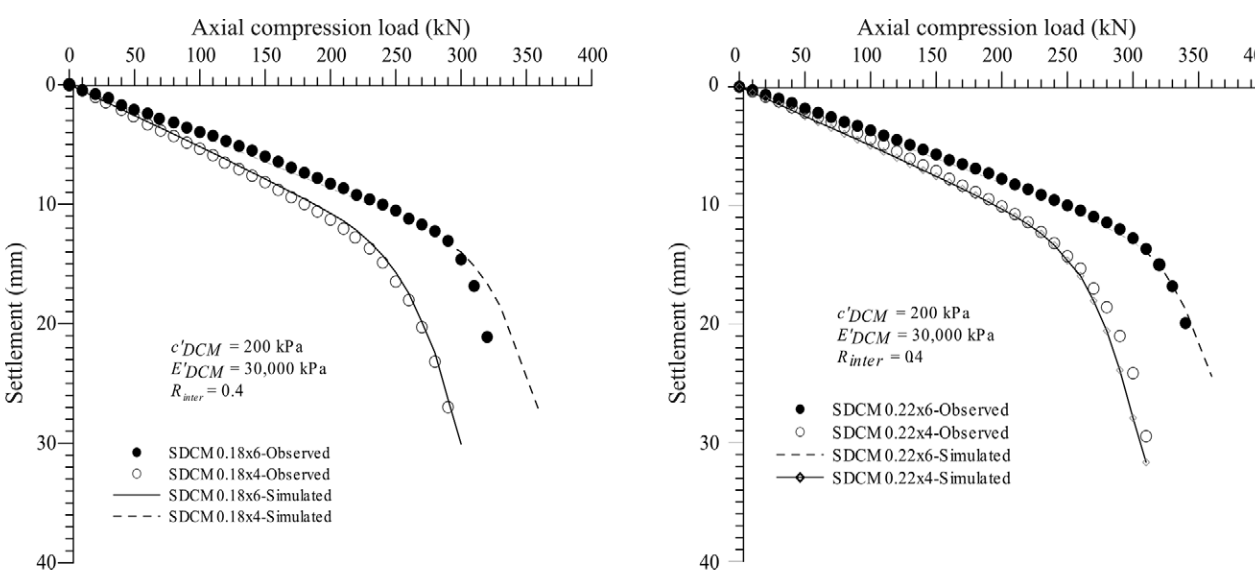

Figure 11 - Comparisons between observed and simulated axial compression load – settlement curves for SDCM.

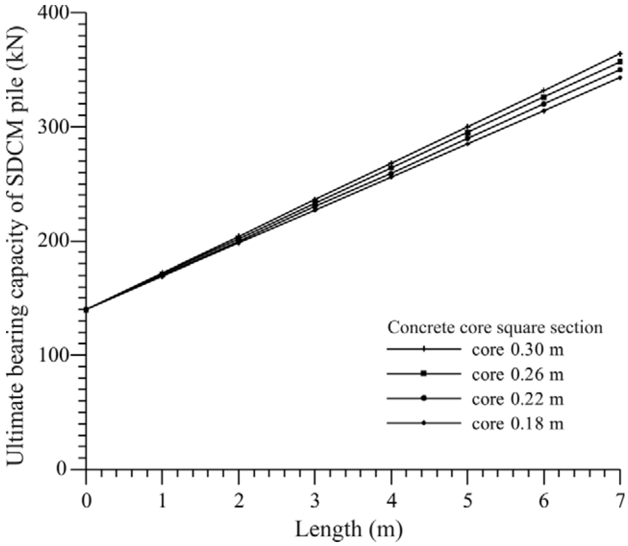

Figure 12 - Effect of lengths and sectional areas of concrete core piles on ultimate bearing capacity.

The mode of failure consisted of three categories, namely: concrete core pile failure, DCM pile failure, and soil failure. The SDCM pile failure occurred in the unreinforced part (DCM pile failure) because the DCM pile was not strong enough to carry and transfer the load to the tip of DCM pile as demonstrated in Fig. 13.

6.2. Lateral load simulation

The appropriate values for mixture of cement-clay cohesion in the DCM pile, C_{DCM}, and mixture of cement-clay modulus, E_{DCM}, obtained from the 3D finite element simulation were similar to that in the axial compression pile. In addition, the tensile strength of DCM pile, T_{DCM}, and tensile strength of concrete core, Tcore, were evaluated in this study. The T_{DCM} obtained from the simulation of DCM pile were 50 kPa and 25 kPa for DCM L-1 and DCM L-2, respectively, and the corresponding values for T_{core} and T_{DCM} obtained from the simulation were 5000 kPa and 50 kPa, respectively (Figs. 14 and 15).

The ultimate lateral load of SDCM pile increased with increasing sectional area because it increased the stiffness of the SDCM pile but the length of concrete core pile did not increase the ultimate lateral load capacity when using concrete core pile lengths longer than 3.5 m. (Fig. 16).

6.3. Embankment load simulation

The surface settlements were measured at the top of DCM, SDCM piles and the unimproved ground in the middle of the embankment (untreated clay). The observed settlements are plotted in Fig. 17 together with the simulated values. Both the magnitude and rate of settlements from simulations agreed well with the observed data from field test as illustrated in Fig. 17. Consequently, the parameters involved were derived and verified. The parametric study was conducted by varying the sectional areas of the concrete core pile of 0.22 x 0.22 m and 0.30 x 0.30 m as well as varying the lengths of concrete core piles of 4, 5, 6 and 7 m to study their effects on the embankment settlements. The effects of lengths and sectional areas of the concrete core

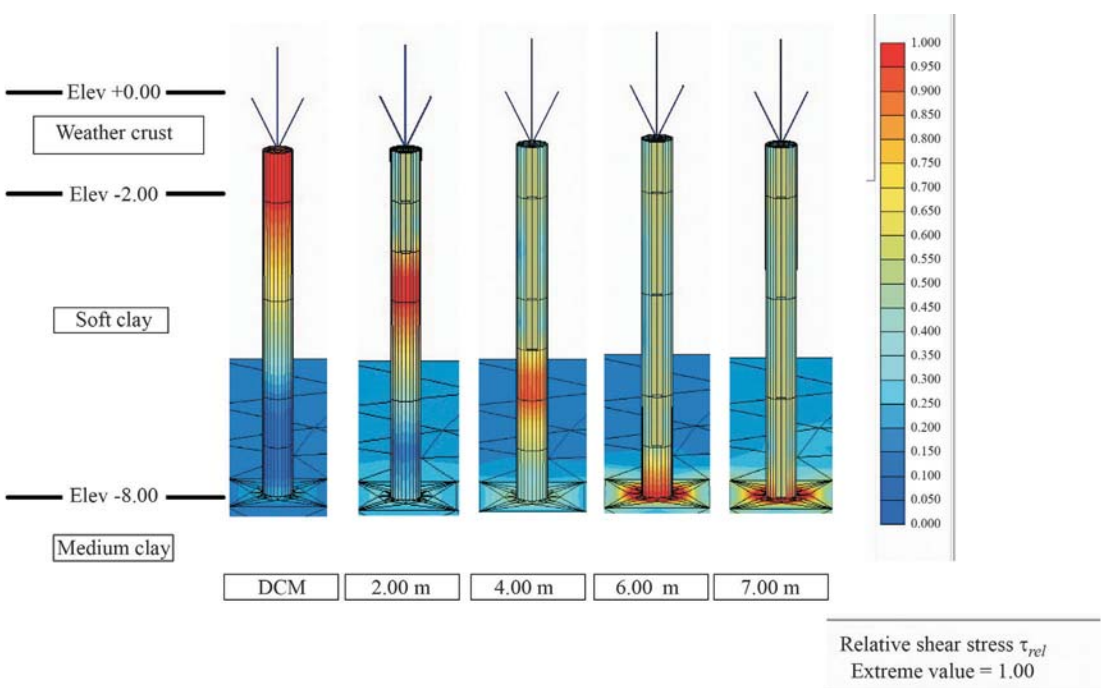

Figure 13 - Relative shear stresses of 0.22 x 0.22 m core piles at failure load from simulations.

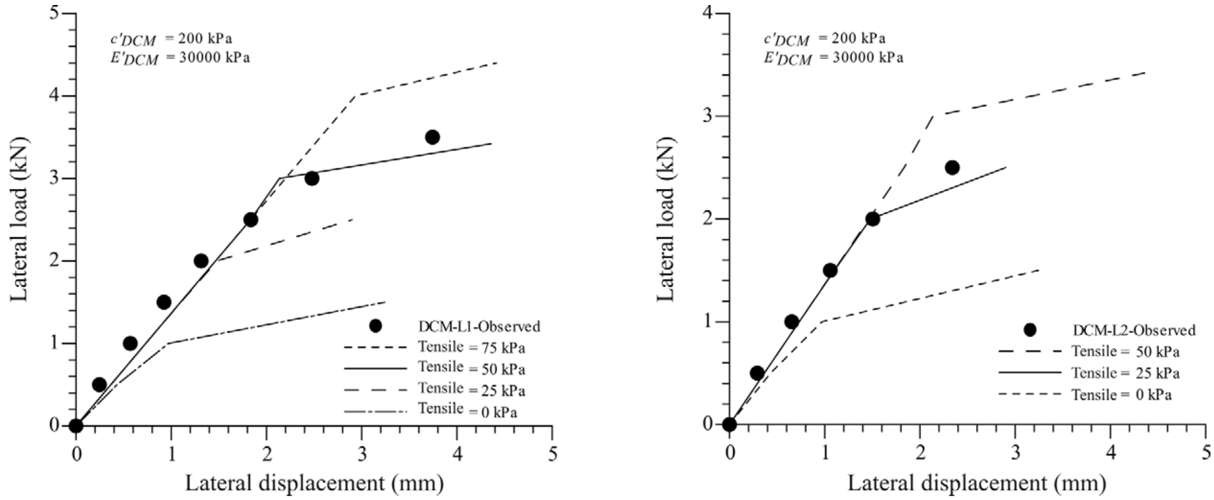

Figure 14 - Comparisons between observed and simulated lateral load – settlement curves for DCM-L1 and DCM-L2.

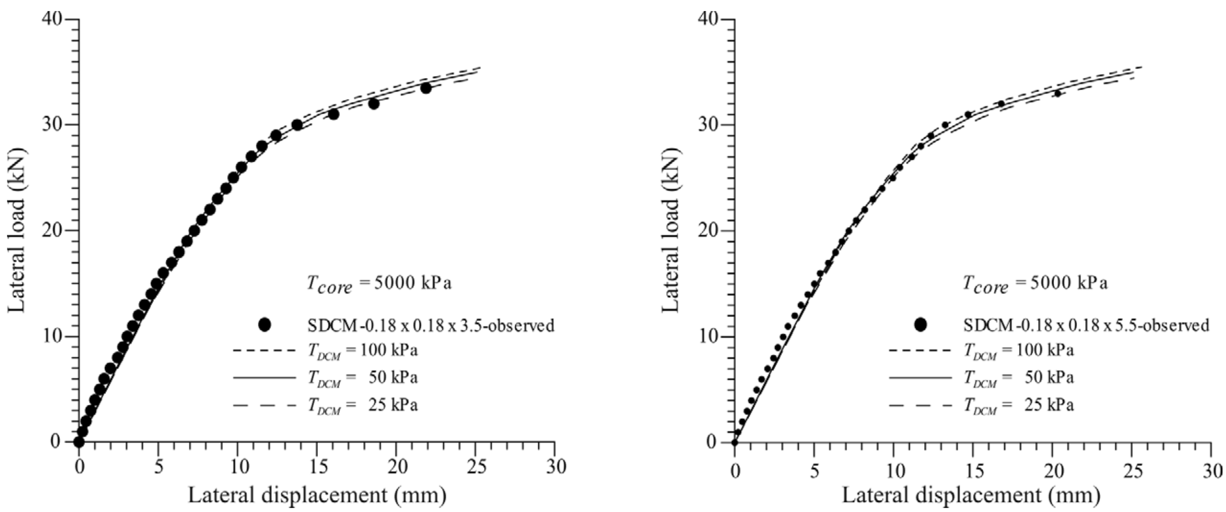

Figure 15 - Comparisons between observed and simulated lateral piles load – settlement curves for SDCM.

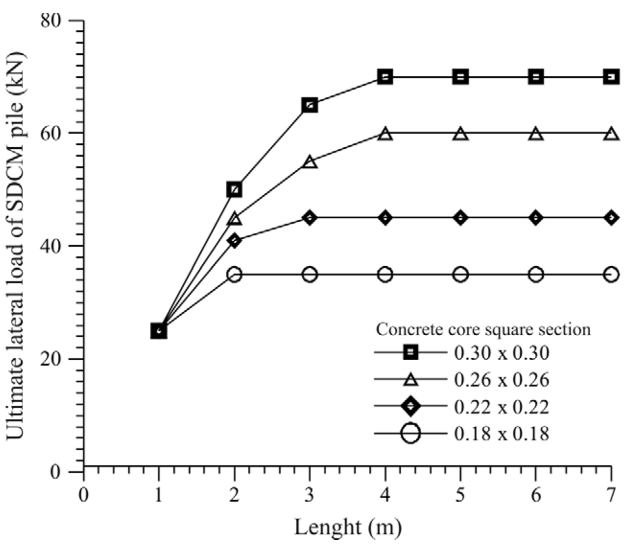

Figure 16 - Effect of lengths and sectional areas of concrete core piles on the ultimate lateral load of SDCM pile.

piles of SDCM piles on the ultimate settlement of embankment simulation are illustrated in Fig. 18. It can be summarized that the ultimate settlement at 600 days after consolidation proportionally decreased with increasing lengths of concrete core piles from 4 to 6 m and only slightly decreased from lengths of 6 to 7 m. Moreover, the ultimate settlement only slightly decreased when increasing the sectional areas of the concrete core piles from 0.22 to 0.30 m.

Figure 19 shows the summary of the effect of core pile length on the settlement at 600 days after consolidation in surrounding clay of SDCM pile. The settlement of surrounding clay of SDCM at surface and 4 m depth decreased with increasing the lengths of concrete core pile and only slightly decreased with increasing the sectional areas. Therefore, it can be concluded that the ultimate settlements proportionally reduced with increasing lengths of concrete core pile. In addition, both the sectional area and length of concrete core pile have no effect in the subsurface settlement at 7 m depth.

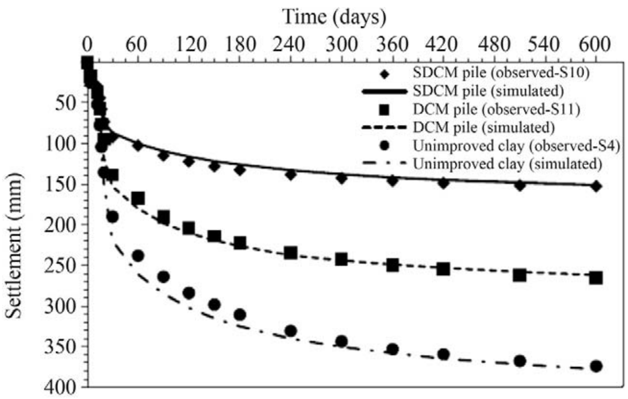

Figure 17 - Comparison of observed and simulated surface settlements.

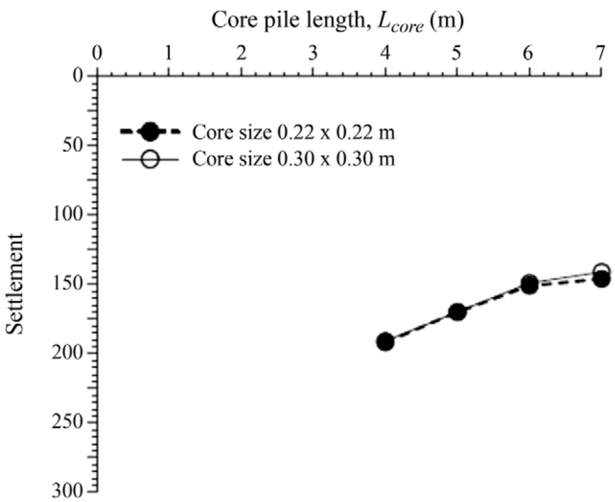

Figure 18 - Effect of lengths and sectional areas of concrete core pile on ultimate settlements of SDCM pile.

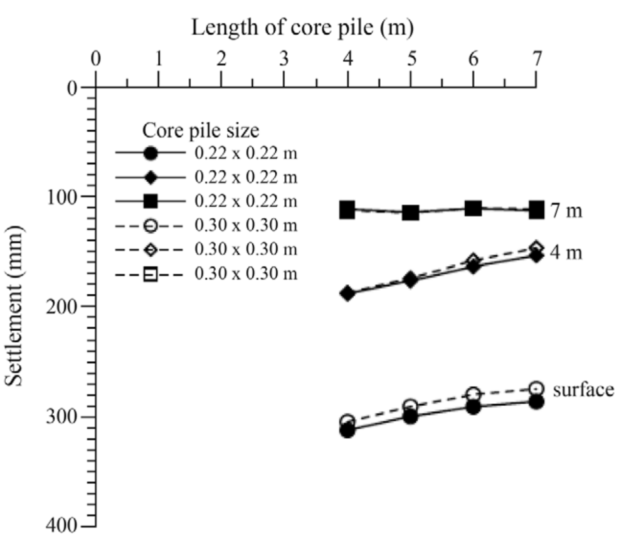

Figure 19 - Effects of core pile lengths on ultimate surface and subsurface settlements in surrounding clay of SDCM pile.

Differential settlements occur in the subsurface at various depths because the stresses proportionally decreased from the surface to the depths 4 and 7 m, respectively. Moreover, the stresses in the surrounding clay of SDCM and DCM piles as well as the unimproved zone are plotted together in Fig. 20. The stresses of surrounding clay of SDCM is the lowest meaning that the lowest settlements at the surface and 4 m depth. For the 7 m depth, the stresses are only slightly different so the settlements were similar.

The effect of length of concrete core pile on the lateral movements are also studied through the simulations by varying the lengths of the concrete core pile from 4 to 7 m as well as their sectional areas consisting of 0.22 x 0.22 m and 0.30 x 0.30 m. The simulated and observed results of the lateral movements for both DCM and SDCM piles at different periods after construction are illustrated in Fig. 21. The observed lateral movements were obtained from inclinometers as indicated in Fig. 5a,b. The measured and simulated lateral movement data agreed well. The effects of concrete core pile lengths longer than 4 m on lateral movements' profiles of SDCM piles at 570 days after construction are illustrated in Fig. 22. The lateral movement reduced with increasing lengths of concrete core piles longer than 4 m. From subsequent simulations as shown in Fig. 23, increasing the lengths and, to a lesser degree, the sectional areas of concrete core piles, reduced the lateral movements of the SDCM piles for concrete core piles longer than 4 m. The lateral movement significantly reduced with increasing lengths as well as with increasing the sectional areas of concrete core piles. It can be summarized that increasing both the lengths and sectional areas of core piles reduced the lateral movement.

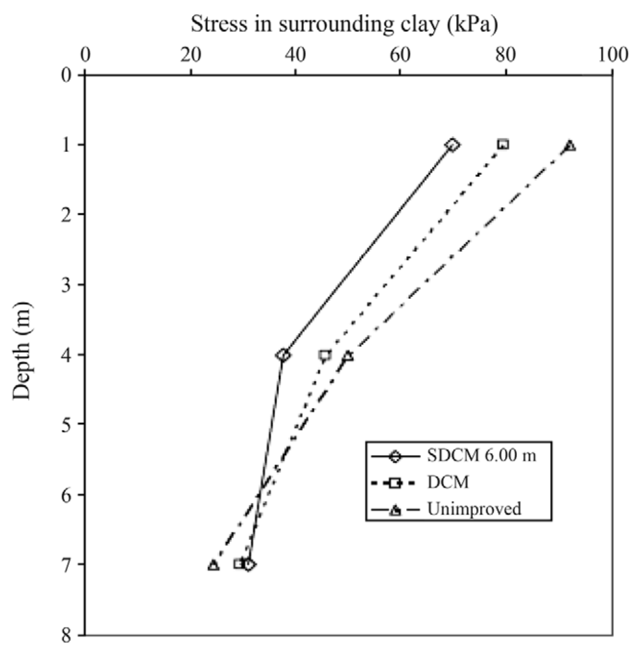

Figure 20 - Stresses in surrounding clay of unimproved zone, SDCM and DCM piles piles at depth 1, 4 and 7 m.

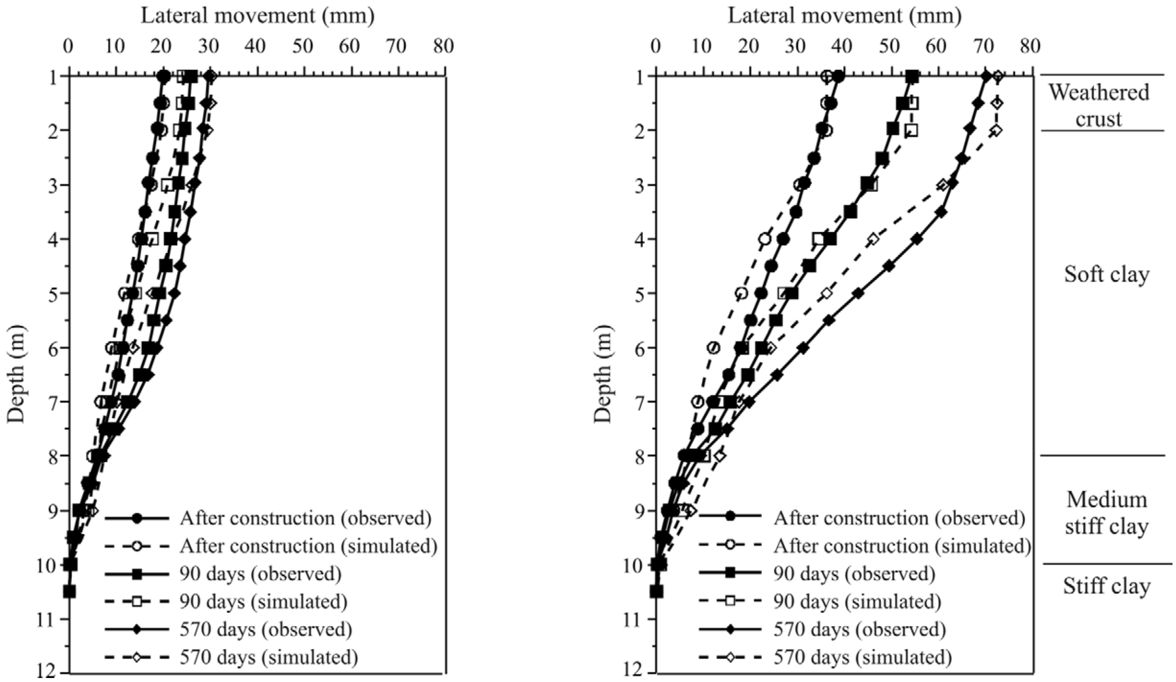

Figure 21 - The simulated and observed lateral movements of SDCM and DCM piles at different periods after construction.

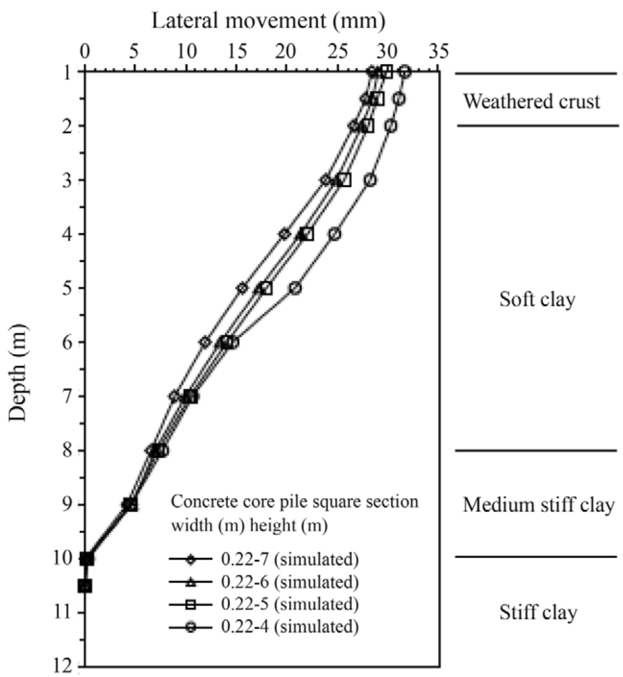

Figure 22 - Effects of concrete core pile lengths on lateral movement profiles of SDCM pile with 0.22 x 0.22 m core pile from simulations.

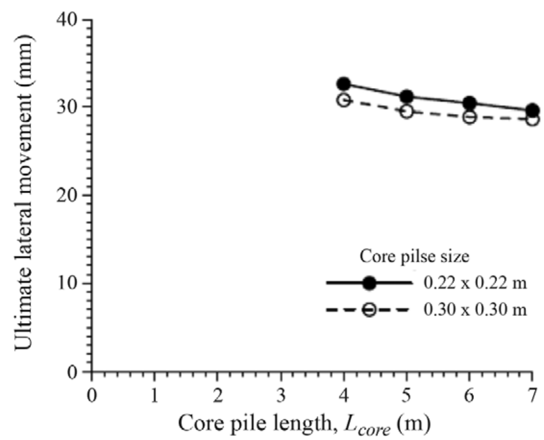

Figure 23 - Effects of sectional areas and lengths of concrete core piles on the maximum lateral movement of SDCM pile.

6.4. Axial compression pile simulation

For the SDCM pile, the corresponding values for cement-clay cohesion in the DCM pile, C_{DCM}, and corresponding modulus, E_{DCM}, were found to be 200 kPa and 30,000 kPa, respectively. The relative shear stresses for both SDCM and DCM piles under embankment load are illustrated in Figs. 24 and 25 corresponding to concrete core pile length of 6.0 m and DCM pile length of 7.0 m. It is indicated that larger relative stresses occurred in the DCM piles compared to the SDCM piles resulting in more compressions in the former than the latter which agree with the vertical deformations in Fig. 17 and lateral deformations plotted in Fig. 21.

7. Conclusions

The full scale embankment loading test supported by SDCM and DCM piles was constructed, monitored and, consequently, simulated by using Plaxis Foundation 3D software in order to study and verify the design parameters.

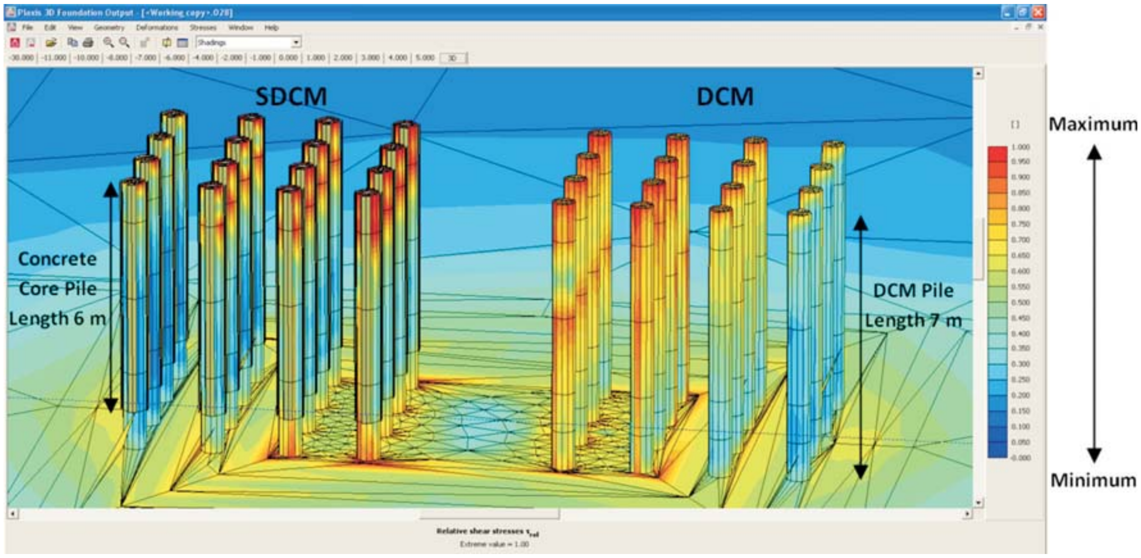

Figure 24 - Relative shear stresses of DCM piles with 7.0 m length and SDCM piles with 0.22 x 0.22 m by 6.0 m concrete core piles under embankment loading.

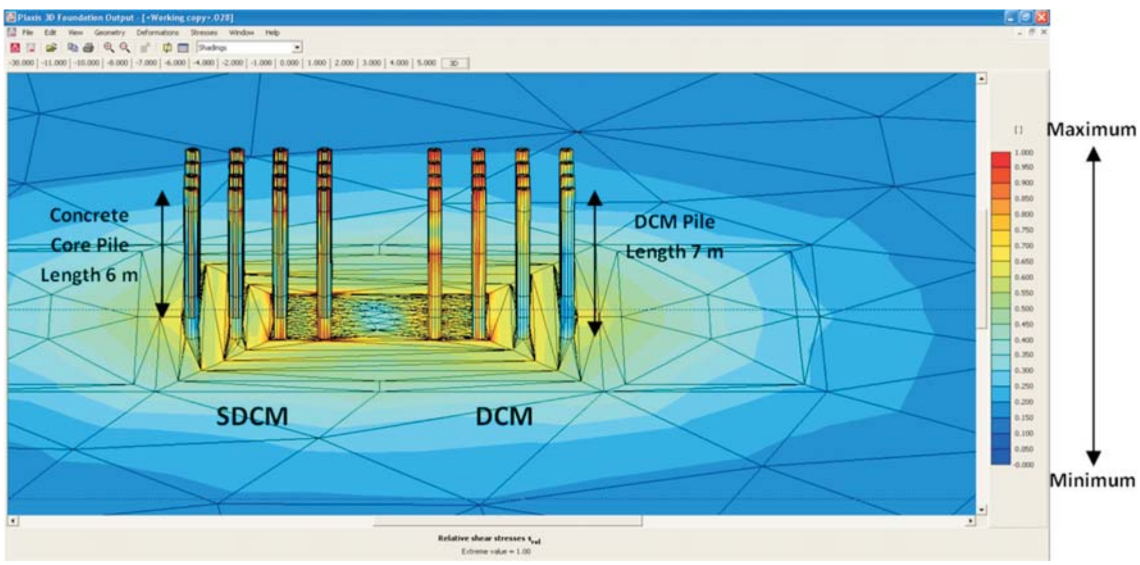

Figure 25 - Cross section view of relative stresses of DCM and SDCM pile under embankment loading.

The parameters were also based on an earlier full scale load tests to failures and subsequent simulations. The appropriate parameter for cement-clay cohesion, C_{DCM}, and cement-clay modulus, E_{DCM}, obtained from the 3D finite element simulations were 200 kPa and 30,000 kPa, respectively. The result indicated that the longer concrete core pile can reduce the vertical displacements of SDCM pile as well as the subsurface portions of the surrounding soil. The settlements reduced with increasing lengths of concrete core piles from 4 to 6 m but slightly reduced from 6 to 7 m core pile length. Moreover, the length of concrete core pile affected both the surface and subsurface settlements at 4 m but did not affect the subsurface settlement at 7 m. In case of lateral deformation, the length and sectional areas of concrete core pile reduced the lateral movement of the embankment. The longer the lengths, the lower the lateral movements. Furthermore, the bigger sectional areas also reduced the lateral movements although with smaller effects. It was also found in the previous and current studies that, the concrete core piles need to be longer than 4 m in order to effectively reduce the lateral movements of the embankment.

References

Bhandari, A. (2006) Laboratory Investigation of Stiffened Deep Cement Mixed (SDCM) Pile. M.Sc. Eng. Thesis

No. GT-78-6, Asian Institute of Technology, Bangkok, 97 pp.

Bergado, D.T.; Ahmed, S.; Sampaco, C.L. & Balasubramaniam, A.S. (1990) Settlement of Bangna-Bangpakong highway on soft Bangkok clay. ASCE Journal of Geotechnical Engineering, v. 116:1, p. 136-154.

Brinkgreve, R.B. & Broere, W. (2006) Manual PLAXIS 3D Foundation ver. 1.6. A.A. Balkema, Rotterdam, 177 pp.

Butler, H.D. & Hoy, H.E. (1997) The Texas Quick Load Method for Foundation Load Testing – User's Manual. Federal Highway Administration, Report No. FHWA-IP-77-8, Texas, 54 pp.

Dong, P.; Qin, R. & Chen, Z. (2004) Bearing capacity and settlement of concrete-cored DCM pile in soft ground. Geotechnical and Geological Engineering, v. 22:1 p. 105-119.

Jamsawang, P. (2008) Full Scale Tests on Stiffened Deep Cement Mixing (SDCM) Pile Including 3d Finite Element Simulation. D. Eng. Diss. No. GE-08-01, Asian Institute of Technology, 235 pp.

Jamsawang, P.; Bergado, D.T.; Bandari, A. & Voottipruex, P. (2008) Investigation and simulation of behavior of stiffened deep cement mixing (SDCM) piles. International Journal of Geotechnical Engineering, v. 2:3, p. 229-246.

Jamsawang, P.; Bergado, D.T.; Bandari, A. & Voottipruex, P. (2009a) Behavior of stiffened deep cement mixing pile in laboratory. Lowland International Journal, v. 11:1, p. 20-28.

Jamsawang, P.; Bergado, D.T. & Voottipruex, P. (2009b) Laboratory and field behavior of stiffened deep cement mixing (SDCM) pile. Ground Improvement Journal, v. 164:G11, p. 33-49.

Petchgate, K.; Jongpradist, P. & Panmanajareonphol, S. (2003a) Field pile load test of soil-cement column in soft clay. In: Proceedings of the International Symposium 2003 on Soil/Ground Improvement and Geosynthetics in Waste Containment and Erosion Control Applications, Asian Institute of Technology, Thailand, pp. 175-184.

Shinwuttiwong, W. (2007) Full Scale Behavior of SDCM Piles under Axial and Lateral Loading with Simulations. M.Sc. Eng. Thesis No GE-07-04, Asian Institute of Technology, Bangkok, 139 pp.

Suksawat, T. (2009) Numerical simulation of SDCM and DCM piles under axial and lateral loads and under embankment load: A parametric study. M.Sc. Eng. Thesis No. GE-08-09, Asian Institute of Technology, Bangkok, 143 pp.

Tand, K.E. & Vipulanandan, C. (2008) Comparison of computed vs. measured lateral load/deflection response of ACIP piles. Plaxis Bulletin, v. 23, p. 10-13.

Wehnert, M. & Vermeer, P.A. (2004) Numerical analysis of load tests on bored piles. NUMOT 9th, Ottawa, pp. 505-511.

Wu, M.; Zhao, X. & Dou, Y.M. (2005) Application of stiffened deep cement mixed column in ground improvement. In: Proceedings International Conference on Deep Mixing Best Practices and Recent Advances, Stockholm, pp. 463-468.

Zheng, G. & Gu, X.L. (2005) Development and practice of composite DMM column in China. In: Proceedings 16th International Conference on Soil Mechanics and Geotechnical Engineering, Osaka, v. 3, pp. 1295-1300.

Analysis and Control of the Stability of Embankments on Soft Soils: Juturnaíba and others Experiences in Brazil

R.Q. Coutinho, M.I.M.C.V. Bello

Abstract. In the design and evaluation of the behavior of embankments on soft clay foundations, geotechnical characterization, along with instrumentation for measurements involving pore pressure and displacements (vertical and horizontal), are required in order to efficiently elaborate a construction. This paper presents the results of stability analysis, and stability control, with emphases on studies carried out by the Geotechnical Group (GEGEP) of the Federal University of Pernambuco, Brazil. Five Brazilian cases are presented: the Juturnaíba trial embankments and Juturnaíba Dam construction, located in Rio de Janeiro; the access embankments for the Jitituba River Bridge in Alagoas; the failure of an embankment alongside highway BR-101-PE in Recife, Pernambuco; and the Sarapuí trial embankment, located in Rio de Janeiro (Ortigão 1980; Ortigão *et al.* 1983). With the exception of the Juturnaiba trial embankment, all of the cases in the stability analysis concerned failure involving embankments on soft clays confirmed the need to apply the Bjerrum (1973) correction factor to field vane tests measuring undrained strength. Effective stress stability analysis utilizing a normally consolidated effective stress parameters for strength measurements, presented results that can be considered satisfactory. Stability control was carried out using measurements of displacements, deformations, and pore pressures. Proposals were presented and analyzed, especially for horizontal displacements, demonstrating good results, and the potential for practical application. Recommendations for use are presented in the paper. The joint results of stability analysis, and stability control, showed the importance of having an FS > 1.3 to guarantee adequate behavior and security.
Keywords: embankments on soft soils, stability analyses, performance, monitoring, and stability control.

1. Introduction

The construction of embankments on soft clays raises an important geotechnical concern that has been studied by various authors, with the sum of their experiences adding to the overall understanding of soft soils when subjected to load increases (*e.g.* Bjerrum 1973; Tavenas & Leroueil 1980; Ladd 1991; Leroueil & Rowe 2000; Coutinho & Bello 2005; Almeida & Marques 2010). In Brazil, important research studies include those carried out by Ortigão (1980), Coutinho (1986) and Magnani de Oliveira (2006). In general, the design of embankments on soft soils should meet the basic stability requirements needed to resist rupture and displacement (vertical and horizontal), during and after construction, while remaining compatible with the objectives involved. Instrumentation is a tool used for monitoring and evaluation (including stability control) during the construction of embankments, where measurements are taken of horizontal and vertical displacements, along with pore-pressure.

This paper presents the results of stability analysis, and stability control, with emphasis on studies carried out by the Geotechnical Group (GEGEP) of the Federal University of Pernambuco, Brazil. Five Brazilian cases are presented: the Juturnaíba trial embankment (Case Study 1), and the Juturnaíba Dam construction (Case Study 2), both located in Rio de Janeiro; the access embankments of the Jitituba River Bridge (Case Study 3), located in Alagoas; the failure of an embankment alongside highway BR-101-PE (Case Study 4), located in Recife, Pernambuco; and the Sarapuí trial embankment, located in Rio de Janeiro (Case Study 5) (Ortigão 1980; Ortigão *et al.* 1983).

2. Behavior of Embankments On Soft Soil

When analyzing embankments on clay foundations, their behavior has commonly been considered to be entirely undrained during construction, with drainage and consolidation starting after construction ends. This approach has been widely utilized, and has generally performed well for conventional designs. Observations during construction have shown that while this approach may often provide reasonable designs, the actual behavior of embankments may be more complicated, and that conventional undrained analyses may over-predict pore pressures and lateral displacements. Thus, if one wishes to predict the actual behavior of an embankment located on clay, it is essential to have good knowledge of the mechanical behavior of natural clays, and to understand what might happen underneath an embankment during construction (Tavenas & Leroueil 1980; Leroueil & Rowe 2000; Coutinho & Bello 2011).

As in most geotechnical problems, understanding soil response only becomes possible when the corresponding stress path is known. Under embankments, the effective

R.Q. Coutinho, D. Sc., Universidade Federal de Pernambuco, Recife, PE, Brazil. e-mail: rqc@ufpe.br.
M.I.M.C.V. Bello, M. Sc., Universidade Federal de Pernambuco, Recife, PE, Brazil. e-mail: isabelamcvbello@hotmail.com.
Submitted on October 28, 2010; Final Acceptance on December 15, 2011; Discussion open until July 31, 2012.

stress path can be deduced from pore pressure observations. Significant partial consolidation during construction has been reported by a number of investigators (*e.g.* Tavenas & Leroueil 1980; Ortigão 1980; Coutinho 1986; Leroueil & Rowe 2000).

If the behavior of the clay foundation under an embankment was perfectly undrained, the effective stress path for a point at or near the centerline would be as O'-U' in Fig. 1a (overconsolidation ratio, OCR < 2.5). As a consequence of the rapid consolidation during early stages of construction (very high coefficient of consolidation, c_v in the pre-consolidation condition), the effective stress path may be O'-P', and reach the limit state curve at P', at a vertical effective stress, σ'_v, close to the pre-consolidation stress, σ'_p, of the clay, corresponding to an increase in pore pressure much smaller than the increase in total stress ($\overline{B}_1 = \Delta u/\Delta\sigma_v < 1.0$; $\overline{B}_m = 0.6$). As the clay becomes normally consolidated, its coefficient of consolidation is reduced by a significant amount, and the behavior becomes essentially undrained. Due to the shape of the limit state curve of natural clays, further loading is associated with a stress path such as P'-A', under a vertical effective stress, which is essentially constant, equal to σ'_p. Such a stress path corresponds to an increase in pore pressure equal to an increase in total stress ($\overline{B}_2 = \Delta u/\Delta\sigma_v = 1.0$) during the second phase of loading.

If the embankment is built to a height in excess of that corresponding to point A (Fig. 1a) the effective stress path will continue up to F', on the strength envelope of the normally consolidated clay, resulting in local failure, possibly to the critical state C''. Between F' and C', the increase in excess pore pressure is larger than the increase in total stress ($\overline{B}_3 = \Delta u/\Delta\sigma_v > 1.0$) as shown in Fig. 1b. It should be noted that $\overline{B}_1$, $\overline{B}_2$ and $\overline{B}_3$ discussed above, are incremental values during different stages of loading and do not correspond directly to the conventional $\overline{B} = \Delta u/\Delta\sigma_v$ under the entire loading (for $\Delta\sigma_v = I\gamma H$). Hence a high value for $\overline{B}_3$ does not necessarily mean that the embankment is unstable. Pore pressure may develop even after construction is completed, *i.e.* when there is no increase in total stress, but when $\overline{B}$ may still be less than unity. The pore pressure generated during the construction of an embankment, and the corresponding stress path, have direct influence on settlements and lateral displacements.

3. Case Studies

3.1. Juturnaíba Dam Project – Case Studies 1 and 2

The Juturnaíba Dam Project, an earth-filled structure located in the Northern portion of the State of Rio de Janeiro, in Brazil, was built from 1981 to 1983 (Fig. 2a). The Project included the Juturnaíba trial embankment (Case Study 1) and the Juturnaíba Dam construction (Case Study 2). The two cases are located in areas with similar geotechnical characteristics. The foundation consisted basically of an organic clay deposit about 8 m thick, with SPT values (blows/length in cm) ranging from 0/111 to 1/33, typically 0/50, along its full depth, underlain by sand sediments with SPT values about 10/30, reaching a depth of 14 m. Visual classification and laboratory tests permitted division of the clayey deposit into six layers, with variations in organic and water content, ranging from light-grey silt clay, to brown clayey peat (Fig. 2b).

Figure 3 shows results involving natural water content, and Atterberg Limit values for the six layers of the profile. Variations of these results can be observed for each layer, and consequently in the plasticity index values. Results are presented in Fig. 4 concerning overburden effective stress (σ'_{vo}) and preconsolidation pressure (σ'_p) obtained by oedometer tests. The foundation deposit exhibits a condition of overconsolidation, with the upper part show-

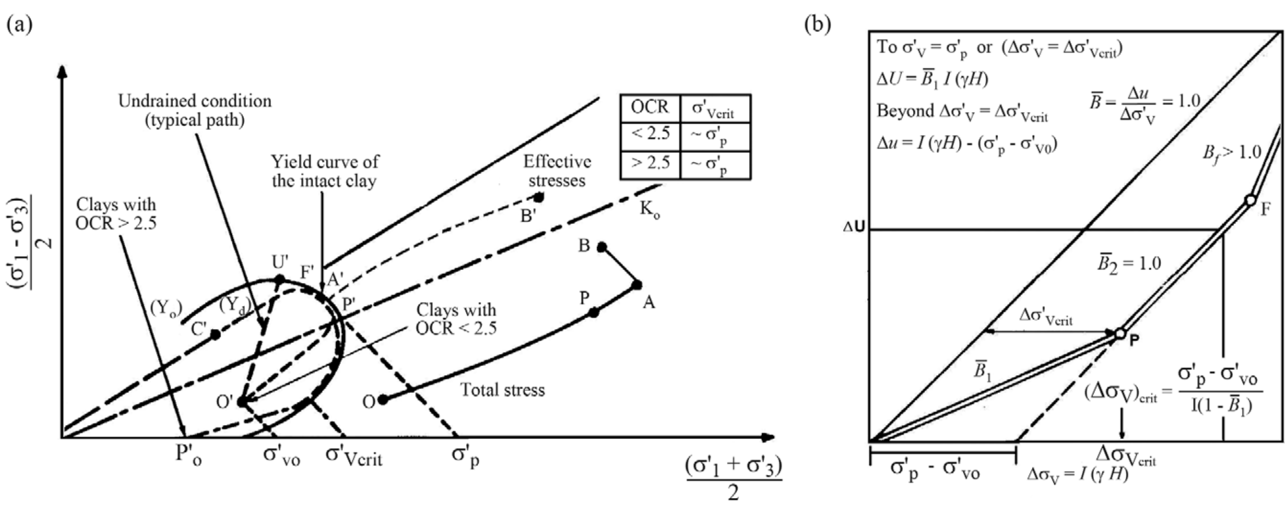

Figure 1 - (a) Total and effective stress path, and (b) increase of pore pressure under the centerline during stage construction of an embankment on soft clays (Coutinho 1986, from Tavenas & Leroueil 1980).

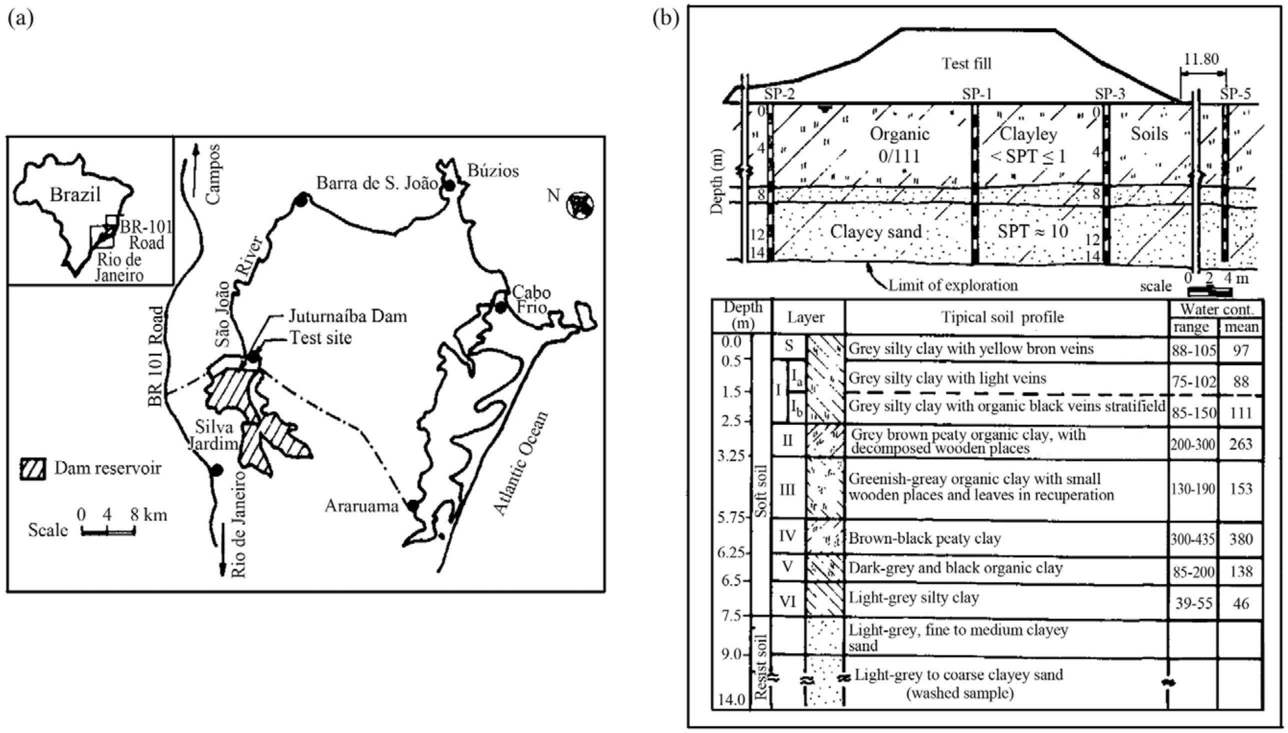

Figure 2 - Juturnaíba Dam Project: (a) Localization; (b) typical soil profile (Coutinho 1986; Coutinho & Lacerda 1987).

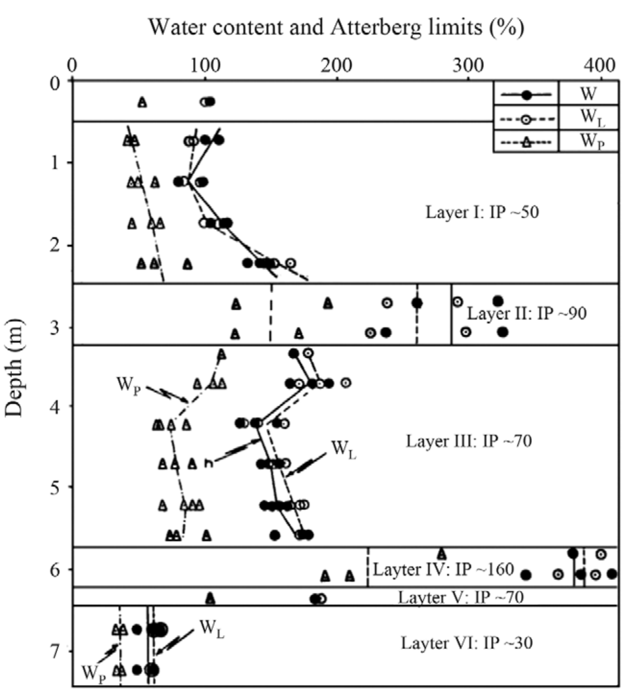

Figure 3 - Water content and Atterberg Limits of the Juturnaíba trial embankment (Coutinho 1986).

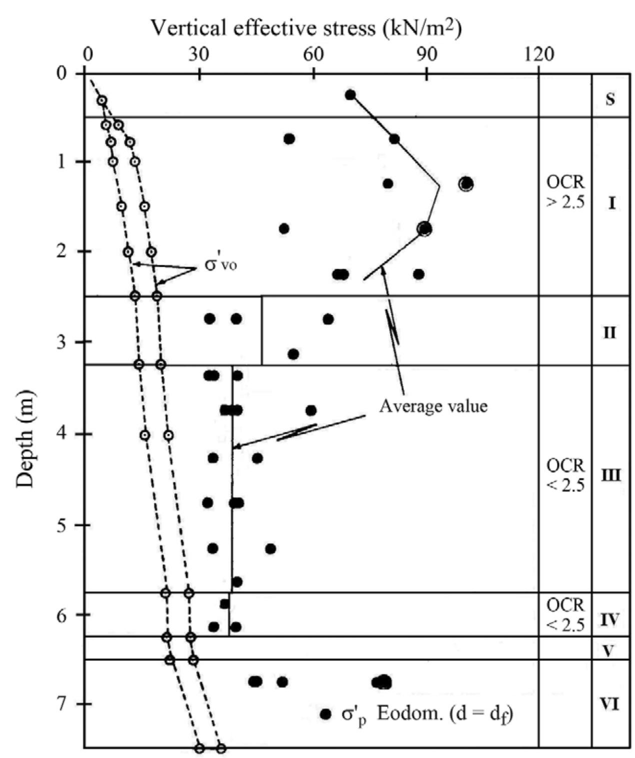

Figure 4 - σ'_{vo}, $\sigma'_{v\,crit}$, σ'_{v}, σ'_{p} laboratory values *vs.* depth – center of the Juturnaíba trial embankment (Coutinho 1986).

ing higher values (OCR > 2.5). Figure 5 shows the results of compressibility parameters, with values indicated for compression ratio (*CR*), swelling ratio (*SR*), void index (e_o), compression index (C_c), and organic content, differing for each layer.

Because 1.2 km of the length of this earth dam was built to rest on organic soft clay, geotechnical studies were

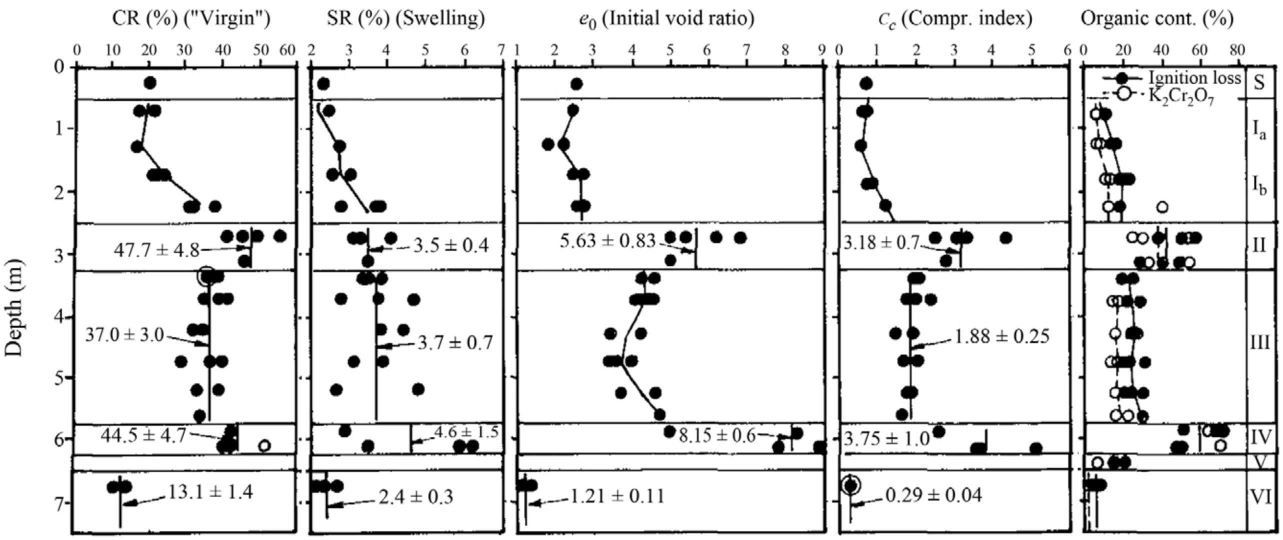

Figure 5 - CR, SR e_o and *Cc vs.* depth – oedometer tests for the Juturnaíba Dam (Coutinho & Lacerda 1987).

quite comprehensive, including laboratory and field investigations, along with construction of a trial embankment leading to failure (Case Study 1), which was instrumented as indicated in Fig. 6 (Coutinho 1986; Coutinho & Lacerda 1987; 1989).

The main purposes of the studies were to provide indications on the undrained strength and compressibility of the clay foundation, and methods to control stability during the construction. Joined by design studies, indications pointed out that the Juturnaíba Dam (Case Study 2) should be built in stages, with berms and flat slopes (Fig. 7). Dam monitoring consisted of placing settlement plates at the embankment-clay interface, with piezometers inside the organic clay, and inclinometers at the slope berm (Coutinho *et al.* 1994; Lucena 1997).

3.2. Access embankments for the Jitituba River Bridge – Case Study 3

Case Study 3 presents the study of the access embankments for the Jitituba River Bridge, located on highway AL-413-Alagoas, with the bridge being built before the access embankments. The geotechnical profile presents a soft clay organic layer between two sand layers, with the thickness of the organic clay increasing towards the direction of the river, to a maximum of 12 m (Fig. 8). Due to the existence of a geotechnical profile composed of soft soil layers, and considering the construction sequence involving the embankments of the Jitituba River Bridge (before the execution of the access embankments), analyses of the vertical and horizontal displacement, and the consequent effects on the pilings of the bridge were recommended. The solution adopted consisted of constructing embankments in

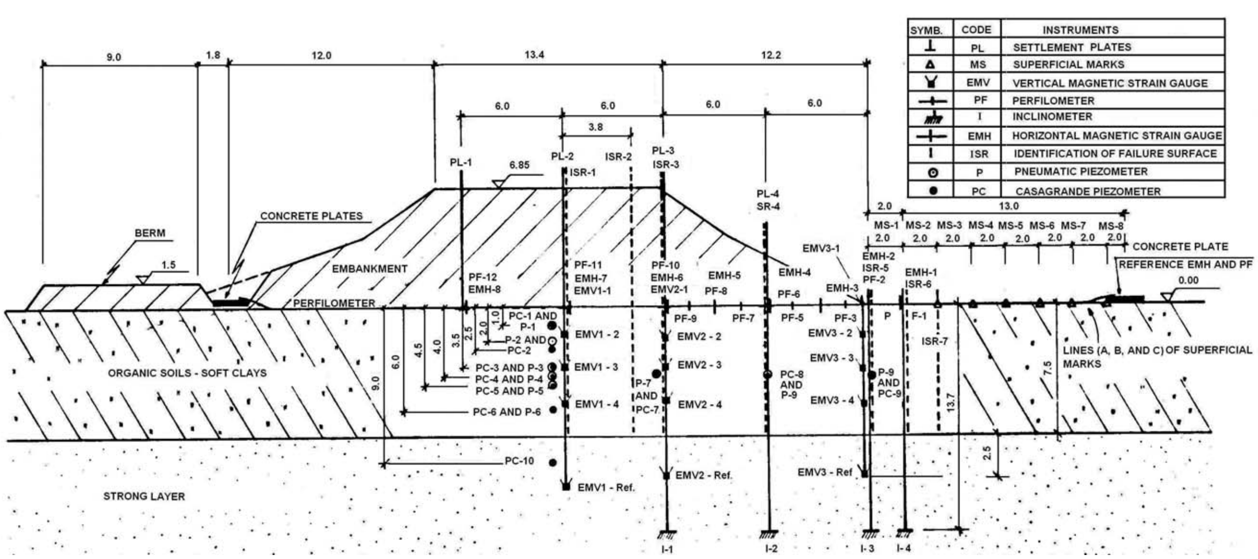

Figure 6 - Instrumentation of the Juturnaíba trial embankment (Coutinho 1986).

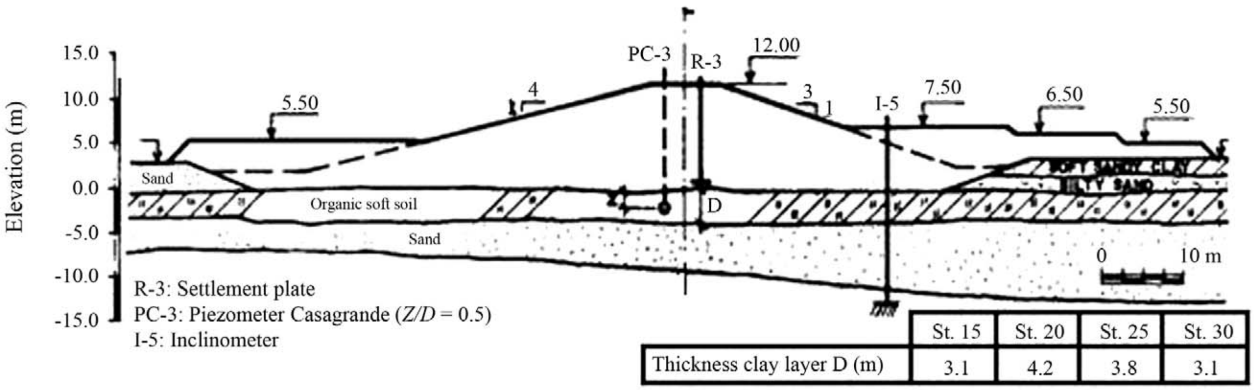

Figure 7 - Transversal geotechnical profile and instrumentation – Juturnaíba Dam (Coutinho & Lacerda 1989).

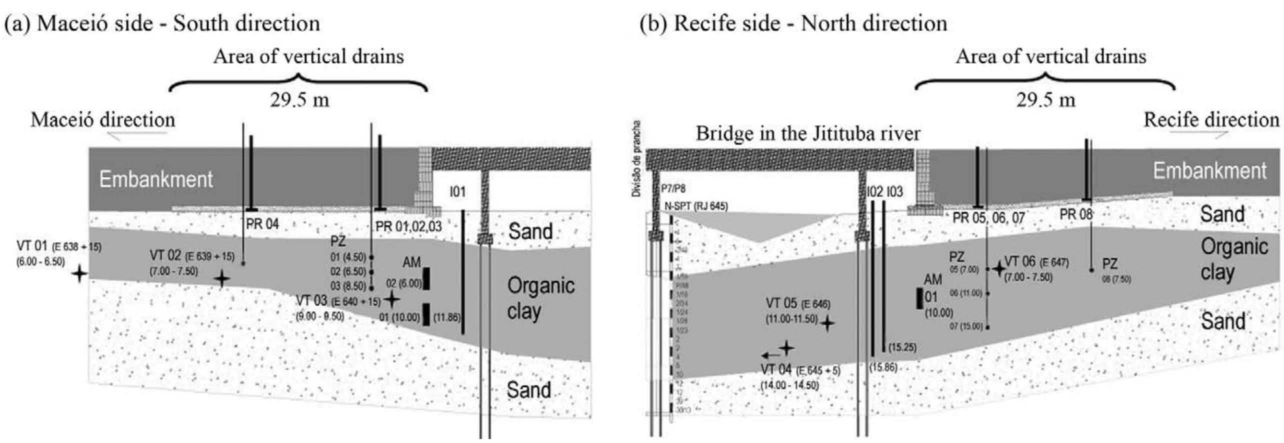

Figure 8 - Longitudinal section, geotechnical profile, and locations of the field investigations for the basic project of the access embankments for the bridge on the Jitituba River (Cavalcante *et al.* 2003; 2004).

stages, allied to the use of prefabricated vertical drains, and geotechnical instrumentation (Casagrande piezometers, settlement plates, and inclinometers) to control and monitor project performance (Cavalcante 2001; Cavalcante *et al.* 2003; 2004). Behavior of the access embankments was analyzed in terms of measurements of pore-pressures, and vertical and horizontal displacements, by applying models proposed in the literature, and by comparison with other case studies of embankments on soft soils.

The research study of the access embankments of the Jitituba River Bridge (Case Study 3) was made possible due to a partnership with Gusmão Engineers Associated.

3.3. Failure of an embankment alongside highway BR-101-PE – Case Study 4

Case Study 4 involves the rupture of an embankment on soft clays that occurred in an area alongside Federal Highway BR-101 - in Pernambuco (Bello 2004; Bello *et al.* 2006; Coutinho & Bello 2005). Figure 9 shows the position of the sheds, and location of the geotechnical field investigations.

Results of the geotechnical profile, natural water content, overconsolidation ratio OCR, and field vane undrained strength *vs.* depth are shown in Fig. 10. Variations can be observed in the results for each soft layer. The geotechnical profile initially presents a fill layer, followed by three layers of soft clays (13 m thick) with different organic content/water content, and finally a silty sand layer. The natural water content, W_n, presented a maximum value (334%) at 7 m of depth, becoming constant (34%). The undrained shear strength S_u demonstrates variation with depth, and a minimum value of 17 kPa at 13 m depth. The OCR value in general is close to 1. The embankment was constructed without any geotechnical investigation project, monitoring, or technological control. After the failure, in order to understand the process, *in situ* and laboratory tests were performed so as to permit total stress stability analysis/back-analysis. The Data Base for Recife Soft Clays (Coutinho *et al.* 1998) was used to complement the technical information needed to carry out the study.

The research work for the embankment alongside highway BR-101-PE (Case Study 4) was made possible thanks to a partnership with Gusmão Engineers Associated.

3.4. Sarapuí trial embankment – Case Study 5

An extensive research program concerning the behavior of embankments located on soft soils, sponsored by the Brazilian Highway Research Institute (IPR), was conducted together with COPPE-UFRJ, at the Federal University of Rio de Janeiro. It included field and laboratory investigations, theoretical analyses, and large-scale field trial embankments on soft soils, and dark grey deposits. The Sarapuí trial embankment (Study Case 5) was the first instrumented embankment taken to failure (Ortigão 1980; Ortigão *et al.* 1983). It was situated in a very flat swampy area, covering a surface area of about 150 km^2 around Guanabara Bay. At the site, the clay deposit is about 11 m thick, and overlies sand and gravel layers. As may be seen from Fig. 11, the liquid limit varies from 120%-160% near the ground surface, to 90%-100% at the bottom of the de-

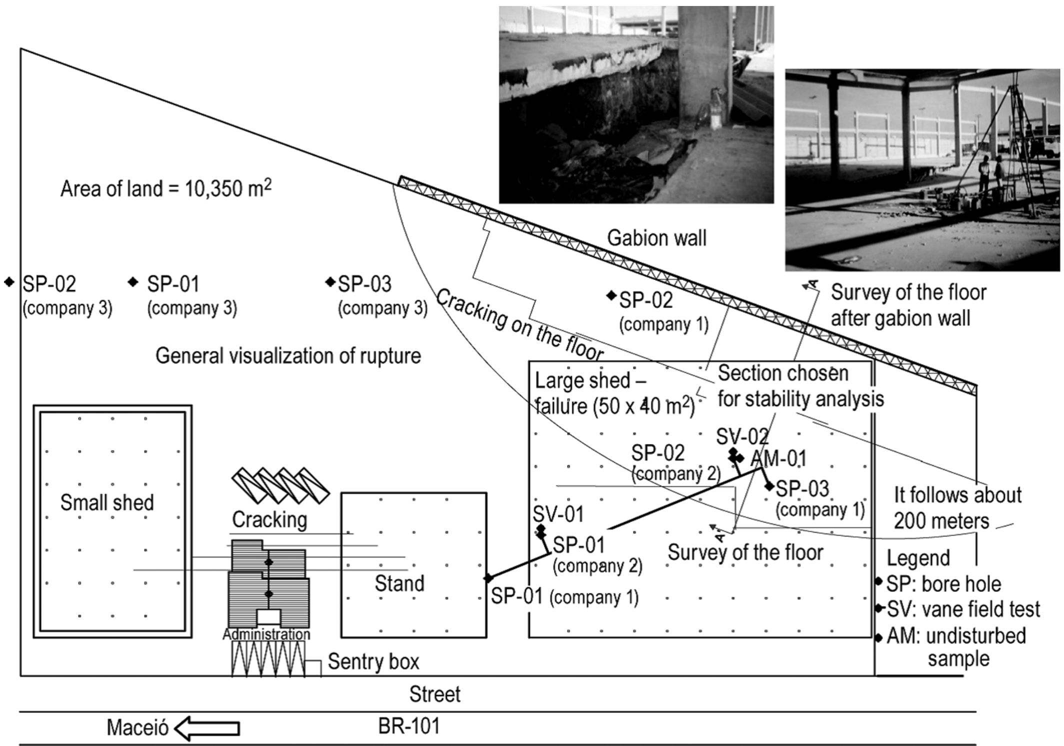

Figure 9 - Situation and localization of SPT soundings, vane field tests and undisturbed sampling – embankment alongside highway BR-101-PE (Bello 2004).

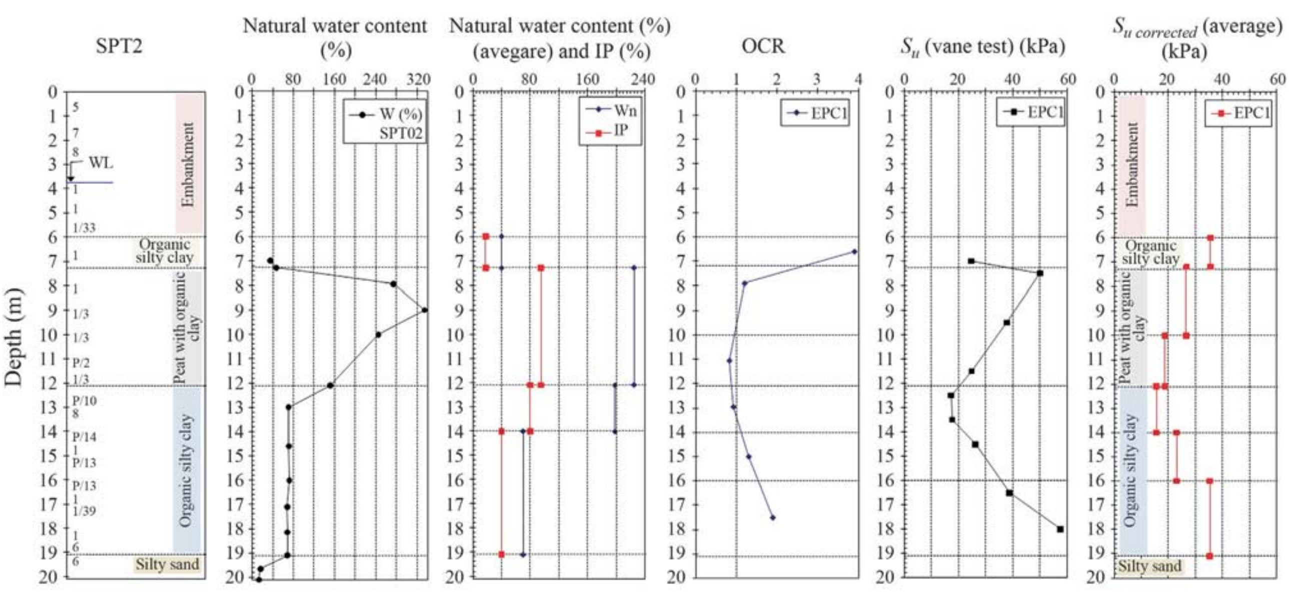

Figure 10 - Profile of embankment alongside highway BR-101-PE – Section AA (Bello 2004).

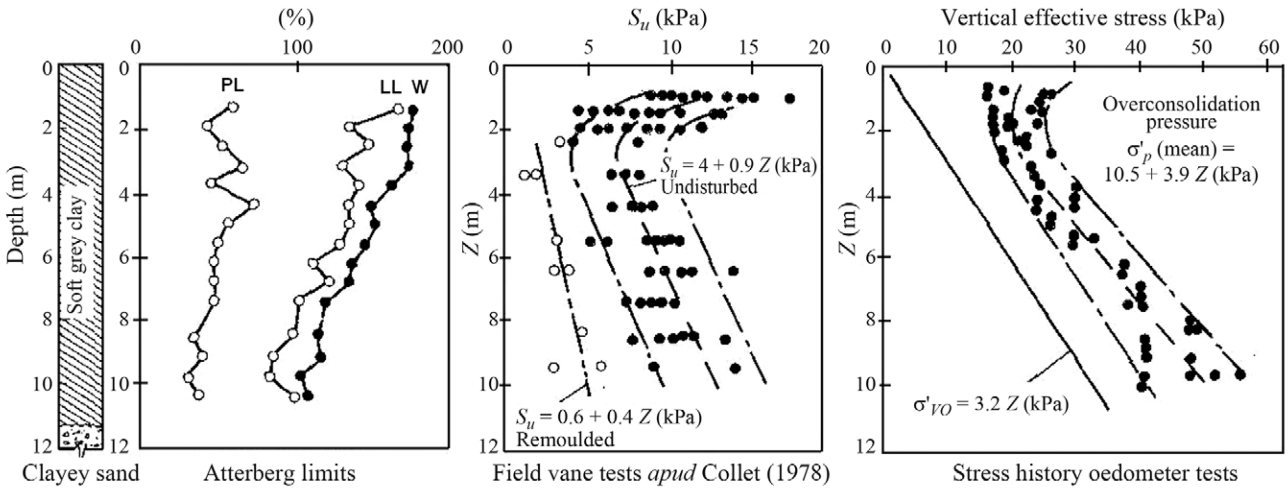

Figure 11 - Summary of Geotechnical properties, Rio de Janeiro soft gray – clay (Ortigão *et al.* 1983).

posit. The natural water content is slightly higher than these liquid limit values. The sensibility of this deposit is low, ranging from 2-4, with an average of 2.6. The plastic limit decreases from 60%-80% near to top, to 50%-60% at the bottom. The results of pre-consolidation pressure (σ'_p) indicated the presence of an upper clay crust, extending down to a depth of 2.5 m. The undrained shear strength (S_u) values seem to initially decrease with the depth, until reaching 2.5 m; below this level, field vane tests indicate increasing S_u values.

4. Stability Analysis

Ladd (1991) defined three types of stability analysis for embankments on soft soils: (a) total stress analysis (TSA); (b) undrained strength analysis (USA), and (c) effective stress analysis (ESA).

Total stress analysis is often used in single-stage construction analysis, and is usually based on the undrained strength profile prior to construction. In undrained strength analysis, the in situ undrained shear strength is computed as a function of the pre-shear effective stress. This analysis is often used in evaluating the stability of embankments that are constructed in stages.

Evaluation of mobilized undrained shear strength S_u, in an embankment constructed in one stage, can be carried out using several approaches: (a) the field vane test approach, with the Bjerrum (1973) correction factor, μ; (b) pre-consolidation pressure $S_u/\sigma'_p = 0.19$ (plasticity index $PI = 10\%$) to about 0.28 (PI = 80%). The upper values often correspond to organic clays; (c) recompression and SHANSEP approaches; (d) the direct simple shear test; (e) the unconfined and unconsolidated undrained compression test, and (f) piezocone penetration tests, and Marchetti dilatometer tests. To gain confidence in the results of stability analyses, it is recommended that at least two of these approaches be considered in practical applications. In the case of an embankment constructed in several stages, the selection of strength can be obtained using several approaches: (a) field vane test approach, without the Bjerrum (1973) correction; (b) CPTU tip resistance approach; (c) vertical effective stress approach ($S_{uv}/\sigma'_{vo} = 0.25$); and (d) SHANSEP approach (Leroueil & Rowe 2000).

Skempton (1957) suggested the general correlation for S_u be determined from the field vane shear test (VST), as a function of the plasticity index. All of the data concerns normally consolidated (NC) clays. A linear depiction of this data results in Eq. (1).

$$S_{u\,(VST)} / \sigma'_{vo} = 0.11 + 0.0037\,PI \tag{1}$$

Coutinho (1986) and Coutinho *et al.* (2000) offered a general discussion concerning field vane testing, and presented results of undrained shear strength for some Brazilian soft clay deposits. Results of the S_{uv}/σ'_p ratio *vs.* plasticity index from Juturnaíba and Recife research site deposits RRS1 and RRS2, and from other Brazilian clays, are presented in Fig. 12. It can be seen that, in general, Brazilian soft clays with $PI < 80\%$ are in agreement with correlations proposed in the literature. If all soils are considered, including organic soils, a modified Skempton (1957) correlation

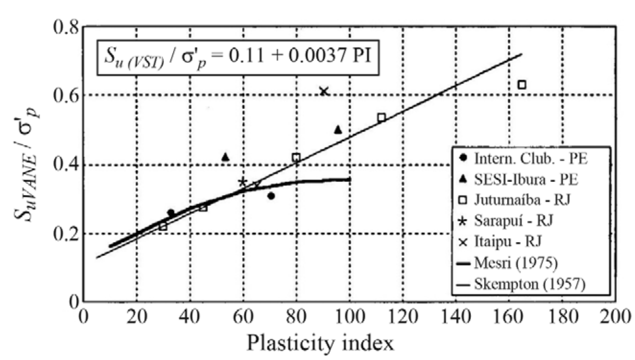

Figure 12 - S_{uVST}/σ'_p *vs. PI* correlation (mod. Skempton 1957, Bjerrum 1973) including values for Brazilian clays (Coutinho *et al.* 2000).

may also be valid for OC clays, using pre-consolidation stress (σ'_p) in place of the overburden effective stress (σ'_{vo}).

In the effective stress analysis approach, mobilized strength parameters are close to those for normally consolidated clay. Theoretical and practical difficulties involving effective stress analysis have been observed, including concerns regarding accurate measurement of pore pressure along the failure surface (Tavenas *et al.* 1980; Ortigão 1980; Coutinho 1986).

In the stability analysis of embankments on soft soils, investigation of the critical shape of the failure surface (circular and non-circular) is important.

This item presents results of the stability analysis performed on the Juturnaíba trial embankment (Case Study 1), and the embankment alongside highway BR-101-PE (Case Study 4). Results of stability analysis performed on the Sarapuí trial embankment (Case Study 5) were used in the discussion as a complement for the Brazilian experiences. Others cases can be seen in Magnani de Oliveira *et al.* (2010) and Almeida *et al.* (2010).

4.1. Total stress analysis results – Case Study 1

Coutinho (1986) performed a total stress stability analysis on the Juturnaíba trial embankment (Case Study 1) to obtain the minimal Safety Factor, SM. The principal analysis was performed using the Modified Bishop method, which takes the circular surface of the rupture into account. The Modified Janbu method was utilized in a complementary analysis (back-analysis) which took into account the specific shape of the failure surface. In the study, a total of seven hypotheses were established considering the S_u profile obtained from the *in situ* vane test (average ± standard deviation), and the cracking of the embankment (Fig. 13). The fill strength parameters (cohesion c = 29,1 kN/m^2, and friction angle ϕ = 29°), were determined from direct shear strength. The analysis was performed for a height of 6.85 m, at which point the failure of the foundation occurred, and also for a height of 8.85 m, to be able to evaluate the behavior of the embankment after failure, which occurred while the embankment was still under construction.

Figure 14 shows S_u values obtained in the field vane test, and in the triaxial UU and CIU ($\sigma'_c \cong \sigma'_{oct}$ *in situ*) laboratory tests, as well as the mean values and the range of field vane shear tests results, with the equations for each of the six soil layers. The following points emerged by analyzing and comparing data: (a) Individual values, and linear regression of the S_u field vane test (Fig. 14a) were basically distinct for each layer. In the tests with "remolded" soil, S_u values were low, with sensitivity near or equal to 10, showing great dispersion and little variation among the layers; b) S_u values from UU and CIU laboratory tests are very similar, and fall close to mean vane shear strength results (Fig. 14b). Results from CIU tests present smaller dispersion than the UU values; c) S_u results in layer III from the triaxial tests are practically constant with the depth, which agrees well with results of the maximum past preconsolidation pressure (Fig. 5); d) The Mesri (1975) proposal for the "mobilized" $S_u = 0.22\sigma'_p$ showed lower results, as expected, than those obtained directly from the triaxial and vane tests (Fig. 14b).

Table 1 shows the summary of the analysis results (minimal Safety Factor, SM values). The stability analysis for the 6.85 m embankment height (Juturnaíba failure condition) considering the average Su from the field vane test performed before construction, without the Bjerrum correction, obtaining values of 1.069, 1.001 and 0.960 for SM, depending on the consideration of embankment cracking in hypotheses 1, 4 and 5 respectively.

With consideration of the S_u vane range (mean values ± standard deviation) and the strength of the embankment (0% cracking), the results of the minimal Safety Factor obtained were 1.274 and 0.888, respectively. The use of the Bjerrum correction would show very low results (SM << 1.0), considering the average high plasticity of the soft deposit, and consequently, the very low correction factor. Back-analysis carried out using the failure surface observed, showed satisfactory results for SM, displaying values close to the preliminary analysis values (in the order of 5 to 9% higher).

Figure 15 presents the minimal Safety Factor results for embankment heights considering the hypothesis of average S_u from the field vane test, and the effect of embankment cracking on the results. An appreciable reduction in SM value can be observed with the continuity of loading, particularly at embankment heights over 5.65 m (SM = 1.31). The influence of cracks in the embankment on

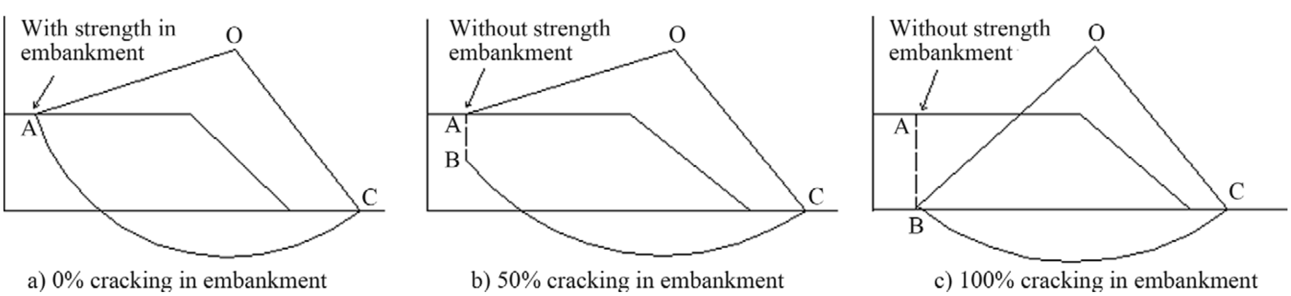

Figure 13 - Consideration of strength of the embankment in the stability analysis (Bello 2004).

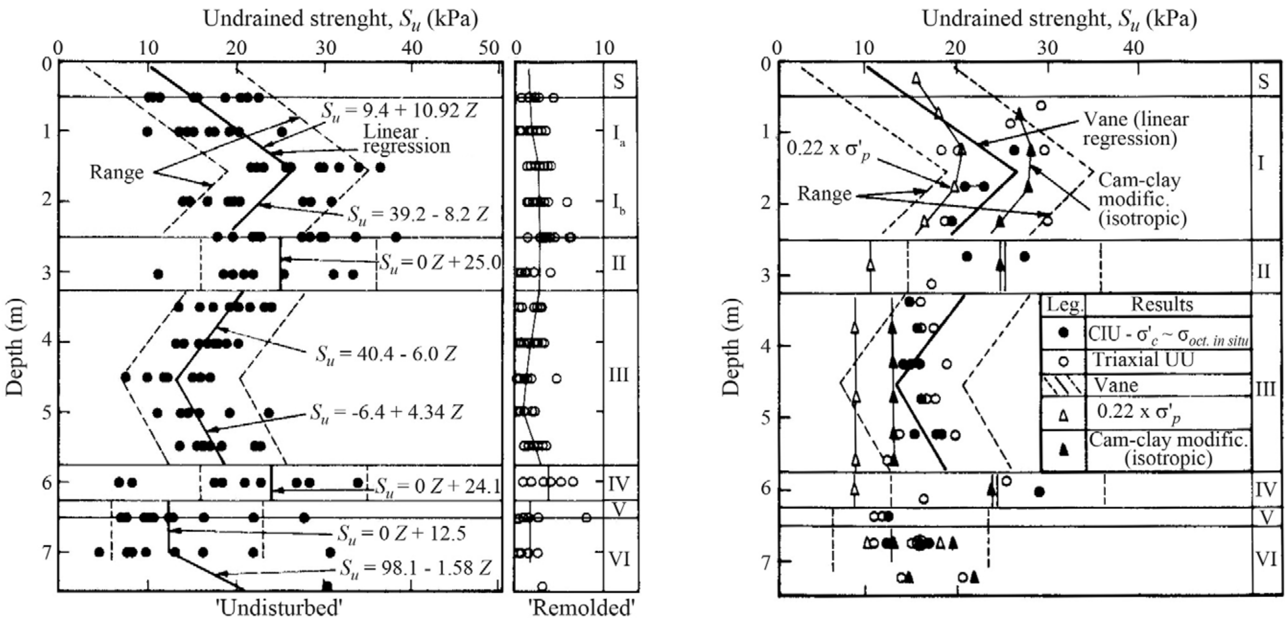

Figure 14 - Undrained strength values S_u *vs.* depths – Juturnaíba trial embankment: (a) S_u from field vane tests; (b) S_u triaxial tests (Coutinho & Lacerda 1989).

the SM values was in the order of 10%. The stability analysis for the 8.85 m high embankment (construction post failure) demonstrated SM results of around 1.0, confirming the rupture condition.

The dissimilar behavior involving the Juturnaíba foundation, which did not need the Bjerrum correction, can be attributed to the organic condition of the soil deposits, extensive drainage, and significant deformation from the increase in stress during the construction phase (see Coutinho 1986; Coutinho & Bello 2011). The analysis also shows that the Mesri (1975) proposal does not adequately

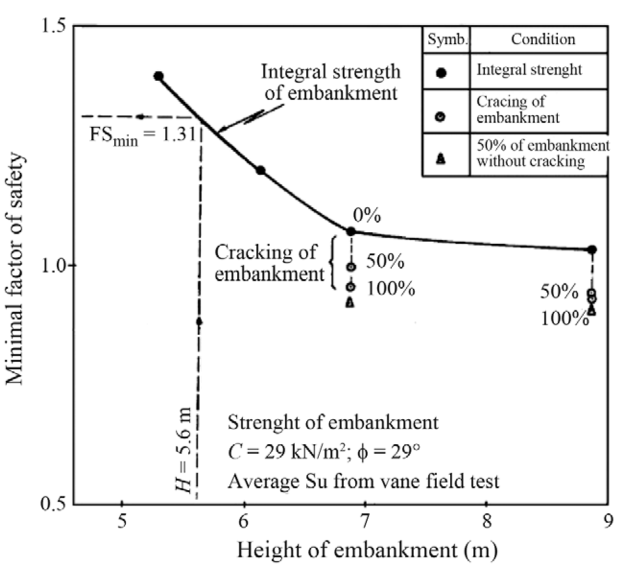

Figure 15 - Summary of the total stability analysis results for the Juturnaíba trial embankment (Coutinho 1986).

represent the mobilized strength. Sandroni (1993) presents another organic soil case (Camboinhas trial excavation-RJ) where application of the Bjerrum (1973) S_u correction proposal is not necessary.

To understand the failure process better, after construction of the 8.85 m high embankment was completed, the embankment was excavated to be able to observe its condition, along with that of the foundation during the work. Figure 16 represents what was observed, demonstrating a shared failure for both sides, with a slick side zone in the foundation, and a loose zone in the embankment. Because of this type of shared failure, what was not observed was the traditional movement of embankment mass in one horizontal direction (during the failure of the 6.85 m embankment).

In the Juturnaíba trial embankment, the critical circle predicted was very similar to the failure surface observed *in situ*, and only slightly dislocated towards the left. It was observed that a circular surface (or similar shape) tangent to the resistant layer can represent the failure surface (Coutinho & Bello 2011).

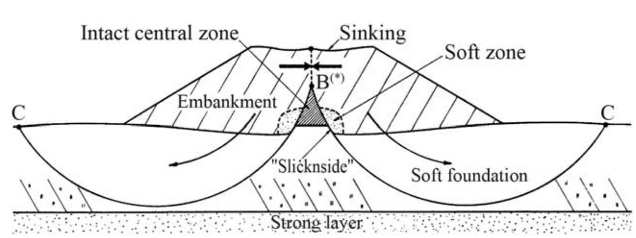

Figure 16 - Shared failure of the Juturnaíba trial embankment (Coutinho 1986).

Table 1 - Summary of the total stress stability analysis, SM_{min} calculated (modified from Coutinho & Bello 2007).

Case study	Hypothesis	(%) Cracking of embankment			S_u			Circular surface		Non circular surface			
								Analysis		Back-analysis			
		0	50	100	Correction	Average	Standard deviation	Bishop	Spencer	Bishop	Janbu	Spencer	Morgenstern-Price
(Case 1) Juturnaíba trial	1	X	-	-	-	X	-	1.069	-	1.165	1.205	-	-
embankment – Coutinho (1986)	2	X	-	-	-	X	(-) X	0.888	-	-	-	-	-
	3	X	-	-	-	X	(+) X	1.274	-	-		-	-
H_{emb} = 6.85 m (Hypothesis 1 to 7)	4	-	X	-	-	X	-	1.001	-	1.046	-	-	-
	5	-		X	-	X	-	0.960	-	1.007	-	-	-
	6	-	X	-	-	X	(+) X	1.200	-	-	-	-	-
	7	-	-	X	-	X	(+) X	1.195	-	-	-	-	-
H_{emb} = 8.85 m (Hypothesis 8)	8	-	X	-	-	X		0,948					
(Case 4) Embankment alongside	1	X	-	-	X	-	-	1.045	1.048	-	1.240	1.232	1.232
highway-101-PE – Bello (2004)	3	-	X	-	X	-	-	1.000	0.995	-	1.128	1.141	1.141
	7	-	X	-	X	-	-	1.082	1.076	-	1.153	1.186	1.186

The stability study was also performed using empirical methods (Load Capacity Equation; the Sliding Wedge Method; Pillot and Moreau Chart; Pinto Chart, and representative use of S_u. Table 2 shows results obtained from the Juturnaíba and Sarapuí trial embankments. The results were satisfactory, which encourages application of these methods for preliminary results, especially the load capacity and sliding wedge methods.

The three-dimensional effect was also studied using the Azzouz *et al.* (1983) proposal. In the Juturnaíba trial embankment, the results from the three-dimensional minimal Safety Factor (SM_{3D}) were on the order of 10% higher than the bi-dimensional value.

The initial Sarapuí embankment analysis suggested that the first indication that failure was being approached occurred when the embankment height was 2.5 m. Until then the instruments had not shown any signs of imminent failure. On the following day, the embankment height was lifted to 2.8 m and after was raised to 3.1 m. The height of embankment of 2.8 m was considered that produced the failure. The total stability analysis suggested that Bjerrum (1973) correction factor, μ, may not be applicable (Ortigão 1980; Ortigão *et al.* 1983). Later Sandroni (1993) presented a discussion about the Sarapuí embankment demonstrating the Bjerrum (1973) proposal applicable when the failure height embankment was reevaluated, and the three-dimensional effect was considered (μ is 0.7 for SM of 1.45).

4.2. Total stress analysis results – Case Study 4

Bello (2004) performed total stability analysis of the embankment alongside highway BR-101-PE. The study seeks to comprehend the failure, and confirm the necessity to correct S_u from the vane field test on Recife soft clays. Sub-layers were defined, with varying soils and respective S_u values from field vane tests, corrected by the Bjerrum (1973) proposal. SM calculations were made using the Modified Bishop, Janbu, Spencer and Morgenstern-Price methods. Table 1 shows a summary of the minimal Safety Factor results obtained from stability analysis, together with back-analysis for three hypotheses regarding the cracking of the embankment, and the use of the corrected S_u value. In the stability analysis, the SM values are in the range of 0.995 to 1.082 for the circular surface condition, depending on the strength of the embankment. Hypothesis 3 (embankment 50% cracking and S_u corrected) presented SM equal to 1.00, explaining the rupture (Table 1 and Fig. 17). The influence of embankment cracks on the SM values ranged from 10% to 15%. In the back-analysis, SM results indicated a range of values close to those for the preliminary stability analysis (around 15% higher). This difference may be due to the difficulty of defining the failure surface for this case while in the field. The predicted critical circle was very similar to the failure surface observed *in situ*, and dislocated only slightly towards the left.

Table 2 - Summary of the S_u (back-analysis) and SM values obtained from empirical methods (Coutinho & Bello 2007).

Method	Height of embankment in a rupture (m)			Representative S_u value (kPa)			S_u (kPa) back-analysis (SM = 1)			SM representative S_u (kPa) value		
	(1)	(2)	(3)	(1)	(2)	(3)	(1)	(2)	(3)	(1)	(2)	(3)
Load capacity equation (Terzaghi 1943)	2.5	6.85	6.0	9.0	19.0	20.59	9.4	19.7	19.63	1.07	0.96	1.05
Sliding Wedges (NAVFAC 1971)							9.7	-	19.08	*	-	1.06
Pillot & Moreau (1973)							9.5	17.3	20.52	*	1.06	1.10
Abacus of Pinto (1966)							-	-	18.00		-	1.14

*The author did not calculate SM for representative S_u value.
Number of authors: (1) Sarapuí (Ortigão 1980); (2) Juturnaíba (Coutinho 1986); (3) Recife (Bello 2004).
Specific weight of embankment: (1) γ_{emb} = 18.4 kN/m^3; (2) γ_{emb} = 15.8 kN/m^3; (3) γ_{emb} = 18.0 kN/m^3.

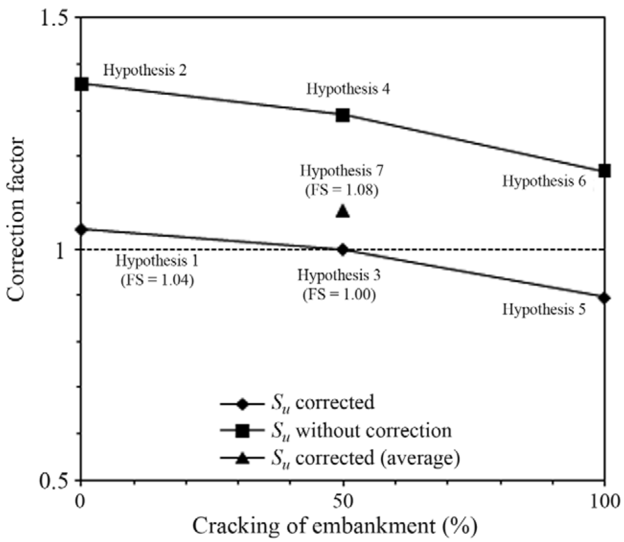

Figure 17 - Results of stability / back analysis (circular surface) - Bishop Method, embankment alongside highway BR-101-PE (Bello 2004).

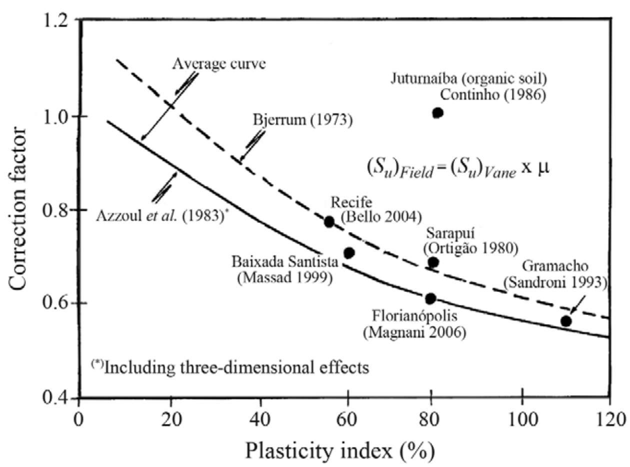

Figure 18 - Correction factors from back-analysis of rupture embankments (Bello 2004; Coutinho & Bello 2005; Coutinho 2006; Sandroni 2006).

The stability study was also performed using empirical methods (Load Capacity Equation; the Sliding Wedge Method; Pillot and Moreau Chart; Pinto Chart), and using a representative Su value for each case. Table 2 shows results obtained for the embankment alongside highway BR-101-PE. The results were satisfactory, which encourages application of these methods for preliminary results, particularly the load capacity and sliding wedge methods.

The three-dimensional effect was also studied using the Azzouz *et al.* (1983) proposal. The results showed a small increase in the three-dimensional SM value, on the order of 5% for the embankment alongside highway BR-101-PE.

4.3. Bjerrum (1973) correction factor, μ - Study Cases 1 and 4

Figure 18 presents the Bjerrum (1973) and Azzouz *et al.* (1983) proposal for the correction factor, μ, to be applied in Su values from field vane test, in order to obtain the undrained strength for design. The results from Brazilian experiences are also shown. It can be seen that the Brazilian results (high plasticity clays) validated the Bjerrum proposal (in general the two proposals). The Juturnaíba trial embankment results lie outside of the proposal, as it involves a highly organic soil foundation (see item 4.1). Stability analysis for the embankment alongside highway BR-101-PE showed the need for the correction factor, μ to be applied in S_u values from field vane tests, in order to obtain the undrained strength for design involving the Recife soft clays. In this case, the average result obtained was μ = 0.8.

4.4. Effective stress analysis results – Case Study 1

Coutinho (1986) carried out effective stress stability analysis on the Juturnaíba trial embankment in order to obtain the minimal Safety Factor SM, for the height that caused failure of the embankment (H_{emb} = 6.85 m). This analysis was performed basically through use of the Modified Bishop method, using preconsolidated, and normally consolidated effective strength parameters, and pore pressure measurements obtained through the use of pneumatic piezometers (Figs. 4 and 19). The fill strength parameters (cohesion $c = 29$ kN/m^2 and friction angle $\phi = 29°$) were determined from direct shear strength.

Analysis considering normally consolidated effective stress parameters for strength ($c = 0$ and $\phi' =$ average of 39°; ϕ' different in each layer of soft soil) presented satisfactory results, particularly when cracking of the embankment was considered to simulate the failure. The SM value obtained ranged from 0.95 to 1.23. In the case of 50% cracking of the embankment, the SM value equaled 1.05.

The predicted critical circle for the effective analysis was distinct for the failure surface observed in situ. The predicted circle presented a smaller extension in area and maximum depth. The observed failure surface showed values for the minimal Safety Factor greater than the corresponding ones obtained in the study of SM. For the case of 50% of cracking of the embankment, and the same effective strength, the SM value was 1.169.

Estimation of pore pressure values at points without piezometers, and the difficulties of measuring the pore pressure at the moment of failure, can cause a reduction in the accuracy of effective stress analysis.

Ortigão (1980) and Ortigão *et al.* (1983) present results of effective stability analysis of the Sarapuí trial embankment. A Minimal Safety Factor well below 1.0 was obtained for failure conditions from the effective stress analysis, considering normally consolidated effective stress parameters for strength. This case shows the difficulties in obtaining good results.

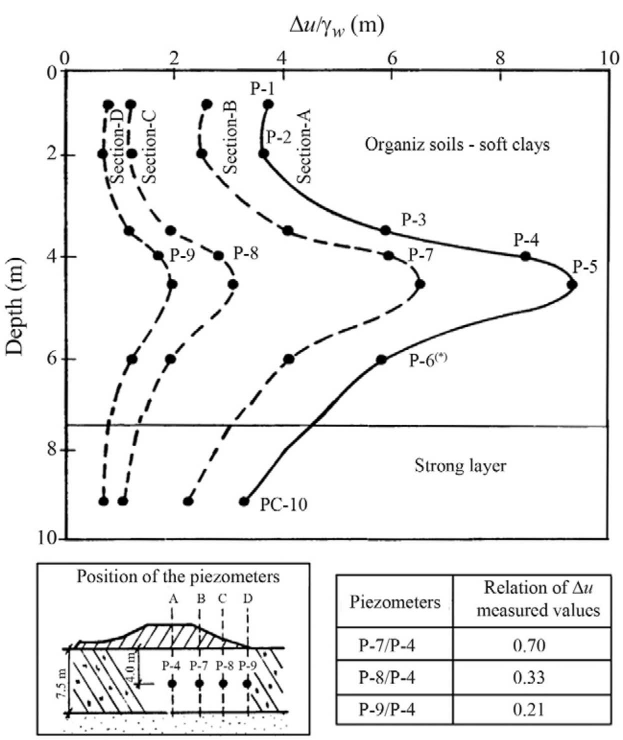

Piezometers	Relation of Δu measured values
P-7/P-4	0.70
P-8/P-4	0.33
P-9/P-4	0.21

Figure 19 - Estimation of pore pressure *vs.* depth – pneumatic piezometer (Coutinho 1986).

5. Stability Control

Field control of the stability of embankments on soft foundations is frequently a means of reducing, or even avoiding the risk of an undesirable failure, and also enables construction on a more rational, and economical basis. Stability control of an embankment can be carried out during construction using the measurement of displacements, deformations, and pore pressures.

This item presents results of stability control carried out on the Juturnaíba trial embankment (Case Study 1), the Juturnaíba Dam (Case Study 2); the access embankments for the Jitituba River Bridge (Case Study 3), and the Sarapuí trial embankment (Case Study 5).

5.1. Pore pressure

Stability control through observation of pore pressures can be carried out using interstitial pressure measurements in an effective stability analysis. In this method, it is necessary to obtain the effective strength parameters, adequate measurement of pore pressures, and the time needed to analyze the results. Results of an effective stability analysis are presented in item 4.3.

The results of increases in pore pressures measured near the middle of a soft deposit of foundation under the center of the embankment may show substantial increases in values when nearing failure. In this case, pore pressure parameter $\overline{B}_3$ ($\Delta u/\Delta\sigma_v$) presents values greater than 1.0 (Fig. 1). According to Tavenas & Leroueil (1980), and Leroueil & Rowe (2000), this condition would be a signal of local failure. The Juturnaíba trial embankment (Case Study 1) showed this behavior, and the result ($\overline{B}_3 > 1.0$) was considered to be a signal of the beginning of failure (Coutinho 1986; Coutinho & Bello 2011).

5.2. Horizontal displacements

Table 3 shows a summary of the stability control proposals for horizontal displacements presented and discussed in this study. In the analysis, two different conditions were considered: (a) embankments designed to be stable: the Juturnaíba Dam (Case Study 2) and the access embankments of the Jitituba River Bridge (Case Study 3); (b) trial embankments induced to rupture: Juturnaíba (Case Study 1) and Sarapuí (Case Study 5). In the stability control process, it is recommended that all behavior be analyzed, not just the value of the measurements, and in practice, more than one stability control proposal be used. Other experiences can be seen in Magnani de Oliveira *et al.* (2010) and Almeida *et al.* (2010).

Table 3 - Summary of the stability control proposals from horizontal displacements.

Analysis methods			Classification
	Maximum value (Y_{max}) *vs.* time (Kawamura 1985)		Convergent behavior → Stable Divergent behavior → Unstable
Y_{max} *vs.* time	Maximum value normalized in function of the thickness of the clay level (Y_{max}/D) *vs.* time		Convergent behavior → Stable Divergent behavior → Unstable
	Velocity of the maximum value normalized $(\Delta Y_{max}/D)/\Delta t$ *vs.* time (Cavalcante 2001; Cavalcante *et al.* 2003)		<< 0,2% / day → Stable > 0.2% / day → beginning to be Unstable
Angular distortion *vs.* time	Maximum value (vd) *vs.* time Construction end value (Ortigão 1980; Coutinho 1986; Cavalcante 2001; Cavalcante *et al.* 2003)		< 3% - Convergent behavior → Stable > 3% - Divergent behavior → beginning to be Unstable
	Velocity of the maximum value (vd) *vs.* time (Almeida *et al.* 2001)		vd ≥ 1.5%/day → Tendency to be unstable 0.5% ≤ vd ≤ 1.5% → Alert, especial attention vd ≤ 0.5%/day → Stable, to continue monitoring
Displaced vertical volume / Displaced horizontal volume	(Vv/Vh) or (ΔVv/ΔVh) *vs.* time	Sandroni *et al.* 2004	(ΔVv/ΔVh > 5) → Stable (3 < ΔVv/ΔVh < 5) → Medium (alert) (ΔVv/ΔVh < 3) → Unstable
		Johnston 1973	3.5-4.2 < ΔVv/ΔVh ≤ 20 → Stable (ΔVv/ΔVh ~ 2.4-1.8) → Unstable
	H_{emb} *vs.* Vh	Sandroni *et al.* 2004	H_{emb} *vs.* Vh increase significantly → Unstable
Y_{max}/D *vs.* SM	(Bourges & Mieussens 1979; Coutinho 1980); Cavalcante 2001; Cavalcante *et al.* 2003)		> 1.8% → Unstable = 1.0% → Stable (SM~1.5) < 0.8%→Stable minimum horiz. displacements

5.2.1. Tendency for horizontal displacements

Analysis of the horizontal displacements was carried out with three considerations: (a) maximum horizontal displacements (Y_{max}) *vs.* time; (b) maximum horizontal displacements, normalized in function of the thickness of the clay layer (Y_{max}/D) *vs.* time; (c) and velocity of the maximum horizontal displacements normalized $(\Delta Y_{max}/D)/\Delta t$ *vs.* time.

(a) Figures 20a and 20b present the evolution of the maximum horizontal (lateral) displacements (Y_{max}) through time, considering the access embankments of the Jitituba River Bridge, and Juturnaíba trial embankment. The main objective of this analysis is to evaluate the possibility of creep rupture (Kawamura 1985). Using this model, rupture from undrained creep is associated with the divergent behavior in the evolution of displacements through time, while the convergent behavior would indicate consolidation and stabilization.

The tendency observed in the access embankments of the Jitituba River Bridge is clearly convergent during and af-

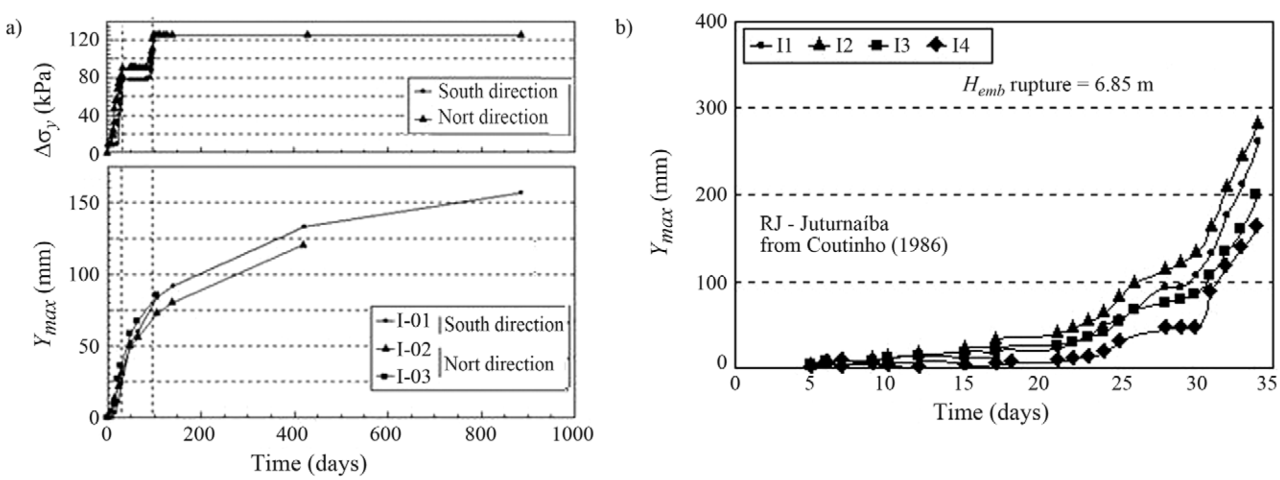

Figure 20 - Maximum horizontal displacements through time: (a) Juturnaíba trial embankment (Coutinho 1986); (b) access embankments of the Jitituba River – up to 885 days (Cavalcante *et al.* 2003).

ter construction, thus indicating the stabilization condition. The maximum horizontal displacement measured just after the end of construction (140 days) was on the order of 80-97 mm, and in the long term (885 days), on the order of 155 mm. In Juturnaíba Dam construction was observed convergent behavior and stabilization condition. Inclinometer I-3 showed values of Y_{max} on the order of 180 mm in 650 days (H_{emb} = 10.70 m) (Lucena 1997; Cavalcante *et al.* 2003).

The tendency observed in the Juturnaíba trial embankment is clearly divergent, particularly after 30 days (H_{emb} = 5.60 m; FS = 1.31), with inclinometer I-3 showing a maximum stable horizontal displacement value on the order of 100 mm, and the last reading corresponding to H_{emb} just before failure, with Y_{max} values on the order of 270 mm. The Sarapuí trial embankment also presented divergent behavior, being more evident after 25 days (H_{emb} = 2.5 m). Inclinometers I-2 and I-4 showed values limit of Y_{max} on the order of 100 mm. In the failure (H_{emb} = 2.8 m), the value of Y_{max} was on the order of 300 mm (Coutinho 1986; Cavalcante *et al.* 2003).

(b) Figure 21 presents the maximum horizontal displacement normalized as a function of the thickness of the clay layer (Y_{max}/D) *vs.* time for the access embankments of the Jitituba River Bridge, and for the Juturnaíba trial embankment. The tendency observed is in agreement with what is proposed, and with the design conditions of each embankment. The convergent behavior in access embankments of the Jitituba River bridge becomes more evident after 140 days, with Y_{max}/D values of 0.6% (H_{emb} = 4.8 m), and 0.9% (H_{emb} = 7.0 m) after 170 days. The Juturnaíba Dam construction showed convergent behavior (stable) with higher values in inclinometers I-1, I-3 and I-4, with Y_{max}/D values of 1.8%, 3.4% and 3.6% for H_{emb} of 10.7 m (Lucena 1997; Coutinho *et al.* 1994; Cavalcante *et al.* 2003).

The divergent behavior of the Juturnaíba trial embankment becomes more evident after 30 days (H_{emb} = 5.60 m; FS = 1.31), with inclinometer I-3 showing Y_{max}/D values of around 1.22% (limit of stability), and for the last reading corresponding to Hemb just before failure, the Y_{max}/D value is 2.75% (beginning to be unstable). The Sarapuí trial embankment showed divergent behavior (inclinometers I-2 and I-4), with values limit of Y_{max}/D of 0.7% and 0.9% (H_{emb} = 2.50 m), and Y_{max}/D values of 1.5 and 1.7% for H_{emb} of 2.8 m (unstable).

(c) The divergent and convergent behavior of the Y_{max}/D curve *vs.* time directly relates to the velocity of the horizontal deformation. Cavalcante *et al.* (2003) verified the possibility of evaluating the unstable or stable situation of the foundation soil through the velocity of the horizontal deformation. Figure 22a shows the results of the velocity of maximum horizontal displacement normalized $(Y_{max}/D)/\Delta t$ *vs.* time for a stable embankment (the access embankments of the Jitituba River bridge), presenting maximum values on the order of 0.024%/day. Figure 22b shows the results of $(Y_{max}/D)/\Delta t$ with time for an embankment induced to rupture (Juturnaíba trial embankment). It is observed that after 30 days, a large increment occurs in the rate of variation of the $(Y_{max}/D)/\Delta t$ value, showing a stable limit value of around 0.20%/day (H_{emb} = 5.6 m), with the last reading corresponding to H_{emb} just before failure, the $(Y_{max}/D)/\Delta t$ value is 0.5%/day. Coutinho (1986) and Cavalcante *et al.* (2003) found similar divergent behavior results in the Sarapuí trial embankment. After 25 days, a stable limit value around 0.20%/day (H_{emb} = 2.5 m) was shown, and for the failure (H_{emb} = 2.8 m), the $(Y_{max}/D)/\Delta t$ value is 0.5%/day. Lucena (1997) and Coutinho *et al.* (1994) showed $(Y_{max}/D)/\Delta t$ results for the Juturnaíba Dam, with stable behavior and values of around 0.03%/day. The maximum $(Y_{max}/D)/\Delta t$ value observed at the recommended limit for stable condition (SM = 1.30) was about 10 times greater in the embankment induced to failure, in comparison with the embankments constructed to be stable.

5.2.2. Angular distortion with time

Analysis of angular distortion was carried out considering two proposals: (a) maximum angular distortions *vs.*

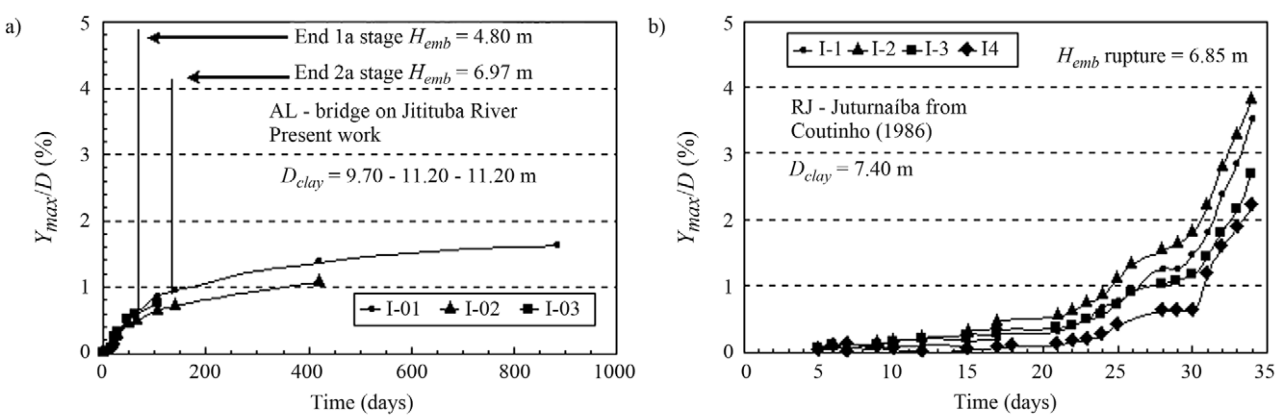

Figure 21 - Relation Y_{max}/D (horizontal maximum displacements / thickness of the clay layer) with time - a) stable embankments; b) embankments induced to the rupture (Cavalcante 2001; Cavalcante *et al.* 2003).

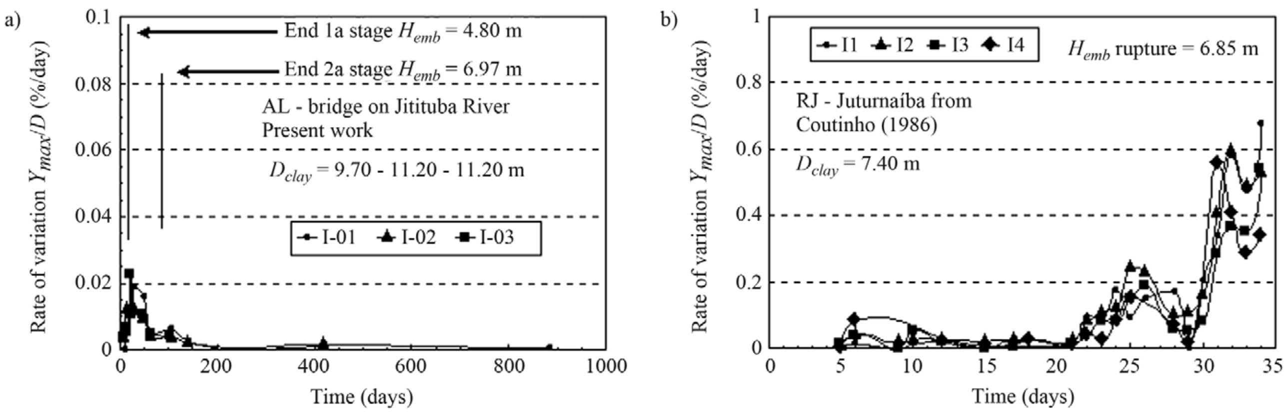

Figure 22 - Rate of variation of the relation Y_{max}/D (horizontal maximum displacements / thickness of the clay layer) through time: a) Stable embankments – access embankments of the Jitituba River Bridge; b) embankments induced to rupture - Juturnaíba trial embankment (Cavalcante 2001; Cavalcante *et al.* 2003).

time and maximum construction end values; and (b) velocity of maximum angular distortion (vd) *vs.* time.

(a) Figure 23 presents the results of maximum angular distortions (10^{-2} radians or %) through time, for the access embankments of the Jitituba River Bridge. The convergent stable behavior is similar to that observed in the analysis of the maximum horizontal displacement. The curve showed a stable maximum value of 2% for just after the end of construction (140 days), and in the long term 3.5% for 885 days.

The tendency observed in the Juturnaíba trial embankment is clearly divergent behavior (Fig. 24). Coutinho (1986), in the analysis of the behavior of the Juturnaíba and Sarapuí trial embankments, found the maximum angular distortions to show divergent behavior for values in the rupture, measuring around 12 and 17%, respectively. The embankments remained stable during construction, with the maximum angular distortion value lower than 4% in the Juturnaíba trial embankment, and 3% in the Sarapuí trial embankment.

(b) Figure 25 presents the value for the maximum rate of angular distortion (vd) *vs.* time for the access embankments of the Jitituba River Bridge. The maximum value observed was 0.07%/day during the initial construction period, showing a much lower value than the vd < 0.5%/day limit proposed by Almeida *et al.* (2001) for a stable situation (Table 3).

Table 4 shows the vd results obtained for the Juturnaíba trial embankment. The values were relatively small (vd < 0.6%/day), and the embankment remained stable to an embankment height of 5.60 m (SM = 1.31). However, in considering Table 3, inclinometer I-2 was practically within the stable limit when beginning to show the alert signal. When the embankment height was increased from 5.60 to 6.10 m, a significant increase in vd occurred for all inclinometers, particularly for I-2, showing extremely high values (H_{emb} = 6.40 m), indicating imminent collapse. The failure occurred with H_{emb} = 6.85 m.

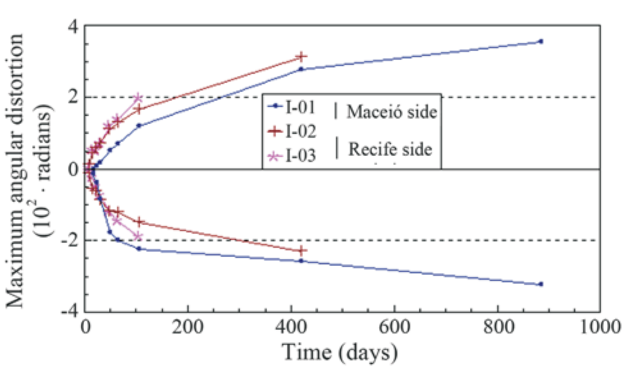

Figure 23 - Maximum angular distortion through time, I-01, I-02, I-03, access embankments of the Jitituba River Bridge (Cavalcante *et al.* 2003).

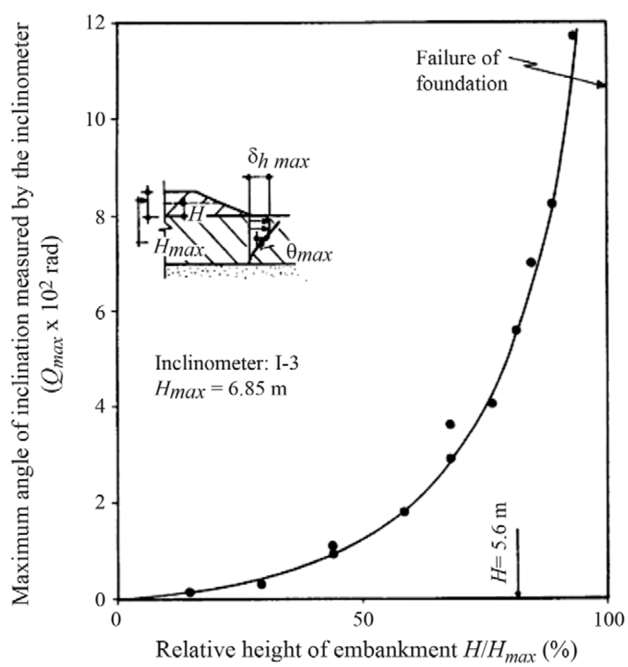

Figure 24 - Maximum angular distortion *vs.* the height of embankment,- Juturnaíba trial embankment (Coutinho 1986).

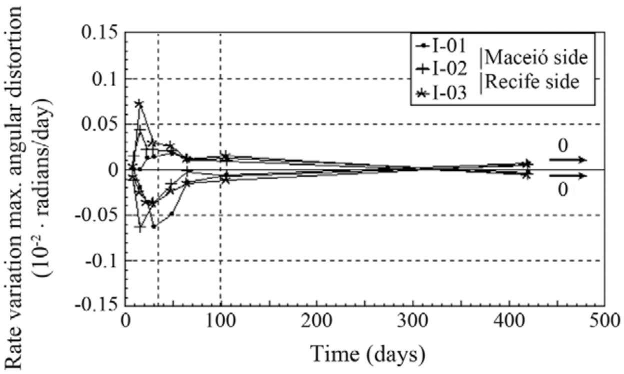

Figure 25 - Rate of variation of the maximum angular distortion with time, access embankments of the Jitituba River Bridge (Cavalcante *et al.* 2003).

5.2.3 Relationship between the variation of vertical volume, and the variation of horizontal volume

Sandroni *et al.* (2004) presented a stability control proposal with analysis and discussion on this topic. The proposed methodology (Table. 3) is based on the displaced vertical volume (Vv) and the displaced horizontal volume (Vh) involving two relations: (a) Vv/Vh or dVv/dVh *vs.* time (t) or embankment height (H_{emb}); and (b) Vh *vs.* H_{emb}. In the methodology, it is recommended that analysis be given to the behavior of all the relations proposed, in order to be able to verify the condition of stability. Johnston (1973) developed earlier studies and observed a range of $3.5\text{-}4.2 < Vv/Vh \leq 20$, corresponding to partial drainage behavior, without failure of embankments; in the embankment which presented failure, Vv/Vh was in the range of 2.4-1.8 (Table 3).

(a) Figure 26a shows the results of Vv/Vh and dVv/dVh *vs.* H_{emb} obtained from the Juturnaíba trial embankment. The values for Vv/Vh were higher that 14 until H_{emb} = 3.25 m, decreasing to 7 between H_{emb} = 3.25 and 5.6.m (SM = 1.31), presenting the stability limit. The values between H_{emb} = 5.6 and 6.4 m decrease to 4.5, presenting a signal of failure. In the case of dVv/dVh, values were higher than 14 in the beginning of loading, decreasing to

Table 4 - Angular distortion rate, vd in the Juturnaíba trial embankment (Coutinho 1986; Almeida *et al.* 2001).

H (m)	I-1 (%/day)	I-2 (%/day)	I-3 (%/day)	I-4 (%/day)	I-5 (%/day)
4.65	0.3	0.6	0.5	0.5	0.5
5.60	0.3	0.6	0.4	0.4	0.4
6.10	1.3	2.3	1.3	1.4	1.6
6.40	2.7	2.5	3.1	1.4	2.4

4.0 when the embankment height was increased from 3.25 m to 5.60 m. Finally, at H_{emb} = 6.4 m, the results of this relation equaled 2.0, presenting a signal of failure.

In the Sarapuí trial embankment, the Vv/Vh results were higher than 7.0, until H_{emb} = 2.5 m. An abrupt decrease to values under 3.0 was observed. The dVv/dVh values ranged from 1.0 to 2.0 for H_{emb} = 2.5 m, indicating that the beginning of the rupture that occurred at the 2.5 m embankment height (Sandroni *et al.* 2004).

This proposal was applied to the access embankments of the Jitituba River Bridge (Cavalcante *et al.* 2003). The $\Delta Vv/\Delta Vh$ results ranged from 8.4 to 28.0 (Southern direction) and 4.2 to 28.0 (Northern direction), which in general was classified as a stable condition, and only in some intervals, during the first phase of the construction, did the embankment present a situation classified as medium/alert.

(b) Another unstable condition is when the H_{emb} *vs.* Vh relation shows divergent behavior, with a significant increase in inclination. Figure 26b shows the results of H_{emb} *vs.* Vh obtained from the Juturnaíba trial embankment. Above the embankment height of 5.60 m (FS = 1.3), the behavior changed significantly, showing results that correspond to the beginning of a possible failure process, which occurred shortly afterwards, with H_{emb} = 6.85 m.

5.2.4 Relationship between horizontal displacements and safety factor (or embankment height)

For use as a stability control proposal, Bourges & Mieussens (1979) related the maximum horizontal dis-

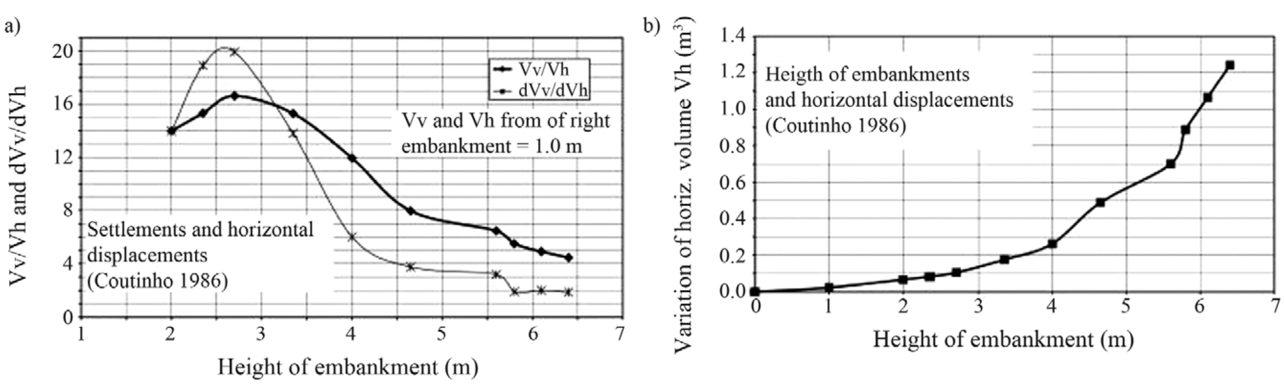

Figure 26 - Juturnaíba trial embankment: a) failure around 35 days; b) evolution of horizontal volume with the height of embankment (Coutinho 1980; Sandroni *et al.* 2004).

placement corresponding to the end of construction, and normalized it in function of the thickness of the clay layer (Y_{max}/D) *vs.* embankment height (H_{emb}), or the Minimal Safety Factor (SM).

Coutinho (1986), in the stability control for the Juturnaíba trial embankment, discussed the use of the Y_{max}/D *vs.* relative height of embankment, H/H_{max} (%). Figure 27 presents the observed results, where divergent behavior can be seen, including a sharp increase after H_{emb} = 5.6 m, and a maximum value of 3% (H_{emb} = 6.4 m) just before failure. In this case, it is recommended that the relation be less than 1.5% in order to have a stable condition. Ortigão (1980) and Ortigão *et al.* (1983) in the Sarapuí trial embankment, found Y_{max}/H_{emb} results of 2.7% for an embankment height of 2.8 m (failure condition).

Cavalcante *et al.* (2003) presented and discussed Y_{max}/D *vs.* SM results obtained for a number of Brazilian embankments on soft clays (Fig. 28). It can be observed that the tendency is for SM values to decrease when the Y_{max}/D values increase. For the stable Jitituba embankment, the maximum values for the Y_{max}/D relation for the 1st and 2nd stages of construction were 0.54% and 0.32%, respectively. Lucena (1997) and Coutinho *et al.* (1994) in the Juturnaíba Dam construction, encountered Y_{max}/H_{emb} results of 1.93%, 0.90%, and 2.09% (inclinometers I-1, I-2 and I3) for an embankment height of 6.0 m (1st stage), demonstrating marginally stable behavior (Fig. 28).

Considering these cases, Cavalcante *et al.* (2003) proposed values for stability control during the construction phase: (a) Y_{max}/D > 1.8% indicates the proximity of rupture situations (SM ~ 1.0); (b) Y_{max}/D = 1.0% is generally adopted in practical application as the safety factor (SM ~ 1.5); (c) Y_{max}/D < 0.8% indicates limit of horizontal displacement.

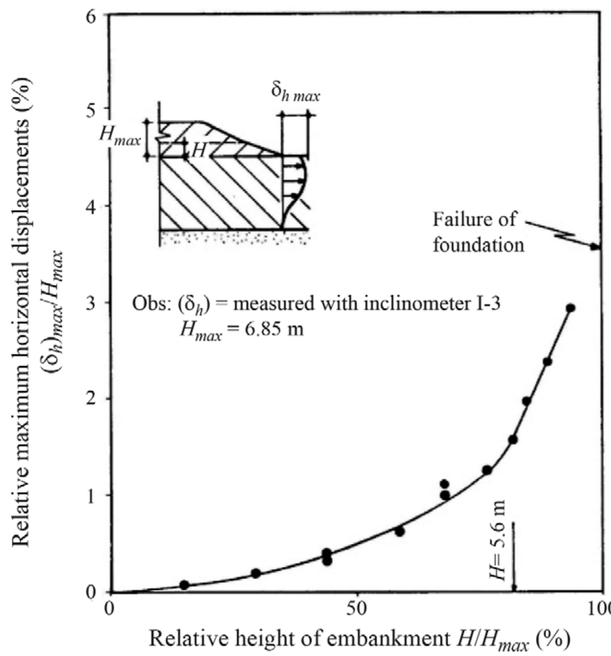

Figure 27 - Relation between the horizontal displacement and the relative height of the embankment, I-3 (Coutinho 1986).

5.2.5. Summary of the stability control (horizontal displacements) results

Table 5 presents a summary of the results obtained in the analysis of stability control from horizontal displacements using all of the proposals from Table 3. Two different conditions were considered: (a) a trial embankment induced to rupture: Juturnaíba (Case Study 1) and Sarapuí (Case Study 5); (b) embankments designed to be stable: the Juturnaíba Dam (Case Study 2) and the access embankments of the Jitituba River Bridge (Case Study 3). The be-

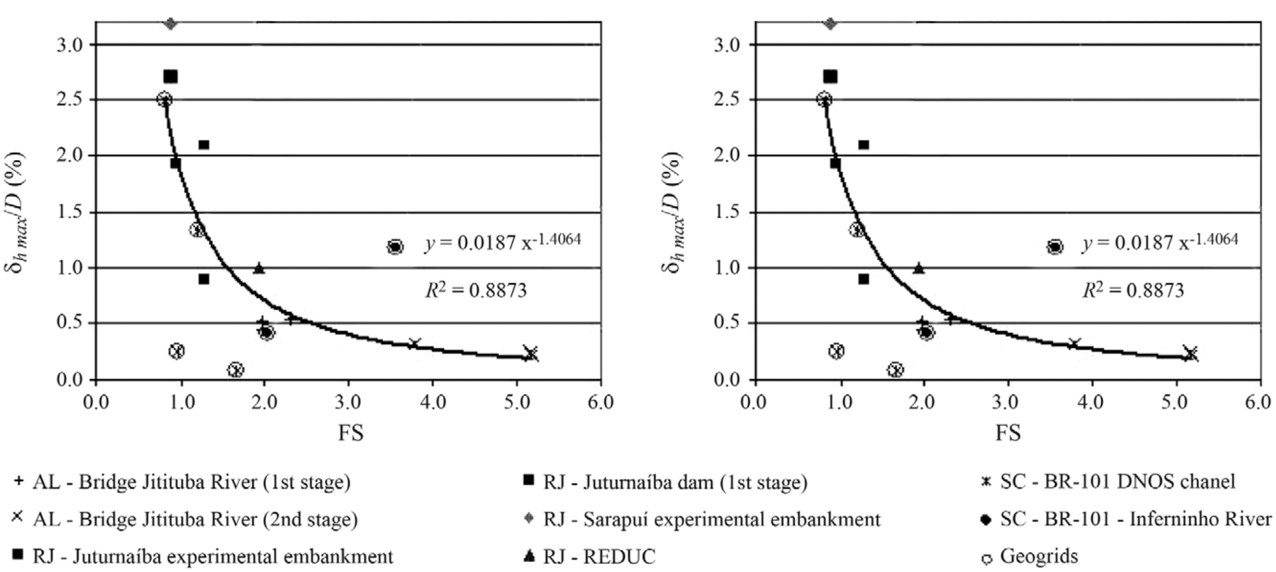

Figure 28 - Y_{max}/D *vs.* FS (or SM relation): Brazilian embankments (Cavalcante *et al.* 2003).

Table 5 - Summary of the stability control results from horizontal displacements proposals.

Analysis methods		Results / classification			
		(Case Study 1) Sarapuí trial embankment	(Case Study 2) Juturnaíba trial embankment	(Case Study 3) Juturnaíba Dam	(Case Study 4) Access embankments of the Jitituba River Bridge
Horizontal displacement *vs.* time	Maximum value normalized in function of the thickness of the clay level (Y_{max}/D) *vs.* time	*I2 and I4 - Divergent* H_{emb} = 2.5 m - 0.7-0.9% Safe Limit H_{emb} = 2.8 m - 1.5-1.7% Unstable	*I3 - Divergent* H_{emb} = 5.6 m - 1.22% Safe Limit H_{emb} = 6.4 m - 2.75% Beginning to be Unstable	*I1, I3 and I4 Convergent* H_{emb} = 10.7 m 1.8; 3.4; 3.6% Stable	*Convergent* H_{emb} = 4.8 m - 0.6% H_{emb} = 6.97 m - 0.9% Stable
	Velocity of the maximum value normalized ($\Delta Y_{max}/D$) *vs.* time (Cavalcante 2001; Cavalcante *et al.* 2003)	*I3 and I4* H_{emb} = 2.5 m - 0.20%/day Safe Limit H_{emb} = 2.8 m - 0.5%/day Unstable	*I1, I2, I3 and I4* H_{emb} = 5.6 m - 0.25%/day Safe Limit H_{emb} = 6.4 m - 0.5%/day Beginning to be Unstable	0.030% / day Stable	0,024% / day Stable
Angular distortion *vs.* time	Maximum value (vd) *vs.* time Construction end value (Ortigão 1980; Coutinho 1986; Cavalcante 2001; Cavalcante *et al.* 2003)	*I3 and I4 - Divergent* 3.0% - Safe Limit 12% - Unstable	*I3 - Divergent* H_{emb} = 5.6 m - *3%* Safe Limit H_{emb} = 6.4 m -12% Beginning to be Unstable	-	*Convergent behavior* Stable < 2%
	Velocity of the maximum value (vd) *vs.* time (Almeida *et al.* 2001)	H_{emb} = 2.5 m -1.00%/day Safe Limit H_{emb} = 2.8 m - 3.5%/day Unstable	H_{emb} = 5.6 m - 0.4%/day Safe Limit H_{emb} = 6.4 m- 3.1%/day Beginning to be Unstable	-	0.07% / day Stable
Displaced vertical volume *vs.* Displaced horizontal volume	(Vv/Vh) or (ΔVv/ΔVh) *vs.* H_{emb} or time (Sandroni & Lacerda 2001; Sandroni *et al.* 2004	ΔVv/ΔVh: H_{emb} = 2.5 m - 7.0 - Safe Limit H_{emb} = 2.8 m = 1.0- Unstable Vv/Vh: H_{emb} = 2.5 m - 7.0 - Safe Limit H_{emb} = 2.8 m = 3.0- Unstable	ΔVv/ΔVh: H_{emb} = 5.6 m - 4.0 - Safe Limit H_{emb} = 6.4 m = 2.0 - Beginning to be Unstable Vv/Vh: H_{emb} = 5.6 m - 7.0 - Safe Limit H_{emb} = 6.4 m = 4.0 - Beginning to be Unstable	-	Southern direction (8.4 to 28.0) Stable Northern direction (4.2 to 28) Medium to Stable
	Vh *vs.* H_{emb}	-	H_{emb} = 5.6 m - 0.6 Safe Limit H_{emb} = 6.4 m - 1.25 Beginning to be Unstable	-	-
Y_{max}/D x SM or Y_{max}/D x H_{emb} (Bourges & Mieussens 1979; Coutinho,1980 Cavalcante 2001; Cavalcante *et al.* 2003)		*I3 and I4 - Divergent* H_{emb} = 2.8 m - 3.0% Unstable	*I3 - Divergent* H_{emb} = 5.6 m - 1.5% Safe Limit H_{emb} = 6.4 m - 3.0% Beginning to be Unstable	*I1, I2 and I3* H_{emb} = 6.0 m (1st Stage) 1.93%; 0.90%; 2.09% Marginally Stable	0.44 to 0.54% Stable (minimum horizontal displacements)

havior tendency, limit values for stable condition (safe limit) and values on unstable condition were presented. The results in general agreed with the stability control proposals for horizontal displacements, showing potential for use in practical work, depending on each problem. It was seen that it is important for more than one proposal be employed, in order to have additional confidence in decisions, and that all behavior has to be analyzed, not just the measurement values. The trial embankments induced to rupture studied in this paper shown that is possible to predict the rupture, with the Juturnaíba embankment showing more anticipating and clearly change from stable to unstable condition. The joint results of stability analysis and stability control show the importance of having SM > 1.3 to guarantee adequate behavior and security.

Ladd (1991) presents and discusses the use and interpretation of displacement data from the field for use in stability control. It is pointed out that this requires experience and judgment, along with the use of different graphs for each problem. The authors recommend the use of many of the graphs / proposals shown in this paper. It must also be remembered that the behavior of a soft clay foundation may be brittle or ductile. In soils with brittle behavior, such as sensitive clays, the rupture can be abrupt and difficult to anticipate. In soils with ductile behavior, the process tends to be more gradual, with greater possibly for advanced warning.

6. Final Comments and Conclusions

This paper presents the results of stability analysis and stability control, with emphases on studies carried out by the Geotechnical Group (GEGEP) of the Federal University of Pernambuco, Brazil. Five Brazilian cases are presented: the Juturnaíba trial embankments and Juturnaíba Dam construction, located in Rio de Janeiro; the access embankments of the Jitituba River Bridge in Alagoas; the failure of an embankment alongside highway BR-101-PE, located in Recife, Pernambuco; and the Sarapuí trial embankment, located in Rio de Janeiro.

Some of the approaches presented and discussed here were used for evaluation of mobilized undrained shear strength S_u in an embankment constructed in one stage. In the total stability analysis, cases of failure in Brazilian embankments on soft clays (the exception being the Juturnaíba trial embankment) show the need for application of the Bjerrum (1973) correction factor to the field vane test measurements for undrained strength. The presence of organic soil layers in the Juturnaíba foundation, combined with strong drainage and deformation/increases from effective stress during the construction, seem to be a possible explanation for the "different" behavior.

Effective stress stability analysis performed on the Juturnaíba trial embankment presented satisfactory results, considering normally consolidated effective stress parameters of strength, particularly when cracking of the embankment was considered to induce failure.

Stability control is one of the important steps in the design and construction of embankments on soft soils, and can be carried out through the measurement of displacements, deformations or pore pressures. Proposals were presented and analyzed, particularly for horizontal displacements, showing potential for use in practical work, depending on each problem. Due to the limits of each proposal, and many variables involved in the process, it is recommended that more than one proposal be used to obtain more confidence in decisions, and that all behavior be analyzed, not just the value of measures. The Juturnaíba trial embankments induced to rupture showed that would be possible to avoid the rupture, with reasonable anticipating and clearly change from stable to unstable condition.

The joint results of stability analysis and stability control show the importance of having SM > 1.3 to guarantee adequate behavior and security.

Acknowledgments

An acknowledgement is due to both CNPq and CAPES for their financial support. Special thanks to Maria Helena Lucena and Sarita Cavalcante, who contributed data for use in this paper, and to Gusmão Associated Engineers, for entering into a partnership with GEGEP.

References

Almeida, M.S.S.; Oliveira, J.R.M.S. & Spotti, A.P. (2001) Previsão e desempenho de aterro sobre solos moles: Estabilidade, recalques e análises numéricas. In: Encontro das Argilas Moles Brasileiras. COPPE/UFRJ e ABMS, Rio de Janeiro e São Paulo, pp. 166-191.

Almeida, M.S.S. & Marques, M.E.S. (2010) Aterros Sobre Solos Moles. Editora Oficina de Textos, São Paulo, 254 pp.

Almeida, M.S.S.; Marques, M.E.S. & Lima, B.T. (2010) Overview of Brazilian construction practice over soft soils. Márcio Almeida (ed) New Techniques on Soft Soils. Oficina de Textos, São Paulo, pp. 247-268.

Azzouz, A.S.; Baligh, M. & Ladd, C. (1983) Corrected field vane strength for embankment design. ASCE JGE, v. 109:5, p. 730-734.

Bello, M.I.M.C.V. (2004) Estudo de Ruptura em Aterros Sobre Solos Moles – Aterro do Galpão localizado na Br-101-PE. M.Sc. Thesis, Universidade Federal de Pernambuco, Recife, 207 pp. (in Portuguese).

Bello, M.I.M.C.V.; Coutinho, R.Q. & Gusmão, A.D. (2006) Estudo de ruptura de um aterro sobre solos moles localizado em Recife, Pernambuco. Proc. XIII COBRAMSEG, Curitiba. v. 4, pp. 2115-2120.

Bjerrum, L. (1973) Problems of soil mechanics and construction of soft clays and structurally unstable soils. 8th ICSMFE, Moscow, v. 3, pp. 111-159.

Bourges, F. & Miussens, C. (1979) Déplacement latéraux à proximité des remblais sur sols compressibles – Méthod de prévision. Bull. Liaison Labo. P. et Ch., n. 101, p. 73-100.

Cavalcante, S.P. (2001) Análise de Comportamento de Aterros sobre Solos Moles – Aterros de Encontro da Ponte sobre o Rio Jitituba- AL. M.Sc. Thesis, Universidade Federal de Pernambuco, Recife, 232 pp.

Cavalcante, S.P.; Coutinho, R.Q. & Gusmão, A.D. (2003) Evaluation and control of stability in field of embank on soft soils. Proc. XII PCSMGE, Cambridge, pp. 2649-2660.

Cavalcante, S.P.P.; Coutinho, R.Q. & Gusmão, A.D. (2004) Analysis of behavior of embankments on soft soils geotechnical investigations and instrumental access embankments of the Jitituba River Bridge. Prof. 15th ICCHGE, New York, paper 2.83, pp. 1-9.

Coutinho, R.Q. (1986) Aterro Experimental Instrumentado Levado à Ruptura Sobre Solos Orgânicos-Argilas Moles Barragem de Juturnaíba. D.Sc. Thesis, COPPE/Universidade Federal do Rio de Janeiro, Rio de Janeiro, 634 pp.

Coutinho, R.Q. (2006) Characterization and Engineering Properties of Recife Soft Clays – Brazil. Charact. and Eng. Properties of Natural Soils, Singapor. v. 3, pp. 2049-2100.

Coutinho, R.Q.; Oliveira, J.T.R. & Oliveira, A.T.J. (1998) Geotechnical site characterization of Recife soft clays. Proc. ISC'98 - I International Symposium on Site Characterization, ISSMGE/ASCE/CGS, Balkema, Atlanta, v. 2, pp. 1001-1006.

Coutinho, R.Q.; Almeida, M.S.S. & Borges, J.B. (1994) Analysis of the Juturnaíba embankment dam built on soft clay. ASCE, Geot. Spec. Public. N. 40, v. 1, p. 348-363.

Coutinho, R.Q. & Lacerda, W.A. (1987) Characterization-consolidation of Juturnaíba organic clays. Proc. ISGESS, Mexico City, México, v. 1, pp. 17-24.

Coutinho, R.Q. & Lacerda, W.A. (1989) Strength characteristics of Juturnaíba organic clays. Proc. 12th ICSMFE, Rio de Janeiro, v. 3, pp. 1731-1734.

Coutinho, R.Q.; Oliveira, A.T.J. & Oliveira, J.T.R. (2000) Palheta: Experiência, Tradição e Inovação. Conferência IV Seminário de Engenharia de Fundação Especiais e Geotecnia / Seminário Brasileiro de Investigação de Campo, São Paulo, v. 3. pp. 53-80.

Coutinho R.Q. & Bello M.I.M.C.V. (2005) Geotecnia do Nordeste – Aterro sobre Solos Moles. ABMS/ Núcleo Nordeste, Recife, Editora Universitária / UFPE, v. 3, pp. 111-153.

Coutinho, R.Q. & Bello, M.I.M.C.V. (2007) The empirical methods for stability analysis in total tensions for embankments on soft soils. Proc. XIII Conferencia Panamericana de Mecánica de Suelos e Ingeniería Geotécnica, Isla Margarita, pp. 868-873.

Coutinho, R.Q. & Bello, M.I.M.C.V. (2010) Analysis and control of the stability of embankments on soft soil: Juturnaíba and other experiences in Brazil. M. Almeida (ed) New Techniques on Soft Soils. Oficina de Textos, São Paulo, pp. 247-268.

Coutinho, R.Q. & Bello, M.I.M.C.V. (2011) Monitoring and performance of embankments on soft soil: Juturnaíba trial embankment and other experiences in Brazil. Soils and Rocks, v. 34:4, p. 353-378.

Johnston, I.W. (1973) Discussion – Session 4. In: Field Instrumentation in Geotechnical Engineering, Halsted Press Book, John Wiley, New York, pp. 700-702.

Kawamura, K. (1985) Methodology for landslide prediction. Proc. XI ICSMFE, San Francisco, v. 3, pp. 1155-1158.

Ladd, C.C. (1991) Stability evaluation during staged construction. JGE, ASCE, v. 117:4 p. 540-615.

Leroueil, S & Rowe, R.K. (2000) Embankments Over Soft Soil and Peat. Geotechnical and Geoenviromental Engineering Handbook. R.K. Rowe (ed) Kluwer Academic Publishers, Norwell, USA, pp. 463-498.

Lucena, M.H.L. (1997) Análise do Comportamento da Fundação da Barragem de Juturnaíba – Techos III-2 e V. M.Sc. Thesis, Universidade Federal University de Pernambuco, Recife, 219 pp. (in Portuguese).

Magnani de Oliveira, H.; Almeida, M.S.S & Ehrlich, M. (2010) Reinforced test embankments on Florianopolis very soft clay. In: Almeida, M.S.S. (ed) New Techniques on Soft Soils. Oficina de Textos, São Paulo, pp. 65-76.

Magnani de Oliveira, H. (2006) Comportamento de Aterros Reforçados sobre Solos Moles Levados à Ruptura. D. Sc. Thesis, COPPE/ Universidade Federal do Rio de Janeiro, Rio de Janeiro, 495 pp. (in Portuguese).

Mesri, G. (1975) Discussion: New design procedure for stability of soft clays. ASCE JGE, Division v. 101:GT4, p. 409-412.

NAVFAC DM-7 (1971) Design Manual of Soil Mechanics, Foundations and Earth Structures, Naval Facilities Engineering Command, Washington, D.C.

Ortigão, J.A.R. (1980) Aterro Experimental Levado à Ruptura sobre Argila Cinza do Rio de Janeiro. D.Sc. Thesis, COPPE/ Universidade Federal do Rio de Janeiro, Rio de Janeiro, 715 pp. (in portuguese).

D.Sc. Thesis, COPPE/UFRJ, Rio de Janeiro.

Ortigão, J.A.R.; Werneck, M.L.G. & Lacerda, W.A. (1983) Embankment failure on clay near Rio de Janeiro. Journal of Geotechnical Engineering ASCE, v. 109:11, p. 1460-1479.

Pillot, G. & Moreau, M. (1973) La Stabitité des Remblais sur sol Mous – Abaqus de Calcul. Editions Eyrolles, Paris, 151 pp.

Pinto, C.S. (1966) Capacidade de carga de argilas com coesão linearmente crescente com a profundidade. Jornal de Solos, v. 3:1, p. 21-44.

Sandroni, S.S. (1993) Sobre o uso do ensaio de palheta *in situ* em aterros sobre argilas moles. Solos & Rochas, v. 16:3, pp. 207-213.

Sandroni, S.S. (2006) Sobre a prática brasileira de projeto geotécnico de aterros rodoviários em terrenos com solos muito moles. In: Congresso Luso-Brasileiro, Curitiba, pp. 507-512.

Sandroni, S.S. & Lacerda, W. (2001) Discussão sobre Controle de Estabilidade em Aterros sobre Solos Moles. Encontro Propriedades das Argilas Moles Naturais Brasileiras, COPPE/UFRJ-ABMS, Rio de Janeiro e São Paulo, pp. 245-257.

Sandroni, S.; Lacerda, A.W. & Brandt, J.R.T. (2004) Método dos volumes para controle de campo da estabilidade de aterros sobre argilas moles. Solos & Rochas, v. 27:1, p. 37-57.

Skempton, A.W. (1957) Discussion. Proc. Institution of Civil Engineers, v. 7, p. 305-307.

Tavenas, F. & Leroueil, S. (1980) The behavior of embankments on clay foundations. Canadian Geotechnical Journal, v. 17:2, p.236-260.

Tavenas, F.; Trak, B. & Lerouiel, S. (1980) Remarks on the validity of stability analysis. Canadian Geotechnical Journal, v. 17:1, p. 61-73.

Terzaghi, K. (1943) Theoretical Soil Mechanics, Wiley, New York, 510 pp.

Monitoring and Performance of Embankments on Soft Soil: Juturnaíba Trial Embankment and Other Experiences in Brazil

R.Q. Coutinho, M.I.M.C.V. Bello

Abstract. The accurate performance of instrumentation is fundamental to the adequate use of the results obtained from analyzing the behavior of constructions of embankments on soft soils. When evaluating embankment behavior, the geotechnical instrumentation for pore pressure and vertical and horizontal displacements measurements can be an extremely useful tool, including when there are adjacent structures. This paper presents the results of monitoring and analysis of the performance of embankments on soft soil, carried out by the Geotechnical Group (GEGEP) of the Federal University of Pernambuco. Three Brazilian cases are presented: the Juturnaíba trial embankment and Juturnaíba Dam construction, in Rio de Janeiro; and the access embankments of the Jitituba River Bridge, in Alagoas. The analysis of embankment behavior was performed by using the traditional model (undrained condition during construction) and the Tavenas & Leroueil (1980) model (partially drained condition during construction). The results showed that it is possible to predict embankment behavior. They also showed the complexity of this topic and the importance of monitoring and evaluating each case in accordance with the location and the type of instrument, subsoil and embankment conditions.

Keywords: embankments, soft soils, monitoring, performance.

1. Introduction

The construction of an embankment on soft clay represents an important geotechnical problem and has been studied by various authors. Their papers form a body of experiences for a better understanding of soft soils bearing load increases (*e.g.* Bjerrum 1973; Tavenas & Leroueil 1980; Leroueil & Rowe 2000). In Brazil, important studies have been published by Ortigão (1980), Coutinho (1986), Pinto (1992), Almeida (1996), Massad (1999); Coutinho & Bello (2005), and Magnani de Oliveira (2006). In general, the design of embankments on soft soils should meet the basic requirements of stability against rupture and vertical and horizontal displacements, during and after construction, compatible with its objective. Trial embankments have been used to increase the understanding on the behavior of embankments on soft soils, as well as to support projects for which conventional procedures presented in studies do not seem sufficient for the adequate prediction of their behavior. Instrumentation is a tool for monitoring and evaluating the construction of embankments by measuring pore-pressures, vertical and horizontal displacements, etc.

This paper presents the results of monitoring and analysis of the performance of embankments on soft soil, carried out by the Geotechnical Group (GEGEP) of the Federal University of Pernambuco. Three Brazilian cases are presented: the Juturnaíba trial embankment and Juturnaíba Dam construction, in Rio de Janeiro; and the access embankments of the Jitituba River Bridge, in Alagoas. The topics on analysis and stability control are presented by Coutinho & Bello (2010).

1.1. Behavior of embankments on soft soil

When analyzing the behavior of embankments on clay foundations, it has commonly been assumed that such is perfectly undrained during construction and that drainage and consolidation start only after the end of construction. This approach has been widely used and has generally performed well for conventional designs. Observations in construction sites have shown that while this approach may often provide reasonable designs, the actual behavior of embankments may be more complicated and that conventional undrained analyses may overpredict pore pressures and lateral displacements. Thus, if one wishes to predict the actual behavior of an embankment on clay, it is essential to have a good knowledge of the mechanical behavior of natural clays and to understand what may happen under an embankment during construction (Tavenas & Leroueil 1980; Leroueil & Rowe 2000).

As in most geotechnical problems, it becomes possible to understand soil response only when the corresponding stress path is known. Under embankments, the effective stress path can be deduced from pore pressure observations. Significant partial consolidation during construction has been reported by a number of investigators (*e.g.* Tavenas & Leroueil 1980; Ortigão 1980; Coutinho 1986; Leroueil & Rowe 2000). The pore pressure increase observed during

R.Q. Coutinho, D. Sc., Universidade Federal de Pernambuco, Recife, PE, Brazil. e-mail: rqc@ufpe.br.
M.I.M.C.V. Bello, M. Sc., Universidade Federal de Pernambuco, Recife, PE, Brazil. e-mail: isabelamcvbello@hotmail.com.
Submitted on December 29, 2010; Final Acceptance on December 15, 2011; Discussion open until July 31, 2012.

the first phase of loading under more than 30 embankments ($\bar{B}_1 = \Delta u/\Delta\sigma_v$) is plotted in Fig. 1 as a function of the normalized depth, z/D, with D being the thickness of the clay layer. Two observations were made by Leroueil *et al.* (1978): $\bar{B}_1$ is smaller than predicted when perfectly undrained behavior is assumed; and the $\bar{B}_1$ *vs.* z/D relationship has the shape of a consolidated isochrone, indicating that in these cases there is significant consolidation during the early stages of construction when the soil is overconsolidated.

If the behavior of the clay foundation under an embankment was perfectly undrained, the effective stress path for a point at or near the centerline would be as O'-U' in Fig. 2a (OCR < 2.5). As a consequence of the rapid consolidation during early stages of construction (very high c_v in the preconsolidation condition), the effective stress path may be O'-P', and reach the limit state curve at P', at a vertical effective stress, σ'_v, close to the preconsolidation pressure, σ'_p, of the clay. As the clay becomes normally consolidated, its coefficient of consolidation is reduced by a significant amount and the behavior becomes essentially undrained. Due to the shape of the limit state curve of natural clays, further loading is associated with a stress path such as P'-A' under a vertical effective stress, which is essentially constant, equal to σ'_p. Such a stress path corresponds to an increase in pore pressure equal to increase in total stress ($\bar{B}_2 = \Delta u/\Delta\sigma_v = 1.0$) during the second phase of loading.

The change in pore pressure generation during construction is thus associated with the soil yielding when the effective stress path reaches the limit state curve. This *in situ* vertical yield stress, (σ'_{vy} or σ'_{vcrit}), has been compared with the preconsolidation pressure measured in conventional 24-h oedometer tests, σ'_{pconv} (Morin *et al.* 1983; Leroueil 1996). The results can be summarized as follows: for overconsolidation ratios (OCRs, estimated on the basis of laboratory tests) between 1.2 and 2, there is good agreement between the two parameters; at lower OCRs, laboratory tests generally slightly underestimate *in situ* values, typically by 10%; for OCRs larger than 2, laboratory tests generally overestimate *in situ* values. The overestimation of σ'_{vy} by laboratory tests in overconsolidated clays with OCR > 2 can be explained by the shape of the limit state curve of natural clays and the fact that the coefficient of earth pressure at rest (Ko) is high in these materials (Fig. 2a) (Leroueil *et al.* 1978).

If the embankment is built to a height that exceeds the corresponding to point A (Fig. 2a) the effective stress path will continue up to F', on the strength envelope of the normally consolidated clay, where there is local failure and then possibly to the critical state C'. Between F' and C', the increase in excess pore pressure is larger than the increase in total stress ($\bar{B}_3 = \Delta u/\Delta\sigma_v > 1.0$) as shown in Fig. 2b. It should be noted that $\bar{B}_1$, $\bar{B}_2$ and $\bar{B}_3$ discussed above are incremental values during different stages of loading and do not

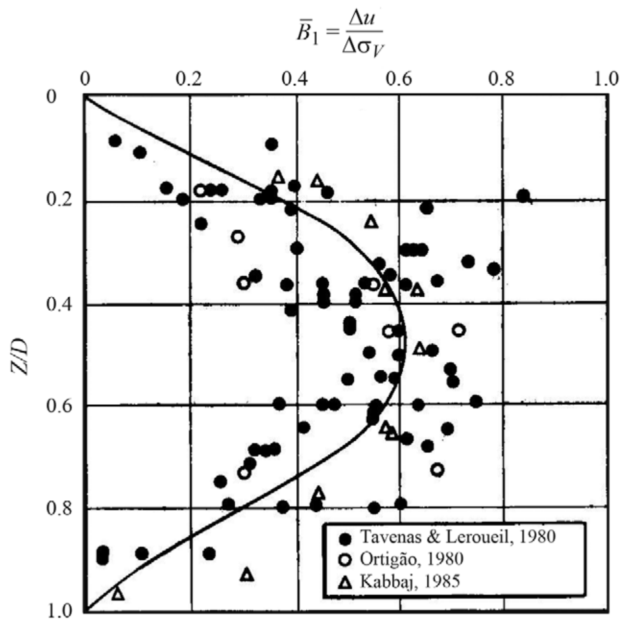

Figure 1 - Compilation of observed excess pore pressures in clay foundation in the first phase of embankment construction (Leroueil & Rowe 2000).

correspond directly to the conventional $\bar{B} = \Delta u/\Delta\sigma_v$ under the entire loading (where $\Delta\sigma_v = \gamma H$). Hence a high value of $\bar{B}_3$ does not necessarily mean that the embankment is unstable. Pore pressure may develop even after construction is completed, *i.e.* when there is no increase in total stress, but $\bar{B}$ may still be less than unity. The pore pressure generated during the construction of an embankment and the corresponding stress path has a direct influence on settlements and lateral displacements.

As indicated by Folkes & Crooks (1985) and Leroueil & Tavenas (1986) the behavior of an embankment on soft clay is not expected to be unique. It has been observed that there are: some field cases where the behavior is essentially undrained; many cases like those discussed here where there is some yielding after partial dissipation of pore pressure; and there have been some cases in which yielding was not reached during construction. In this latter situation, the pore pressures rapidly decrease after the end of construction.

Isochrones shown are given by equation:

$$\bar{B}_1 = \bar{B}_m\left[1-\left(\frac{z}{\Lambda}-1\right)^2\right], \text{For } \bar{B}_m = 0.6 \qquad (1)$$

where z = the distance from the upper drainage boundary; Λ = the drainage path (Λ = 0.5D) and $\bar{B}_m$ = the maximum pore pressure ratio.

1.2. Cases studied

This paper presents results of monitoring and performance of embankments on soft soil carried out by the

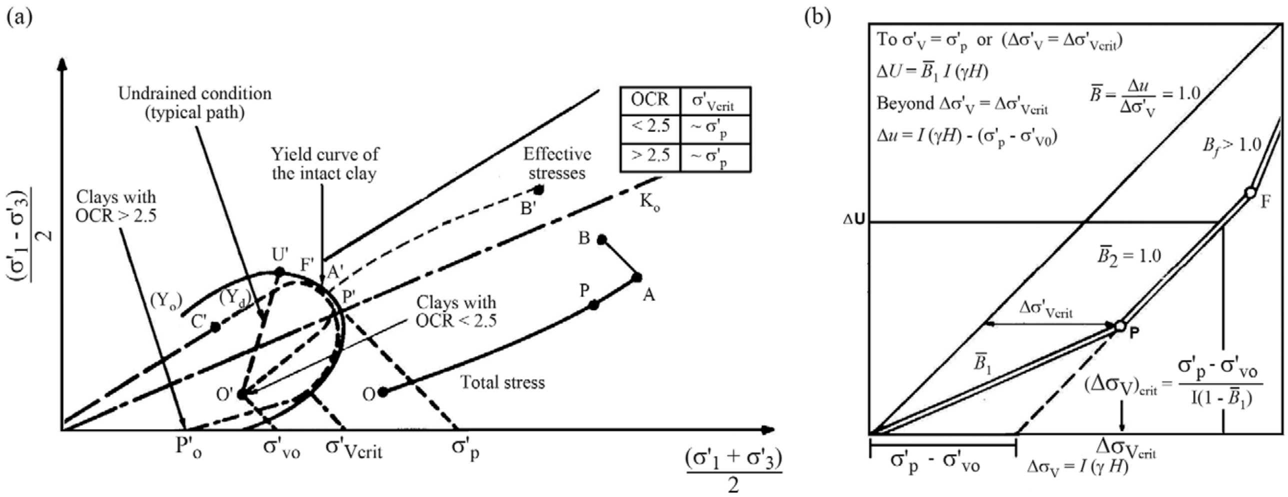

Figure 2 - (a) Total and effective stress paths, and (b) increase of pore pressure under the centerline during stage construction of an embankment - clays with OCR < 2.5 (Coutinho 1986, from Tavenas & Leroueil 1980).

Geotechnical Group (GEGEP) of the Federal University of Pernambuco. The study realized on the Juturnaíba Dam project was used as the basis for this paper.

The Juturnaíba Dam project, an earth-fill structure located in the north of the state of Rio de Janeiro, was built in 1981-1983 (Fig. 3a). The foundation consisted basically of an organic clay deposit about 7.5-8 m thick, with SPT values (blows / length in cm) ranging from 0/111 to 1/33, typically 0/50, along its full depth, underlain by sand sediments with SPT values about 10/30 to a depth of 14 m. Visual classification and laboratory tests permitted a subdivision of clayey deposit into six layers, with varying organic and water content, ranging from light-grey silt clay to a brown clayey peat (Fig. 3b).

Because a 1.2 km length of this earth dam was supposed to rest on organic soft clay, geotechnical studies were quite comprehensive, including laboratory and field investigations and the construction of a trial embankment led to failure (first case), which was instrumented as indicated in Fig. 4 (Coutinho 1986, Coutinho & Lacerda 1987; 1989).

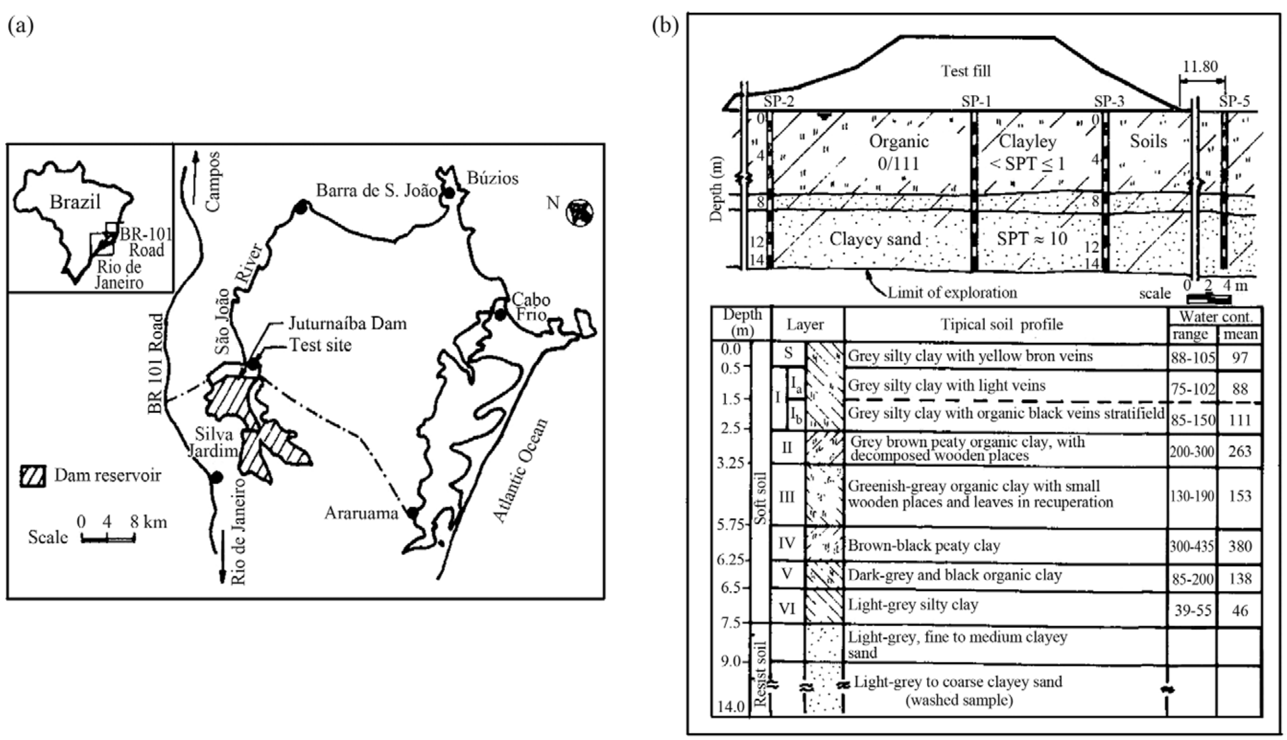

Figure 3 - Juturnaíba Dam: (a) test site; (b) typical soil profile (Coutinho & Lacerda 1987).

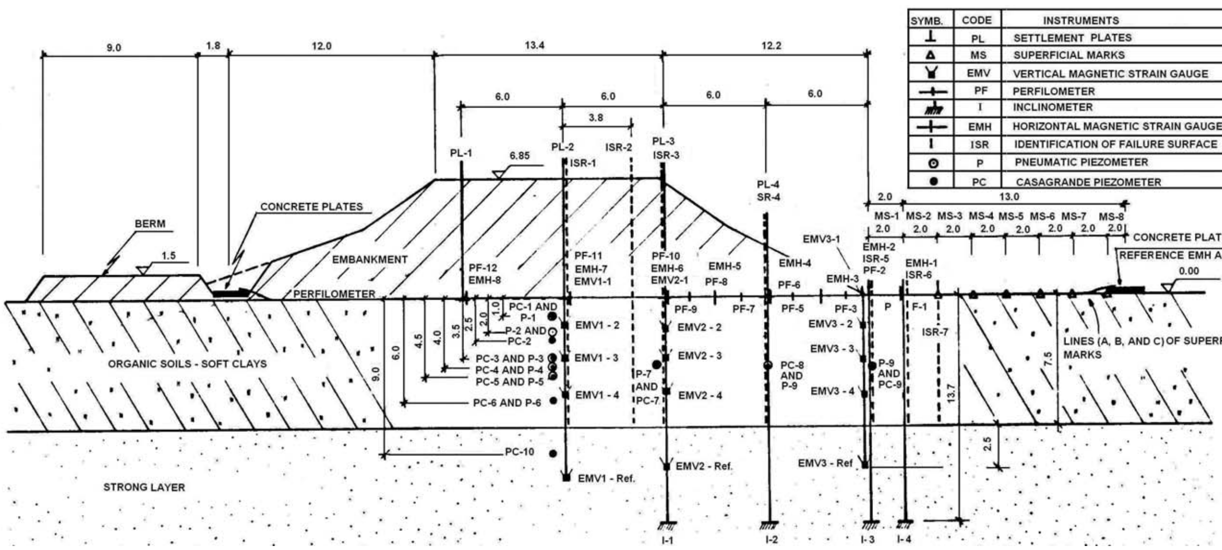

Figure 4 - Instrumentation of the Juturnaíba trial embankment (Coutinho 1986) - First case.

Figure 5 shows results of the water content and Atterberg Limits for six layers of the profile. It can be observed the variation of these results for each layer and consequently in the plasticity index values. Figure 6 presents the results of the overburden effective stress (σ'_{vo}) and preconsolidation pressure (σ'_p) obtained by the oedometric tests. The foundation deposit presents overconsolidation condition with the upper part showing higher values (OCR > 2.5). Figure 7 shows the compressibility parameters, and it can be seen that compression ratio (CR) and swelling ratio (SR) are distinct for each layer. Values of initial void index (e_o), compression index (C_c), and organic content are also different for each layer. The main purposes of these studies were to provide indications on the undrained strength and compressibility in the clay foundation and on methods to control stability during construction.

The design studies indicated that the dam should be built in stages with berms and flat slopes and the 1.2 km length being divided in three sections (II, III.2 and V). Dam monitoring (second case) consisted of placing settlement

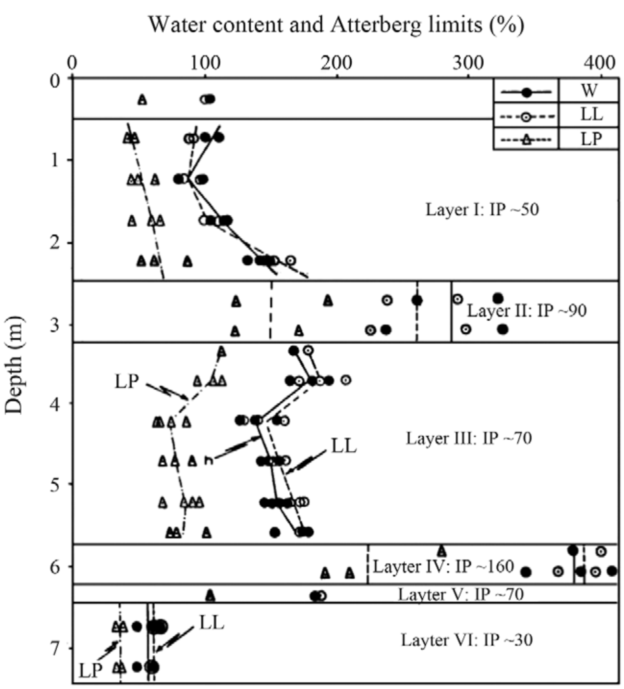

Figure 5 - Water content and Atterberg Limits of the Juturnaíba trial embankment (Coutinho 1986).

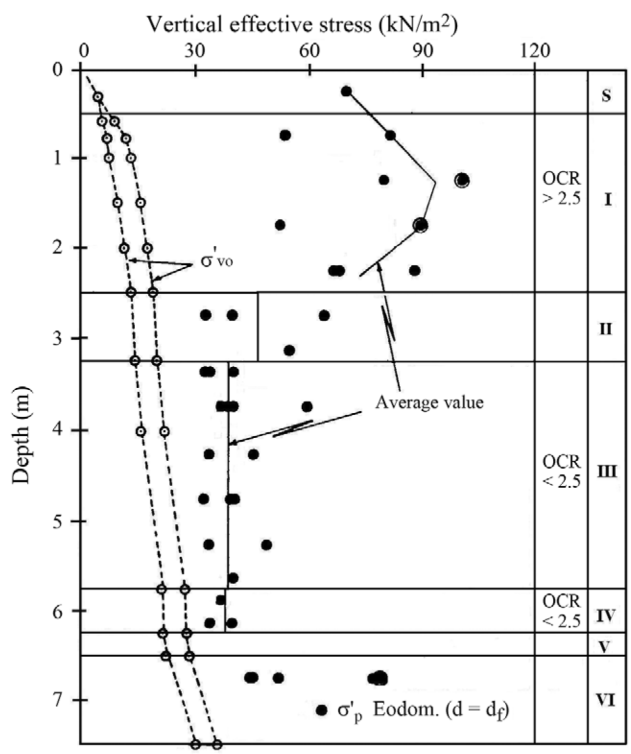

Figure 6 - σ'_{vo}, $\sigma'_{v\,crit}$, σ'_v and σ'_p laboratory values *vs.* depth - center of the Juturnaíba trial embankment (Coutinho 1986).

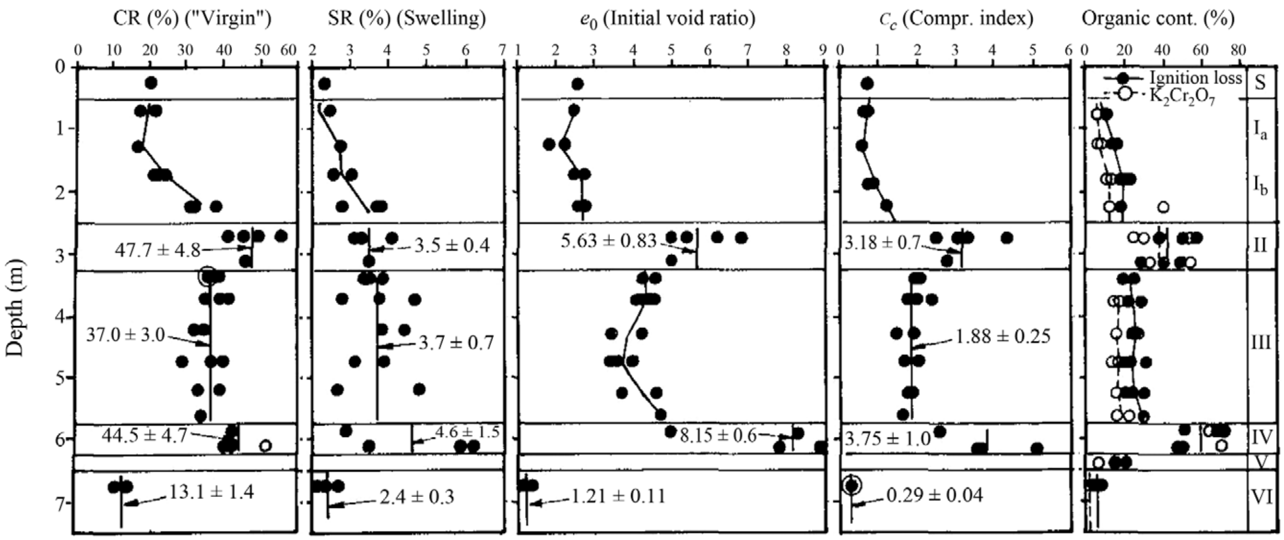

Figure 7 - CR, SR e_o and *Cc vs.* depth - oedometer tests in the Juturnaíba Dam (Coutinho & Lacerda 1994).

plates at the embankment clay interface, piezometers inside the organic clay, and inclinometers at the slope berm. Eleven stakes (15 to 60) were instrumented and Fig. 8 examplifies (Coutinho *et al.* 1994; Lucena 1997).

The third case presents the study on the access embankments for the Jitituba River Bridge, located on the Alagoas - 413 Highway. This bridge was built before the access embankments. Due to the existence of a soft soil layer (12 m thick) and to the construction sequence of the bridge, there was a need to analyze the vertical and horizontal displacements and the consequent efforts on the piles of the bridge (Fig. 9). The behavior of the access embankments was analyzed in terms of measurements of pore-pressures, and vertical and horizontal displacements, by applying models proposed in the literature and by comparison with other case studies of embankments on soft soils. The solution adopted consisted of constructing the embankments in stages, along with the use of prefabricated vertical drains and geotechnical instrumentation (Casagrande piezometers, settlement plates and inclinometers) to control and monitor the performance of the project (Cavalcante 2001; Cavalcante *et al.* 2003; 2004). The research studies on this case were made possible due to the partnership with Gusmão Engineer Associated.

2. Instrumentation

The accurate performance of instrumentation is fundamental to the adequate use of its results obtained during embankment construction. The general objectives of the instrumentation are: to evaluate the general behavior of the embankment; to obtain signs of imminent rupture thus allowing a control methodology to be adopted during construction; and to evaluate the behavior of instrumentation, by comparing measurements obtained from more than one instrument at the same location.

In order to evaluate the degree of consolidation and the strength of the clay, it is desirable to instrument the clay foundation with piezometers and settlement gauges. This is particularly important in stage construction as it estimates when the following stage may be constructed and to what level. When there are services, structures or bridge piles close to the embankment, it can be important to monitor the

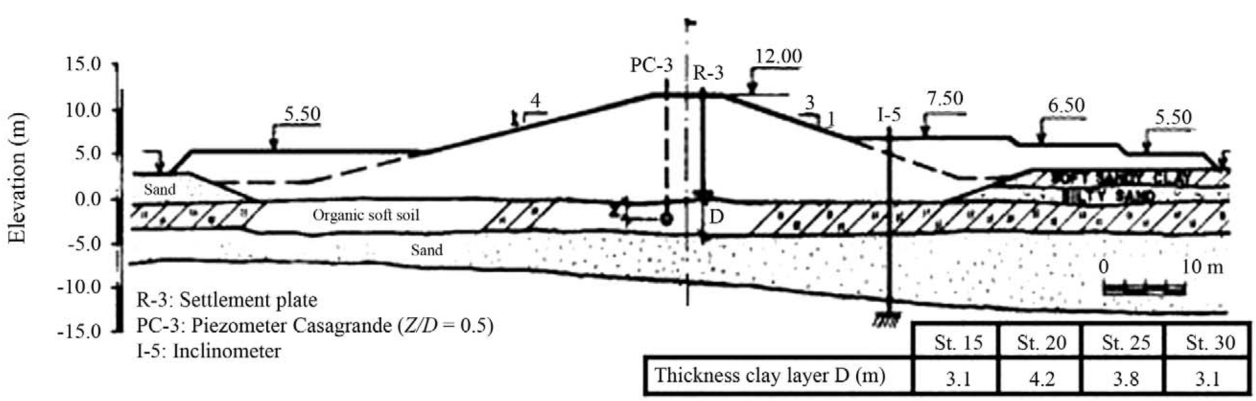

Figure 8 - Geotechnical profile and instrumentation of Juturnaíba Dam (Coutinho *et al.* 1994) - Second case.

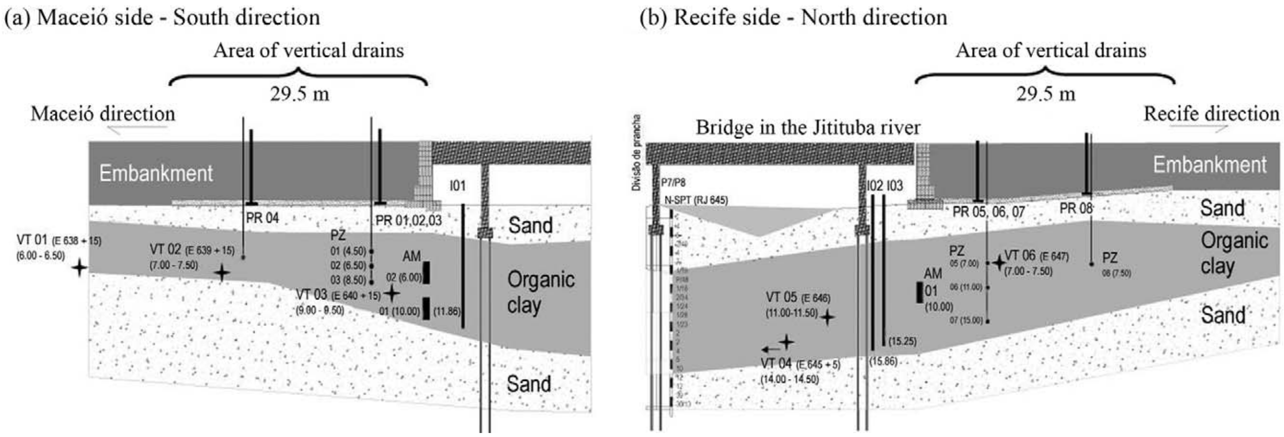

Figure 9 - Longitudinal section, geotechnical profile and the location of the field investigations of the basic project of the access embankments of the bridge on the Jitituba River (Cavalcante 2001; Cavalcante *et al.* 2004).

lateral displacements using inclinometers (Leroueil & Rowe 2000).

In most cases, the behavior of the embankment is monitored with respect to the following variables: vertical displacements (at surface and depth); horizontal displacements (at surface and depth); pore pressure; and total stress in the embankment (not common).

As a practical consideration, the observation of the pore pressures generated during construction under the centerline of an embankment can generally be used to calculate the vertical yield stress of the clay at the level of the piezometers. It can also give an indication of local shear failure when the ratio $\Delta u/\Delta\sigma$ becomes larger than 1.0. The strain between two deep settlement gauges can be used in conjunction with pore pressure measurements to define an *in situ* effective stress-strain curve that can then be compared with the compression curve assumed for the sublayer considered. When the clay deposit and the consolidation conditions are relatively simple, Asaoka's (1978) method can be used during the consolidation process to evaluate the approximate magnitude of the final settlement as well as to determine a representative coefficient of consolidation (Leroueil & Rowe 2000).

Figure 4 shows the instrumentation used in Juturnaíba trial embankment. The following instruments were used:

• Measurement of vertical displacements: 4 settlement plates placed throughout the instrumented section (Pli); 12 magnetic strain gauges, placed in the foundation deposit throughout the instrumented section (EMVi); 1 continuous pipe at the base of the embankment with 12 points for measurements with a full-profile settlement gauge (Pfi); 18 surface marks installed on the soil surface in the central region of the failure zone (Msi). A bench-mark (RNP) was utilized - it was installed at a location far from the region of influence of the displacements.

• Measurement of horizontal displacements: 4 inclinometer tubes (Ii); 8 measuring points, using a horizontal magnetic strain gauge, distributed throughout a continuous tube at the base of the embankment (EMHi); 18 surface marks placed on the soil surface in the central region of the failure zone (Msi).

• Measurement of pore pressure: 9 pneumatic (Pi) and 10 Casagrande piezometers (PCi), placed in the foundation deposit.

• Identification of the failure surface: 7 pipes were placed to help defining the failure surface (ISRi); 4 inclinometer pipes (Ii).

Two water level measuring gauges and one Casagrande piezometer were installed in the underlying sand layer, in front of the embankment, outside the zone of influence of the construction. The instruments were arranged in order to concentrate them in a single section, with redundancy towards the amount and the type of instrument, thus allowing relevant information at surface and depth in the foundation soil to be obtained. Initial measures were taken so as to evaluate the behavior of the instruments with regard to repeatability of the measurement technique. The accuracy of the measurements was evaluated by comparing results from different systems for a given position.

Coutinho (1986) evaluated the performance of the instruments used for measuring the vertical displacement (settlement plates, vertical magnetic strain gauge, full-profile settlement gauge and superficial marks) and horizontal displacement (horizontal magnetic strain gauge, inclinometer and superficial marks) in the Juturnaíba trial embankment. Tables 1 and 2 show the sensitivity, precision, reliability and accuracy of the instruments for vertical and horizontal displacement, respectively. The formation of groups on the accuracy of the results of vertical displacements can be observed, namely settlement plates, surface marks and vertical magnetic strain gauge. Accuracy was in the order of ±5 to 7 mm; and the accuracy of the full-profile settlement gauge was of the order of ±17 mm. The accuracy of the measurements of horizontal displacements for all instruments was of the order of ±5 mm.

Table 1 - Sensitivity, precision, reliability and accuracy of vertical displacements - Juturnaíba (Coutinho 1986).

Instruments		Settlement plates	Perfilometer	Vertical magnetic strain gauge	Surface marks
Sensitivity (mm)	1	~7	1	1	
Precision (mm)	± 2	± 10	± 1	± 2	
Reliability	Very good	Good	Good	Excellent	
Accuracy (mm)	5	17	7	5	
Deviation in relation of average observed values (mm)	Average	Position (2)	3.0	5.0	5.0
		Position (3)	8.9	6.7	16.5
	Standard deviation	Position (2)	2.3	4.3	4.8
		Position (3)	4.1	4.8	6.3
	Range 90% (mm)	Position (2)	6.8	12.1	12.9
		Position (3)	15.6	14.6	26.9

Note: Positions (2) and (3) - see Fig. 4.

Table 2 - Sensitivity, precision, reliability and accuracy of horizontal displacements-Juturnaíba (Coutinho 1986).

Instruments		Surface marks		Inclinometers		Horizontal magnetic strain gauge	
		MS (1)	MS (2)	IN (1)	IN (2)	EMH (1)	EMH (2)
Sensitivity (mm)		1		1:10,000 rad		1	
Precision (mm)		± 3		± 2		± 2	
Reliability		Excellent		Very good		Good	
Accuracy (mm)		5		5		5	
Deviation in relation of observed values (mm) - Pos (3)	Average	3.0	6.0	1.0	3.0	4.0	8.0
	Standard deviation	1.0	2.5	1.0	2.7	1.2	2.3
	Range (90%)	4.6	10.1	2.6	7.4	6.0	11.8

Notes: a) Values for height of embankment: (1) until 4.0 m; (2) greater than 4.0 m. b) Position (3) - see Fig. 4.

Figure 10 shows the summary of the vertical and horizontal displacements measured by different instruments at the base of the Juturnaíba trial embankment during construction, before the failure. These measurements show the occurrence of significant displacements of the foundation surface, which increase gradually as the height of the embankment increases. The maximum vertical values were greater than 500 mm at a height of 6.4 m just before failure. In the case of horizontal displacements, the maximum value was 200 mm and there is a position in the base of the embankment at which a change of the displacement direction occurred, causing tensile stresses.

The measurement of pore pressure taken before the construction of the trial embankment started, showed a deviation of less than ±1 kPa for both instruments (pneumatic and hydraulic Casagrande). Figures 11 and 12 present pore pressure isochronous measured under the center of the embankment and the results of the comparative study between the two types of piezometers, respectively. The excess of pore pressure (Δu) values measured, using the pneumatic piezometers, were always higher than the corresponding Casagrande's values.

As the height of the embankment increases, to near the failure of the foundation, the values measured by pneumatics piezometers in the center of the soft layer present significant increases, unlike the values measured with the Casagrande piezometers. In general, the values obtained for the ratio between measurements from the two piezometer types were in the range of 0.8 to 1.0 for heights of up to 4.65 m (Fig. 12). As the embankment height increases, that ratio decreases (range of 0.8 to 0.5) until the embankment reaches failure. The average value is in the order of 0.75.

Measurements from inclinometer, failure surface indicator (ISR's) and failure visual signs (cracks) were used to localize the failure surface (Fig. 13). Considering all the points observed it was verified that a circular surface tan-

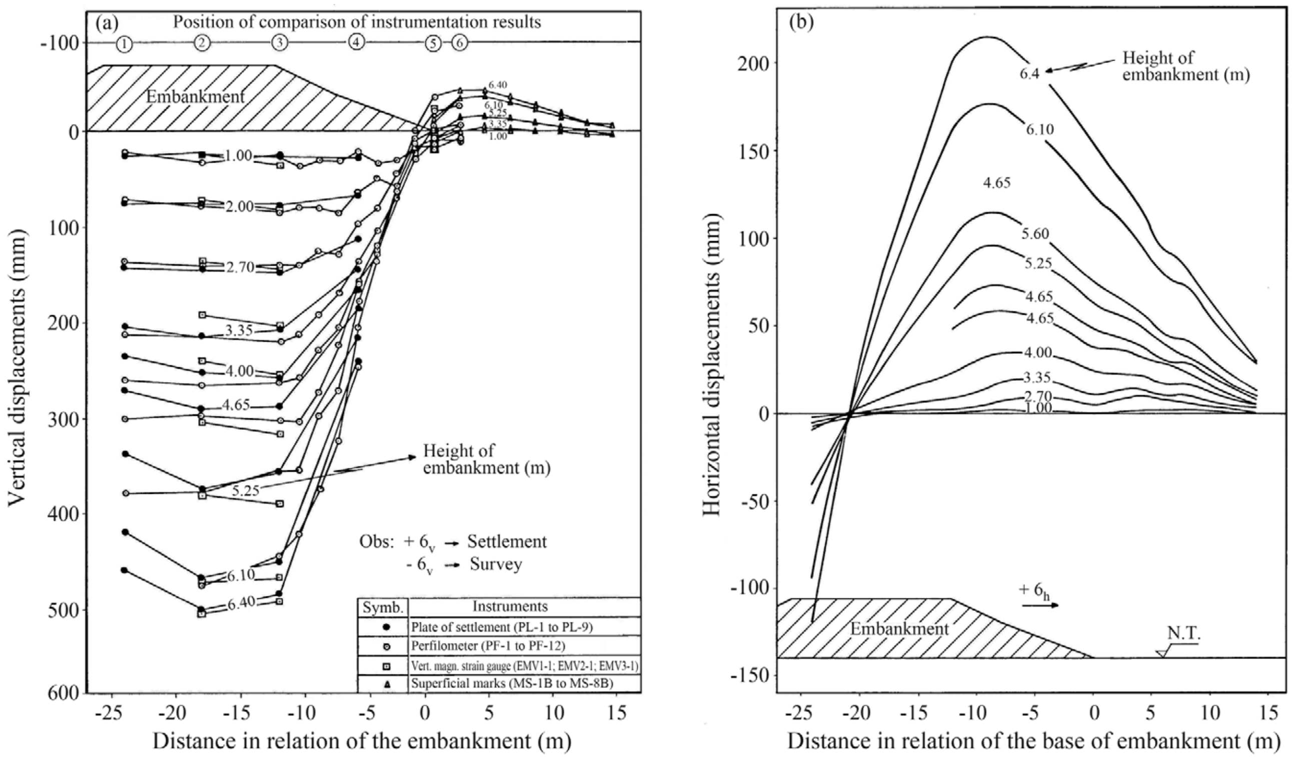

Figure 10 - Comparison between displacements measured in the base of the Juturnaíba trial embankment during construction, before the failure: (a) vertical and (b) horizontal (Coutinho 1986).

gent near to the resistant layer can represent the failure surface. These results were close to those indicated by the measurements from the inclinometers. A mechanism of failure of the planar type, in blocks, also seems to explain the phenomenon of the failure. Examples of possible failure surface are presented in Fig. 13.

Figure 14 presents the results of the geotechnical instrumentation obtained in the first 140 days in the access embankments of the bridge over the Jitituba River. After this period, the construction was paralyzed. Later, paving was carried out and the operation of the bridge was permitted, and only measurements of horizontal displacements could be performed.

3. Pore Pressure

As to the conventional design of embankment on clay foundations, it has been assumed that the behavior is perfectly undrained during the construction. For this case the pore pressure generated Δu can be given by Eq. (2).

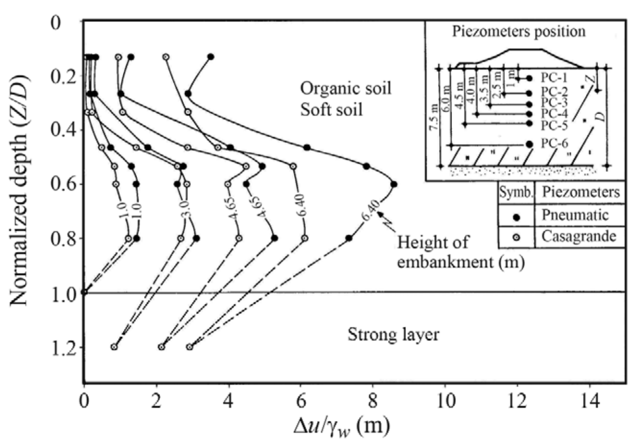

Figure 11 - Pore pressure *vs.* depth - Casagrande and pneumatic piezometers- Juturnaíba trial embankment (Coutinho 1986).

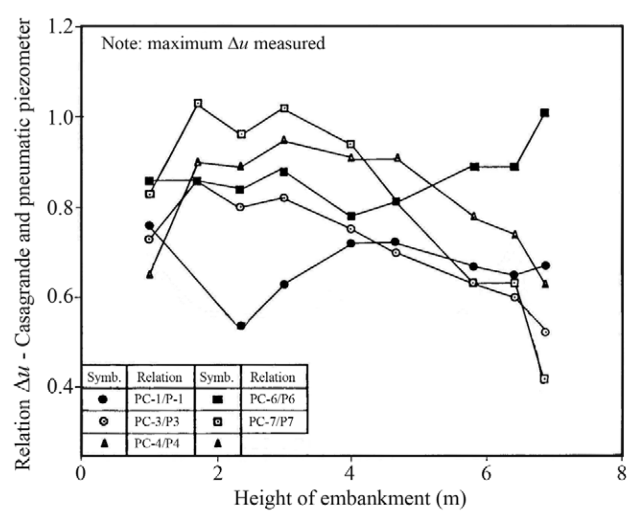

Figure 12 - Comparison among pore pressure measured by Casagrande and pneumatic piezometers - Juturnaíba trial embankment (Coutinho 1986).

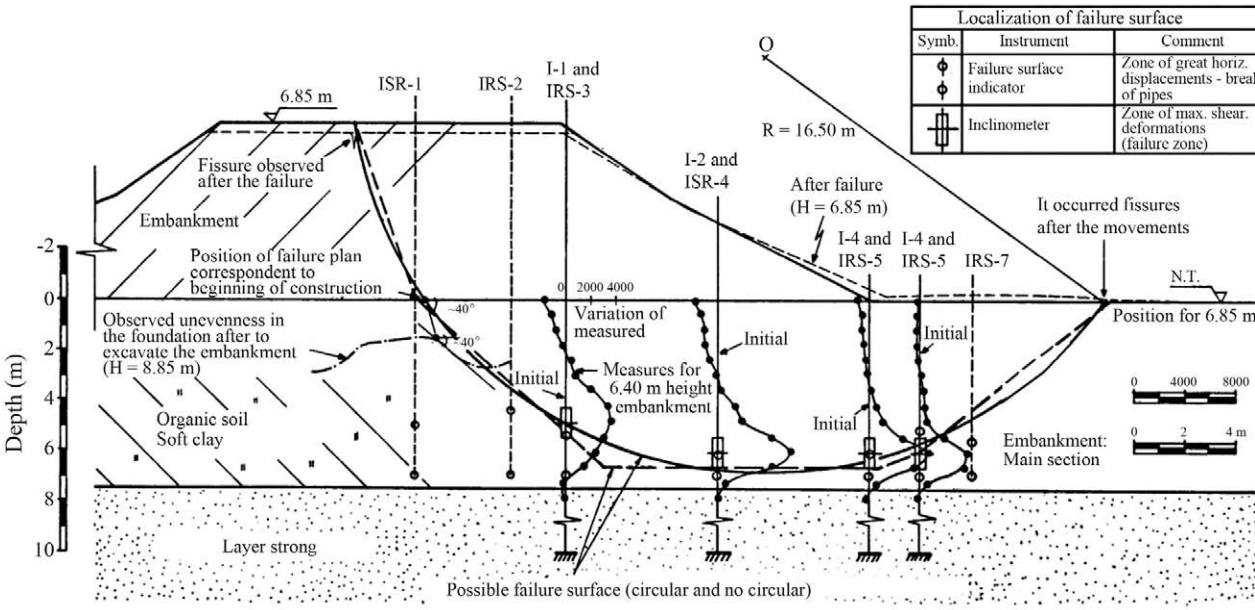

Figure 13 - Localization of the failure surface - Juturnaíba trial embankment (Coutinho 1986).

$$\Delta u = f(\Delta\sigma) \quad (2)$$

As the total stress varies, the pore pressure increase is given by the octaedrical stress increase $\Delta\sigma_{oct}$ (Eq. (3)). This methodology is based on the direct application of the elastic theory, and it is used when the pressure conditions that were imposed are in the limit of elastic behavior of the clayey soil. The principal total stress increases are $\Delta\sigma_1$, $\Delta\sigma_2$, $\Delta\sigma_3$.

$$\Delta u = \Delta\sigma_{oct} = 1/3\,(\Delta\sigma_1 + \Delta\sigma_2 + \Delta\sigma_3) \quad (3)$$

In the case of the oedometer test, where an one-dimensional compression occurs, the pore pressure increase due to undrained loading is given by the vertical stress increase $\Delta\sigma_v$ (Eq. (4)).

$$\Delta u = \Delta\sigma_1 = \Delta\sigma_v \quad (4)$$

In many cases, significant partial consolidation during construction has been reported (item 1.1). In these cases pore pressures generated can, in general, be illustrated as in Fig. 2b, with $\overline{B}_1$, during the early stages of loading (Fig. 1) being given by:

$$\overline{B}_1 = 0.6\text{-}2.4\,(Z/D - 0.5)^2 \quad (5)$$

This equation is applicable until the local vertical effective stress reaches the preconsolidation pressure σ'_p, of the clay (O-P', Fig. 2a; OCR < 2.5). After that the clay behaves as normally consolidated and the corresponding height of embankment H_{nc} can be obtained by:

$$\gamma H_{nc} = \sigma'_{vy} \text{ or } \sigma'_{crit} = (\sigma'_p - \sigma'_{vo}) / I\,(1 - \overline{B}_1) \quad (6)$$

where $\overline{B}_1$ = pore pressure parameter; Z/D = normalized depth; D = thickness of the clay layer; I = influence factor; γ = unit weight of the embankment; γ'_{vy} = in situ vertical yield stress; σ'_{crit} = critical pressure; σ'_p = preconsolidation pressure; σ'_{vo} = initial vertical effective stress.

In the second phase of loading (P'-A', Fig. 2a) the increase in pore pressure is equal to the increase in total stress ($\overline{B}_2 = \Delta u/\Delta\sigma_v = 1.0$). At the end of construction, the excess pore pressure that will dissipate after construction is defined as the horizontal distance between A (total stress) and A' (effective stress) and given by:

$$\Delta u = \Delta\sigma_v - (\sigma'_p - \sigma'_{vo}) = I\gamma H - (\sigma'_p - \sigma'_{vo}) \quad (7)$$

If the third phase of loading occurs, local failure may be reached, and there may be softening of the clay (F' - C', Fig. 2a) associated with an increase in excess pore pressure larger than the increase in total stress ($\overline{B}_3 = \Delta u/\Delta\sigma_v > 1.0$). It should be noted that $\overline{B}_1$, $\overline{B}_2$ and $\overline{B}_3$ are incremental values during different stages of loading.

Coutinho (1986) presents and discusses results of pore pressure generated during the construction of the Juturnaíba trial embankment. Figures 11, 15 and 16 show examples of comparisons between predicted and observed values of Δu for some piezometers. The main conclusions are:

• It is clear that partial drainage occurred during construction. The piezometers located at the depths of 1.0 m and 2.0 m showed significant initial dissipation because they were placed close to the drainage boundary and in organic soils with high OCR values (OCR > 2.5)

• Δu values obtained by the Leroueil *et al.* method generally presented good estimates, particularly for the piezometers in the middle of the clay layer and for the highest height of the embankment. Near the failure height, other methods showed Δu values close to the values measured by

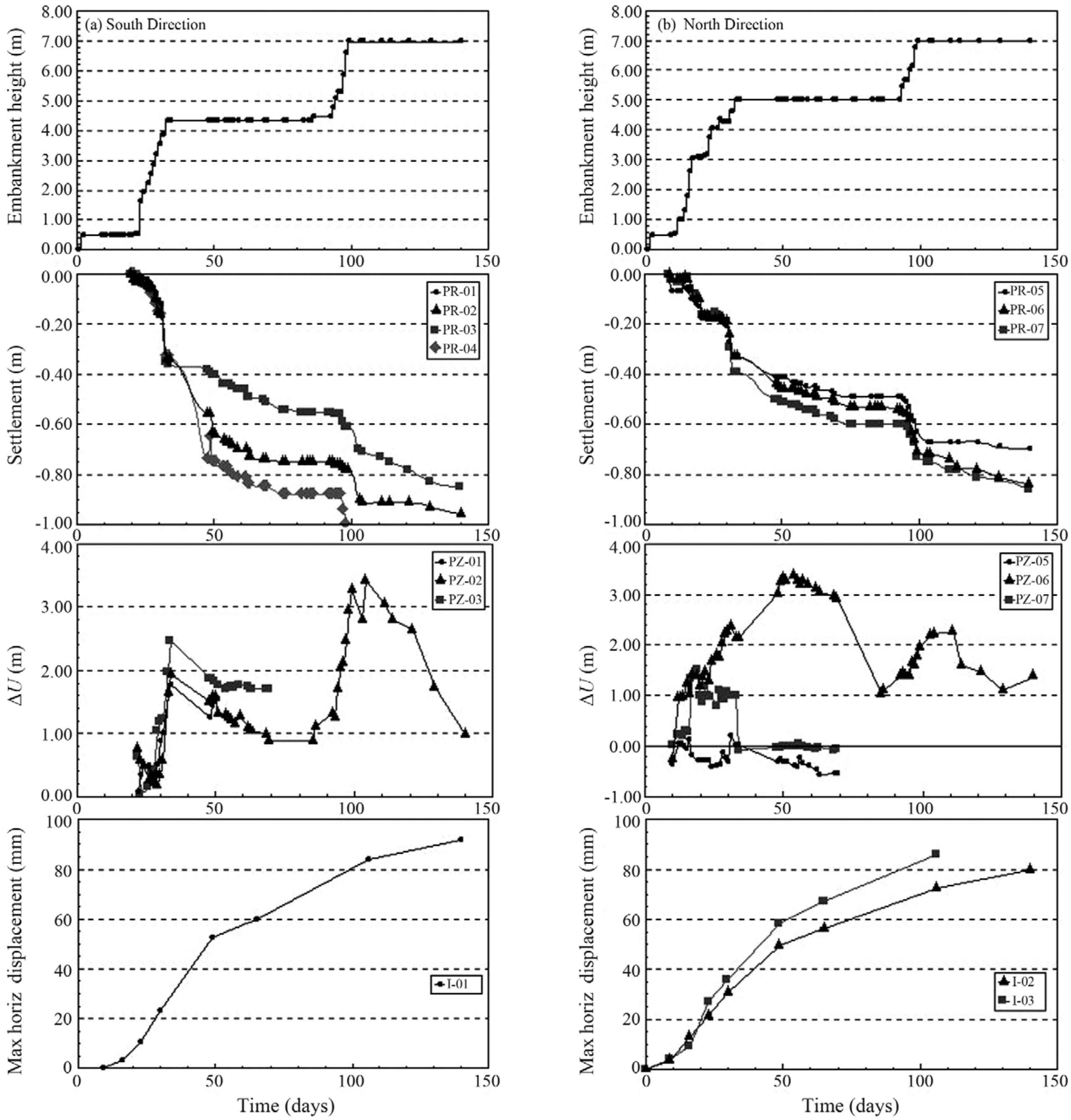

Figure 14 - Results of the geotechnical instrumentation measurements performed in the access embankments of the bridge on the Jitituba River (Cavalcante *et al.* 2004).

the piezometers in the middle of the clay layer (for example $\Delta u = \Delta\sigma_{oct}$).

• It is possible to see that the behavior of the clayey sand layer underneath the clay foundation was not completely drained (partial drainage occurred).

• In the central piezometers P-4 and P-5, a sign of local failure ($B_f > 1.0$) was observed, as indicated by Leroueil *et al.* (1978).

• It is observed that the pore pressure *vs.* depth curves (Figs. 11 and 16) takes the shape of a bell, with the axis of symmetry located below half the height of the soft layer. The behavior was not of the conventional type, because significant drainage in the upper stretch of the foundation occurred up to an embankment height of almost 3.0 m, whereas there was only partial draining in the underlying sand layer.

Figure 17 and Table 3 show results of the preconsolidation pressure (σ'_p) and vertical effective stress σ'_{crit} (σ'_{vy}) obtained in the Juturnaíba trial embankment by two procedures: oedometric tests and field pore pressure using Le-

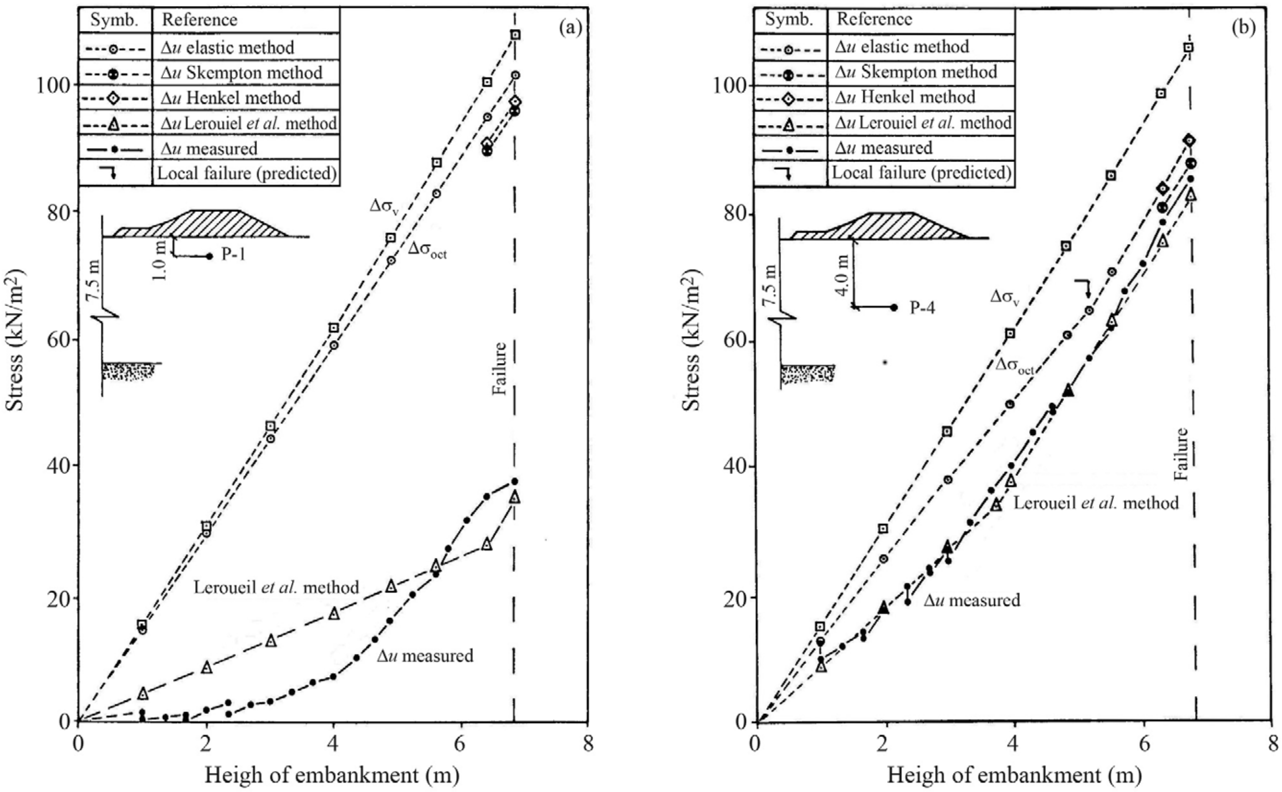

Figure 15 - Comparison between predicted and observed Δu value in the Juturnaíba trial embankment - Piezometer: (a) P1; (b) P4 (Coutinho 1986).

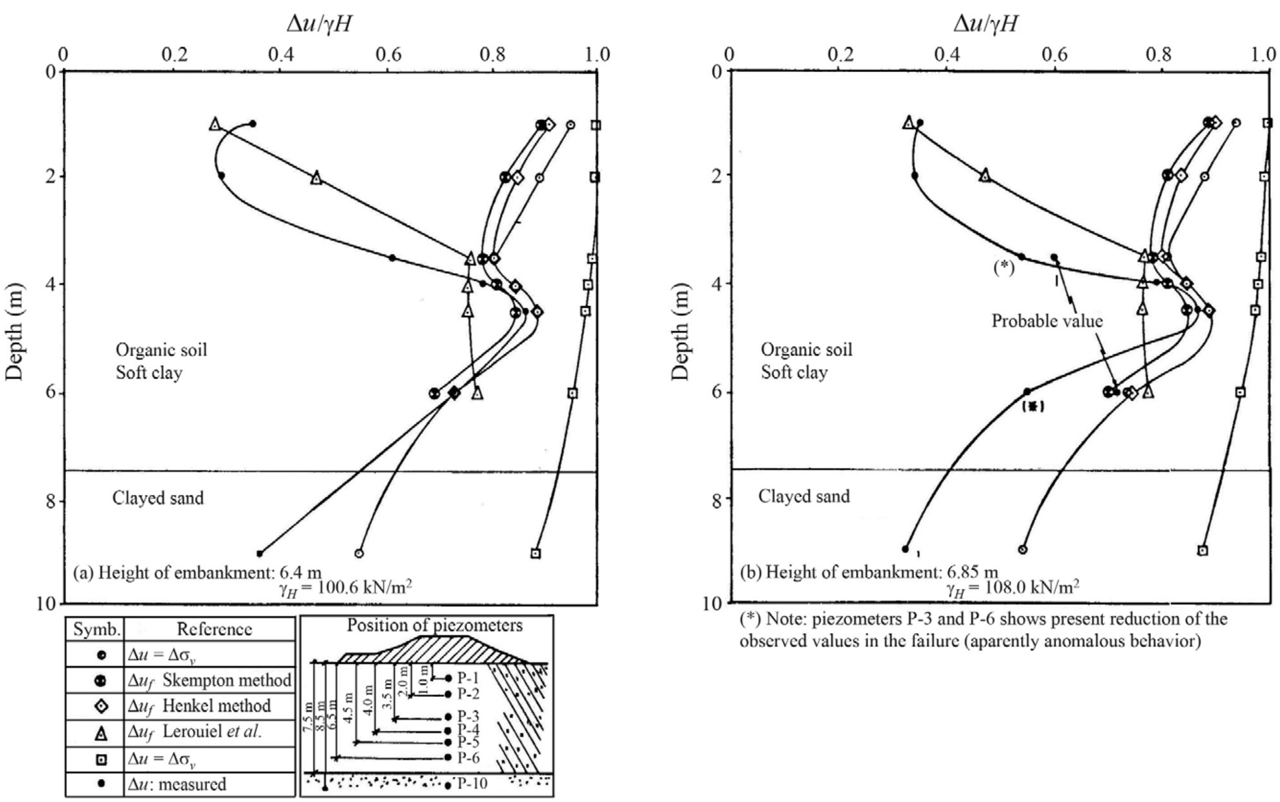

Figure 16 - Comparison between predicted and observed values of Δu *vs.* depth - piezometer at the center of the Juturnaíba trial embankment - height of embankment: 6.40 and 6.85 m (Coutinho 1986).

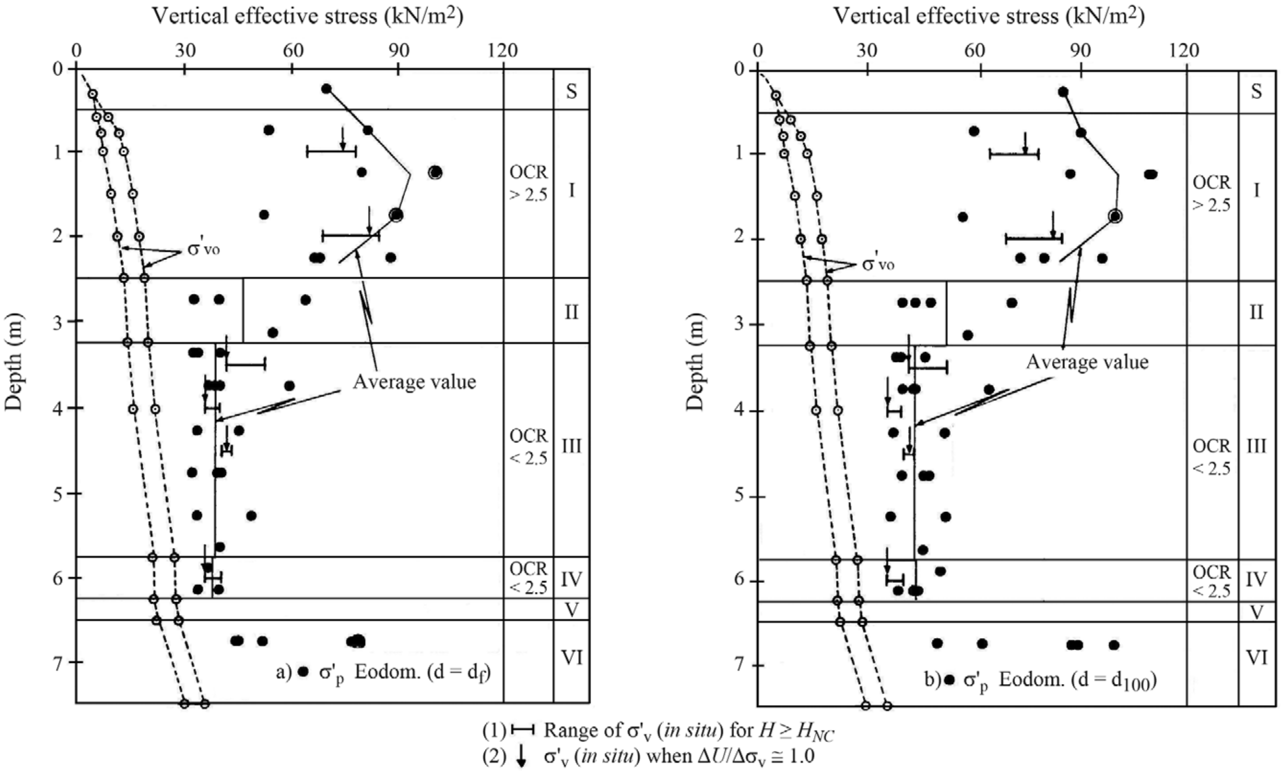

Figure 17 - σ'_{vo}, $\sigma'_{v\,crit}$, σ'_v and σ'_p values (laboratory and *in situ*) *vs.* depth - center of the Juturnaíba trial embankment (Coutinho 1986).

roueil *et al.* (1978) proposal. Field results showed reasonable agreement with described in item 1.1. For OCR > 2.5, the σ'_{crit} values were smaller than σ'_p showing an increase as the construction continued and reaching values close to σ'_p for an embankment height of 5.6 m. For OCR < 2.5, the σ'_{crit} values were in the same order as σ'_p values, remaining constant in the same range while the construction continued. The condition $\Delta u \cong \Delta\sigma_v$ was obtained for an embankment height of 3.0 m for the foundation zone with OCR < 2.5, and for an embankment height of 5.6 m in the foundation zone with OCR > 2.5.

Table 3 also shows a summary of the observed values of pore pressure coefficient ($\overline{B}$) and effective stresses in comparison with those predicted by Leroueil *et al.* (1978). The relation observed between Δu and $\Delta\sigma_v$ for the OCR > 2.5 presents a further stage in relation to soils with OCR < 2.5, due to the difference between the effective stress paths in each case (Fig. 2a), showing the "specificity" and complexity of the behavior of the clay foundation of the Juturnaíba trial embankment.

Coutinho *et al.* (1994) presented an analysis of the Juturnaíba Dam behavior with primary emphasis on pore pressure and settlement data. One procedure consisted of comparing numerical finite difference (CONMULT PROGRAM) predictions with instrumentation data. Another approach made use of the classical method (undrained condition) and the Tavenas & Leroueil method (partial drained condition) to estimate the pore pressure increases during construction.

The correction in the measurements of pore pressures from the Casagrande piezometers proposed by Coutinho (1986) was applied in the analysis of the response to the stress increase, where Δu corrected ($\Delta u_{pneumatic}$) = $\Delta u_{Casagrande}$ / 0.75 (see item 2, Fig. 12). The predicted and measured Δu values at piezometers C1 and C3 are shown in Fig. 18a. Reasonable agreement is reached at loading stages 1 and 2, but for stages 3 and 4 the agreement is poor. The discrepancy seems to be related to the generated Δu calculated by the CONMULT PROGRAM (undrained condition) and the condition in the field.

Generally Δu generated during construction is related to the increasing vertical load from the embankment. Predicted and measured Δu values at piezometers C3 (typical example) are showing in Fig. 18b, where the measured Δu is much lower than the predicted values from conventional methods, considering undrained condition throughout construction. Good agreement is observed between measured Δu and predicted values by Leroueil *et al.* method, which considers partial drainage during construction, until the embankment rises to a height of 5.6 m. As the embankment height increases, the clay layer is supposed to reach a normally consolidated condition. Under this condition, the measured values are lower than the predicted ones, show-

Table 3 - Comparison between observed and predicted excess pore pressure values by Leroueil *et al.* (1978) Method - Juturnaíba trial embankment (Coutinho 1986).

Piezometer			$\bar{B}_{measur.} = \Delta U / \Delta\sigma_V$				$\bar{B}_{measur.} = \Delta U / \Delta\sigma_V$				H_{nc} (m)	Effective stress kN/m²			Velocity of construction
Nº	Depth (m)	Layer	$\sigma'_v \le \sigma'_{crit}$ $\bar{B}_1$	$\sigma'_v > \sigma'_{crit}$			$\sigma'_v \le \sigma'_{crit}$ $\bar{B}_1$	$\sigma'_v > \sigma'_{crit}$			Observed	σ'_{vo}	σ'_p	σ'_{crit}	
				1° stage $\bar{B}_2$	2° stage $\bar{B}_3$	Final stage $\bar{B}_f$		1° stage $\bar{B}_2$	2° stage $\bar{B}_3$	Final stage $\bar{B}_f$					
P-1	1.0	Ia	0.117	0.63	0.90	-	(2)	(3)	1.0	1.0	4.0	10.0	86.0	64.6	square below
P-2	2.0	Ib	0.100	0.48	0.85	-			1.0	1.0	4.0	10.9	82.5	68.7	

(a) Piezometers installed in clayey soils with OCR > 2.5.
(1) σ'_p value adopted corresponding to representative value in the position of piezometer in Fig. 5.
(2) The average $\bar{B}_1$ value throughout the layer was 0.22.
(3) $\bar{B}_2$ value varied between 0.42 and 1.01, with average of 0.75.

Piezometer			$\bar{B}_{measur.} = \Delta U / \Delta\sigma_V$			$\bar{B}_{measur.} = \Delta U / \Delta\sigma_V$			H_{nc} (m)		Effective stress (kN/m²)			Velocity of construction	
Nº	Depth (m)	Layer	(4) $\sigma'_v \le \sigma'_{crit}$ $\bar{B}_1$	$\sigma'_v > \sigma'_{crit}$		$\sigma'_v > \sigma'_{crit}$	$\sigma'_v \le \sigma'_{crit}$ $\bar{B}_1$		Obs	Pred	σ'_{vo}	σ'_p	σ'_{crit}	Height of embankment (m)	Velocity average (kN/m² / day)
				1° stage $\bar{B}_2$	(5) Final stage $\bar{B}_f$		1° stage $\bar{B}_2$	(2) Final stage $\bar{B}_f$							
P-3	3.0	III	0.278	0.85	~0.85	0.597	1.0	> 1.0	2.35	3.8	14.6	38.75	42.0	0-3.0	2.20
P-4	4.0	III	0.556	0.91	1.25	0.597	1.0	> 1.0	3.0	3.76	15.6	38.75	36.0		
P-5	4.5	III	~0.547	~1.0	1.45	0.576	1.0	> 1.0	~3.0	3.45	16.5	38.75	42.4	3.0-6.85	4.30
P-6	4.5	IV	0.640	0.92	~0.92	0.384	1.0	> 1.0	3.0	2.0	19.9	38.3	36.1		

(b) Piezometers installed in clayey soils with OCR < 2.5.
(4) $\bar{B}_1$ value corresponding to the last measurement of pore pressure for $\sigma'_v = \sigma'_{crit}$.
(5) $\bar{B}_f$ value corresponding to the representative value for an embankment height of 5.6 m to 6.4 m.
Obs: Observed; Pred: Predict.

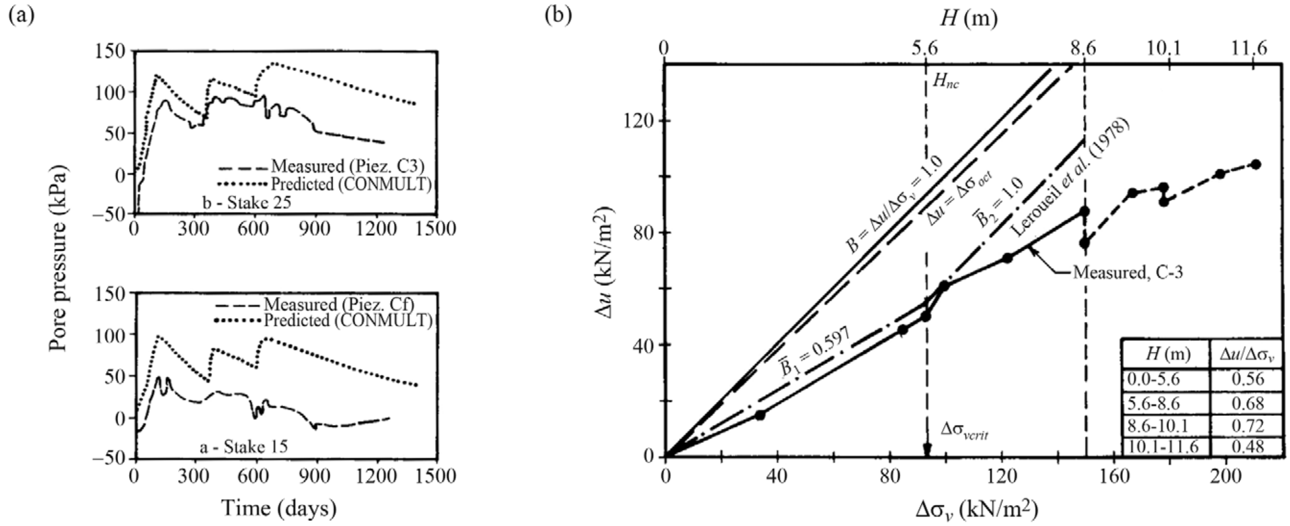

Figure 18 - Predicted and measured Δu in the Juturnaíba Dam: (a) against time; (b) during construction (Coutinho *et al.* 1994).

ing a ratio $\Delta u/\Delta\sigma_v$ of about 0.7, instead of 1.0, as predicted by the method. It seems that partial drainage continues to occur during construction.

The main objective to the follow up of pore pressures in the Jitituba embankments was to evaluate the efficiency of the adopted solution to accelerate the settlements and dissipate the pore-pressures, that is to say, prefabricated vertical drains (Cavalcante *et al.* 2003; 2004). The large time-lag of the Casagrande piezometer allied to the variations of the water level makes the analysis of data from piezometers more difficult. The results obtained from piezometers PZ-02 (South Direction) and PZ-06 (North Direction) were evaluated in relation to the response to the increase in stress and the dissipation of pore pressures with time, including the coefficient of horizontal consolidation by Orleach method (1983). This method is based in the Terzaghi Theory (1943) to obtain the coefficient of vertical consolidation and in the Barron Theory (1948) to obtain the coefficient of radial consolidation.

In order to minimize the effect of the Casagrande piezometer limitations, in this case the corrections on the measurements of pore pressures from Casagrande piezometers were also applied as proposed by Coutinho (1986) (see item 2).

Figure 19 presents the graph Δu *vs.* $\Delta\sigma_v$ (including stages construction) for the piezometer PZ-02 (South Direction), which relates the pore-pressure increase (measured and corrected) to the stress increase. Table 4 presents the values of Δu, $\Delta\sigma_v$, $\Delta u/\Delta\sigma_v$ and $\Delta u_{corrected}/\Delta\sigma_v$ for two piezometers and for both stages of construction. It is observed that the ratios of both $\Delta u/\Delta\sigma_v$ and $\Delta u_{corrected}/\Delta\sigma_v$ presented a compatible maximum value of 0.58 with a partially drained behavior during construction ($\Delta u/\Delta\sigma_v < 0.6$) (see item 1.1). This behavior is due to the possible overconsolidated behavior (high c_v or c_h) at the start of the construction,

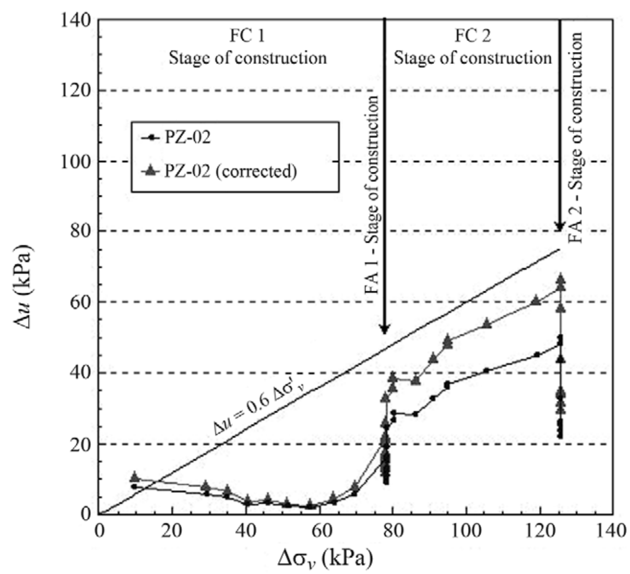

Figure 19 - Pore-pressures responses - South direction of Jitituba embankment (Cavalcante 2001).

Table 4 - Pore Pressure increase (Δu) *vs.* stress increase ($\Delta\sigma_v$) - Jitituba embankment (Cavalcante 2001).

Direction	South PZ-02	North PZ-06
Δu (kPa)	12	34
$\Delta\sigma_v$ (kPa)	69	82
$\Delta u/\Delta\sigma_v$	0.17	0.41
$\Delta u_{corrected}/\Delta\sigma_v$	0.23	0.55
Δu (kPa)	21	13
$\Delta\sigma_v$ (kPa)	48	35
$\Delta u/\Delta\sigma_v$	0.43	0.36
$\Delta u_{corrected}/\Delta\sigma_v$	0.58	0.48

and/or to the use of vertical drains in order to accelerate settlement, where both cause a faster dissipation of the pore-pressures generated.

The Orleach (1983) method was applied to obtain the coefficient of radial consolidation for piezometers PZ-02 South Direction (Fig. 20) and PZ-06 North Direction. It is observed in Table 5 that the PZ-06 (North) presents smaller consolidation coefficients than the PZ-02 (South), in both construction stages. The second stage of the construction presents a higher consolidation coefficient than the first one, on both sides. When compared with the laboratory average (normally consolidated interval) they become 1.04 and 1.50 times higher for the South and North Direction, respectively. When compared to the value used in the project, they are lower. The samples used in the laboratory were of low quality, which influenced the results of the consolidation parameters, reducing the values of c_v and σ'_P (Coutinho *et al.* 1998). In spite of the mechanical limitations (time-lag) of the Casagrande piezometers, the application of the Orleach (1983) method yielded reasonable results in comparison with laboratory results with low quality samples.

4. Vertical Displacements

The analysis of vertical displacements of an embankment consists of one or more stages, and usually requires the prediction of the initial and long-term settlements and

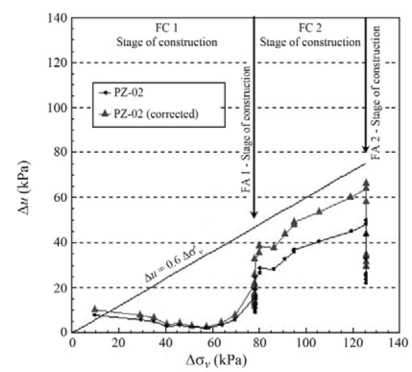

Figure 20 - Log (Δu) *vs.* time - Application of the Orleach (1983) method, Jitituba embankment (Cavalcante 2001).

Table 5 - Consolidation coefficient obtained by Orleach (1983) Method in the laboratory and adopted in the project - Jitituba embankment (Cavalcante 2001).

		1° Stage		2° Stage	
		$\alpha 1$	c_h 10^{-8}. m^2/s	$\alpha 1$	c_h 10^{-8}. m^2/s
Orleach (1983)	South	0.024	7.65	0.032	10.29
	North	0.008	2.51	0.031	9.98
	Average	-	5.08	-	10.14
Laboratory	-	4.0-8.0	-	4.0-8.0	
Project	-	15.0	-	15.0	

their variation with time. The total settlement will be the sum of the settlements during construction and settlements in the long term. As described in item 1.1, the behavior of an embankment on clay foundations can occur in some cases when it is essentially undrained and in many cases with partial drainage during construction.

4.1 Construction settlements

4.1.1. Undrained condition (“Conventional Design Approach”)

When a load is applied quickly to a limited area on a clay deposit, the strain induced in the clay causes lateral deformation of the soil, resulting in settlement. This settlement is generally considered as an instantaneous response to the load applied, occurring under undrained conditions and known as immediate or initial settlement, S_c. The prediction of the initial settlement uses a model derived from elasticity theory and has the form:

$$S_c = \rho_i = [q\, B\,(1 - \upsilon^2)\, I\rho] / E_u \qquad (8)$$

where ρ_i = immediate or initial settlement; q = stress applied to soil foundation; B = width or diameter of the loaded area; υ = Poisson coefficient, in this case 0.5; $I\rho$ = influence factor, which depends on the geometry of the problem; E_u = undrained Young modulus of the soil.

The initial settlement tends to be small in comparison with the settlement due to consolidation. This occurs when the base of the loaded area “B” is much bigger than the thickness of the clay layer “H”, for which “$I\rho$” values become very small. Foot & Ladd (1981) presented situations where the “ρ_i” value was very significant. Soils with high plasticity and/or high organic content are susceptible to these movements especially when loaded with a low factor of safety. Using the calculation procedure considered by D’Appolonia *et al.* (1971), the authors proposed a method to predict “ρ_i” values for use in this project.

Figure 21a presents results of construction settlements (predicted and measured by plate PL-2) under the center of Juturnaíba trial embankment (Coutinho 1986). The agreement between the theoretical results and the values observed was not satisfactory. Only the results corresponding to circular loading and for a height of 6.40 m presented values close to the results observed. The low value of the relation H/B corresponds to very small values of $I\rho$ and, consequently, to small settlement values. The circular load presented higher values for $I\rho$. Coutinho *et al.* (1994) and Lucena (1994) used the same procedure to calculate the initial settlements in two sections of the Juturnaíba Dam and observed similar behavior.

4.1.2. Construction settlement (“Partial Drainage”)

Leroueil *et al.* (1978) and Tavenas & Leroueil (1980) presented an empirical method for evaluating construction settlements of overconsolidated clay, with OCR < 2.5, where partial drainage of the foundation during construction was considered to have occurred. Figure 2a presents the effective stress path and considers the settlement takes place over two stages: initially a rapid consolidation in the Ko condition (preconsolidation compression) and after that, an essentially undrained shear deformation under the limit state curve.

The settlement of the first stage can be obtained from the results of oedometer tests on the overconsolidation clays, and can be calculated by the conventional expression:

$$S_r = \sum_{i=1}^{n} H \times RR \times \log \frac{\sigma'_p}{\sigma'_{vo}} \tag{9}$$

where RR = recompression index; H = clay layer thickness; σ'_p = preconsolidation pressure; σ'_{vo} = initial vertical effective stress.

When one significant part of the foundation becomes normally consolidated (second stage - $H_{emb} = H_{nc}$), the velocity of the occurrence of the settlement increases. The clay foundation, now with reduced rigidity and low permeability (Fig. 2a - P'A'), is deformed because of undrained shear distortion. After reviewing historical cases, Eq. 10) was proposed by the authors to obtain the undrained settlement S_u, corresponding to the second stage.

$$S_u = (0.07 \pm 0.03)\,(H - H_{nc}) \tag{10}$$

where: $\gamma H_{nc} = (\sigma'_p - \sigma'_{vo}) / I\,(1 - \overline{B}_1)$; I = influence factor; γ = unit weight of the embankment; $\overline{B}_1$ = pore pressure parameter.

The settlement S_c at the end of construction results from the sum of the recompression settlement, S_r (O' towards P' in Fig. 2a), and the undrained settlement, S_u (P'-A' in Fig. 2a):

$$S_c = S_r + S_u \tag{11}$$

Figure 21b presents results of calculated and observed (settlement plate PL-2) construction settlements in the center of the Juturnaíba trial embankment as a function of the height of the embankment. For this method (partial drainage) the agreement between predicted and measured values was satisfactory, and showed slightly higher values for lower embankment heights and slightly smaller values for greater embankment heights.

4.2. Long term settlement

The equation usually used in conventional designs to calculate the primary settlement of a deposit considers overconsolidated and normally consolidated compressions:

$$S_p = \sum_{i=1}^{n} \left(H \times RR \times \log \frac{\sigma'_p}{\sigma'_{vo}} + H \times CR \times \log \frac{\sigma'_{vf}}{\sigma'_p} \right) \tag{12}$$

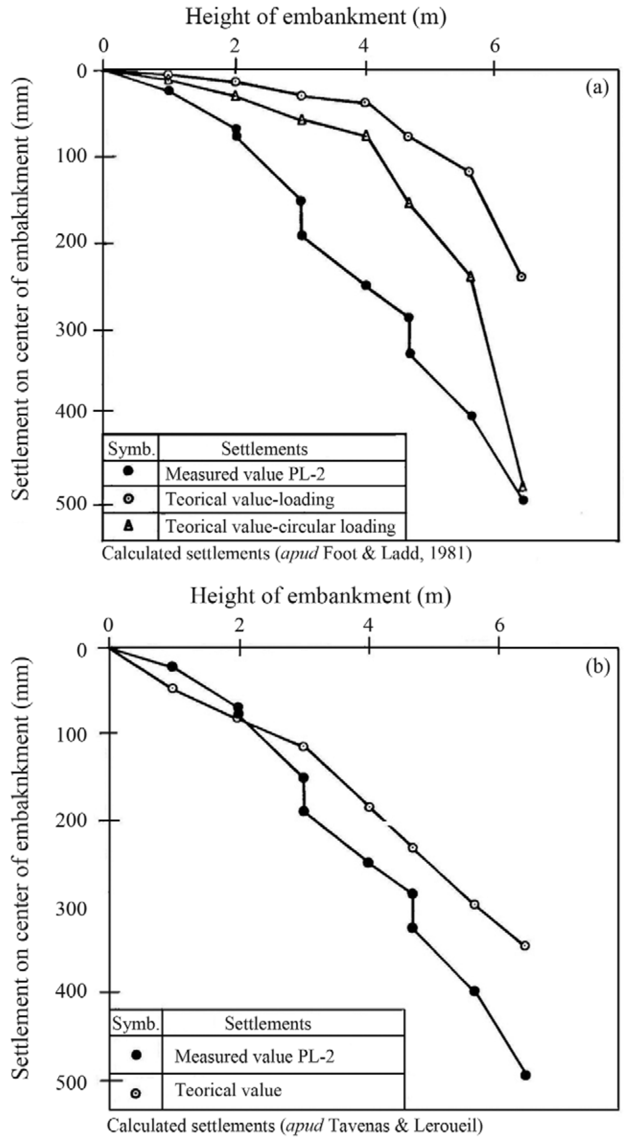

Figure 21 - Measured and calculated settlements - Juturnaíba trial embankments (Coutinho 1986).

where i = layer number; n = number of sub-layers; $RR = C_r / (1 + e_o)$, recompression coefficient; $CR = C_c / (1 + e_o)$, virgin compression coefficient; σ'_{vf} = final vertical effective stress.

In the case of the partial drainage method, the long term settlement, S_d, is the second part of the consolidation settlement (normally consolidated compression) associated with effective stress increase from σ'_p to σ'_{vf} ($\sigma'_{vo} + \Delta\sigma'$). Thus:

$$S_d = \frac{H}{1 + e_{oi}} C_{ci} \log\left(\frac{\sigma'_{voi} + \Delta\sigma'}{\sigma'_{pi}} \right) \tag{13}$$

The total settlement, S, for both cases (Leroueil *et al.* and conventional methods) is given by the sum of the construction and long term settlements, namely:

• Leroueil *et al.* method: $S = S_c + S_d = S_r + S_u + S_d$ (14)

• Conventional design: $S = S_c + S_p = \rho\, i + S_r + S_d$ (15)

The differences between the two approaches are basically: during construction, the Leroueil *et al.* method presents higher settlement; in the total settlement, the difference is between the values of ρi (the conventional method) and S_u (the Leroueil *et al.* method).

After the end of primary consolidation, settlement continues with time due to secondary consolidation, S_s, and in conventional design has been estimated by:

$$S_s = DC_{\alpha\varepsilon} \log\left(\frac{t}{t_p}\right) = \frac{DC_{\alpha e}}{1+e_p} \log\left(\frac{t}{t_p}\right) \quad (16)$$

Where $C_{\alpha\varepsilon}$ and $C_{\alpha e}$ are measured in oedometer tests or estimated from C_c; t_p = time at the end-of-primary consolidation; t = time to estimate the settlement; e_p = the void ratio at time t_p.

In fact, the influence of the viscous behavior of the clays (and also peats) in the settlement during primary consolidation is more complex. There are two extreme possibilities: (a) the creep occurs only after the end-of-primary consolidation, and consequently, the strain at the end-of-primary consolidation would be the same in situ and in laboratory; (b) the viscous strains develop during primary consolidation and, consequently, the strain at the end-of-primary consolidation is larger in situ than in the laboratory. In addition, there is also a discussion about a finite final value for the secondary compression (see Leroueil & Rowe 2000; Rémy *et al.* 2010a).

Coutinho *et al.* (1994) and Lucena (1994) present an analysis of the Juturnaíba Dam settlement behavior considering undrained condition during construction using two approaches: (a) classical conventional method (Terzaghi's Theory) and (b) CONMULT PROGRAM. Settlements were measured by settlement plates installed at the embankment-clay interface. The final primary settlement and the in situ coefficient of consolidation were obtained from settlement data using Asaoka's method (Asaoka 1978; Magnan & Deroy 1980). Computed and measured total settlements are show in Table 6 for the three sections and the eleven stakes analyzed. Good agreement between the results of settlements computed and the Asaoka's method is generally observed. Relative differences [(Asaoka - Terzaghi) / Asaoka] varied from -7.7 to +13% for the eleven points. Another good example of results and discussion about primary and secondary consolidation can be seen in Rémy *et al.* (2010a,b).

Computed and measured settlement curves are shown in Figs. 22a and 22b for two of the four stakes (section 2) analyzed by CONMULT PROGRAM. Good agreement between numerical and measured settlements is observed at stakes 15 and 30 (5 to 10%). Settlements are slightly overpredicted at stakes 20 and 25 (25 to 30%). Computed initial settlement rates are greater than the ones measured. In the classical method, consolidation analysis was conducted by using Terzaghi's theory, considering the loading stages and the load increase with time. The final settlement and the average coefficient of consolidation to be used in the analysis were also computed on the basis of the surface settlement using Asaoka's method. A typical example of classical consolidation analysis is shown in Fig. 22c. Very close agreement is observed in this case provided that a proper c_v and total settlement values are used for each construction stage and the load increase with time is considered. These results show the applicability of Terzaghi's Theory for this particular case. When the use of c_v of laboratory and settlements obtained from Terzaghi, the corrected predicted curves show some difference from the result measured by plate R-3.

Values of average *in situ* c_v were back-calculated from the settlement data for different loading stages using

Table 6 - Comparison between measured and predicted settlements Juturnaíba Dam (Borges 1991; Coutinho *et al.* 1994; Lucena 1997).

Section	Stake	Asaoka (mm) (1)	Plate R-3 (mm) (2)	Terzaghi (mm) (3)	Difference (%) (1)-(3)/(1)	Difference (%) (1)-(2)/(1)
III-2	46	1436	1400	1547	-7,73	2.51
	50	1346	1200	1371	-1.86	10.85
	55	318	312	297	6.60	1.89
	60	310	310	298	3.87	0
V	35	1196	1130	1040	13.04	5.52
	37+10	1349	1070	1436	-6.45	20.68
	40	1170	1150	1185	-1.28	1.71
II	15	1153	1155	1005	12.8	-0.17
	20	1270	1210	1350	-6.3	4.72
	25	1457	1430	1320	9.4	1.85
	30	-	1093	975	10.8	-

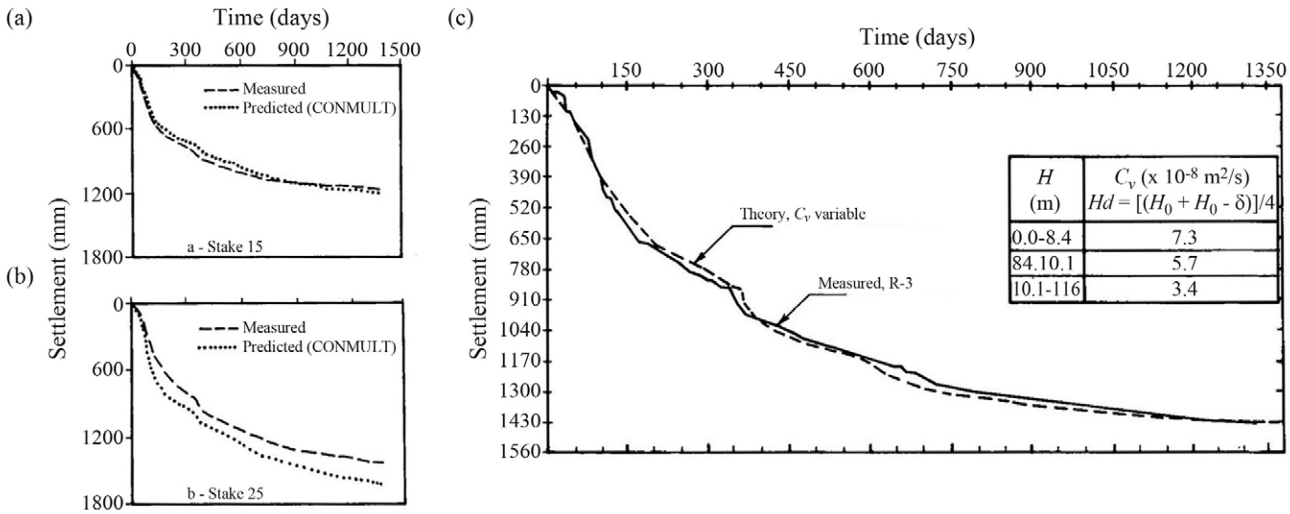

Figure 22 - Predicted and measured settlements against time - Juturnaíba Dam: (a) and (b) Conmult analysis; (c) Terzaghi analysis (Coutinho *et al.* 1994).

Asaoka's method. Table 7 compares such results with average values obtained in the laboratory for the range of the total stress applied. It can be seen that *in situ* values are higher than average laboratory values, but with the ratio c_v *in situ* / c_v lab in the order of 2 or less. The analysis performed using CONMULT showed that c_v values generally increase slightly up to the overconsolidation (yield) pressure, decrease abruptly afterwards and then show a slow decrease (Coutinho *et al.* 1994).

Cavalcante (2001) and Cavalcante *et al.* (2003) measured and analyzed vertical displacements in Jitituba embankment (Fig. 9). The maximum settlement and consolidation coefficient in the field were obtained, considering the period of the curve settlement *vs.* time, after the end of the construction of each stage (consolidation phase) (Fig. 23).

In the analysis of stress-deformation behavior, it is observed that estimated settlements using laboratory parameters (in normally consolidated soil) presented values about 40% to 60% higher than the maximum values measured in the field (Table 8). A possible reason for this difference is disturbance effects on the laboratory results. The stress-deformation behavior obtained in the laboratory was compared graphically to that in the field (settlement plates located in the center of embankments) with the final vertical effective stress (σ'_{vf}) values in the field being obtained through the difference between the estimated total stresses and the pore pressure measured in the field. The disturbance effects in the laboratory samples can be observed through the deformation corresponding to the initial effective stress σ'_{vo} (~14%) and the overconsolidation stress results to be lower than σ'_{vo} values (Fig. 24).

Table 8 - Settlement estimated using laboratory and maximum values measured in the field - Jitituba embankment (Cavalcante *et al.* 2003).

Direction	South	North
$\Delta\sigma_{v1}/\Delta\sigma v_{o1}$	3.0	2.4
CR	22%	22%
Layer thickness	9.70 m	11.20 m
Settlement laboratory	1.30 m 13.2%	1.30 m 11.6%
Settlement field	0,91 m 9.38%	0,80 m 7.14%
Difference lab-field	42.86	62.5

The coefficient of horizontal consolidation values obtained by the Asaoka (1978) method was higher in the North Direction than in the South Direction (around 26%). With regard to those obtained in laboratory, the field values

Table 7 - Coefficient of consolidation values: Section II - Juturnaíba Dam (Coutinho *et al.* 1994).

H (cm)	Laboratory (m²/s)		*In situ* (x 10^{-8} m²/s)			
	c_v		c_v Asaoka's method			
	Range	Mean stress	STAKE 15	STAKE 20	STAKE 25	MEAN
0.0-8.5	40.0-3.5	7.0	8.1	11.2	7.3	8.9
8.5-10.0	3.5-2.1	2.7	5.9	4.8	5.7	5.5
10.0-11.5	2.1-2.1	2.1	3.5	2.8	3.4	3.2

were from about 2.6 to 7.7 times higher (Table 9). The possible causes for this difference are the disturbance effects in the compressibility and consolidation parameters, that is, induces σ'_p and c_h values that are underestimated in the laboratory (Coutinho *et al.* 1998).

Results of c_h obtained from the Asaoka method were 2.3 to 3.1 times the values from the Orleach method (interpretation of Δu measured). In both methods, c_h was found to be higher in the second stage (1.18 and 2.65 times). One reason may be the low stress increment ratio, which results in a larger participation of the secondary settlement in the total settlement (Martins & Lacerda 1985) and/or it is not sufficient to exceed the overconsolidation caused by the secondary consolidation from previous stress stage (Leonards & Altschaefl 1964).

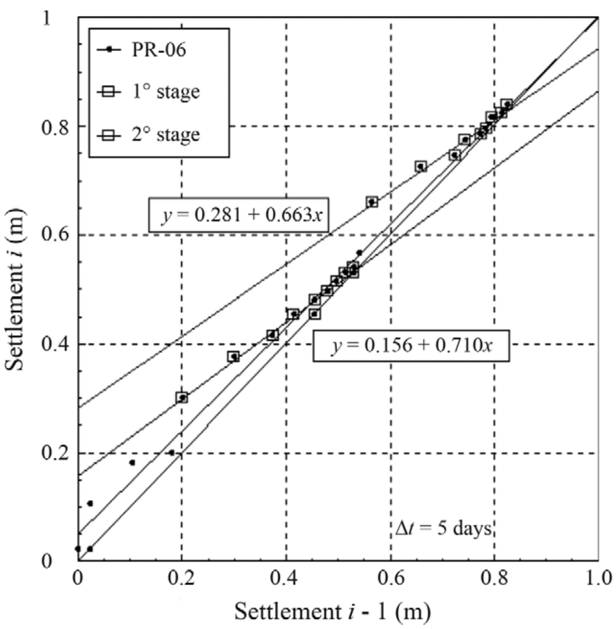

Figure 23 - Application of the Asaoka graphic construction, plate PR-06, North Direction - Jitituba embankment (Cavalcante *et al.* 2003).

Cavalcante (2001) and Cavalcante *et al.* (2003), based on Massad (1988; 1999), proposed the estimation of an overconsolidation parameter in the field, OCR_{GLOBAL}, given the settlement expressed and the collected data of maximum settlements estimated / measured in the field and the estimated stresses σ'_{vo} and $\Delta\sigma'_v$. For all cases studied CR = 40% and SR = 5% were considered due to the similarity between the compressibility parameters of Brazilian soft clays. Figure 25 presents OCR_{GLOBAL} values obtained for several embankments. The influence of overconsolidation stress on the magnitude of deformations can be observed. In the Jitituba embankment, the OCR_{GLOBAL} presented average values of 2.1 and 2.6 for each stage of loading. In other embankments, this parameter presented values in the range of 1.3 and 6.7.

5. Horizontal Displacement

Using empirical correlations and the Ylight model, Tavenas *et al.* (1979) present a method that allows the hori-

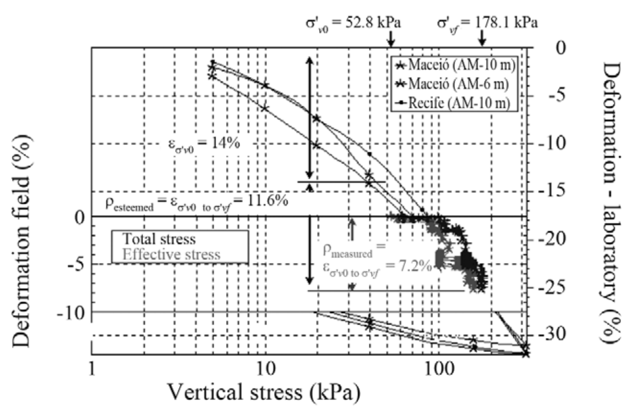

Figure 24 - Comparison between the behavior stress deformations observed in the field and in the laboratory, North Direction - Jitituba embankment (Cavalcante *et al.* 2003).

Table 9 - Comparison between c_h obtained through field measurements, from laboratory tests and used in the project - Jitituba embankment (Cavalcante *et al.* 2003).

Direction			South PZ-02		North PZ-06	
		Stage	1°	2°	1°	2°
Stress increase		$H_{emb\ end}$ (m)	4.34	6.98	5.03	6.96
		σ'_{V0i} (kPa)	41.80	119.92	52.80	143.3
		$\Delta\sigma_{Vi}$ (kPa)	78.12	47.52	90.54	34.74
		$\Delta\sigma_{Vi}/\Delta\sigma'_{Vi}$	1.87	0.40	1.71	0.24
c_h (10^{-8}.m^2/s)	Field	Asaoka (1978)	20.55	24.34	26.32	30.8
		Orleach (1983)	7.65	10.29	2.51	9.98
		Laboratory	4.00-8.00 normally consolidated range			
		Project	15.00			

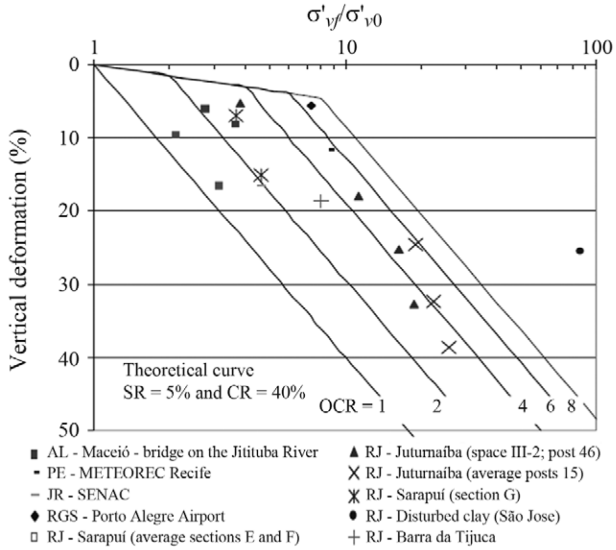

Figure 25 - Influence of the overconsolidation ratio on the magnitude of the settlements of several Brazilian embankments on soft soils (Cavalcante *et al.* 2003).

zontal deformation to be expressed as a ratio between maximum vertical displacement, S, measured in the center of embankment and maximum horizontal displacement y_m, measured in a vertical under the foot of the embankment.

According to the Ylight model (Tavenas & Leroueil 1980), during the construction of an embankment on overconsolidated soft soil foundation (OCR < 2.5), the effective stress path for a point at or near the centerline is O'P'A' (Fig. 2a). What is observed initially in the overconsolidated clay is drained consolidation near the Ko condition. In this condition, the horizontal displacements are much smaller than the settlements (preconsolidation compression - S_r) and in fact, all the deformation components are small because of the rigidity of the clay - O'P'. Based on field observations, Bourges & Mieussens (1979) and Tavenas *et al.* (1979) (see also Leroueil & Rowe 2000) proposed an empirical method to calculate horizontal displacements. It was observed that in cases of embankments with slopes of the order of 1.5 to 2.5 (H): 1 (V), this initial maximum horizontal displacement would be correlated with the maximum settlement (Fig. 26) using the equation:

$$y_{mr} = (0.18 \pm 0.09)\, S_r \tag{17}$$

When reaching the P' point in the path (Fig. 2a), the clay foundation becomes normally consolidated and is subjected to an approximately undrained state of plastic shear during which the horizontal displacements increase quickly, at the same rate as the settlements (P'A') until construction ends.

The statistical expressions proposed that relates the increase of horizontal displacements to the settlement (Fig. 27) is:

$$\Delta y_{mu} = (0.91 \pm 0.2)\, S_u \tag{18}$$

The total maximum horizontal displacement, y_m, at the end of construction will be represented by the addition of two parcels of displacement:

$$y_m = y_{mr} + y_{mu} \tag{19}$$

where y_{mr} is the lateral displacements during the preconsolidation compression, and y_{mu} is the lateral displacements during the following phase, when the soil is normally consolidated.

With the time, after construction ends, the effective stress increases following a path such as A'B' (Fig. 2a), with the settlements due to consolidation of the normally consolidated clay. Tavenas *et al.* (1979) concluded that the maximum horizontal displacement continues to increase linearly with the settlement yielding, for definitive conditions of geometry and stability, in:

$$\Delta y_m = (0.16 \pm 0.02)\, \Delta S \tag{20}$$

where ΔS corresponds to consolidation settlement "S_c".

The value of the ratio $\Delta y_m/\Delta S$ during consolidation can be a function of the width L or angle β of the embankment slope, of the thickness of clay (D or H) and of the fac-

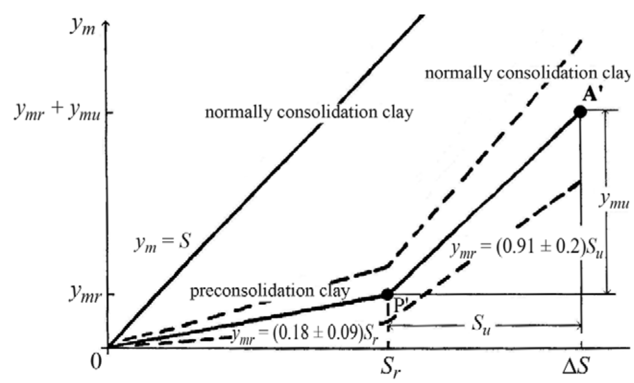

Figure 26 - Calculation of horizontal displacement in function of the settlement during construction (Tavenas *et al.* 1979).

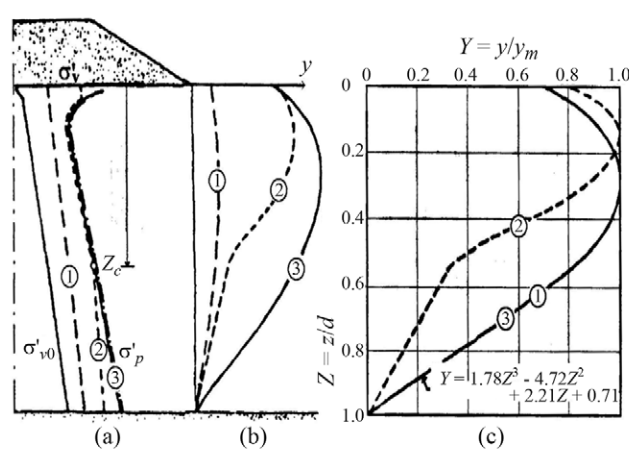

Figure 27 - Method of estimating the distribution of the horizontal deformation with the depth under the base of the embankment (Tavenas *et al.* 1979).

tor of safety, which limits the level of the shear stress at point A' (Fig. 2a).

The similarity between Eq. (20) and the corresponding one at the beginning of the construction (Eq. (17)) provides additional evidence of the drained nature of the response of the clayey foundation at the initial stage, according to the literature. The observed relationship shows as a general occurrence in the initial period of consolidation, that is, about 5 years later for investigated soils. For long periods of consolidation, the $\Delta y_m/\Delta S$ ratio can decrease by to about 1/3 of the observed value at the start of consolidation, that is, the $\Delta y_m/\Delta S$ ratio could also be a function of time.

The distribution of the horizontal displacement with the depth can be estimated using the relation between the normalized deformation, $Y = y/y_m$, and the relative depth $Z = z/D$, where "D" is the thickness of the clayey layer (Fig. 27). The empirical relation between Y and Z depends directly on the consolidation state of the foundation clay. During the initial period of construction, when all the clay is in an overconsolidated state, the deformation is of type 1, which corresponds to the classic solution of elasticity theory. If, during the final phase of construction, all clay layer moves to the normally consolidated state the deformation, when construction ends, reflects this final homogeneity final of the foundation soil (situation type 3, Fig. 27b). Bourges & Mieussens (1979) showed empirically that, in these cases, the normalized deformations are identical (Fig. 27c). The distribution of horizontal displacements when construction ends can be obtained using Eq. (21):

$$Y = 1.78\,Z^3 - 4.72\,Z^2 + 2.21\,Z + 0.71 \tag{21}$$

where $Y = y/y_m$ and $y_m = y_{mr}$, and $Z = z/D$.

If only part of the soil foundation reaches the normal consolidated state during the construction, then the final deformations will reflect this heterogeneity with a form of type 2 (Fig. 26c - see Tavenas *et al.* 1979 for the equation).

The results of horizontal displacements observed in the Juturnaíba trial embankment were represented as indicated by Tavenas *et al.* (1979) and Bourges & Mieussens (1979) (Figs. 4, 28, 29 and 30). Analyzing the results, it can be observed that (Coutinho 1986):

• Figure 29 presents the horizontal displacements measured using the four inclinometers set up in one cross section. It is possible to see that the behavior observed is similar to I-1 and I-2 and shows some influence from the strength of the embankment. The I-3 and I-4 show the foundation deformation in a vertical under or near the foot of the embankment.

• The observed values (Fig. 29a) of y_m (foot of embankment) *vs.* S (center of embankment) showed three rectilinear intervals, instead of only two as indicated by Tavenas *et al.* (1979). The first and the third intervals showed values of $\Delta y_m/\Delta S$ in very good agreement with the Tavenas *et al.* proposal. The soft clay foundation under the trial embankment presents a shallow part (depth: 0-2.5 m) with OCR > 2.5 (Fig. 16) and the proposed method was developed for clays with OCR < 2.5. This characteristic of the soft deposit may be one reason for the different behavior.

• The inclinometers (under the embankment, I-1 and I-2) showed similar behavior for the relation of y_m *vs.* S, with the ratio $\Delta y_m/\Delta S$ presenting, in general, higher values than the reference inclinometer at the toe of embankment (Fig. 27b).

Analyzing the pore pressure and the increases in stress developed because of the construction of the em-

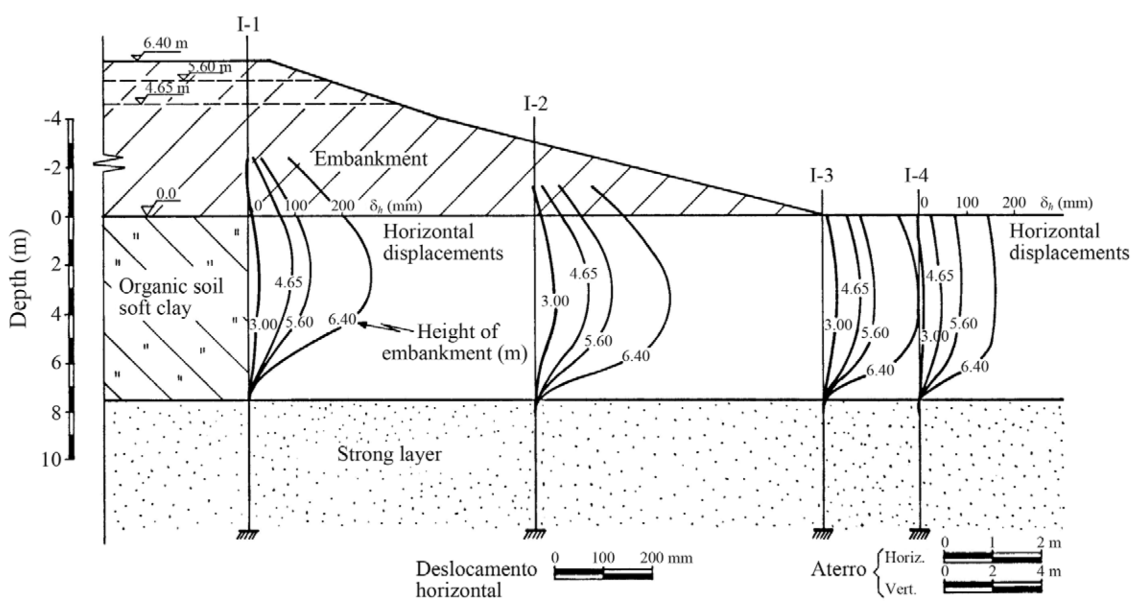

Figure 28 - Horizontal displacements measured for inclinometers - embankment with 3.00; 4.65; 5.60 and 6.40 heights, Juturnaíba trial embankment (Coutinho 1986).

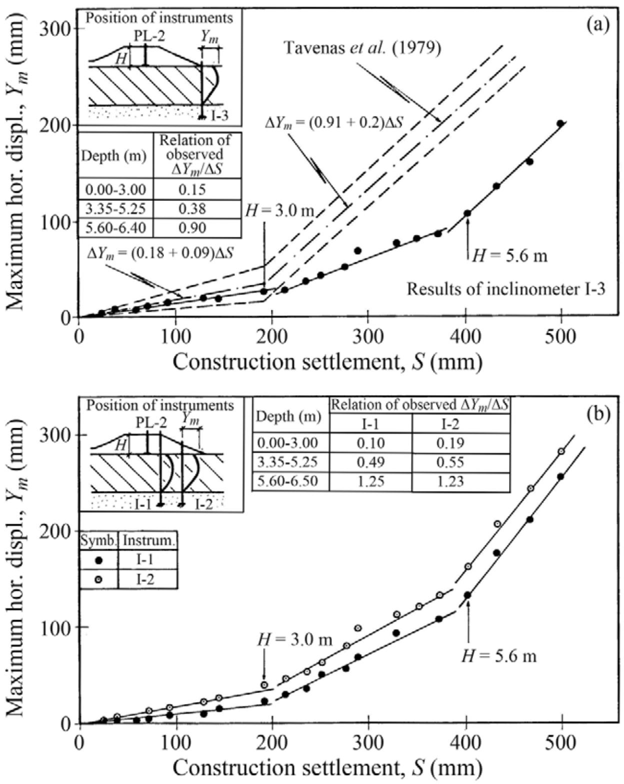

Figure 29 - Maximum horizontal displacement vs. settlement of the construction in the center of the Juturnaíba trial embankment: (a) inclinometer at the foot of the embankment and (b) inside the emban kment (Coutinho 1986).

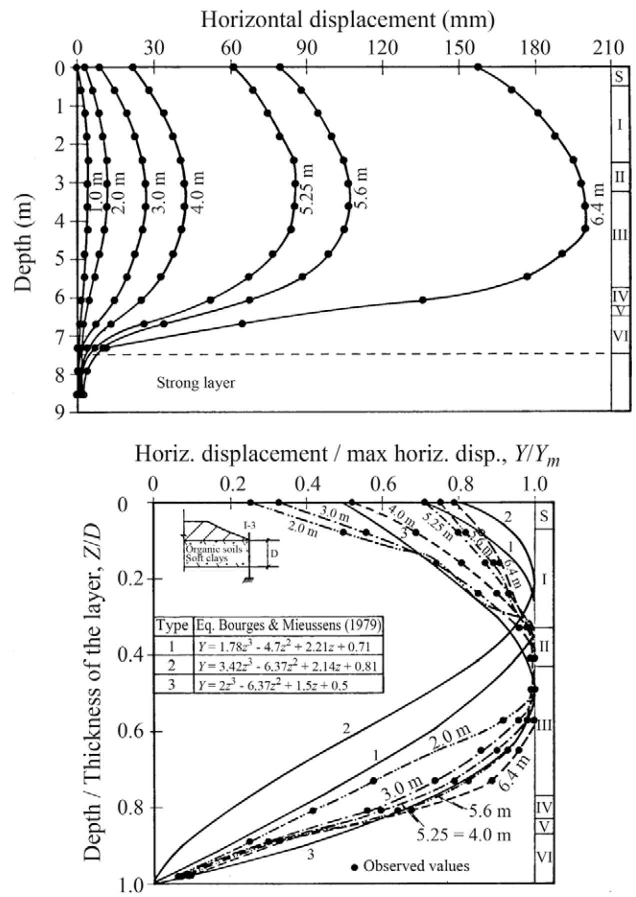

Figure 30 - Distribution of horizontal displacements with depth, foot of Juturnaíba embankment:(a) horizontal displacement; (b) horizontal displacement/maximum horizontal displacement (Coutinho 1986).

bankment, it was observed that for the part of the foundation with OCR > 2.5 (Fig. 16; 0-2.5 m depth), the σ'_{crit} values were smaller than σ'_p from the oedometer laboratory tests and tended to increase as the construction continued, reaching values similar to σ'_p for an embankment height of 5.6 m. For the part of the foundation with OCR < 2.5 (Fig. 16; 2.5-7.5 m depth), the σ'_{crit} values were in the same range as the σ'_p values, and remained constant in the same range while the embankment continued to be constructed. The condition $\Delta u \cong \Delta\sigma_v$ was obtained for an embankment height of 3.0 m for the foundation zone with OCR < 2.5 and for a height of 5.6 m in the foundation zone with OCR > 2.5. This condition has a strong influence on the horizontal displacements observed:

• The normalized distribution of the horizontal displacement with the corresponding depth along the vertical line under the foot of embankment, $y/y_m = f(z/D)$ seems to be in agreement with the Bourges & Mieussens' proposal (depending on the strength condition of the deposit), being stationary in the zones of the foundation that is normally consolidated. The good agreement with curve type 3 for the entire foundation occurred when the height of the embankment was between 3.0 and 4.0 m (Fig. 30).

• The existence of a relatively thick layer with OCR > 2.5 seems to be responsible for the differences observed between the predicted and the observed values, and for the variation of $y/y_m = f(Z/D)$ behavior during the construction.

In the Juturnaíba trial embankment it was possible to have different instruments in the same location to measure vertical and horizontal displacements (Fig. 4). Figure 31 shows the resultant displacements (vectors) at points of the foundation for different embankment heights. It can be seen that the tendency is for vectors to be displaced during construction basically until failure, showing an expected behavior.

Coutinho *et al.* (1994) and Lucena (1994) present an analysis of the horizontal displacement of the Juturnaíba Dam in which they show measured and predicted maximum horizontal displacement *vs.* settlement under the center of the embankment are presented (Fig. 32). Horizontal displacements were measured at the inclinometer set up at the slope-berm interface. During the construction stages, the values measured are in agreement with those proposed only up to an embankment height of 5.6 m, when the soft clay appeared to become normally consolidated. Above this height, the measured values are much lower than the

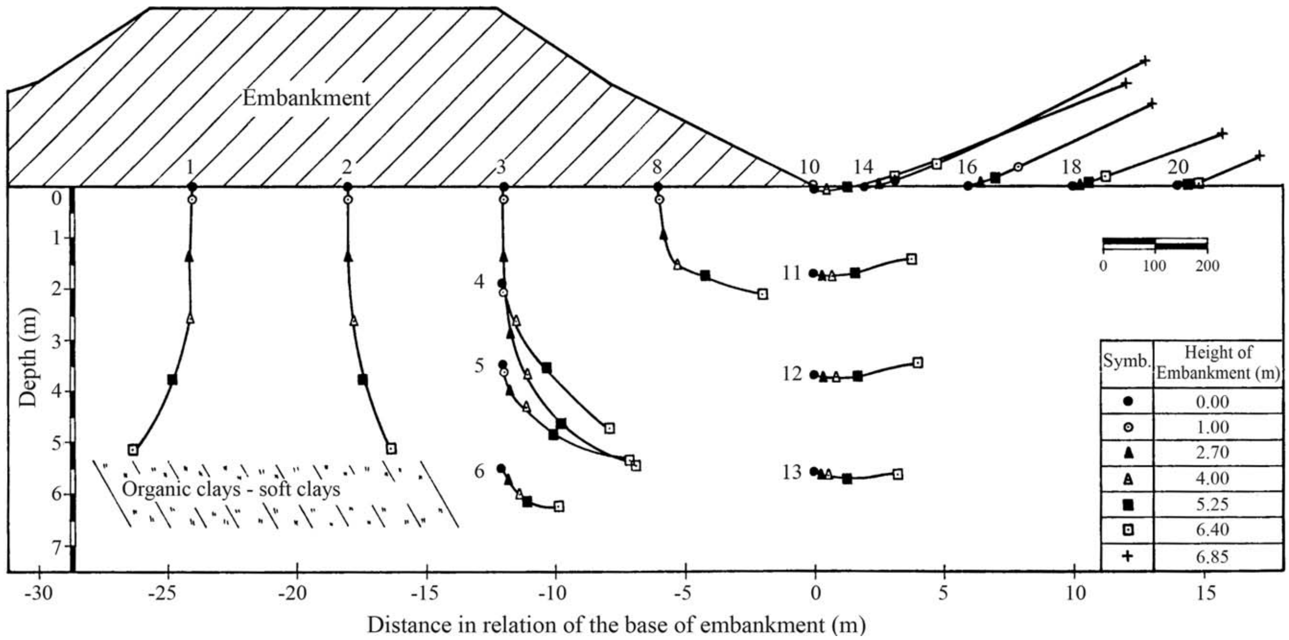

Figure 31 - Resultants (vertical + horizontal) displacements in points of foundation - Juturnaíba trial embankment (Coutinho 1986).

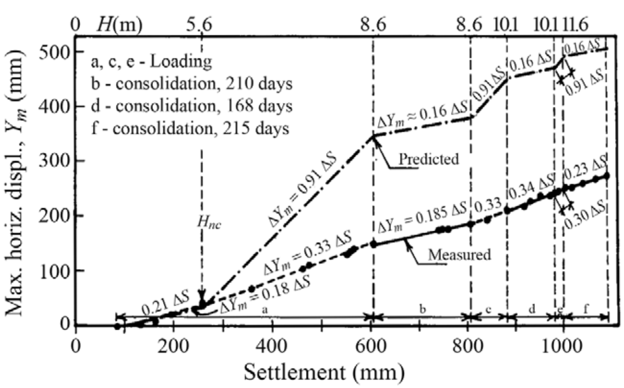

Figure 32 - Maximum Horizontal Displacements *vs.* Settlements - Juturnaíba Dam (Coutinho *et al.* 1994).

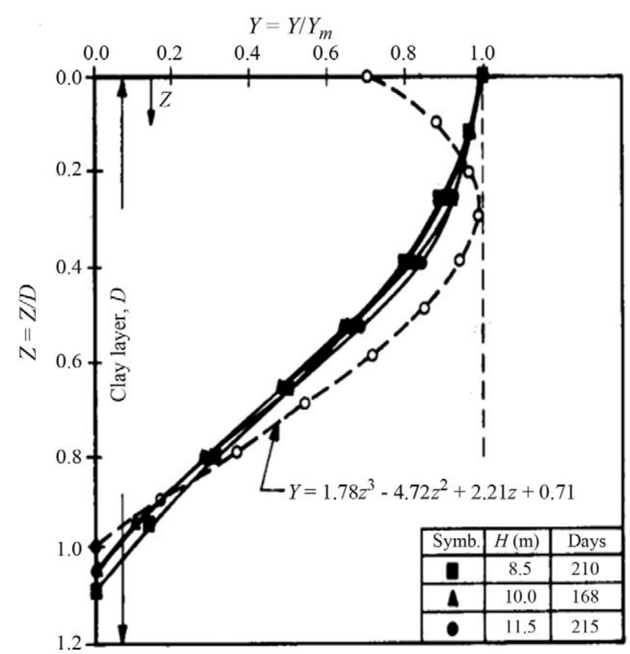

Figure 33 - Distribution of Horizontal Deformation with depth - Juturnaíba Dam (Coutinho *et al.* 1994).

predicted ones. The $\Delta Y_m/\Delta S$ measured values were in the range of 0.30-0.33 instead of 0.91 as predicted by the method. During the consolidation periods, the agreement is generally good, where the ratio $\Delta Y_m/\Delta S$ values are generally in the range of 0.18-0.23, close to the predicted values which average about 0.16. The results appear to show that partial drainage occurred during all the construction stages. One possible explanation for this behavior is the combination of the following factors: the large width of the embankment, the relatively small thickness of the compressible layer, and perhaps the location of the inclinometer.

The distribution of the lateral displacement with respect to depth depends directly on the consolidation state of the clay beneath the embankment. Figure 33 shows for Juturnaíba Dam the predicted (Tavenas *et al.* 1979) and measured $Y = f(Z)$ for the consolidation period under different loading stages, after the clay layer has become normally consolidated. As proposed by Tavenas *et al.* (1979), the distribution of lateral displacement regarding depth remained essentially unchanged with respect to time and construction stages. In addition, reasonable agreement between predicted and measured $Y = (Z)$ curves is also observed. The main discrepancy is the displacement at the top of the clay foundation.

Cavalcante (2001) and Cavalcante *et al.* (2003 and 2004) performed horizontal displacement analysis and stability control in the Jitituba embankment. The main purpose of following up horizontal displacements was to check the stability of the foundation soil during and after the construction of the access embankments of the Jitituba River Bridge, in order to ensure these displacements were maintained within safe limits and that they presented the least possible minimal values, because of proximity of piles of the bridge foundation. Figures 34 and 35 present measured and predicted maximum horizontal displacement *vs.* settlement under the center of the embankment and the normalized profile of the horizontal displacements with the depth, respectively.

It is observed in Fig. 34 that the ratio $\Delta Y_{max}/\Delta S$ presented in general values in all the construction and consolidation phases (except in the phase of the consolidation for inclinometer I-01) that were lower than the values proposed by Tavenas *et al.* (1979). During the construction phases, the $\Delta Y_{max}/\Delta S$ values were between 0.08 and 0.46, indicating a range of values correspondent to predominantly partially drained condition during construction. In the consolidation phases, it is observed that the values presented a reasonable range within 0.04 and 0.22, basically in the range proposed by Tavenas *et al.* (1979). This behavior can be due to the use of vertical drains, which accelerates consolidation as well as the increase of soil strength and/or to a possible overconsolidated state during the first construction phase.

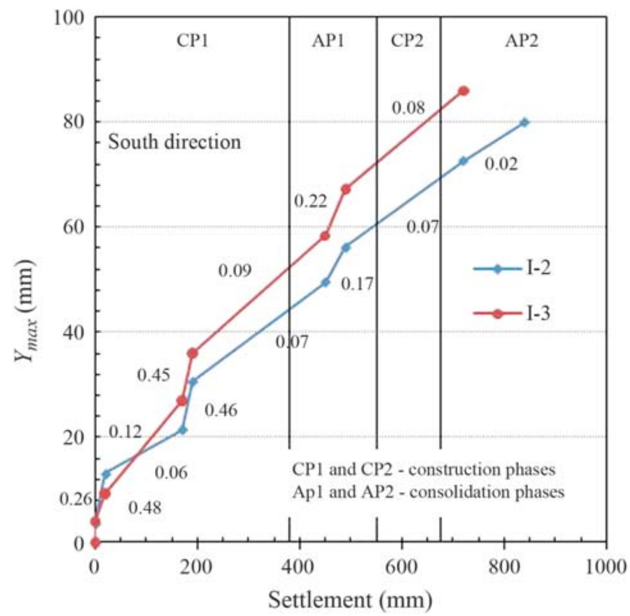

Figure 34 - Graphics Y_{max} (mm) *vs.* S (m) - Check of the ratio $\Delta Y_{max}/\Delta S$ proposed by Tavenas *et al.* (1979) Jitituba embankment (Cavalcante e*t al.* 2004).

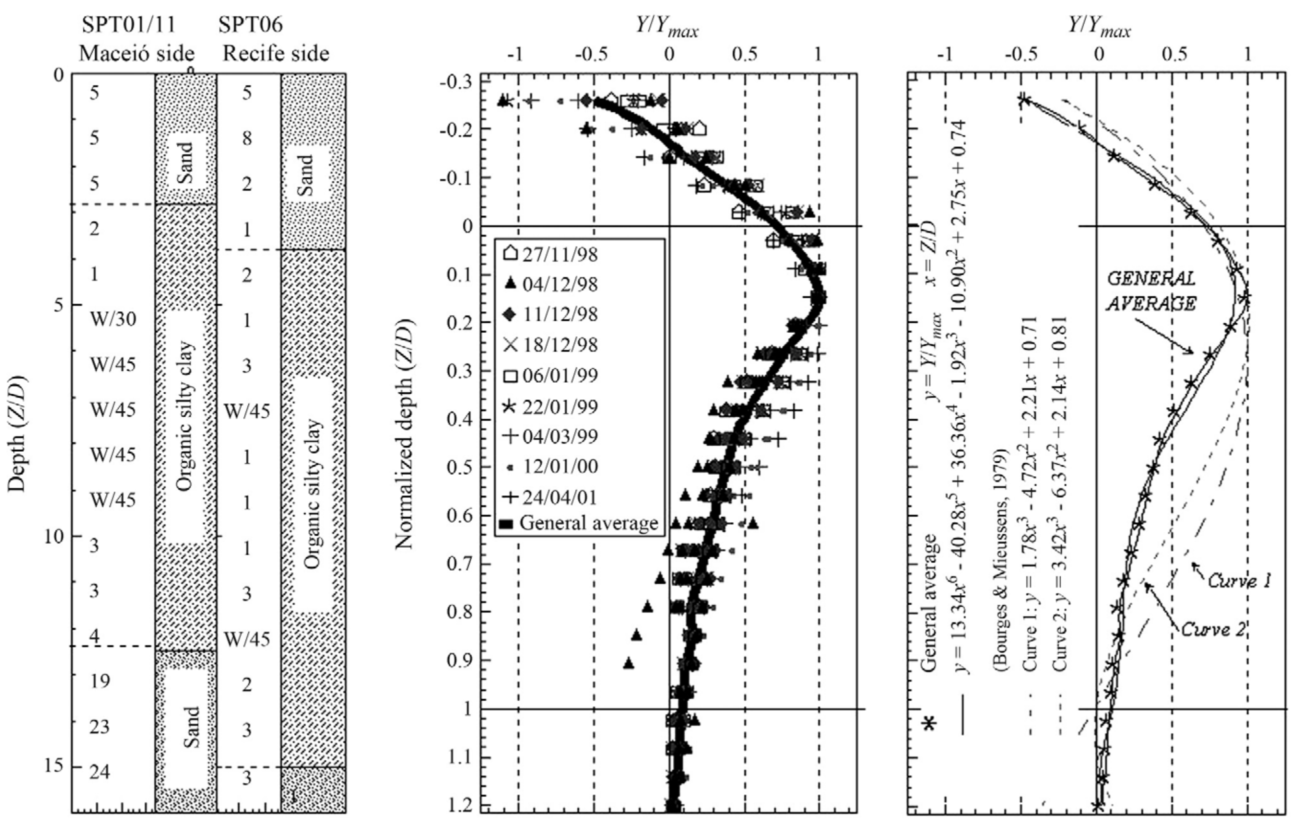

Figure 35 - Comparison between the average of the profiles normalized with the curves proposed by Bourges & Mieussens (1979) - Jitituba embankment (Cavalcante *et al.* 2004).

6. Final Comments and Conclusions

This paper presented and discussed concepts and results of monitoring and the performance of an embankment on soft soil deposits. Research and practical cases were used in the paper with emphasis on a well-instrumented and extensive study performed on the Juturnaíba trial embankment. The conventional ("undrained condition during construction") and the Tavenas & Leroueil models ("partial drainage during construction") were used in the analysis of the behavior of the embankments. In general, all the embankments studied presented partial drainage during construction, thus showing that actual behavior can be more complicated and that the conventional undrained analysis overpredicts pore pressure and horizontal displacements.

For the well-instrumented Juturnaíba trial embankment, in principle, the Tavenas & Leroueil model presented good results. Due to the specific soil foundation conditions of the area with the presence of organic soil layers and with part (~30%) of the deposit with OCR > 2.5, the effective stress path and the behavior observed showed more partial drainage and an "intermediate" interval in the behavior of pore pressure and lateral displacements during construction / failure. This case can be as an "extension of the Tavenas & Leroueil model proposed for the cases where the foundation deposit has a significant part with OCR > 2.5 but most of the soft deposit has OCR < 2.5.

Above an embankment height of 5.60 m (FS = 1.31), the foundation behavior (pore pressure, vertical and horizontal displacements) changes significantly showing the beginning of a possible process of failure, which occurred shortly after with H_{emb} = 6.85 m. This result confirms the importance of having a factor of safety in a project higher than 1.3-1.4, as indicated in the literature.

The cases studied in this paper show how complicated actual embankment behavior can be but they also point out to the possibility of predicting embankment behavior, depending on the condition of the foundation deposit, embankment geometry, location and type of instrument, etc. The importance of monitoring and evaluating each case based on an appropriate model is fundamental for the success of a project.

Acknowledgments

The authors are indebted to CNPq and CAPES for their financial support. Special thanks to Sarita Cavalcante and Maria Helena Lucena who contributed with part of the data used in this paper, and to Gusmão Associated Engineers for the partnership of in this project.

References

Almeida, M.S.S. (1996) Aterros Sobre Solos Moles: Da Concepção à Avaliação do Desempenho. Editora UFRJ, Rio de Janeiro, 216 pp.

Asaoka, A. (1978) Observational procedure of settlement prediction. Japanese Society of Soil Mechanics and Foundation Engineering, v. 18:4, p.87-101.

Barron, R.A. (1948) Consolidation of Fine-Grained Soils by Drain Well. Journal of the Geotechnical Engineering Division, ASCE, Transactions, paper 2346, v. 113, pp. 718-742.

Bjerrum L. (1973) Problems of soil mechanics and construction of soft clays and structurally unstable soils. Proc. of the 8th ICSMFE, Moscow, v. 3, pp. 111-159.

Bourges, F. & Miussens, C. (1979) Déplacement Latéraux à Proximité des Remblais Sur Sols Compressibles - Méthod de Prévision. Bull. Liaison Labo. P. et Ch., n. 101, p. 73-100.

Cavalcante, S.P.P. (2001) Análise de Comportamento de Aterros sobre Solos Moles - Aterros de Encontro da Ponte sobre o Rio Jitituba- AL. M.Sc. Thesis, Universidade Federal de Pernambuco, Recife, 232 pp. (In Portuguese).

Cavalcante, S.P.P.; Coutinho, R.Q. & Gusmão, A.D. (2003) Evaluation and control of stability of embankments on soft soils. Proc. XII PCSMGE, Cambridge, pp. 2649-2660.

Cavalcante, S.P.P.; Coutinho, R.Q. & Gusmão, A.D. (2004) Analysis of behavior of embankments on soft soils geotechnical investigations and instrumental access embankments of the Jitituba River Bridge. Proc. 15th ICCHGE, New York, paper 2.83, pp. 1-9.

Coutinho, R.Q. (1986) Aterro Experimental Instrumentado Levado à Ruptura Sobre Solos Orgânicos - Argilas Moles da Barragem de Juturnaíba. D.Sc. Thesis, COPPE/Universidade Federal do Rio de Janeiro, Rio de Janeiro, 634 pp. (In Portuguese).

Coutinho, R.Q. & Lacerda, W.A. (1987) Characterization-consolidation of Juturnaíba organic clays. Proc. ISGESS, Mexico City, v. 1, pp. 17-24.

Coutinho, R.Q. & Lacerda, W.A. (1989) Strength characteristics of Juturnaíba organic clays. Proc.12th ICSMFE, Rio de Janeiro, v. 3, pp.1731-1734.

Coutinho, R.Q.; Almeida, M.S.S. & Borges, J.B. (1994) Analysis of the Juturnaíba embankment dam built on soft clay. Vertical and horizontal deformations of foundations and embankments. Proc. of Settlement 94, Texas, v. 1, pp. 348-363.

Coutinho, R.Q.; Oliveira, J.T.R. & Oliveira, A.T.J. (1998) Estudo quantitativo da qualidade de amostras de argilas moles brasileiras - Recife e Rio de Janeiro. Proc. XI COBRAMSEG - Congresso Brasileiro de Mecânica dos Solos e Engenharia Geotécnica, Brasília, v. 2. pp. 927-936.

Coutinho, R.Q. & Bello, M.I.M. (2005) Geotecnia do Nordeste. ABMS / Núcleo Nordeste, Recife, Editora Universitária / UFPE, v. 3, p. 111-153.

Coutinho, R.Q. & Bello, M.I.M. (2010) Analysis and control of the stability of embankments on soft soil: Juturnaíba and other experiences in Brazil. Proc. Symp. of New Techniques for Design and Construction in Soft Clays, Guarujá, pp. 247-268.

D'Apolonia, D.J.; Poulos, H.G. & Ladd, C.C. (1971) Initial Settlement of Structures on Clay. ASCE, JSMFE, No. 10 0, pp. 1359-1377.

Folkes, D.J. & Crooks, J.H.A. (1985) Effective stress paths and yielding in soft clays below embankments. Canadian Geotechnical Journal, v. 22: 3, p. 357-374.

Foot, R. & Ladd, C.C. (1981) Undrained settlement of plastic and organic clays. ASCE, JTGED, v. 107:GT8, p. 1079-1094.

Leonards, G.A. & Altschaeffl, H.G. (1964) Compressibility of Clay. Journal of the Soil Mechanics and Foundation Division, Transactions of ASCE, v. 90:5, p. 133-155.

Leroueil, S.; Tavenas, F.; Mieussens, C. & Peignaud, M. (1978) Construction pore pressures in clay foundation under embankments. Part II: Generalized behaviour. Canadian Geot. Journal, v. 16:1, p. 66-82.

Leroueil, S. & Tavenas, F. (1986) Discussion on "Effective stress paths and yielding in soft clays below embankments". Canadian Geotechnical Journal, v. 23:3, p. 410-413.

Leroueil, S. (1996) Compressibility of clays: Fundamental and practical aspects. Journal of Geot. Eng. ASCE, v. 122:7, p. 534-543.

Leroueil, S & Rowe, R.K. (2000) Embankments Over Soft Soil and Peat. Geotechnical and Geoenviromental Engineering Handbook. R. K.Rowe (ed) Kluwer Academic Publishers, Norwell, pp. 463-498.

Lucena, M.H.L. (1994) Análise do Comportamento da Fundação da Barragem de Juturnaíba - Techos III-2 e V. M.Sc. Thesis, Universidade Federal de Pernambuco, Recife, 219 pp (In Portuguese).

Massad, F. (1988) Baixada Santista: Aterros sobre solos moles interpretados à luz dos novos conhecimentos sobre a gênese das argilas quaternárias. Proc. Simp. Depósitos Quaternários das Baixadas Litorâneas Brasileiras, São Paulo, v. 1. pp. 5.1-5.10.

Massad, F. (1999) Baixada Santista: Implicações da história geológica no projeto de fundações. Solos e Rochas, v. 22:1, p. 3-49.

Magnan, J.P. & Deroy, J.M. (1980) Analyse graphique des tassement observés sons les ouvrages. Bull. Liaison Laboratoire des Ponts e Chaussés, 109, p. 9-21.

Magnani de Oliveira, H. (2006) Comportamento de Aterros Reforçados sobre Solos Moles Levados à Ruptura. D. Sc. Thesis. COPPE/ Universidade Federal do Rio de Janeiro, Rio de Janeiro, 495 pp. (In Portuguese).

Martins, I.S.M. & Lacerda, W.A. (1985) A theory of consolidation with secondary compression. Proc. 11th ICSMFE, San Francisco, p. 567-570.

Morin, P.; Leroueil, S. & Sampson, L. (1983) Preconsolidation pressure of champlain clays. Part. I. In-situ determination. Canadian Geotechnical Journal, v. 20:4, p. 782-802.

Orleach, P. (1983) Techniques to Evaluate the Field Performance of Vertical Drains. Msc. Thesis, MIT, Cambridge.

Ortigão, J.A.R. (1980) Aterro Experimental Levado à Ruptura sobre Argila Cinza do Rio de Janeiro. D.Sc. Thesis, COPPE/ Universidade Federal do Rio de Janeiro, Rio de Janeiro, 715 pp. (In Portuguese).

Pinto, C.S. (1992) Primeira conferência Pacheco Silva: Tópicos de contribuição de Pacheco Silva e considerações sobre a resistência não drenada as argilas. Solos e Rochas, São Paulo, v.15:2, p. 49-87.

Rémy, J.P.P.; Martins, I.S.M.; Santa Maria, P.E.L.; Aguiar, V.N. & Andrade, M.E.S. (2010a) The embraport pilot embankment - Primary and secondary consolidations of Santos soft clay with and without wick drains - Part 1. Proc. Symp. of New Techniques for Design and Construction in Soft Clays, Guarujá, pp. 289-310.

Rémy, J.P.P.; Martins, I.S.M.; Santa Maria, P.E.L.; Aguiar, V.N. & Andrade, M.E.S. (2010b) The Embraport pilot embankment - Primary and secondary consolidations of Santos soft clay with and without wick drains - Part 2. Proc. Symp. of New Techniques for Design and Construction in Soft Clays, Guarujá, pp. 311-330.

Tavenas, F.; Mieussens, C. & Bougens, F. (1979) Lateral displacements in clay foundations under embankments. Canadian Geotechnical Journal, v. 16:3, p. 532-550.

Tavenas, F. & Leroueil, S. (1980) The behavior of embankments on clay foundations. Canadian Geotechnical Journal, v. 17:2, p. 236-260.

Terzaghi, K. (1943) Theoretical Soil Mechanics, Wiley, New York, 510 pp.

Soft Soils Improved by Prefabricated Vertical Drains: Performance and Prediction

B. Indraratna, C. Rujikiatkamjorn, X.-Y. Geng, G. McIntosh, R. Kelly

Abstract. The use of prefabricated vertical drains with vacuum preloading and surcharge preloading is now common practice and is proving to be one of the most effective ground improvement techniques known. The factors affecting its performance, such as the smear zone, the drain influence zone, and drain unsaturation, are discussed in this paper. In order to evaluate these effects a large scale consolidation test was conducted and it was found that the proposed Cavity Expansion Moreover, the procedure for converting an equivalent 2-D plane strain multi-drain analysis that considers the smear zone and vacuum pressure are also described. The conversion procedure was incorporated into finite element codes using a modified Cam-clay theory. Numerical analysis was conducted to predict excess pore pressure and lateral and vertical displacement. Three case histories are analyzed and discussed, including the sites of Muar clay (Malaysia), the Second Bangkok International Airport (Thailand), and the Sandgate railway line (Australia). The predictions were then compared with the available field data, which include settlement, excess pore pressure, and lateral displacement. Further findings verified that smear, drain unsaturation, and vacuum distribution can significantly influence consolidation so they must be modeled appropriately in any numerical analysis to obtain reliable predictions.

Keywords: analytical model, cyclic loading, numerical model, soft soils, vacuum preloading, vertical drains.

1. Introduction

Preloading of soft clay with vertical drains is one of the most popular methods used to increase the shear strength of soft soil and control its post-construction settlement. Since the permeability of soils is very low, consolidation time to the achieved desired settlement or shear strength may take too long (Holtz, 1987; Indraratna *et al.*, 1994). Using prefabricated vertical drains (PVDs), means that the drainage path is shortened from the thickness of the soil layer to the radius of the drain influence zone, which accelerates consolidation (Hansbo, 1981). This system has been used to improve the properties of foundation soil for railway embankments, airports, and highways (Li & Rowe, 2002).

Over the past three decades the performance of various types of vertical drains, including sand drains, sand compaction piles, prefabricated vertical drains (geosynthetic) and gravel piles, have been studied. Kjellman (1948) introduced prefabricated band shaped drains and cardboard wick drains for ground improvement. Typically, prefabricated band drains consist of a plastic core with a longitudinal channel surrounded by a filter jacket to prevent clogging. Most vertical drains are approximately 100 mm wide and 4 mm thick.

To study consolidation due to PVDs, unit cell analysis with a single drain surrounded by a soil cylinder has usually been proposed (*e.g.* Barron, 1948; Yoshikuni & Nakanodo, 1974). PVDs under an embankment not only accelerate consolidation, they also influence the pattern of subsoil deformation. At the centre line of an embankment where lateral displacement is negligible, unit cell solutions are sufficient but elsewhere, especially towards the embankment toe, any prediction from a single drain analysis is not accurate enough because of lateral deformation and heave (Indraratna *et al.*, 1997).

Figure 1 shows the vertical cross section of an embankment stabilised by a vertical drain system, with the instruments required to monitor the soil foundation. Before PVDs are installed superficial soil must be removed to ease the installation of the horizontal drainage, the site must be graded, and a sand platform compacted. The sand blanket drains water from the PVDs and supports the vertical drain installation rigs.

Figure 2 illustrates a typical embankment subjected to vacuum preloading (membrane system). Where a PVD system is used with vacuum preloading, horizontal drains must be installed after a sand blanket has been put in place (Cognon *et al.*, 1994). The horizontal drains are connected to a peripheral Bentonite slurry trench, which is then sealed

B. Indraratna, PhD, Professor and Head, School of Civil, Mining & Environmental Engineering, Director, Centre for Geomechanics & Railway Engineering, University of Wollongong, Wollongong City, NSW 2522, Australia. e-mail: indra@uow.edu.au.
C. Rujikiatkamjorn, PhD, Senior Lecturer, Centre for Geomechanics & Railway Engineering, School of Civil, Mining and Environmental Engineering, Faculty of Engineering, University of Wollongong, Wollongong City, NSW 2522, Australia. e-mail: cholacha@uow.edu.au.
X.-Y. Geng, PhD, Research Fellow, Centre for Geomechanics & Railway Engineering, School of Civil, Mining and Environmental engineering, Faculty of Engineering, University of Wollongong, Wollongong City, Australia. e-mail: xgeng@uow.edu.au.
G. McIntosh, BEng, MEng, Principal Engineer, Douglas Partners Pty Ltd, Unanderra, NSW Australia. e-mail: Geoff.McIntosh@douglaspartners.com.au.
R. Kelly, PhD, Associate Engineer, Coffey Geotechnics, Sydney, Australia. e-mail: Richard_Kelly@coffey.com.
Submitted on November 1, 2010; Final Acceptance on December 15, 2011; Discussion open until July 31, 2012.

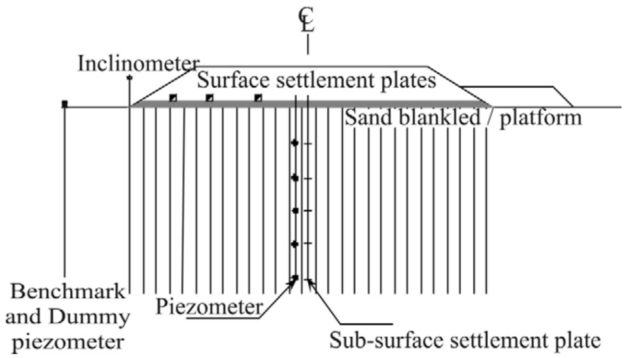

Figure 1 - Vertical drain system with preloading.

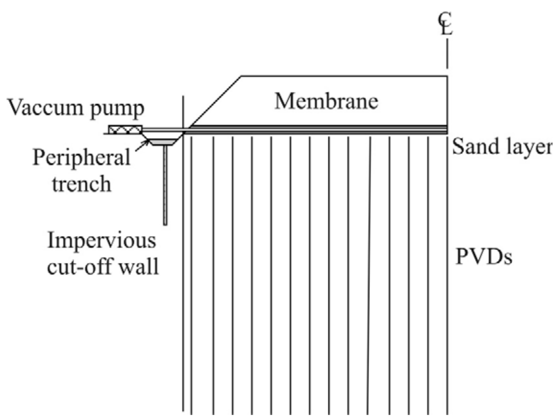

Figure 2 - Vacuum preloading system.

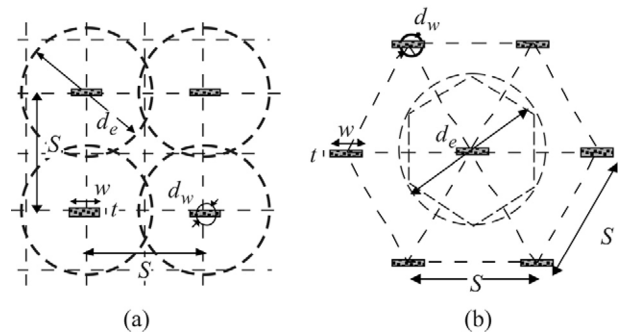

Figure 3 - Drain installation pattern (a) square pattern; (b) triangular pattern.

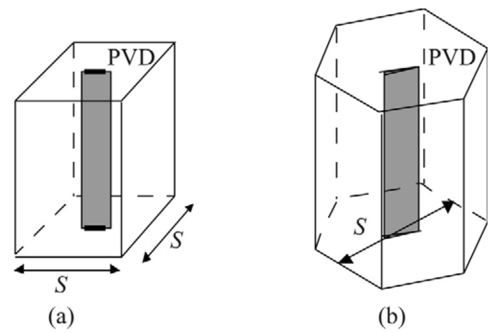

Figure 4 - Vertical drain and its dewatered soil zone (a) unit cell with square grid installation and (b) unit cell with triangular grid installation.

with an impermeable membrane and cut-off walls to prevent possible vacuum loss at the embankment edges. The vacuum pumps are connected to the discharge module extending from the trenches. The vacuum generated by the pump increases the hydraulic gradient towards the drain which accelerates the dissipation of excess pore water pressure.

2. Factors Influencing The Performance of A Vacuum Or Surcharge Preloading With Consolidated Pvds

2.1. Equivalent drain diameter and drain influence zone

As shown in Fig. 3, PVDs with a rectangular cross section are usually installed in a triangular or square pattern. Their shapes are not the same as the circular cross section considered in the unit cell theory so a PVD with a polygon influence zone must be transformed into a cylindrical drain with a circular influence zone (Fig. 4). The approximate equations proposed for the equivalent drain diameter are based on various hypotheses, hence the different results. The formulations for an equivalent cylindrical drain conversion available from previous studies are highlighted below:

$$d_w = \frac{2(w+t)}{\pi} \quad \text{(Hansbo, 1979)} \tag{1}$$

$$d_w = \frac{(w+t)}{2} \quad \text{(Atkinson \& Eldred, 1981)} \tag{2}$$

$$d_w = 0.5w + 0.7t \quad \text{(Long \& Covo, 1994)} \tag{3}$$

where d_w = equivalent PVDs diameter and w and t = width and thickness of the PVD, respectively.

2.2. Smear zone

The smear zone is the disturbance that occurs when a vertical drain is installed using a replacement technique. Because the surrounding soil is compressed during installation there is a substantial reduction in permeability around the drain, which retards the rate of consolidation. In this section the Elliptical Cavity Expansion Theory was used to estimate the extent of the smear zone (Ghandeharioon *et al.* 2009; Sathananthan *et al.* 2008). This prediction was then compared with laboratory results based on permeability and variations in the water content. The detailed theoretical developments are explained elsewhere by Cao *et al.* (2001) and Ghandeharioon *et al.* (2009), so only a brief summary is given below. The yielding criterion for soil obeying the MCC model is:

$$\eta = M\sqrt{\frac{p'_c}{p'} - 1} \quad (4)$$

where p'_c = the stress representing the reference size of yield locus, p' = mean effective stress, M = slope of the critical state line and η = stress ratio. Stress ratio at any point can be determined as follows:

$$\ln\left(1 - \frac{(a^2 - a_0^2)}{r^2}\right) = -\frac{2(1+\nu)}{3\sqrt{3}(1-2\nu)}\frac{\kappa}{\upsilon}\eta - 2\sqrt{3}\frac{\kappa\Lambda}{\upsilon M} f(M, \eta, \mathrm{OCR}) \quad (5)$$

$$f(M, \eta, \mathrm{OCR}) = \frac{1}{2}\ln\left[\frac{(M+\eta)(1-\sqrt{\mathrm{OCR}-1})}{(M-\eta)(1+\sqrt{\mathrm{OCR}-1})}\right] - \tan^{-1}\left(\frac{\eta}{M}\right) + \tan^{-1}(\sqrt{\mathrm{OCR}-1}) \quad (6)$$

In the above expression, a = radius of the cavity, a_0 = initial radius of the cavity, ν = Poisson's ratio, κ = slope of the over consolidation line, υ = specific volume, OCR = over consolidation ratio and λ is the slope of the normal consolidation line).

Figure 5 shows the variation of the permeability ratio (k_h/k_v), obtained from large scale laboratory consolidation and predicted plastic shear strain along the radius. Here the radius of the smear zone was approximately 2.5 times the radius of the mandrel, which agreed with the prediction using the cavity expansion theory.

2.3. Drain unsaturation

Due to an air gap from withdrawing the mandrel, and dry PVDs, unsaturated soil adjacent to the drain can occur. The apparent delay in pore pressure dissipation and consolidation can be observed during the initial stage of loading (Indraratna *et al.*, 2004). Figure 6 shows how the top of the drain takes longer to become saturated than the bottom. Figure 6 illustrates the change in degree of saturation with the depth of the drain. Even for a drain as short as 1 m, the time lag for complete drain saturation can be significant.

2.4. The effect of vacuum consolidation on the lateral yield of soft clays

In order to investigate the effect of a combined vacuum and surcharge load on lateral displacement, a simplified plane strain (2-D) finite element analysis could be used (Indraratna *et al.* 2008). The outward lateral compressive strain due to surcharge can be reduced by applying suction (vacuum preloading). The optimisation of vacuum and surcharge preloading pressure to obtain a given settlement must be considered in any numerical model to minimise lateral displacement at the embankment toe (Fig. 7a), while identifying any tension zones where the vacuum pressure may be excessive.

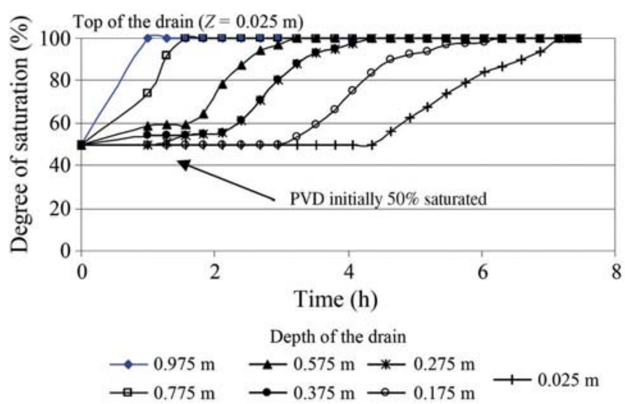

Figure 6 - Degree of drain saturation with time (after Indraratna *et al.* 2004).

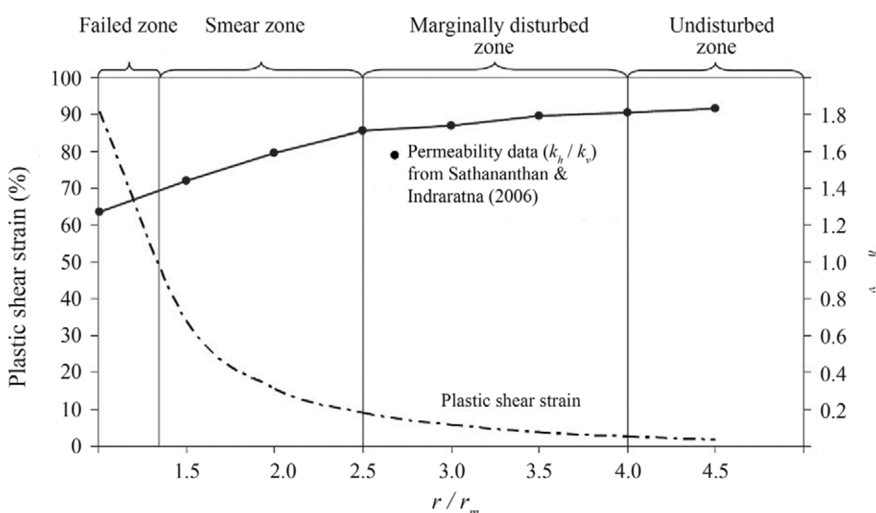

Figure 5 - Variations in the ratio of the horizontal coefficient of permeability to the vertical coefficient of permeability and the plastic shear strain in radial direction (adopted from Ghandeharioon *et al.* 2009).

As expected, the vacuum pressure alone can create inward lateral movement, whereas preloading without any vacuum may contribute to an unacceptable outward lateral movement. The particular situations for most clays is generally a combination of 40% surcharge preloading stress with a 60% vacuum, which seems to maintain a lateral displacement close to zero. Figure 7b presents the various profiles of surface settlement with an increasing surcharge loading. A vacuum alone may generate settlement up to 10 m away from PVD treated boundary while the application of VP can minimise the value of soil heave beyond the embankment toe.

3. Equivalent Plane Strain For Multi-Drain Analysis

In order to reduce the calculation time, most available finite element analyses on embankments stabilised by PVDs are based on a plane strain condition. To obtain a realistic 2-D finite element analysis for vertical drains, the equivalence between a plane strain condition and an in-situ axisymmetric analysis needs to be established. Indraratna and Redana (2000); Indraratna *et al.* (2005) converted the unit cell of a vertical drain shown in Fig. 8 into an equivalent parallel drain well by determining the coefficient of permeability of the soil.

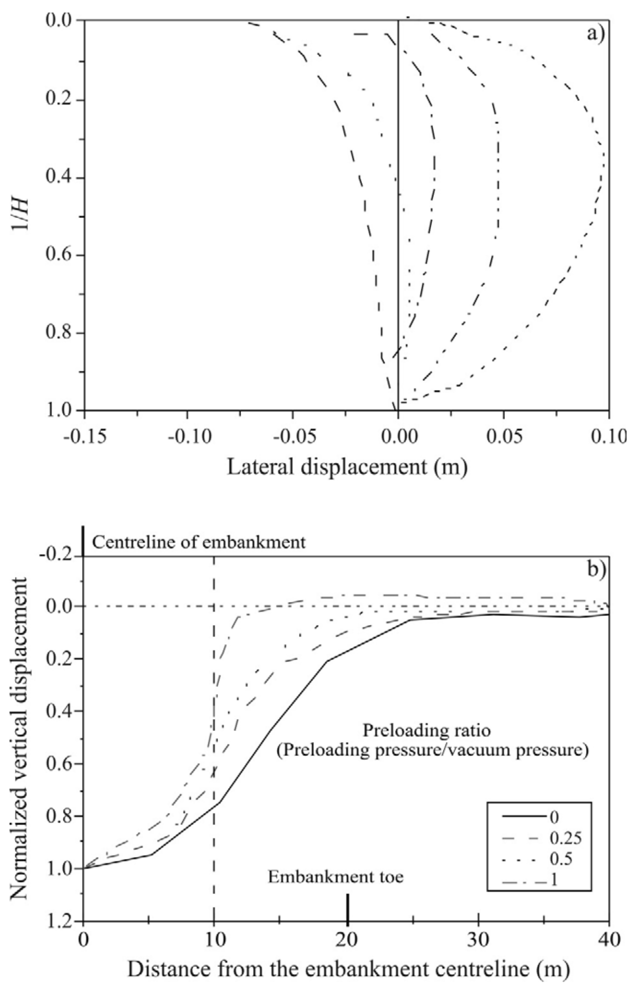

Figure 7 - (a) Lateral displacements; and (b) surface settlement profiles (Indraratna *et al.* 2008).

By assuming that the diameter of the zone of influence and the width of the unit cell in a plane strain to be the same, Indraratna & Redana (2000) presented a relationship between k_{hp} and k'_{hp}, as follows:

$$k_{hp} = \frac{k_h\left[\alpha + \beta\dfrac{k_{hp}}{k'_{hp}} + \theta(2lz - z^2)\right]}{\left[\ln\left(\dfrac{n}{s}\right) + \left(\dfrac{k_h}{k'_h}\right)\ln(s) - 0.75 + \pi(2lz - z^2)\dfrac{k_h}{q_w}\right]} \tag{7}$$

In Eq. (7), if well resistance is neglected, the smear effect can be determined by the ratio of the smear zone permeability to the undisturbed permeability, as follows:

$$\frac{k'_{hp}}{k_{hp}} = \frac{\beta}{\dfrac{k_{hp}}{k_h}\left[\ln\left(\dfrac{n}{s}\right) + \left(\dfrac{k_h}{k'_h}\right)\ln(s) - 0.75\right] - \alpha} \tag{8}$$

$$\alpha = \frac{2}{3} - \frac{2b_s}{B}\left(1 - \frac{b_s}{B} + \frac{b_s^2}{3B^2}\right) \tag{8a}$$

$$\beta = \frac{1}{B^2}(b_s - b_w)^2 + \frac{b_s}{3B^2}(3b_w^2 - b_s^2) \tag{8b}$$

$$\theta = \frac{2k_{hp}^2}{k'_{hp}q_z B}\left(1 - \frac{b_w}{B}\right) \tag{8c}$$

where k_{hp} and k'_{hp} are the undisturbed horizontal and the corresponding smear zone equivalent permeability, respectively.

The simplified ratio of plane strain to axisymmetric permeability by Hird *et al.* (1992) is readily obtained when the effect of smear and well resistance are ignored in the above expression, as follows:

$$\frac{k_{hp}}{k_h} = \frac{0.67}{[\ln(n) - 0.75]} \tag{9}$$

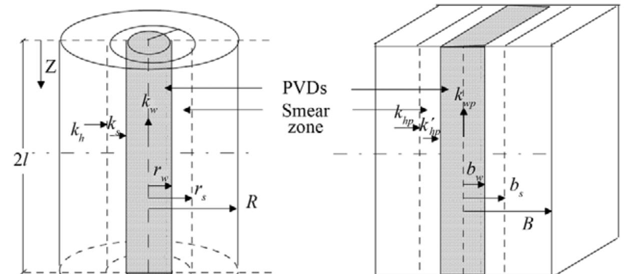

Figure 8 - Conversion of an axisymmetric unit cell into plane strain condition (after Indraratna & Redana 2000).

The well resistance is derived independently and yields an equivalent plane strain discharge capacity of drains, which can be determined from the following equation:

$$q_z = \frac{2}{\pi B} q_w \quad (10)$$

With vacuum preloading, the equivalent vacuum pressures in plane strain and axisymmetric are the same.

4. Application To Case Histories

4.1. Muar clay embankment

One of the test embankments on Muar plain was constructed to failure. The failure was due to a "quasi slip circle" type of rotational failure at a critical embankment height at 5.5 m, with a tension crack propagating through the crust and the fill layer (Fig. 9). Indraratna *et al.* (1992) analysed the performance of the embankment using a finite element Plane strain finite element analysis employing two distinct constitutive soil models, namely, the Modified Cam-clay theory using the finite element program CRISP (Woods, 1992) and the hyperbolic stress-strain behaviour using the finite element code ISBILD (Ozawa & Duncan, 1973). Two modes of analysis were used, undrained and coupled consolidation. Undrained analysis was used when the loading rate was much faster than the dissipation rate of excess pore pressure. This will cause excess pore pressure to build up during loading but will not alter the volume. While excess pore pressure is generated simultaneously with drainage, a positive or negative change in volume is allowed for coupled consolidation analysis.

The essential soil parameters used for the Modified Cam-clay model are summarised in Table 1 and a summary of soil parameters for undrained and drained analyses by ISBILD is tabulated in Table 2. Because properties of a topmost crust were not available it was assumed that the soil properties were similar to the layer immediately below. The properties of the embankment surcharge (E = 5100 kPa, ν = 0.3 and γ = 20.5 kN/m^3), and related shear strength parameters (c' = 19 kPa and ϕ' = 26°), were obtained from drained tri-axial tests.

The finite element discretisation is shown by Fig. 10. The embankment was constructed at a rate of 0.4 m/week. Instruments such as inclinometers, piezometers, and settlement plates were installed at this site (Fig. 11).

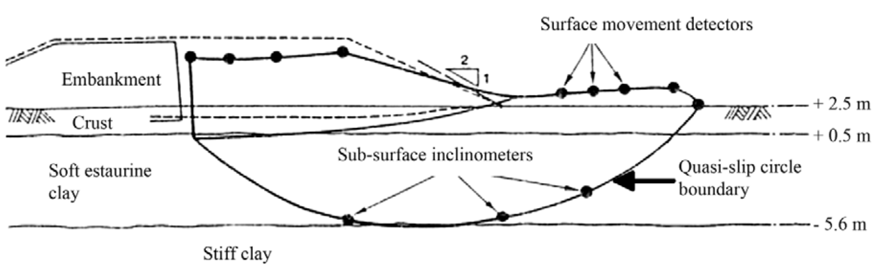

Figure 9 - Failure mode of embankment and foundation (modified after Brand & Premchitt, 1989).

Table 1 - Soil parameters used in the Modified Cam-clay model (CRISP) (Source: Indraratna *et al.*, 1992).

Depth (m)	κ	λ	M	e_{cs}	K_w x 10^4 (cm^2/s)	γ (kN/m^3)	k_h x 10^{-9} (m/s)	k_v x 10^{-9} (m/s)
0-2.0	0.05	0.13	1.19	3.07	4.4	16.5	1.5	0.8
2.0-8.5	0.05	0.13	1.19	3.07	1.1	15.5	1.5	0.8
8.5-18	0.08	0.11	1.07	1.61	22.7	15.5	1.1	0.6
18-22	0.10	0.10	1.04	1.55	26.6	16.1	1.1	0.6

Table 2 - Soil parameters for hyperbolic stress strain model ISBILD (Source: Indraratna *et al.*, 1992).

Depth (m)	K	c_u (kPa)	K_{ur}	c' (kPa)	ϕ' (degree)	γ (kN/m^3)
0-2.5	350	15.4	438	8	6.5	16.5
2.5-8.5	280	13.4	350	22	13.5	15.5
8.5-18.5	354	19.5	443	16	17.0	15.5
18.5-22.5	401	25.9	502	14	21.5	16.0

Note: K and K_{ur} are the modulus number and unloading-reloading modulus number used to evaluate the compression and recompression of the soil, respectively.

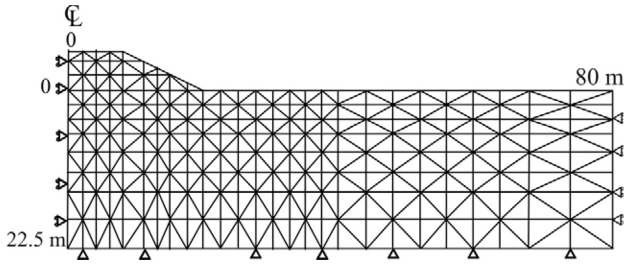

Figure 10 - Finite element discretisation of embankment and subsoils (modified after Indraratna *et al.*, 1992).

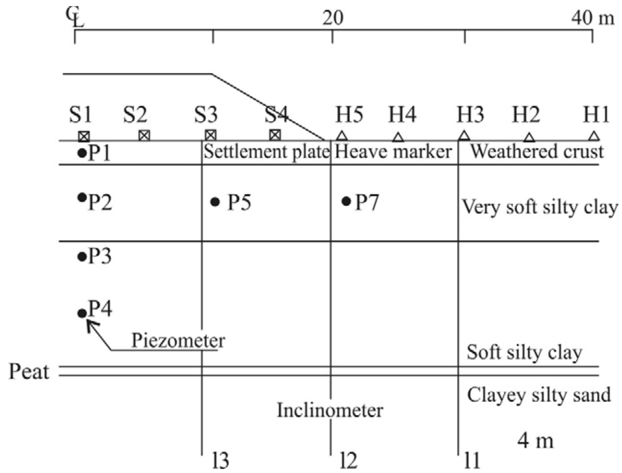

Figure 11 - Cross section of Muar test embankment indicating key instruments (modified after Ratnayake, 1991).

The yielding zones and potential failure surface observed were based on the yielded zone boundaries and maximum displacement vectors obtained from CRISP. Figures 12 and 13 show the shear band predicted, based on the maximum incremental displacement and the boundaries of yielded zone approaching the critical state, respectively. The yielded zone was near the very bottom of the soft clay layer but it eventually spread to the centre line of the embankment, which verified that the actual failure surface was within the predicted shear band.

4.2. Second Bangkok International Airport

The Second Bangkok International Airport or Suvarnabhumi Airport is about 30 km from the city of Bangkok, Thailand. Because the ground water was almost at the surface, the soil suffered from a very high moisture content, high compressibility and very low shear strength. The compression index ($C_c/(1 + e_0)$)varied between 0.2-0.3. The soft estuarine clays in this area often pose problems that require ground improvement techniques before any permanent structures can be constructed.

As reported by AIT (1995), the profile of the subsoil showed a 1 m thick, heavily over-consolidated crust overlying very soft estuarine clay which was approximately 10 m below the bottom of a layer of crust. Approximately 10 to 21 m beneath this crust there was a layer of stiff clay. The ground water level varied from 0.5 to 1.5 m below the sur-

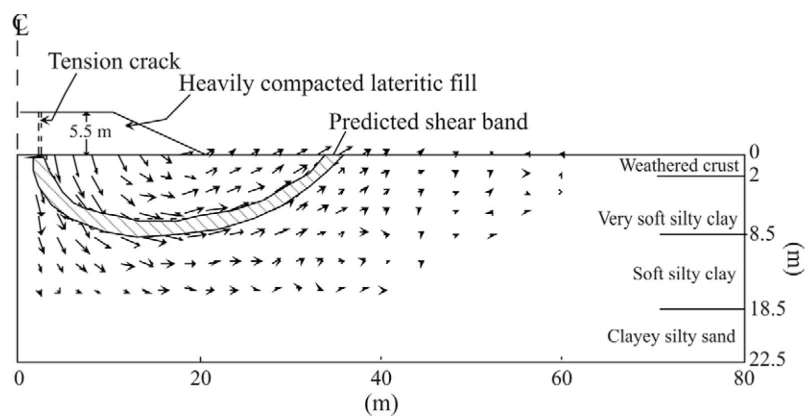

Figure 12 - Maximum incremental development of failure (modified after Indraratna *et al.*, 1992).

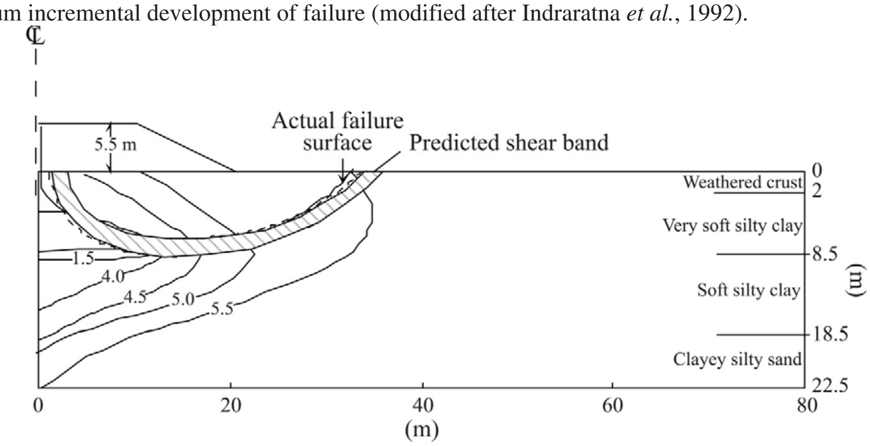

Figure 13 - Boundary zones approaching critical state with increasing fill thickness (CRISP) (modified after Indraratna *et al.*, 1992).

face. The parameters of these layers of subsoil, based on laboratory testing, are given in Table 3.

Two embankments stabilised by vacuum combined with surcharge loading (TV2) and surcharge loading alone (TS1) are described in this section. The performances of embankments TV2 and TS1 were reported by Indraratna & Redana (2000), and Indraratna *et al.* (2005), respectively. The vertical cross section of Embankment TS1 is shown in Fig. 14. TS1 was constructed in multi-stages, with 12 m long PVDs @ 1.5 m in a square pattern. The embankment was 4.2 m high with a 3H:1V side slope. Embankment TV2 was stabilised with vacuum combined surcharge and 12 m long PVDs. A membrane system was also used on this site.

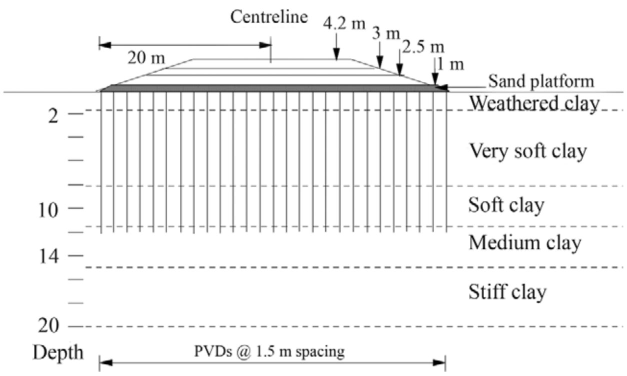

Figure 14 - Cross section at embankment TS1 (After Indraratna & Redana, 2000).

Both embankments were analysed using the finite element software ABAQUS. The equivalent plane strain model (Eqs. (7)-(10)) and modified Cam-clay theory were incorporated into this analysis. The comparisons of the degree of consolidation based on settlement from the FEM and field measurement at the centre line of the embankment are presented in Fig. 15. It can be seen that the application of vacuum pressure reduced the time from 400 to 120 days to achieve the desired degree of consolidation. Figure 16 shows the time dependent excess pore water pressure during consolidation. The vacuum loading generated negative excess pore pressure in TV2 whereas the surcharge fill in embankment TS1 created a positive excess pore pressure. These predicted excess pore pressures agreed with the field measurements. The maximum negative excess pore pressure was approximately 40 kPa, probably caused by a puncture in the membrane and subsequent loss of air. The total applies stresses for both embankment were very similar and therefore yielded similar ultimate settlements (90 cm). The reduction in negative pore pressure at various times was caused by the vacuum being lowered. Despite these problems the analysis using the proposed conversion procedure, including the smear effects, could generally predict the field data quite accurately.

4.3. Sandgate railway embankment

Under railway tracks where the load distribution from freight trains is typically kept below 7-8 m from the surface,

Table 3 - Selected soil parameters in FEM analysis (Indraratna *et al.* 2005).

Depth (m)	λ	κ	ν	k_v 10^{-9} m/s	k_h 10^{-9} m/s	k_s 10^{-9} m/s	k_{hp} 10^{-9} m/s	k_{sp} 10^{-9} m/s
0.0-2.0	0.3	0.03	0.30	15.1	30.1	89.8	6.8	3.45
2.0-8.5	0.7	0.08	0.30	6.4	12.7	38.0	2.9	1.46
8.5-10.5	0.5	0.05	0.25	3.0	6.0	18.0	1.4	0.69
10.5-13	0.3	0.03	0.25	1.3	2.6	7.6	0.6	0.30
13.0-15	1.2	0.10	0.25	0.3	0.6	1.8	0.1	0.07

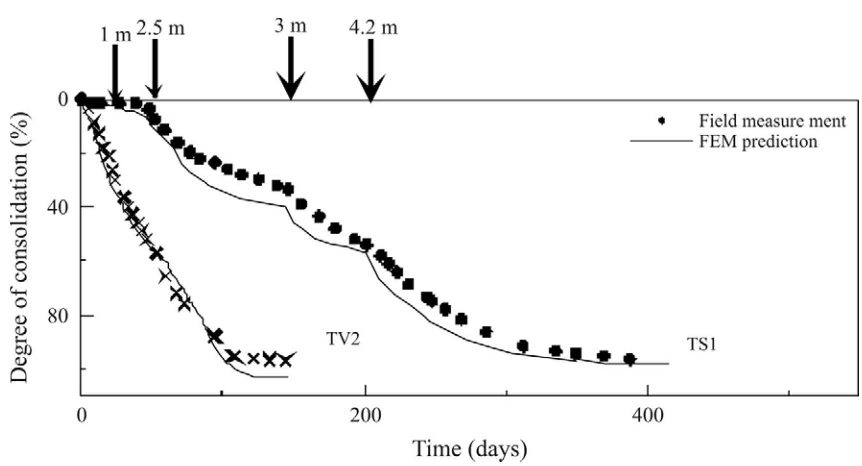

Figure 15 - Degree of Consolidation at the centreline for embankments (after Indraratna & Redana, 2000 and Indraratna *et al.*, 2005).

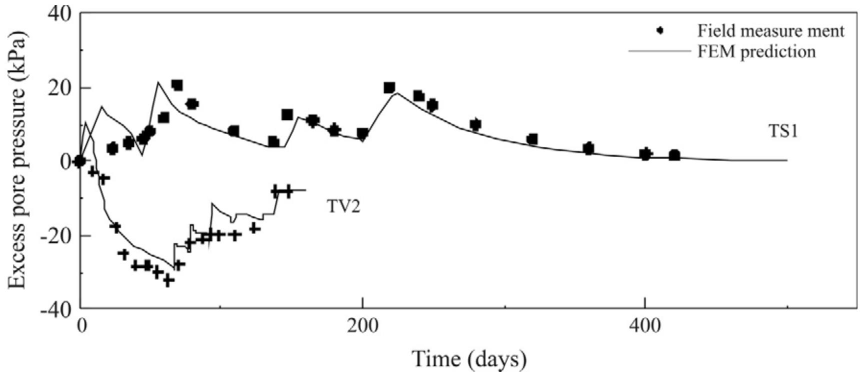

Figure 16 - Excess pore pressure variation at 5.5 m depth (after Indraratna & Redana, 2000 and Indraratna *et al.*, 2005).

relatively short PVDs may still dissipate cyclic pore pressures and curtail any lateral movement of the soft formation. It was expected that any excessive settlement of deep estuarine deposits during the initial stage of consolidation may compensate for continuous ballast packing. However, the settlement rate can still be controlled by optimising the spacing and pattern of drain installation. In this section a case history where short PVDs were installed beneath a rail track built on soft formation is presented with the finite element analysis (Indraratna *et al.* 2010). The finite element analysis used by the Authors to design the track was a typical Class A prediction for a field observation because it was made before it was constructed.

To improve the conditions for rail traffic entering Sandgate, Kooragang Island, Australia, where major coal mining sites are located, two new railway lines were needed close to the existing track. An in-situ and laboratory test was undertaken by GHD Longmac (Chan, 2005) to obtain the essential soil parameters. This investigation included boreholes, piezocone tests, in-situ vane shear tests, test pits, and laboratory tests that included testing the soil index property, standard oedometer testing, and vane shear testing.

The existing embankment fill at this site overlies soft compressible soil from 4 to 30 m deep over a layer of shale bedrock. The properties of this soil, with depth, are shown in Fig. 17, where the groundwater level was at the surface. Short, 8 m long PVDs were used to dissipate excess pore pressure and curtail lateral displacement. There was no preloading surcharge embankment provided due to stringent time commitments. The short PVDs were only expected to consolidate a relatively shallow depth of soil beneath the track where it would be affected by the train load. This initial load was considered to be the only external surcharge. An equivalent static approach based on the dynamic impact factor was used to simulate the field conditions, in this instance a static load of 80 kPa and an impact factor of 1.3 in conjunction with a speed of 40 km/h and a 25 tonne axle load. The Soft Soil model and Mohr-Coulomb model incorporated into the finite element code PLAXIS, were used in this analysis (Brinkgreve, 2002). Figure 18 illustrates a cross-section of the rail track formation.

In the field the 8 m long PVDs were spaced at 3 m intervals, based on the Authors' analysis and recommendations. Figures 19 and 20 show a comparison between the predicted and measured settlement at the centre line of the

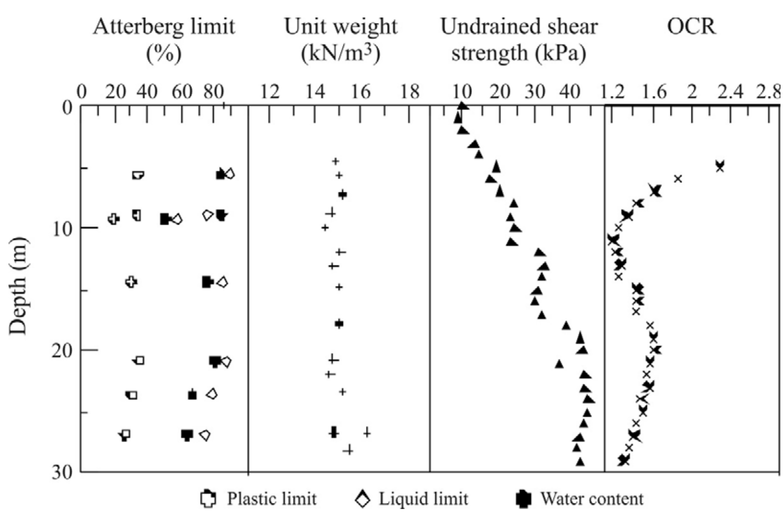

Figure 17 - Soil properties at Sandgate Rail Grade Separation Project (adopted from Indraratna *et al.* 2010).

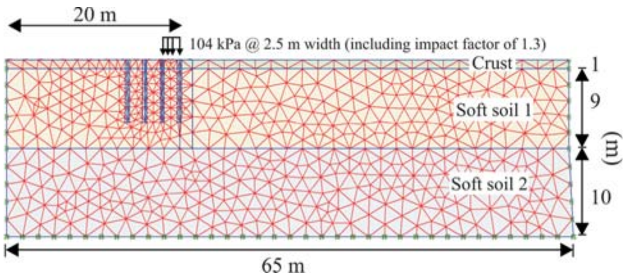

Figure 18 - Vertical cross section of rail track foundation (after Indraratna *et al.* 2010).

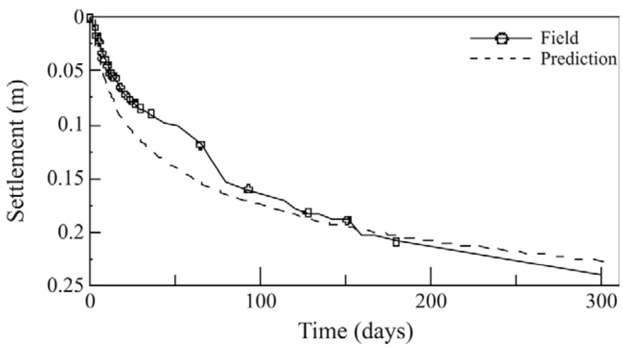

Figure 19 - Predicted and measured at the centre line of rail tracks (after Indraratna *et al.* 2010).

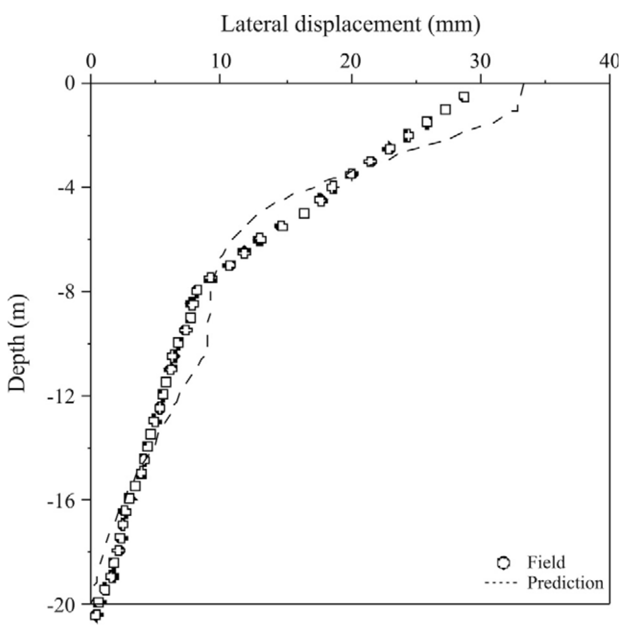

Figure 20 - Measured and predicted lateral displacement profiles near the rail embankment toe at 180 days (after Indraratna *et al.* 2010).

rail track and lateral displacement after 180 days, respectively. The predicted settlement agreed with the field data for a Class A prediction, with the maximum displacement being contained within the top layer of clay. The "Class A" prediction of lateral displacement agreed with what occurred in the field.

5. Conclusion

Various types of vertical drains have been used to accelerate the rate of primary consolidation. A comparison between embankments stabilised with a vacuum combined with a surcharge, and a surcharge alone, were analysed and discussed. Consolidation time with a vacuum applied was substantially reduced and lateral displacement curtailed, and if sufficient vacuum pressure is sustained, the thickness of the surcharge fill required may be reduced by several metres.

A plane strain finite element analysis with an appropriate conversion procedure is often enough to obtain an accurate prediction for large construction sites. An equivalent plane strain solution was used for selected case histories to demonstrate its ability to predict realistic behaviour. There is no doubt that a system of vacuum consolidation via PVDs is a useful and practical approach for accelerating radial consolidation because it eliminates the need for a large amount of good quality surcharge material, via air leak protection in the field. Accurate modelling of vacuum preloading requires both laboratory and field studies to quantify the nature of its distribution within a given formation and drainage system.

It was shown from the Sandgate case study that PVDs can decrease the buildup of excess pore water pressure during cyclic loading from passing trains. Moreover, during rest periods PVDs continue to simultaneously dissipate excess pore water pressure and strengthen the track. The predictions and field data confirmed that lateral displacement can be curtailed which proved that PVDs can minimize the risk of undrained failure due to excess pore pressure generated by cyclic train loads.

Acknowledgments

The authors appreciate the support given by the Australian Rail Track Corporation (ARTC), and John Holland Pty Ltd. They wish to thank the CRC for Rail Innovation (Australia) for its continuous support. The embankment data provided by the Asian Institute of Technology are appreciated. A number of other current and past doctoral students, namely, Mr. Somalingam Balachandran, Ms. Pushpachandra Ratnayake, Dr. I Wayan Redana, Dr. Chamari Bamunawita, Dr. Iyathurai Sathananthan, Dr. Rohan Walker, and Mr. Ali Ghandeharioon also contributed to the contents of this keynote paper. More elaborate details of the contents discussed in this paper can be found in previous publications of the first author and his research students in Geotechnique, ASCE, Canadian Geotechnical Journals, since mid 1990's and Dr. Rujikiatkamjorn PhD thesis for the work related to Bangkok case histories.

References

AIT (1995) The Full Scale Field Test of Prefabricated Vertical Drains for The Second Bangkok International Airport (SBIA). AIT, Bangkok, 259 pp.

Atkinson, M.S. & Eldred, P. (1981) Consolidation of soil using vertical drains. Geotechnique, v. 31:1, p. 33-43.

Barron, R.A. (1948) Consolidation of fine-grained soils by drain wells. Transactions ASCE, v. 113, p. 718-724.

Brand, E.W. & Premchitt, J. (1989) Moderator's report for the predicted performance of the Muar test embankment. Proc. International Symposium on Trial Embankment on Malysian Marine Clays, Kuala Lumpur, v. 2, pp. 1/32-1/49.

Brinkgreve, R.B.J. (2002) PLAXIS (Version 8) User's Manual. Delft University of Technology and PLAXIS B.V., Netherlands, 162 pp.

Cao, L.F.; Teh, C.I. & Chang, M.F. (2001) Undrained cavity expansion in modified cam clay I: Theoretical analysis. Geotechnique, v. 51:4, p. 323-334.

Chan, K. (2005) Geotechnical Information Report for the Sandgate Rail Grade Separation, Hunter Valley Region. Australia, 67 pp.

Cognon, J.M.; Juran, I. & Thevanayagam, S. (1994) Vacuum consolidation technology-principles and field experience. Proc. Conference on Foundations and Embankments Deformations, College Station, Texas, v. 2, pp. 1237-1248.

Ghandeharioon, A.; Indraratna, B. & Rujikiatkamjorn, C. (2009) Analysis of soil disturbance associated with mandrel-driven prefabricated vertical drains using an elliptical cavity expansion theory. International Journal of Geomechanics, ASCE, v.20:2, p. 53-64.

Hansbo, S. (1979) Conslidation of clay by band-shaped prefabricated drains. Ground Eng., v. 12:5, p. 16-25.

Hansbo, S. (1981) Consolidation of fine-grained soils by prefabricated drains. Proceedings of 10th International Conference on Soil Mechanics and Foundation Engineering, Stockholm, Balkema, v. 3, pp. 677-682.

Hird, C.C.; Pyrah, I.C. & Russell, D. (1992) Finite element modelling of vertical drains beneath embankments on soft ground. Geotechnique, v. 42:3, p. 499-511.

Holtz, R.D. (1987) Preloading with prefabricated vertical strip drains. Geotextiles and Geomembranes, v. 6(1-3), p. 109-131.

Indraratna, B. & Redana, I.W. (2000) Numerical modeling of vertical drains with smear and well resistance installed in soft clay. Canadian Geotechnical Journal, v. 37:1, p. 132-145.

Indraratna, B.; Bamunawita, C. & Khabbaz, H. (2004) Numerical modeling of vacuum preloading and field applications. Canadian Geotechnical Journal, v. 41:6, p. 1098-1110.

Indraratna, B.; Balasubramaniam, A.S. & Balachandran, S. (1992) Performance of test embankment constructed to failure on soft marine clay. Journal of Geotechnical Engineering, ASCE, v. 118:1, p. 12-33.

Indraratna, B.; Balasubramaniam, A.S. & Ratnayake, P. (1994) Performance of embankment stabilized with vertical drains on soft clay. J. Geotech. Eng., ASCE, v. 120:2, p. 257-273.

Indraratna, B.; Balasubramaniam, A.S. & Sivaneswaran, N. (1997) Analysis of settlement and lateral deformation of soft clay foundation beneath two full-scale embankments. International Journal for Numerical and Analytical Methods in Geomechanics, v. 21:9, p. 599-618.

Indraratna, B.; Rujikiatkamjorn C. & Sathananthan, I. (2005) Analytical and numerical solutions for a single vertical drain including the effects of vacuum preloading. Canadian Geotechnical Journal, v. 42:4, p. 994-1014.

Indraratna, B. & Rujikiatkamjorn, C. (2008) Effects of partially penetrating prefabricated vertical drains and loading patterns on vacuum consolidation. In: K.R. Reddy, M.V. Khire and A.N. Alshawabkeh (eds), GeoCongress, ASCE, pp. 596-603.

Indraratna, B.; Rujikiatkamjorn, C.; Adams, M. & Ewers, B. (2010) Class A prediction of the behaviour of soft estuarine soil foundation stabilised by short vertical drains beneath a rail track. International Journal of Geotechnical and Geo-environmental Engineering, ASCE, v. 136:5, p. 686-696.

Kjellman, W. (1948) Accelerating consolidation of fine grain soils by means of cardboard wicks. Proc. 2nd ICSMFE, Rotterdam, v. 2, pp. 302-305.

Li, A.L. & Rowe, R.K. (2002) Combined effect of reinforcement and prefabricated vertical drains on embankment performance. Canadian Geotechnical Journal, v. 38:6, p. 1266-1282.

Long, R. & Covo, A. (1994) Equivalent diameter of vertical drains with an oblong cross section. Journal of Geotechnical Engineering, v. 20:9, p. 1625-1630.

Ozawa, Y. & Duncan, J.M. (1973) ISBILD: A Computer Program for Static Analysis of Static Stresses and Movement in Embankment. University of California, Berkeley, 144 pp.

Ratnayake, A.M.P. (1991) Performance of test embankments with and without vertical drains at Muar flats site, Malaysia. Master Thesis, GT90-6, Asian Institute of Technology, Bangkok, 190 pp.

Sathananthan, I. & Indraratna, B. (2006) Laboratory evaluation of smear zone and correlation between permeability and moisture content. J. of Geotechnical & Geo-environmental Engineering, ASCE, v. 132:7, p. 942-945.

Sathananthan, I.; Indraratna, B. & Rujikiatkamjorn C., (2008) The evaluation of smear zone extent surrounding mandrel driven vertical drains using the cavity expansion theory. International Journal of Geomechanics, ASCE, v. 8:6, p. 355-365.

Woods, R. (1992) SAGE CRISP Technical Reference Manual. The CRISP Consortium Ltd., Cambridge, 223 pp.

Yoshikuni, H. & Nakanodo, H. (1974) Consolidation of fine-grained soils by drain wells with finite permeability. Japanese Society Soil Mechanics and Foundation Engineering, v. 14:2, p. 35-46.

Behaviour of Three Test Embankments Taken to Failure on Soft Clay

M.S.S. Almeida, H.M. Oliveira, D. Dias, L.O.G. Deotti

Abstract. This article compares and analyses the behaviour of three test embankments. The soil foundation consisted of normally consolidated clay overlain by a thick sand surface layer. The embankments were rapidly constructed until failure, which occurred after approximately 50 days. Two of the embankments were reinforced, one including prefabricated vertical drains (PVD), while the third had neither reinforcement nor PVDs. The two reinforced embankments presented similar net embankment heights (fill thickness minus average settlement) at failure, owing to the similarity in the undrained strength values of the two clay layers. The test embankment with PVDs showed that this drainage feature improved overall behaviour but the benefit was less than suggested in the literature, owing to the low coefficient of consolidation of the normally consolidated clay, rapid construction and drain disturbance effects. Numerical analyses of the test embankment with PVDs showed good overall agreement between measured and computed values and confirmed overall field observations. The embankment without reinforcement and PVDs reached a greater embankment height than the two reinforced embankments, owing to its greater clay strength.

Keywords: displacements, embankment, pore pressure, soft clay, vertical drains, numerical analyses.

1. Introduction

The construction of embankments on very soft soils requires careful control of settlement and stability (Bergado *et al.*, 1994; Rowe & Leroueil, 2001). Prefabricated vertical drains (PVD) are commonly adopted for the acceleration of settlement by providing short horizontal drainage paths (Holtz, 1987; Almeida *et al.*, 2001, Almeida *et al.*, 2005; Lo *et al.*, 2008) and geosynthetic reinforcement (Humphrey & Holtz, 1989; Rowe *et al.*, 1995, 1996; Chai *et al.*, 2002; Kelln *et al.*, 2007) has been used to improve the stability of these soil structures. The combined use of PVDs and geosynthetic reinforcement may allow for higher embankments and short construction times in comparison with conventional construction methods (*e.g.*, Li & Rowe, 2001; Rowe & Li, 2005). Most of the literature studies are related to embankments placed directly on soft clays or placed on top of shallow surface sand layers, which is not the present case.

This article compares the behaviour of three instrumented test embankments constructed until failure on normally consolidated very soft clay layers overlain by working platforms 1.7 to 2.1 m thick. Usually, working platforms are constructed immediately before the actual embankment but in the present case they were constructed six years before embankment construction. Two of the embankments were reinforced, one had PVDs and the other did not have PVDs. A third embankment was constructed without reinforcement and without PVDs.

Horizontal and vertical displacements and pore pressure measurements are presented and compared. The three embankments were loaded until foundation failure occurred also for the reinforced embankments as failure of the reinforcement did not take place. Numerical analyses of the test embankment provided with PVDs were also carried out to clarify the influence of the PVDs on short term construction to failure.

2. The Test Embankments

The test embankments and the motorway are located on Santa Catarina Island in the city of Florianópolis, on the southern coast of Brazil, as shown in Fig. 1. In the southern part of the island, a very soft clay deposit 4 to 22 m thick is found.

Around 1996 a sand hydraulic fill was constructed in a bay where the motorway was planned to pass in order to raise the ground level above sea level, because the area used to be flooded at various times during the year. Although the surface sand layer generally worked well, a number of failures occurred. As a result, three test embankments, TE1, TE2 and TE3, were planned and completed (Magnani, 2006) by late 2002 on the Florianópolis clay, with the aim

M.S.S. Almeida, Ph.D., Graduate School of Engineering, COPPE, Universidade Federal do Rio de Janeiro, Caixa Postal 68506, 21945 Rio de Janeiro, RJ, Brazil. e-mail: almeida@coc.ufrj.br.
H.M. Oliveira, D.Sc., Departamento de Engenharia Civil, Universidade Federal de Santa Catarina, Rua João Pio Duarte da Silva 205, 88040-970 Carrego Grande, Florianópolis, SC, Brazil. e-mail: henriquemagnani@uol.com.br.
D. Dias, D.Sc., LTHE Laboratory, Joseph-Fourier University, UMR 5564 bp 53, 38041 Grenoble, France. e-mail: daniel.dias@ujf-grenoble.fr.
L.O.G. Deotti, M.Sc., COPPE, Universidade Federal do Rio de Janeiro and ELETROBRAS, Rua do Ouvidor 107, 20040-031 Centro, Rio de Janeiro, R.J., Brazil. e-mail: leodeotti@hotmail.com; lguerra@eletrobras.com.
Submitted on February 6, 2012; Final Acceptance on December 15, 2011; Discussion open until July 31, 2012.

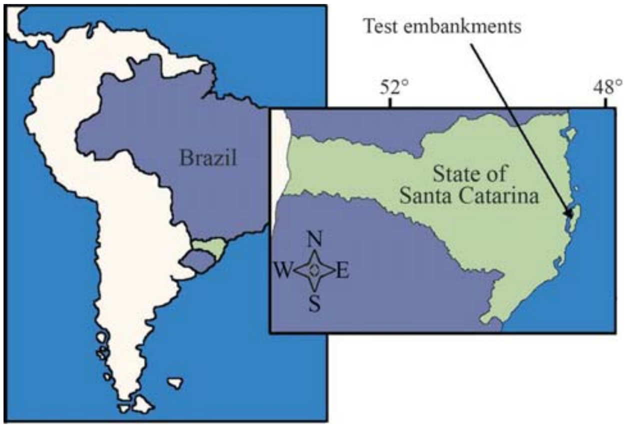

Figure 1 - Location of the test embankments.

of providing relevant data for the construction of the motorway. The motorway embankment would have a thick sand surface layer and be reinforced and provided with PVDs in the clay layer. Therefore, it was decided that the three test embankments should be constructed in areas with pre-existing surface sand layers. Embankments TE1 and TE2 were provided with 200 kN/m x 45 kN/m Stabilenka® polyester reinforcement with a modulus $J_{5\%}$ = 1700 kN/m for 5% strain. Prefabricated Colbonddrain® CX 1000 drains (10 cm x 0.5 cm) in a triangular mesh with 1.30 m spacing were placed in section TE1. Embankment TE3 was constructed without reinforcement and PVDs. The test embankments were raised until failure occurred after around 50 days.

The three test embankments had essentially the same geometry and instrumentation, although their foundations had different clay thicknesses, as explained below. Figure 2 shows the geometry and instrumentation used in embankment TE1. The transverse section of embankment TE1 (before and after failure) is shown in Fig. 2a with slopes 1(V): 1.5(H). The three embankments also had the same plan geometry (see Fig. 2b), platform width 20 m by 30 m and lateral berms 1.0 m high and 12 m long aimed at inducing failure in the intended transverse direction. Given that the base of the embankment had a slight inclination, the direction of the failure was naturally defined by this inclination.

The test embankments were instrumented as exemplified in Fig. 2 for embankment TE1. The embankments were monitored in terms of vertical displacements (eight settlement plates; three verticals of magnetic extensometers and three lines, each with six surface marks), horizontal displacements (three vertical inclinometers) and pore pressure (three electric vibrating wire piezometers) near the embankment centre line. Four specially designed load cells (Almeida *et al.*, 2010) were used to measure the tensile force mobilised in the reinforcement. With the exception of the load cell, all the instruments used are commonly applied in geotechnical engineering (Dunnicliff, 1988).

The measured tensile forces in the reinforcement (Magnani *et al.*, 2009) were relatively small in the present case, owing to the existence of the surface sand layer. Measured tensile forces at the two reinforced embankments for failure conditions were in the range 40-50 kN/m but at service state conditions (factor of safety around 1.4) much lower values, of the order of 4 to 7 kN/m, were developed. Stability analyses (Magnani *et al.*, 2010) using tensile forces measured in the reinforcement indicate that the reinforcement made a very small contribution to the increase in the factors of safety, *i.e.*, at failure conditions the reinforcement increased the factors of safety by 2.4% and 3.6% respectively for embankments TE1 and TE2 with respect to the same (hypothetically) unreinforced embankments. Stability analyses also showed that the surface sand layers contributed by increasing the factors of safety by 43% to 60% with respect to the same (hypothetical) embankments without the surface sand layers, unreinforced in both cases.

This article assesses the behaviour until failure of the three embankments with respect to the importance of reinforcement and PVDs, with emphasis on displacement and pore pressure data. The analysis of the forces measured by the reinforcement load cells, discussed in detail by Magnani *et al.* (2009), is outside the scope of this article. The results of stability analyses are also considered for the overall understanding of the performances of the three embankments. Numerical analyses of the embankment provided with PVDs complemented field observations and clarified the importance of the PVDs in the present cases.

3. Foundation Soils and Fill Materials

Geotechnical investigations were carried out under the auspices of the motorway engineering project and included vane and piezocone tests as well as triaxial and consolidation tests. Table 1 summarises the geotechnical characteristics of the Florianopolis clay, obtained from various investigation projects carried out between 1979 and 2002, the later date referring to the year of the test embankment construction. Florianopolis clay is very soft, with low organic content and medium sensitivity. The results of the present investigation are consistent with the behaviour of clays located along the south and south-east coast of Brazil (Almeida & Marques, 2002; Almeida *et al.*, 2008; Massad, 1994; Pinto, 1994).

Figure 3 shows the continuous undrained strength profiles $S_{u(PZ)}$ in the centre of each test embankment obtained from piezocone tests. The $S_{u(PZ)}$ values shown in Fig. 3 make use of the equation:

$$S_{u(PZ)} = \frac{q_T - \sigma_v}{N_{kt}} \tag{1}$$

where q_T is the corrected point resistance measured in piezocone tests, σ_v is the total in situ vertical stress and N_{kt} the empirical cone factor equal to 12.0, as obtained by local correlations between vane and piezocone tests, and which

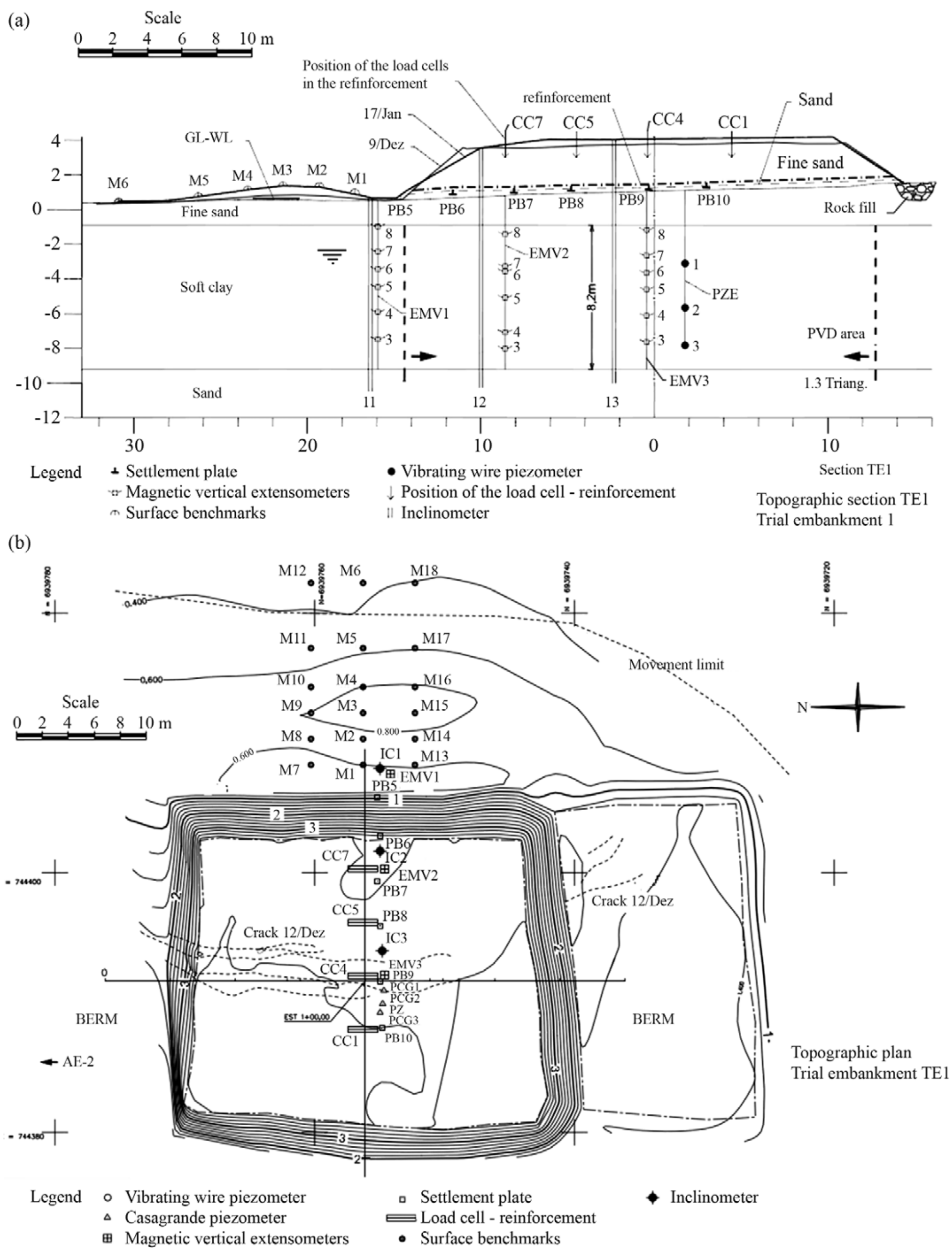

Figure 2 - Test embankment TE-1, with drains and reinforcement: (a) cross-section; (b) plan view.

is also a typical value for Brazilian very soft clays (Schnaid, 2009).

Owing to the local geological variations, the thickness of the soft clay was different for each section of the embankment, as shown in Fig. 3 and Table 2. Thicknesses of the surface sand layer in the three embankments are also indicated in Table 2.

The higher values of S_u measured under embankment TE3 (see Fig. 3) are due to the existence of the sand lens in a less thick clay layer and a thicker surface sand layer acting on the clay surface over a period of six years. Owing to the action of the sand layer surcharge, most of the soft clay layer was close to normally consolidated condition, which was confirmed by oedometer tests and piezocone tests carried out in this clay (Magnani, 2006).

Uniform fine silica sand (95% of the material passing through # 40 sieve and less than 5% passing through # 200 sieve) was used in both the surface sand layer and the embankment. The bulk weight of this sand was $\gamma = 17.5$ kN/m^3, void ratio $e = 0.60$ and degree of saturation $S = 34\%$. Direct

Table 1 - Geotechnical parameters of Florianópolis soft clay.

Parameter	Value
Water content w (%)	100-170
Liquidity index w_L (%)	105-165
Average plasticity index I_P (%)	80
Organic matter content, average percentage in weight (%)	3.8
Bulk weight γ (kN/m^3)	13.2-14.2
Voids ratio e	2.9-4.5
Compression ratio C_c / (1 + e_o)	0.30-0.45
Ratio of compression indices C_s / C_c	0.08-0.14
Vertical coefficient of consolidation c_v - normally consolidated (m^2/s)	0.7-1.0 x 10^{-8}
Vertical coefficient of permeability k_v - (m/s)	1.0 x 10^{-9}
Vane uncorrected undrained strength S_u (kPa)	5-28
Sensitivity (vane)	3-6
Effective friction angle ϕ' (degrees)	30.0
Effective cohesion c (kPa)	0.0
Rigidity Index $I_r = G_{50}/S_u$ - obtained from CIU triaxial tests	50
Cone factor N_{kt} (average)	12.0
Pore pressure ratio B_q	0.4-0.6

shear tests indicated a friction angle ϕ = 33.8°. In embankment TE1 with PVDs, a drainage blanket (medium-to-coarse sand) layer with an average thickness of 0.40 m was used.

4. Vertical Displacements

4.1. Vertical displacements at the embankment bases

Vertical displacements at the base of the test embankments were measured by settlement plates under the embankments and surface marks in front of the embankments (see Fig. 2). Figure 4 compares the vertical displacement data for the three embankments and it is noted that the maximum settlement values are closer to the slope than to the central region (embankment axis), particularly in the final loading stages. This sagged pattern of displacements has been found in some embankments (Almeida *et al.*, 1985; Indraratna *et al.*, 1992) and may be attributed to low factors of safety and the shearing yield of the soft clay foundation under the slope (Almeida *et al.*, 1986) as well as to the large width of the embankment compared to its height (Zhang, 1999).

Figure 4 shows that embankment TE1 has the highest settlement values, followed by embankment TE2 and then embankment TE3. Although for the test embankments constructed to failure, the rotational shear movement may control settlements, the fact that the magnitude of settlement is

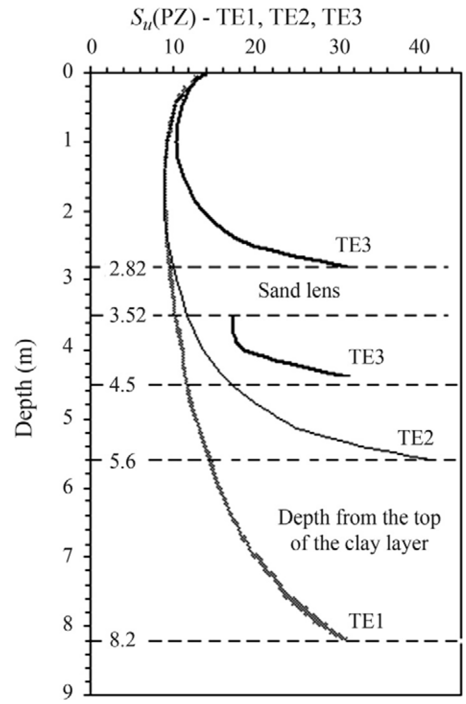

Figure 3 - Undrained strength measured at the three instrumented sections: (a) piezocone S_u profiles (and depth of the clay layers); (b) vane strength S_u *vs.* piezocone measurements.

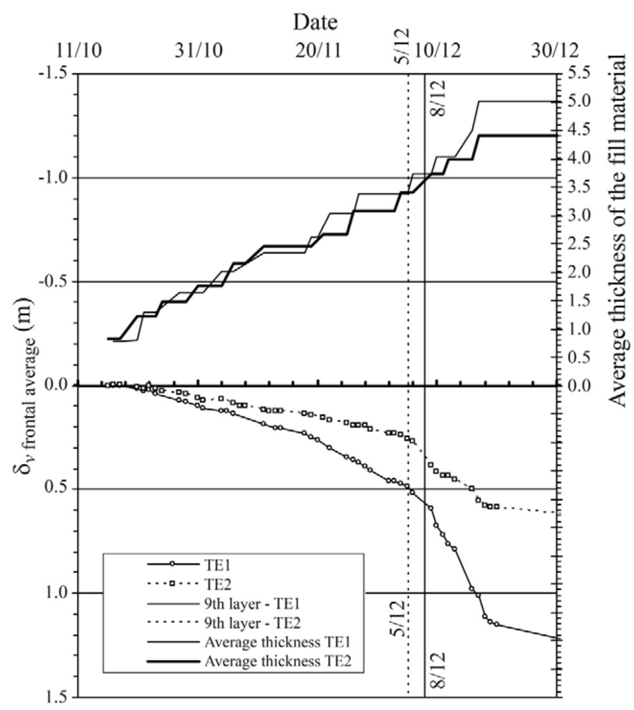

Figure 4 - Vertical displacements of the three test embankments.

proportional to the thickness of the clay layer suggests that consolidation settlements were also relevant in the present case. From the results of the TE2 embankment, the embankment at the centreline was about 0.15 m at the 10th lift

Table 2 - Main features of the three test embankments.

	Embankment		
	TE1	TE2	TE3
Reinforcement	Polyester Stabilenka -200 x 45 kN/m; *J* = 1700 kN/m		No reinforcement
Vertical drains	Colbondrain CX 1000, 10 cm x 0.5 cm, triangular array, 1.30 m spacing	No drains	No drains
Clay thickness (m)	8.2	5.6	4.5 (sand layer from 2.8 to 3.5 m)
Working platform thickness (sand hydraulic fill) (m)	1.7	1.8	2.1

of the embankment fill, corresponding to 2.7% vertical strain (*i.e.* soft clay thickness was 5.6 m). For the case of TE1 test embankment, whose soft clay foundation thickness was 8.2 m, 2.7% vertical strain would be equal to only 0.22 m of settlement while the field measurements show about 0.5 m of settlement, which implies that more than 55% of the settlement was caused by consolidation. This suggests that PVDs had some effect in accelerating consolidation during construction. This topic is further discussed later in this paper using results of numerical analyses.

4.2. Settlements of the frontal plates

Figure 5 compares vertical settlements δ_v in the four frontal plates (located between the failure surface and frontal slope) of embankments TE1 and TE2. The data shown in Fig. 5 represent the average values of settlement plates PB6, PB7, PB8 and PB9 for embankment TE1 (see Fig. 2) as well as the corresponding data for the four settlement plates for embankment TE2. The instant of the increase in settlement rates indicates the start of the process of embankment failure. This instant is indicated in Fig. 5 by vertical lines and corresponds to the placement of the ninth layer, coincidently for the two embankments. It can be noted that the load histories of the two reinforced embankments were quite similar until failure.

Figure 6 compares the fill thickness *vs.* average frontal settlements for the three embankments. The points corresponding to the onset of failure (first crest cracks) and total collapse are indicated in Fig. 6a. It may be observed that embankment TE3 presents smaller settlements and greater fill thickness compared with embankments TE1 and TE2. The comparison of the two reinforced embankments shows that TE1 presents greater thickness and larger settlements than embankment TE2. These data have also been

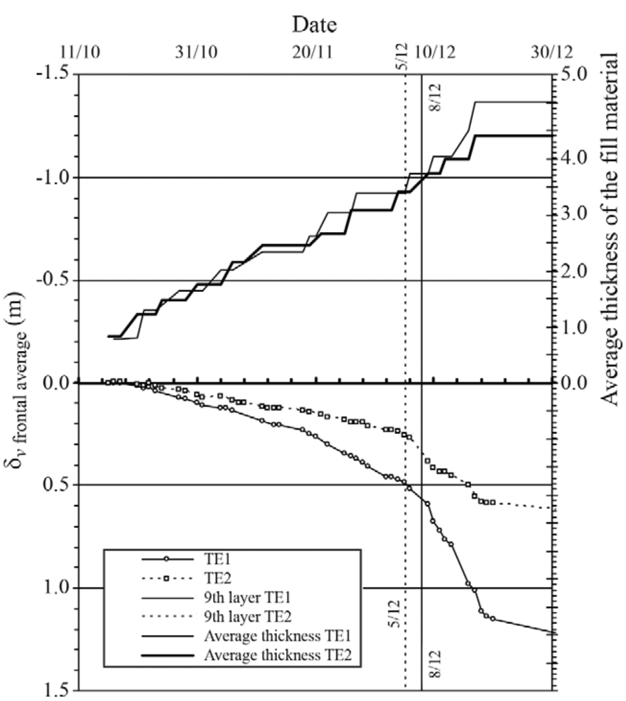

Figure 5 - Average settlement of the frontal settlement plates *vs.* time for embankments TE1 and TE2.

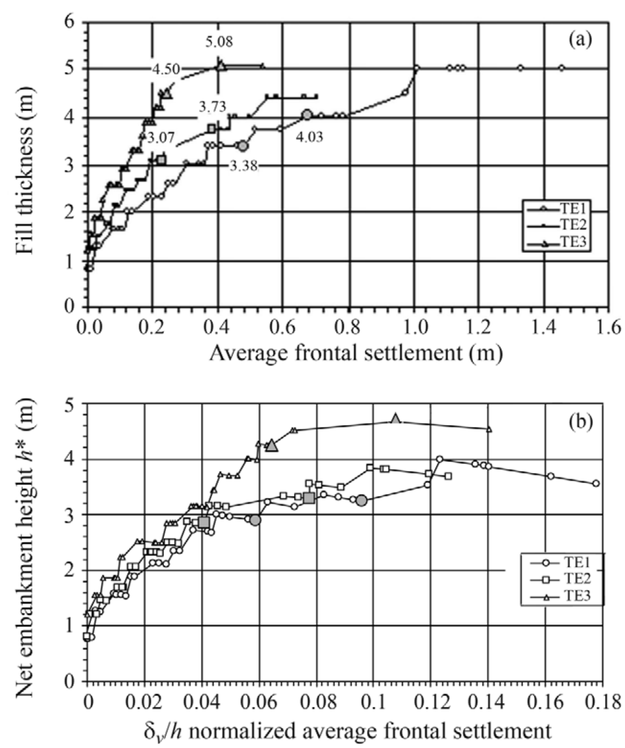

Figure 6 - Average frontal settlement data for embankments TE1, TE2 and TE3.

plotted with respect to net embankment height h^* defined by the embankment thickness minus the average settlement (Rowe & Soderman, 1987; Hinchberger & Rowe, 2003) *vs.* normalised settlement (normalised by the thickness of the clay layer), as shown in Fig. 6b, where the curves of the two reinforced embankments are closer than in Fig. 6a. Thus, the greater thickness in embankment TE1 is compensated by larger settlements and the values of h^* are quite close, particularly at the start of failure and at total collapse. Therefore, the PVDs have increased settlements but not the net embankment height h^*. However, the PVDs may have promoted some gain in strength for two reasons: a) the S_u profile for TE1 showed somewhat lower undrained shear strength than for TE2 (see Fig. 1); b) at failure, both embankments had the same net embankment heights while TE1 had larger settlement (about 0.3 m larger) which means TE1 had higher embankment fill thickness (*i.e.* experienced higher overburden pressure at failure). These two reasons would suggest that PVDs had improved the embankment stability and increased the undrained shear strength of the clay.

It is seen in Fig. 6 that embankment TE3 without reinforcement reaches greater fill thickness and net embankment height than the two reinforced embankments. This is attributed (Magnani, 2006; Magnani *et al.*, 2010) to the greater strength of clay in an undrained state, and also to the presence of the sand lenses under embankment TE3 (see Fig. 3a). For these reasons embankment TE3 may not be considered, in the present cases studied, as a reference unreinforced embankment with respect to the two reinforced embankments.

4.3. Vertical displacements at the embankment toe

The monitoring of vertical displacements at the embankment toe or slightly beyond the toe is an efficient procedure (Hunter & Fell, 2003) to assess the impending failure of embankments on soft clays. Figure 7 shows the results of the vertical magnetic extensometers MTV1 located about 2 m beyond the toe of embankment TE1 (analogous to MTV4 in embankment TE2 – see Fig. 2). It is noted that the extensometers located above the failure surface (indicated by the inclinometers, see item below) experienced upward displacements and the two extensometers located below the failure surface had downward displacements and smaller displacement variations than those above the failure surface.

It can be noted that the displacements of the extensometers closer to the ground surface increased substantially shortly after the placement of the ninth layer, during which cracks at the embankment surface were noted. Data on the frontal plates shown in Fig. 5 support this conclusion. The ninth layer, for that reason, is considered to be the point at which the embankments TE1 and TE2 failed. The results of the inclinometers, discussed at greater length by Magnani *et al.* (2009), support these findings. Similarly,

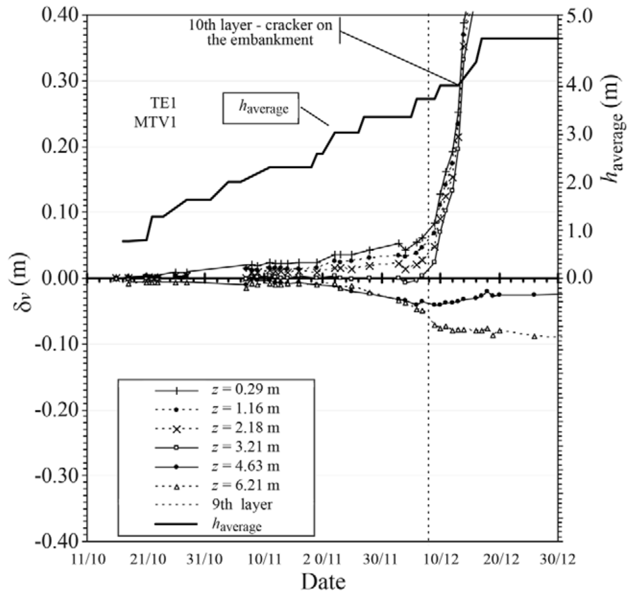

Figure 7 - Vertical displacements measured in vertical extensometers at the embankment toe – test embankment TE1.

the twelfth layer was considered (Magnani, 2006) to be the moment of failure for the unreinforced embankment TE3.

5. Central Settlements, Pore Pressure and Consolidation

5.1. Central settlements data

Data on the central settlement plates of embankments TE1 and TE2 with thicker clay layers are analysed here. The three embankments had central plates in similar positions and for TE1 these were PB7, PB8, PB9 and P10, as shown in Fig. 2. These central plates are less influenced by shear-induced settlements and are useful for assessing the consolidation of these two embankments.

Fig. 8 shows the average settlements in the central region normalised by the clay thickness, before failure, plotted against the net applied embankment vertical stress $\Delta\sigma_v$, *i.e.*, the embankment stress less the embankment submergence owing to settlements. Best linear fit lines through the data are also presented. Normalised settlements of embank-

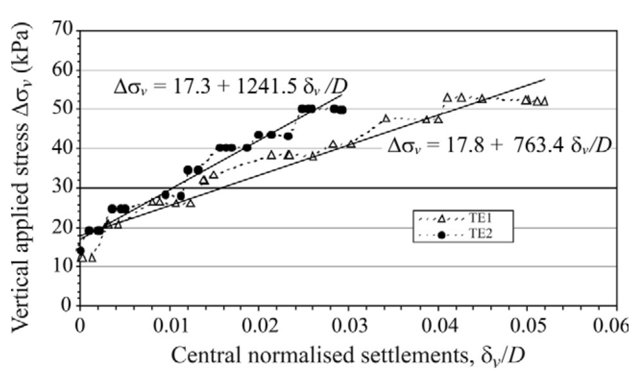

Figure 8 - Central settlements normalised by the clay thickness *vs.* vertical applied stress for embankments TE1 and TE2.

ment TE1 are 1.62 times higher (the ratio between the inclinations of the two best fit lines) than normalised settlements for embankment TE2. TE1 settled more due to its greater clay thickness and the presence of PVDs.

Measured settlements include immediate (undrained) and consolidation settlements. In simple terms, consolidation settlements in Fig. 8 are represented by the settlements under quasi-constant $\Delta\sigma_v$ values and immediate settlements are represented by the settlements owing to the increase in $\Delta\sigma_v$ values; thus the consolidation settlements for embankment TE1 with PVDs in a thicker clay layer are greater than the consolidation settlements for embankment TE2. Despite greater consolidation of embankment TE1 (embankment fill thickness is higher for TE1), however, the net embankment height h^* for embankments TE1 and TE2 was quite similar (see Fig. 6b).

5.2. Excess pore pressures

Measured values of excess pore pressure Δu and the average applied embankment vertical stress $\Delta\sigma_v$ are shown in Fig. 9 for embankments TE1 and TE2. The positions of piezometers under the embankment centre lines are indi-

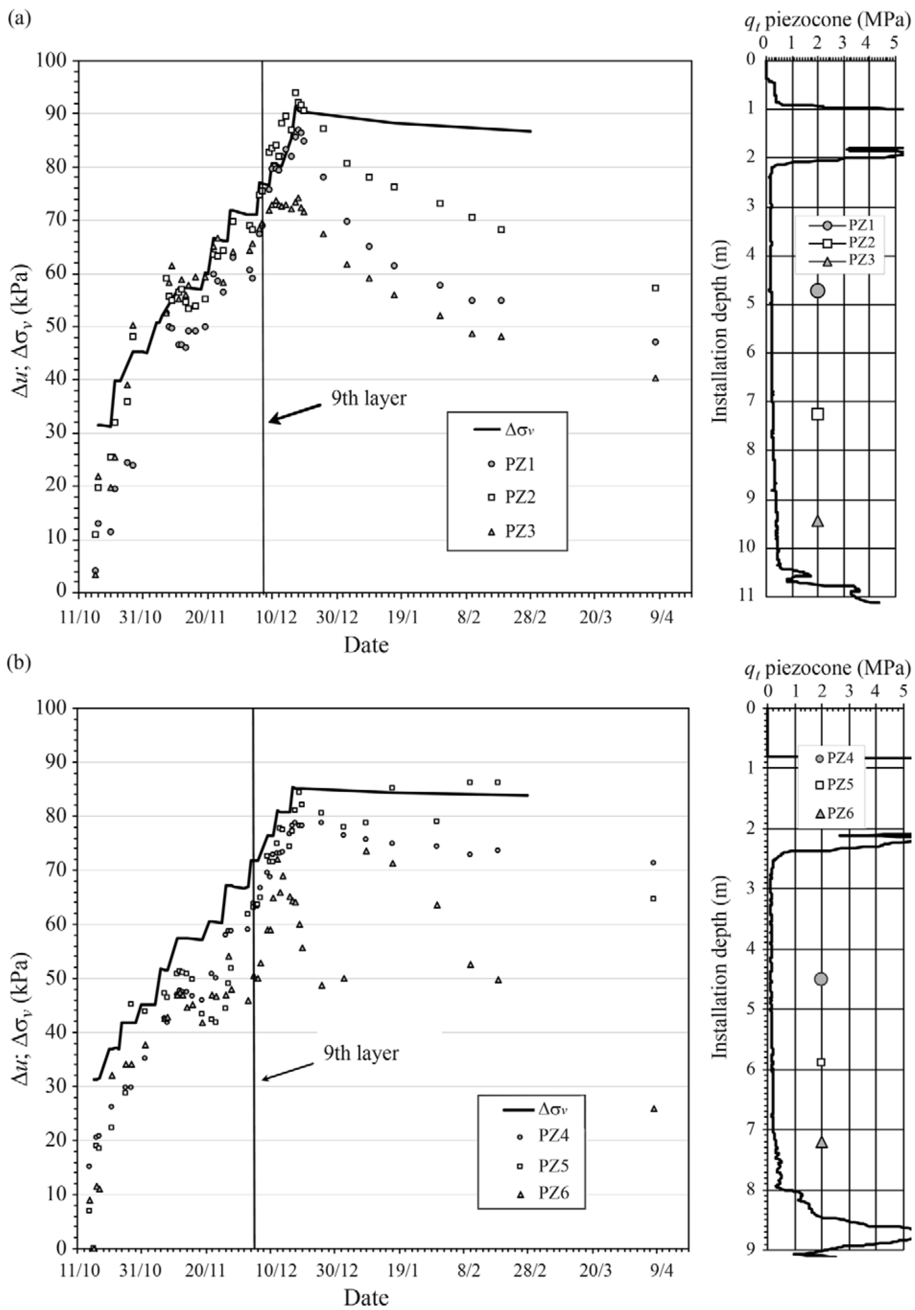

Figure 9 - Excess pore pressure and average vertical stress in clay layers: (a) embankment TE1; (b) embankment TE2.

cated on the right-hand side of Fig. 9 together with piezocone data. Values of $\Delta\sigma_v$ include the vertical stress corresponding to the surface sand layer, as consolidation was still under development. Therefore part of the measured pore pressure (generated and dissipated) was due to the placement of the surface sand layer. The vertical lines indicate the placement of the ninth layer when cracks in the embankment were observed.

The values for Δu and $\Delta\sigma_v$ shown in Fig. 9 are quite close for both embankments, *i.e.*, the ratio $\Delta u/\Delta\sigma_v$ is close to unity, an expected behaviour for normally consolidated clays, which is the present case. Values of $\Delta u/\Delta\sigma_v$ described in the literature are related to lightly over-consolidated clays and lie in the range 0.38 to 0.75 (Leroueil *et al.*, 1978), particularly at the early loading stages, owing to the relatively high value of the coefficient of consolidation of the over-consolidated soil.

The results presented in Fig. 9a suggest that the influence of the PVDs on the dissipation of pore pressures during the construction phase of embankment TE1 was apparently quite small. With regard to the post-construction phase, the data on the two piezometers near the mid-clay depth (see circles and squares in Fig. 9) show, as expected, that the pore pressures under embankment TE1 (Fig. 9a) with PVDs dissipate faster than pore pressures under embankment TE2 (Fig. 9b) without PVDs.

6. Horizontal Displacements

Three inclinometers were installed in each test embankment, one close to the embankment toe, another at the crest of the embankment and a third near the centre of the embankment, namely inclinometers I4, I5 and I6 in embankment TE2 (corresponding to I1, I2 and I3 of TE1 - Fig. 2).

Monitoring of horizontal displacements using inclinometers at the embankment toe is one of the most efficient procedures for assessing impending failure of embankments on soft clays (*e.g.*, Hunter & Fell, 2003; Magnani *et al.*, 2008). For the three embankments studied by Magnani (2006), the inclinometers located at the embankment toe showed the highest values compared with the other inclinometers. The patterns of the inclinometer measurements of the two reinforced embankments TE1 and TE2 are quite similar (Magnani, 2006). Figure 10 shows measurements of the inclinometers in the foundation layers (sand surface layer and clay layer) located at the embankment toe for reinforced test embankment TE2 and unreinforced test embankment TE3. The data shown are horizontal displacements *vs.* depth (Fig. 10a) and vertical deviation *vs.* depth (Fig. 10b). Vertical deviation or vertical inclination angle $\theta_v = \Delta\delta_h/\Delta z$ is defined by the ratio between the increment in horizontal displacements $\Delta\delta_h$ and the distance Δz between the measured points. Both curves kept their shape as embankment loading progressed, which confirms the observations of Tavenas *et al.* (1979) for unreinforced embankments on lightly over-consolidated clays. The depth at which the maximum vertical deviation value θ_{vmax} occurs remains constant during the raising of the embankment and corresponds approximately to the depth of the maximum shear strains, thus indicating the depth of the failure (*e.g.*, Hunter & Fell, 2003). The observed depths of the failure z_f are 5.0 m, 3.8 m and 1.8 m, respectively for embankments TE1, TE2 and TE3, and thus z_f increases with the increase in the thickness of the clay layer.

The depth of maximum horizontal displacements δ_{hmax} ($\theta_v = 0$) is shallower for the unreinforced embankment TE3 owing to the less thick clay layer and no reinforcement adopted.

More comprehensive data on horizontal displacements and the correlation of these with the forces measured in the reinforcement have been presented by Magnani *et al.* (2009).

7. Applied Embankment Stresses and Soft Clay Response

The response of foundation layers to the applied embankment vertical stress is shown in Fig. 11. Figure 11a shows the vertical embankment applied vertical stress $\Delta\sigma_v$ (submersion effects discounted) *vs.* the maximum vertical deviation values θ_{vmax} measured in the inclinometers located at the toe of the embankments (I1 for embankment TE1, I4 for embankment TE2 and I7 for embankment TE3). Similar results were obtained (Magnani, 2006) for the inclinometers located at the crests of the embankments.

It should be noted from Fig. 11a that the two reinforced embankments showed similar behaviour despite the fact that clay under embankment TE1 had PVDs. Figure 11a also shows that embankment TE3 reaches a higher $\Delta\sigma_v$ value than the reinforced embankments. This fact may be explained by the higher strength S_u of the clay layer (see Fig. 3), the smaller thickness of the clay layer and the presence of the sand lens within the clay layer. For these reasons, embankment TE3 cannot be considered as a reference (unreinforced) embankment in relation to the reinforced embankments TE1 and TE2.

Figure 11b shows the data of Fig. 11a normalised by the maximum applied embankment vertical stress $\Delta\sigma_{vmax}$. It is noted that curves of the three embankments get close. This is of great interest as it indicates that the shearing responses of the three clay layers were similar and, in the present case, valid for both reinforced and unreinforced embankments. Therefore, the maximum vertical deviations can be expressed solely by the failure factor of safety and by the clay strain characteristics. For a factor of safety of 1.4 ($\Delta\sigma_v/\Delta\sigma_{vmax} = 0.71$), for example, the maximum vertical deviation value θ_{vmax} for the present case is between 3% and 4% for the data contained in Fig. 11b.

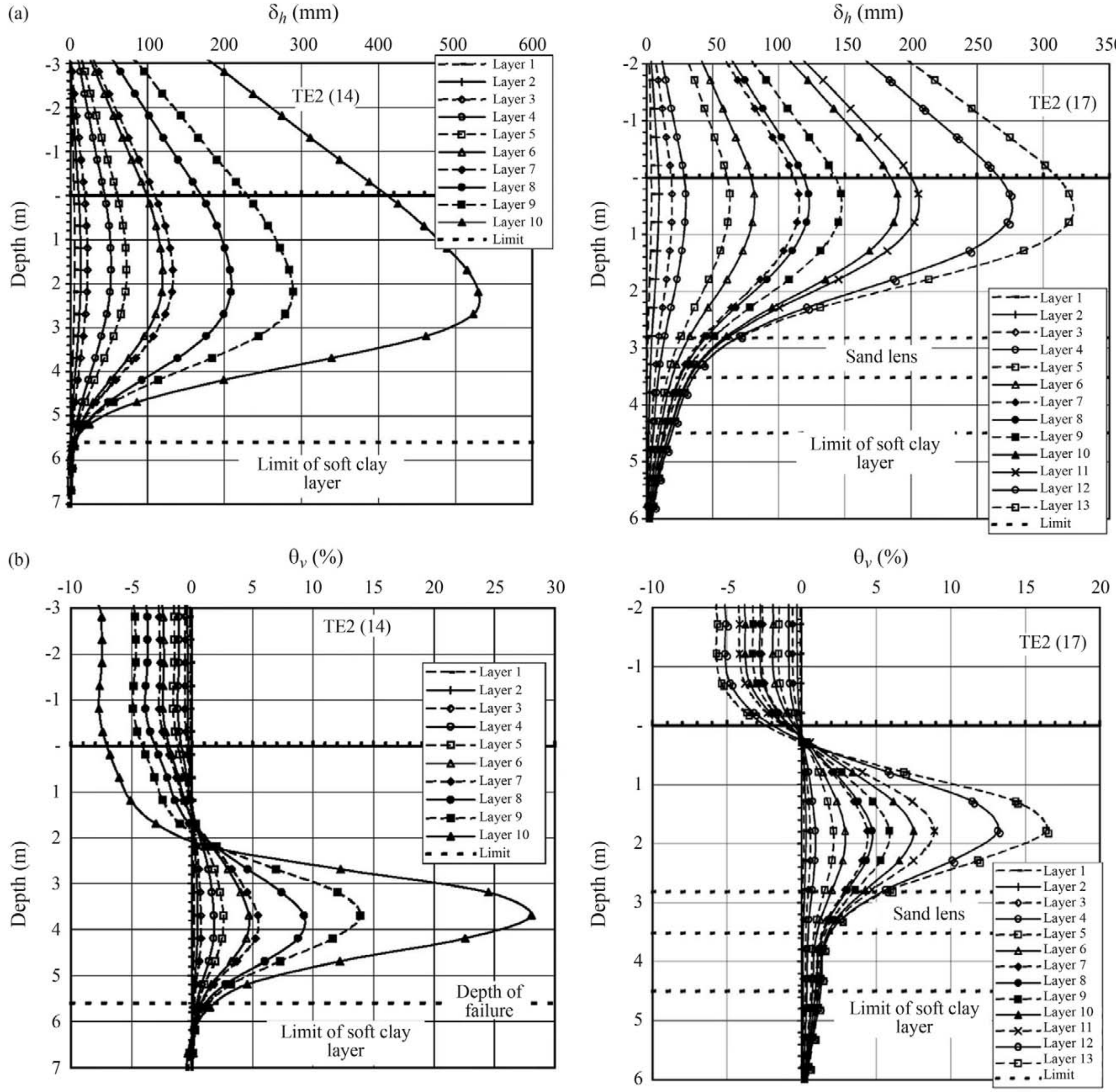

Figure 10 - Inclinometer measurements at the embankment toe: (a) horizontal displacements - δ_h; (b) vertical deviation θ_v.

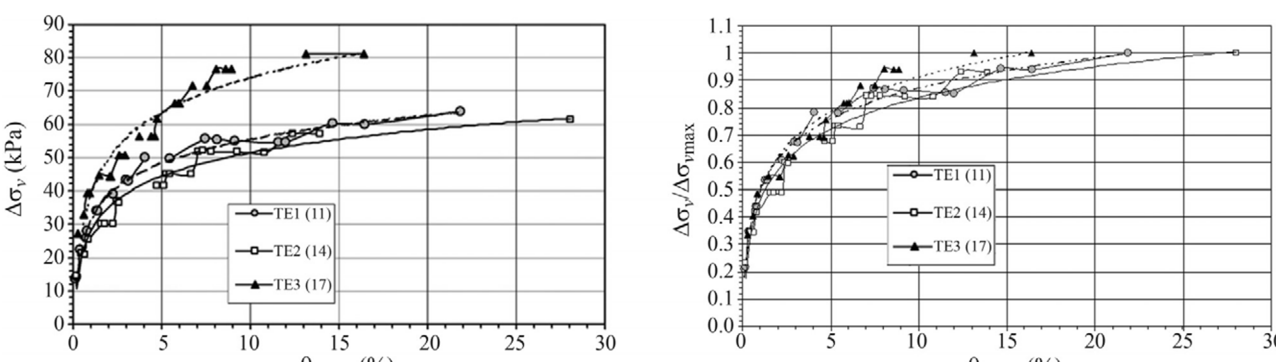

Figure 11 - Vertical embankment stress *vs.* maximum vertical deviation for inclinometers located at the toe of the embankments.

The results of Fig. 11b indicate that, despite the fact that the unreinforced embankment TE3 is a not a reference embankment in relation to the reinforced embankments TE1 and TE2, the results of the three embankments can be analysed together, thereby allowing an overall analysis of the behaviour of the clay foundation when subjected to loading. Therefore, the stability and deformation of the present test embankments on thick surface sand layers were governed by the soft clay whether the embankment was reinforced or not.

8. Stability of the Embankments

Stability analyses of the three test embankments carried out for each loading stage (Magnani *et al.*, 2009; Magnani *et al.*, 2010) produced the variation of the factor of safety *vs.* the applied vertical stress $\Delta\sigma_v$ shown in Fig. 12. These analyses were based on: (a) the measured S_u profiles shown in Fig. 2 (the small gains in strength were disregarded); (b) the measured reinforcement forces for each loading stage; (c) the Bjerrum correction factor (μ = 0.60) applied to the vane strength; (d) the correction for three-dimensional effects of the failure surface (Azzouz *et al.*, 1983), which increased the conventional 2-D factors of safety by 10 to 14% depending on the test embankment; and (e) Bishop's limit equilibrium method, as the observed failure surfaces were consistent with the points of maximum vertical deviation and had circular shapes, as shown in Fig. 12 for TE2. Similar agreement was obtained for TE1 and TE3 (Magnani, 2006).

Figure 12 shows that the variation of the factors of safety F_s with applied vertical stress of embankments TE1 and TE2 are quite close. For the same applied vertical stress, unreinforced embankment TE3 shows higher factors of safety than reinforced embankments. Thus, the results shown in Fig. 12 are consistent with the stress-strain curves shown in Fig. 11a.

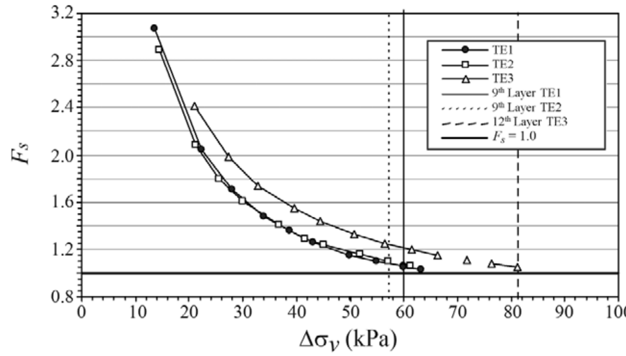

Figure 12 - Factors of safety for the three test embankments for each loading stage considering Bjerrum correction factor μ = 0.60 and 3-D effects.

The overall behaviour of the three embankments can also be observed in the photos of the three embankments shown in Fig. 14. The cracks developed in embankment TE1 with PVDs and reinforcement (Fig. 14a) can hardly be seen in the picture. Embankment TE2 (Fig. 14b), also reinforced but without PVDs, developed slightly bigger cracks at the crest. The unreinforced embankment TE3 (Fig. 14c), however, presented a clear failure at the embankment crest, the step between the two platforms being around 0.70 m.

Irrespective of the fact that TE3 is not a reference embankment, since it was constructed on a thinner clay layer with higher strength and reached a higher elevation, the photos presented in Fig. 14 indicate that the use of rein-

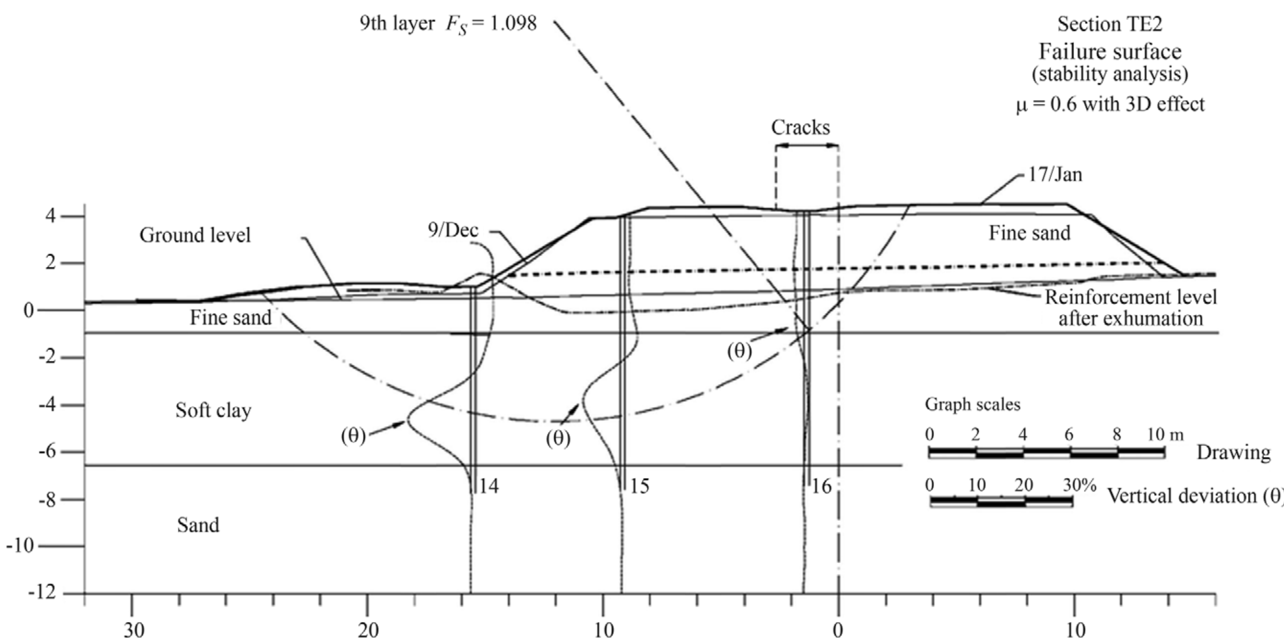

Figure 13 - Theoretical critical failure surface (stability analysis) *vs.* observed failure surface (points of maximum vertical deviation).

forcement as for embankments TE1 and TE2 resulted in better overall performance.

9. Numerical Analyses and the Relevance of PVDs

Literature recommendations (Saye, 2001) regarding PVD installation to minimize smear are drain spacing l greater than 1.50 m and a mandrel area A smaller than 65 cm^2, but values used for TE1 were l = 1.30 m and A = 180 cm^2. Therefore it appears that smear may have played an important role in the performance of test embankment TE1. Therefore, numerical 2-D finite element analyses of TE1 were carried out using the Plaxis program (Brinkgreve, 2010) to assess the importance of the PVDs in this test embankment loaded quickly to failure.

Figure 14 - Photos of the crest of the test embankments at failure.

9.1. Material parameters

For these analyses elasto-plastic soil models available in the Plaxis program were used; the *Soft Soil model,* a Cam-clay type model for the soft clay and the *Hardening Soil model* for the sand materials (embankment and sand fill). Parameters for sand layers and soft clay are presented in Tables 3 and 4, respectively.

The geosynthetic reinforcement was modelled as an elastic material with stiffness J = 1,700 kN/m with 15-node soil finite elements adopted for this 2-D analysis. The geosynthetic layer was modelled using structural finite elements.

9.2. Modelling of PVDs in FE analysis

For test embankment TE1 provided with PVDs, an equivalent 2-D plane strain multi-drain analysis (Indraratna & Redana, 2000; Indraratna, 2009) was carried out.

To perform a multidrain analysis, it is necessary to adopt a coefficient of horizontal permeability for plane strain conditions $k_{h,ps}$ different from the horizontal coefficient of permeability used for axi-symmetric unit cell conditions $k_{h,ax}$. This correspondence uses geometric data and may also assume drain smear as explained below.

Table 3 - Parameters for sand materials – Hardening Soil model.

Parameter	Value
Effective friction angle	35°
Dilatance angle	0°
Effective cohesion (kPa)	0 (*)
Stiffness Modulus $E_{50}^{ref} = E_{oed}^{ref}$ (kN/m^2)	18,000
Stiffness Modulus E_{ur}^{ref} (kN/m^2)	52,000
Poisson ratio	0.3
Bulk weight (kN/m^3)	17.5

(*) for the unsaturated embankment c = 1 kPa was adopted.

Table 4 - Parameters for the soft clay layer – Soft Soil model.

Parameter	Value
Effective friction angle (°)	30
Effective cohesion (kPa)	5.0
$C_c/(1 + e_o)$	0.36
$C_s/(1 + e_o)$	0.039
Over-consolidation ratio – OCR	1.1
Ko	0.53
Bulk weight (kN/m^3)	13.7

As far as drain smear is concerned, a typical literature value equal to 3.0 was adopted for the ratio $k_{h,ax}/k_{s,ax}$ between the coefficient of horizontal permeability in the intact soil ($k_{h,ax}$) and the smeared soil ($k_{s,ax}$).The equivalent coefficient of horizontal permeability in plane strain $k_{h,ps}$ and the equivalent horizontal permeability to the smear zone $k_{s,ps}$ can be computed based on the horizontal soil intrinsic coefficient of horizontal permeability $k_{h,ax}$ and geometric data using the equations (Indraratna & Redana, 2000).

$$\frac{k_{h,ps}}{k_{h,ax}} = \frac{\frac{2}{3}\left[\frac{(n-1)^2}{n^2}\right]}{\left[\ln(n) - \frac{3}{4}\right]} \tag{2}$$

$$\frac{k_{s,ps}}{k_{h,ps}} = \frac{\beta}{\frac{k_{h,ps}}{k_{h,ax}}\left[\ln\left(\frac{n}{s}\right) + \frac{k_{h,ax}}{k_{s,ax}} - \frac{3}{4}\right] - \alpha} \tag{3}$$

$$\alpha = \frac{2}{3}\frac{(n-s)^3}{n^2(n-1)} \tag{4}$$

$$\beta = \frac{2(s-1)}{n^2(n-1)}\left[n(n-s-1) + \frac{1}{3}(s^2+s+1)\right] \tag{5}$$

where $n = d_e/d_w$ is the ratio of the diameter of the unit cell d_e to the equivalent drain diameter d_w and $s = d_s/d_w$ relates the diameter of the smear zone d_s with d_w.

For the triangular drain mesh spaced 1.3 m d_e = 1.3 x 1.05 = 1.365 m. Considering PVD dimensions a = 10 cm and b = 0.5 cm, then $d_w = 2(a + b)/\pi = 0.067$ m. Therefore, $n = d_e/d_w = 20.42$ m.

The diameter of the smear zone d_s is assumed equal to 2.5 times the equivalent mandrel diameter d_m which in turn is a function of the adopted mandrel area equal to 180 cm^2, thus $d_m = (0.018*4/\pi)^{0.5} = 0.0874$ m and d_s = 2.5 x d_m = 0.22 m, and $s = d_s/d_w = 3.27$ m.

The adopted value of the vertical coefficient of permeability k_v was 10^{-9} m/s. Then, if we assume isotropy in terms of the horizontal coefficient of permeability of the intact soil is $k_{h,ax} = 10^{-9}$ m/s. As $k_{s,ax}/k_{h,ax} = 3$, then the horizontal coefficient of permeability of the smeared soil is $k_{s,ax}$ = 3.33 x10^{-10} m/s. Then, substituting these values and the values of n and s obtained above into Eqs. (2) to (5), one obtains for the intact soil $k_{h,ps}$ = 2.66 x10^{-10} m/s and for the smeared zone $k_{s,ps}$ = 0.71 x10^{-10} m/s, which were the values used in the plane strain finite element analyses.

9.3. Numerical results *vs.* measured data

Three finite element analyses were carried out for test embankment TE1: (a) "PVD" which is expected to be the condition closest to the actual conditions of test embankment TE1; (b) "PVD no-smear" assuming that PVDs installation caused no smear, to compare this with "PVD analysis" in which smear is considered; (c) "no-PVD" for a virtual condition for TE1 without PVDs, to assess the influence of the PVDs. The main features of these analyses are summarized in Table 5, which also presents the values of vertical and horizontal coefficients of permeability adopted in these 2-D FE analyses.

The PVDs multi-drain analysis (Indraratna & Redana, 2000) assumes the width of the unit cell in plane strain conditions to be the same as the diameter d_e of the axi-symmetric unit cell. It also assumes that the drain width in plane strain is equal to the equivalent drain diameter d_w and similarly with respect to the smear zone. The finite element mesh adopted following these features is shown in Fig. 15 for the "PVD analysis" and "PVD no-smear analysis" (around 19,000 elements). The "no PVD analysis" used a similar FE mesh (around 8400 elements), obviously without PVDs.

The actual TE1 test embankment loading history was adopted for the three analyses, thus consolidation was allowed during the whole period of about two months of embankment construction, during both loading and waiting periods between each layer placement.

Computed and measured settlements, with and without PVDs, for the settlement plate PB7 (see Fig. 2) are shown in Fig. 16 for the three analyses. Good overall agreement between measured and "PVD analysis" is observed, which suggests that the multidrain analysis and the adopted

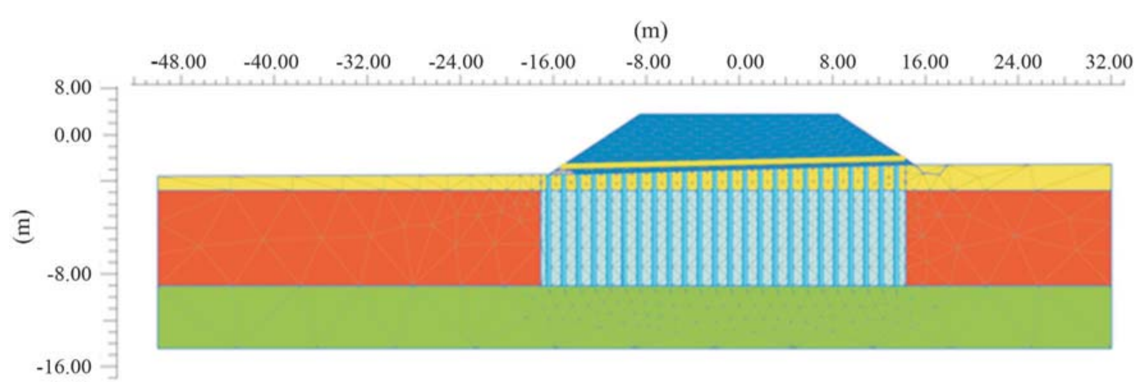

Figure 15 - Finite element mesh adopted for the PVD analyses.

Table 5 - Main features of the 2D multidrain FE analyses performed.

Analysis	PVDs	smear	Region	k_v (10^{-10} m/s)	k_h (10^{-10} m/s)
"PVD"	yes	yes	Drain region (smear)	3.33	0.71
			Drain region	10	2.66
			Outside the drain region	10	10.0
"PVD no-smear"	yes	no	Drain region	10	2.66
			Outside the drain region	10	10
"no-PVD"	no	-	-	10	10

model parameters are adequate. Agreement is quite good until 20 November, but for subsequent times the numerical analysis slightly under-predicts measured settlements.

Figure 16 shows also that settlements of "no-PVD analysis" are smaller than settlements of "PVD analysis" (and measured settlements), thus showing that PVDs had a beneficial effect in accelerating settlements. The influence of smear is also noticed in Fig. 16 by comparing results of "PVD analysis" and "PVD no-smear analysis", the latter presenting larger settlements, as expected.

The three time-settlement curves showed a change in slope, indicating large yield zones and the start of the failure process. The time corresponding to these changes in slope roughly coincides with the time of the actual failure process in test embankment TE1 (layers 9 and 10). It may be observed that this time for the "no PVD analysis" starts slightly earlier than for the two PVD analyses. It may also be observed that FE analysis could not continue much further due to lack of numerical convergence.

Results of computed and measured maximum horizontal displacement are shown in Fig. 17 for the inclinometer I1 located at the embankment toe. It is observed that the computed values are quite close to and slightly larger than the measured values until 10 November. Better agreement is observed for intermediate times, particularly for the "PVD analysis".

For dates after 10 November, differences between the numerical analyses increase. The differences between these analyses follow the same trend observed for vertical displacements, with displacements becoming larger as drainage conditions improve, *i.e.*, smaller horizontal displacements for "no-PVD analysis" which increase for the "PVD analysis" and increase further for the "PVD no-smear analysis".

Results of the computed and measured total pore pressures for piezometer PZ1 are shown in Fig. 18. The measured results increase continuously with time with negligible pore pressure dissipation. A similar pattern is observed for "PVD analysis" which also compares well with the measured results, suggesting that smear was well simulated in this multidrain analysis. Results of "PVD no-smear analysis", also shown in Fig. 18, are close to "PVD analysis" up to 20 November and then show smaller values.

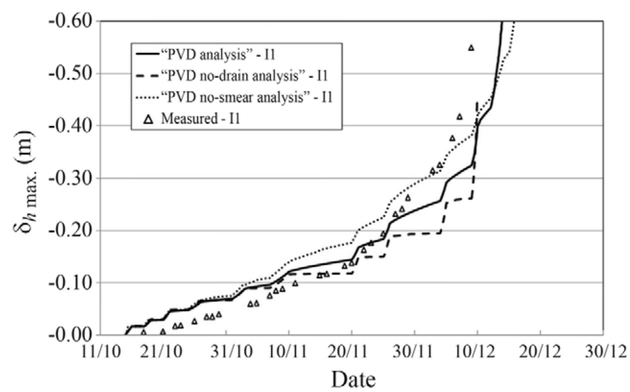

Figure 17 - FE results x field measurements – Maximum horizontal displacement (I1).

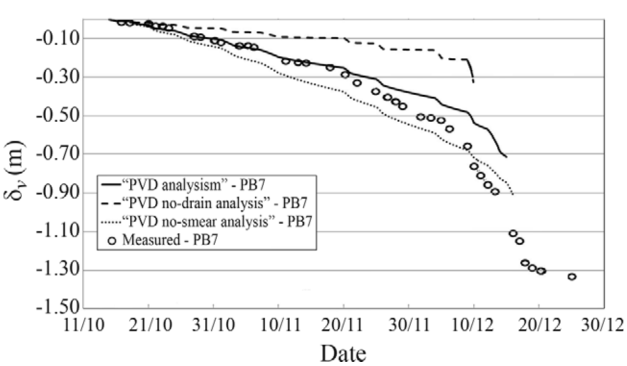

Figure 16 - FE results x field measurements – Vertical displacement (PB7).

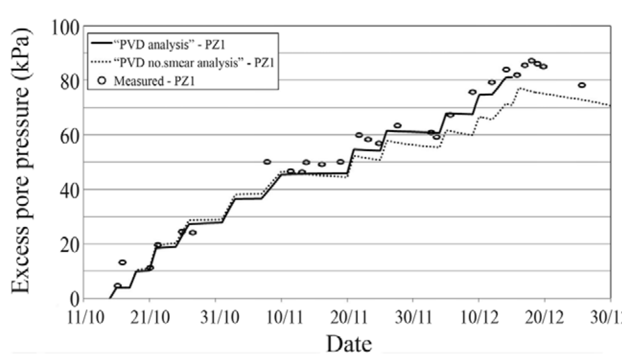

Figure 18 - FE results x field measurements – Excess of pore pressure for PZ1.

These results show more pronounced pore pressure dissipation following loading, thus indicating better drain performance when no smear occurs, as expected.

Overall assessment of the numerical analyses shows that PVDs influenced the performance of TE1 but this influence appears to be smaller than shown in the literature (*e.g.*, Li & Rowe, 2001). The reasons for this appear to be the very low value of the coefficient of consolidation of Florianopolis clay, disturbance effects due to drain installation and the short construction time.

10. Conclusions

Three test embankments (two reinforced and one unreinforced) were rapidly constructed to failure on normally consolidated clay layers overlain by pre-constructed surface sand layers. The foundation of one of the reinforced embankments (TE1) was provided with PVDs.

The embankment without reinforcement and PVDs (TE3) reached a higher vertical stress (or net embankment height) at failure than the two reinforced embankments owing to its greater clay strength. The two reinforced embankments (TE1 and TE2) presented similar maximum vertical stress at failure. This was because of the similarity in the undrained strength values of the two clay layers. Owing to the low coefficient of consolidation of the normally consolidated clay, the rapid construction of the test embankments and drain disturbance (close drain spacing and large mandrel used) the PVDs had, in the present case, a relatively small effect on the behaviour of the reinforced embankment provided with vertical drains. These conclusions are supported by the results obtained by finite element analyses. Numerical analyses showed that the PVD had a greater influence on settlement and on horizontal displacements than on pore pressure results and that smear appears to play an important role in this particular case history.

The curves of variation of factors of safety *vs.* applied embankment stress showed very close values for reinforced embankments TE1 and TE2 and higher factors of safety in general were obtained for unreinforced embankment TE3.

The normalisation of the applied embankment stress by the maximum applied stress *vs.* the clay shearing strains produced close stress-strain curves for the three embankments. Thus the responses of the embankments to the normalised embankment stresses are independent of the thickness of the soft layer and are valid, in the present case, for both reinforced and unreinforced embankments.

The photos of the failures show that the reinforcement was effective in controlling large cracks at failure, and the unreinforced embankment presented a clear failure surface with a step at the crest of the embankment.

Acknowledgments

The authors are indebted to all the individuals and institutions that made the construction of the three test embankments possible, in particular the technical staff of COPPE-UFRJ Geotechnical Laboratory for the installation of the instruments. Maria Cascão, Politechnic School, Federal University of Rio de Janeiro presented important suggestions for the development of the finite element analyses.

References

Almeida, M.S.S.; Britto, A.M. & Parry, R.H.G. (1986) Numerical modeling of a centrifuged embankment on soft clay. Canadian Geotechnical Journal, v. 23:2, p. 103-114.

Almeida, M.S.S.; Davies, M.C.R. & Parry, R.H.G. (1985) Centrifuge tests of embankments on strengthened and unstrengthened clay foundations. Géotechnique, v. 35:4, p. 425-441.

Almeida, M.S.S.; Futai, M.M.; Lacerda, W.L. & Marques, M.E.S. (2008) Laboratory behaviour of Rio de Janeiro soft clays. Part 1: Index and compression properties. Soils and Rocks, v. 31:2, p. 69-75.

Almeida, M.S.S. & Marques, M.E.S. (2002) The behaviour of Sarapuí soft clay. Proceedings of the International Workshop on Characterization and Engineering Properties of Natural Soils, v. 1, pp. 477-504, Balkema, Singapore.

Almeida, M.S.S.; Marques, M.E.S. & Spotti, A.P. (2005) Two case histories of vertical drains in very soft clays. Buddhima, I.; Chu, J. & Hudson, J.A. (eds) Ground Improvement - Case Histories. Geo-Engineering Book Series, Elsevier, chap 5, pp. 145-157

Almeida, M.S.S.; Spotti, A.P.; Santa Maria, P.E.L.; Martins, I.S.M. & Coelho, L.B.M. (2001) Consolidation of a very soft clay with vertical drains. Geotechnique, v. 50:2, p. 633-643.

Almeida, M.S.S.; Ehrlich, M.; Riccio, M.; Magnani, H. & Souza, H. (2010) Development and performance of load cell systems for reinforced embankment and reinforced soil wall. Proceedings 9th International Conference on Geosynthetics, Guarujá, Brazil, v. 4, p. 1869-1874.

Azzouz, A.S.; Baligh, M.M. & Ladd, C.C. (1983) Corrected field vane strength for embankment design. Journal of Geotechnical Engineering ASCE, v. 109:5, p. 730-735.

Bergado, D.T.; Chai, J.; Alfaro, M.C. & Balasubramanian, A.S. (1994) Improvement Techniques of Soft Ground in Subsiding and Lowland Environment. Balkema, Rotterdam, 232 pp.

Brinkgreve, R.B.J. (2010). PLAXIS – 2D User's Manual. Rotterdam, Netherlands, 682 pp.

Chai, J.; Miura, N. & Shen, S. (2002) Performance of embankments with and without reinforcement on soft subsoil. Canadian Geotechnical Journal, v. 39:4, p. 838-848.

Dunnicliff, J. (1988) Geotechnical Instrumentation for Monitoring Field Performance. John Wiley, New York, 608 p.

Hinchberger, S. & Rowe, R.K. (2003) Geosynthetic reinforced embankments on soft clay foundations predicting reinforcement strain at failure. Geotextiles and Geomembranes, v. 21:3, p. 151-175.

Holtz, R.D. (1987) Preloading with prefabricated vertical strip drains. Geotextiles and Geomembranes, v. 6:1-3, p. 109-131.

Humphrey, D.N. & Holtz, R.D. (1989) Effect of surface crust on reinforced embankment. Proceedings of Geosynthetics '89, Industrial Fabrics Association International, St, Paul, v. 1, pp. 136-147.

Hunter, G. & Fell, R. (2003) Prediction of impending failure of embankments on soft ground. Canadian Geotechnical Journal, v. 40:1, p. 209-220.

Indraratna, B.; Balasubramaniam, A.S. & Balachandran, S. (1992) Performance of test embankment constructed to failure on soft marine clay. Journal of Geotechnical Engineering, ASCE, v. 118:1, p. 12-33.

Indraratna, B. & Redana I.W. (2000) Numerical modeling of vertical drains with smear and well resistance installed in soft clay. Canadian Geotechnical Journal, v. 37:1, p. 133-145.

Indraratna, B. (2009) "Recent advances in the application of vertical drains and vacuum preloading in soft soil stabilization", 2009 EH Davis Memorial Lecture – Australian Geomechanics Journal, v. 45, p.603-617.

Kelln, C.; Sharma, J.; Hughes, D. & Gallagher, G. (2007) Deformation of a soft estuarine deposit under a geotextile reinforced embankment. Canadian Geotechnical Journal, v. 44:5, p. 603-617.

Leroueil, S.; Tavenas, F.; Mieussens, C. & Peignaud, M. (1978) Construction pore pressures in clay foundations under embankments. Part II: Generalized behaviour. Canadian Geotechnical Journal, v. 15:1, p. 65-82.

Li, A.L. & Rowe, R.K. (2001) Combined effects of reinforcement and prefabricated vertical drains on embankment performance.Canadian Geotechnical Journal, v. 38:6, p. 1266-1282.

Lo, S.R.; Mak, J.; Gnanendran, C.T.; Zhang, R. & Manivannan, G. (2008) Long-term performance of a wide embankment on soft clay improved with prefabricated vertical drains. Canadian Geotechnical Journal, v. 45:8, p. 1073-1091.

Magnani, H. (2006) Comportamento de Aterros Reforçados Sobre Solos Moles Levados a Ruptura. Tese D.Sc, Programa de Engenharia Civil, COPPE/UFRJ, Rio de Janeiro.

Magnani, H.O.; Almeida, M.S.S. & Ehrlich, M. (2008) Construction stability evaluation of reinforced embankments over soft soils. Proceedings of First Pan American Geosynthetics Conference & Exhibition, March 2008, Cancun, CD-Rom.

Magnani, H.O.; Almeida, M.S.S. & Ehrlich, M. (2009a) Behaviour of two reinforced test embankments on soft clay taken to failure. Geosynthetics International, v. 16:3, p. 127-138.

Magnani, H.O.; Ehrlich, M. & Almeida, M.S.S. (2009b) Embankments over soft clay deposits: the contribution of basal reinforcement and surface sand layer to stability. Journal of Geotechnical and Geoenvironmental Engineering ASCE, v. 136, p. 260-265.

Massad, F. (1994) Propriedades dos sedimentos marinhos. In: Solos do Litoral Paulista. Associação Brasileira de Mecânica dos Solos, São Paulo, pp. 99-128.

Pinto, C.S. (1994) Aterros na baixada, In: Solos do Litoral Paulista. Associação Brasileira de Mecânica dos Solos, São Paulo, pp. 235-264.

Rowe, R.K.; Gnanendran, C.T.; Landva, A.O. & Valsangkar, A.J. (1995) Construction and performance of a full-scale geotextile reinforced test embankment, Sackville, New Brunswick. Canadian Geotechnical Journal, v. 32:3 p. 512-534.

Rowe, R.K.; Gnanendran, C.T.; Landva, A.O. & Valsangkar, A.J. (1996) Calculated and observed behaviour of a reinforced embankment over soft compressible soil. Canadian Geotechnical Journal, v. 33:2, p. 324-338.

Rowe, R.K. & Leroueil, S. (2001) Embankments over soft soil and peat. Rowe, R.K. (ed), Geotechnical and Geoenvironmental Engineering Handbook. Kluwer, Norwell, pp. 463-499.

Rowe, R.K. & Li, L.L. (2005) Geosynthetic-reinforced embankments over soft foundations. Geosynthetics International, v. 12:1, p. 50-85.

Rowe, R.K. & Soderman, K.L. (1987b) Reinforcement of embankments on soils whose strength increases with depth. Proceedings of the Geosynthetics '87 Conference, New Orleans, pp. 266-277.

Saye, S.R. (2001) Assessment of soil disturbance by the installation of displacement sand drains and prefabricated vertical drains. Proceedings of Symposium on Soil Behaviour and Soft Ground Construction, Geotechnical Special Publication no. 119. Geo-Institute ASCE, Cambridge, pp. 325-362.

Schnaid, F. (2009) In Situ Testing in Geomechanics. Taylor and Francis, Oxon, 352 pp.

Tavenas, F.; Mieussens, B. & Bourges, F. (1979) Lateral displacements in clay foundations under embankments. Canadian Geotechnical Journal, v. 16:3, p. 532-550.

Zhang, L. (1999) Settlement patterns of soft soil foundations under embankments. Canadian Geotechnical Journal, v. 36:4, p. 774-781.

List of Symbols

c = cohesion (kPa)
C_c = compression index
C_s = swelling index
c_v = coefficient of vertical consolidation (m/s^2)
e = void ratio (dimensionless)
F_s = factor of safety (dimensionless)

G = shear modulus (kPa)
h = embankment height (m)
h^* = embankment thickness less measured settlement (m)
I_P = plasticity index (%)
J = reinforcement modulus = T/ε_a (kN/m)
N_{kt} = empirical cone factor (dimensionless)
q_T = corrected point resistance (kPa)
S_u = undrained clay strength (kPa)
z = depth (m)
z_f = depth of the failure (m)
w = water content (%)
w_L = liquidity index (%)
δ_h = horizontal displacement (m)
δ_v = vertical displacement (m)
ε_a = reinforcement strain (%)
Δu = excess pore pressure (kPa)
$\Delta\sigma_v$ = applied embankment vertical stress (kPa)
$\Delta\sigma_{vmax}$ = maximum applied (submersion effects discounted) embankment vertical stress (kPa)
ϕ = friction angle (°)
γ = bulk weight (kN/m^3)
μ = Bjerrum correction factor (dimensionless)
θ_v = vertical deviation (dimensionless)
θ_{vmax} = maximum vertical deviation (dimensionless)
σ_v = total vertical stress (kPa)
$k_{h,ps}$ = equivalent coefficient of horizontal permeability in plane strain (m/s)
$k_{s,ps}$ = equivalent coefficient of horizontal permeability to the smear zone in plane strain (m/s)
$k_{h,ax}$ = coefficient of horizontal permeability (m/s)
k_v = vertical coefficient of permeability

SOILS and ROCKS
An International Journal of Geotechnical and Geoenvironmental Engineering

Publication of
ABMS - Brazilian Association for Soil Mechanics and Geotechnical Engineering
SPG - Portuguese Geotechnical Society
Volume 34, N. 4, December 2011

Author index







Instructions to Authors

Category of the Papers

Soils and Rocks is the scientific journal edited by the Brazilian Association for Soil Mechanics and Geotechnical Engineering (ABMS) and the Portuguese Geotechnical Society (SPG). The journal is intended to the divulgation of original research works from all geotechnical branches.

The accepted papers are classified either as an Article paper, a Technical Note, a Case Study, or a Discussion according to its content. An article paper is an extensive and conclusive dissertation about a geotechnical topic. A paper is considered as a technical note if it gives a short description of ongoing studies, comprising partial results and/or particular aspects of the investigation. A case study is a report of unusual problems found during the design, construction or the performance of geotechnical projects. A case study is also considered as the report of an unusual solution given to an ordinary problem. The discussions about published papers, case studies and technical notes are made in the Discussions Section.

When submitting a manuscript for review, the authors should indicate the category of the manuscript, and is also understood that they:

a) assume full responsibility for the contents and accuracy of the information in the paper;

b) assure that the paper has not been previously published, and is not being submitted to any other periodical for publication.

Manuscript Instructions

Manuscripts must be written in English. The text is to be typed in a word processor (MS Word or equivalent), using ISO A4 page size, left, right, top, and bottom margins of 25 mm, Times New Roman 12 font, and line spacing of 1.5. All lines and pages should be numbered. The text should be written in the third person.

The fist page of the manuscript is to include the title of the paper in English, followed by the names of the authors with the abbreviation of the most relevant academic title. The affiliation, address and e-mail is to be indicated below each author's name. An abstract of 200 words is to be written in English after the author's names. A list with up to six keywords at the end of the abstract is required.

Although alteration of the sequence and the title of each section may be required, it is suggested that the text contains the following sections: Introduction, Material and Methods, Results, Discussions, Conclusion, Acknowledgements, References and List of Symbols. A brief description of each section is given next.

Introduction: This section should indicate the state of the art of the problem under evaluation, a description of the problem and the methods undertaken. The objective of the work is to be clearly presented at the end of the section.

Materials and Methods: This section should include all information needed to the reproduction of the presented work by other researchers.

Results: In this section the data of the investigation should be presented in a clear and concise way. Figures and tables should not repeat the same information.

Discussion: The analyses of the results should be described in this section. **Conclusions**: The text of this section should be based on the presented data and in the discussions.

Acknowledgenments: If necessary, concise acknowledgements should be written in this section.

References: References to other published sources are to be made in the text by the last name(s) of the author(s), followed by the year of publication, similarly to one of the two possibilities below:

"*while Silva & Pereira (1987) observed that resistance depended on soil density*" or "*It was observed that resistance depended on soil density (Silva & Pereira, 1987).*"

In the case of three or more authors, the reduced format must be used, *e.g.*: Silva *et al.* (1982) or (Silva *et al.*, 1982). Two or more citations belonging to the same author(s) and published in the same year are to be distinguished with small letters, *e.g.*: (Silva, 1975a, b, c.). Standards must be cited in the text by the initials of the entity and the year of publication, *e.g.*: ABNT (1996), ASTM (2003).

Full references shall be listed alphabetically at the end of the text by the first author's last name. Several references belonging to the same author shall be cited chronologically. Some examples are listed next:

Papers: Bishop, A.W. & Blight, G.E. (1963) Some aspects of effective stress in saturated and unsaturated soils. Géotechnique, v. 13:2, p. 177-197.

Books: Lambe, T.W & Whitman, R.V. (1979) Soil Mechanics, SI Version, 2nd ed. John Wiley & Sons, New York, p. 553.

Book with editors: Sharma, H.D.; Dukes, M.T. & Olsen, D.M. (1990) Field measurements of dynamic moduli and Poisson's ratios of refuse and underlying soils at a landfill site. Landva A. & Knowles, G.D. (eds) Geotechnics of Waste Fills - Theory and Practice, American Society for Testing and Materials - STP 1070, Philadelphia, p. 57-70.

Proceedings (printed matter or CD-ROM): Jamiolkowski, M.; Ladd, C.C.; Germaine, J.T & Lancellotta, R. (1985) New developments in field and laboratory testing of soils. Proc. 11th Int. Conf. on Soil Mech. and Found. Engn., ISSMFE, San Francisco, v. 1, pp. 57-153.(specify if CD – ROM)

Thesis and dissertations: Lee, K.L. (1965) Triaxial Compressive Strength of Saturated Sands Under Seismic Loading Conditions. PhD Dissertation, Department of Civil Engineering, University of California, Berkeley, 521 p.

Standards: ASTM (2003) Standard Test Method for Particle Size Analysis of Soils - D 422-63. ASTM International, West Conshohocken, Pennsylvania, USA, 8 p.

Internet references: Soils and Rocks available at http://www.abms.com.br.

On line first publications must also bring the digital object identifier (DOI) at the end.

Figures shall be either computer generated or drawn with India ink on tracing paper. Computer generated figures must be accompanied by the corresponding digital file (.tif, .jpg, .pcx, etc.). All figures (graphs, line drawings, photographs, etc.) shall be numbered consecutively and have a caption consisting of the figure number and a brief title or description of the figure. This number should be used when referring to the figure in text. Photographs should be black and white, sharp, high contrasted and printed on glossy paper.

Tables shall be numbered consecutively in Arabic and have a caption consisting of the table number and a brief title. This number should be used when referring to the table in text. Units should be indicated in the first line of the table, below the title of each column. Abbreviations should be avoided. Column headings should not be abbreviated. When applicable, the units should come right below the corresponding column heading. Any necessary explanation can be placed as footnotes.

Equations shall appear isolated in a single line of the text. Numbers identifying equations must be flush with the right margin. International System (SI) units are to be used. The symbols used in the equations shall be listed in the List of Symbols. It is recommended that the used symbols be in accordance with Lexicon in 8 Languages, ISSMFE (1981) and the ISRM List of Symbols.

The text of the submitted manuscript (including figures, tables and references) intended to be published as an article paper or a case history should not contain more than 30 pages formatted according to the instructions mentioned above. Technical notes and discussions should have no more than 15 and 8 pages, respectively. Longer manuscripts may be exceptionally accepted if the authors provide proper explanation for the need of the required extra space in the cover letter.

Discussion

Discussions must be written in English. The first page of a discussion paper should contain:

• The title of the paper under discussion in the language chosen for publication;

• Name of the author(s) of the discussion, followed by the position, affiliation, address and e-mail. The discusser(s) should refer himself (herself, themselves) as "the discusser(s)" and to the author(s) of the paper as "the author(s)".

Figures, tables and equations should be numbered following the same sequence of the original paper. All instructions previously mentioned for the preparation of article papers, case studies and technical notes also apply to the preparation of discussions.

Editorial Review

Each paper will be evaluated by reviewers selected by the editors according to the subject of the paper. The authors will be informed about the results of the review process. If the paper is accepted, the authors will be required to submit a version of the revised manuscript with the suggested modifications. If the manuscript is refused for publication, the authors will be informed about the reasons for rejection. In any situation comprising modification of the original text, classification of the manuscript in a category different from that proposed by the authors, or refusal for publication, the authors can reply presenting their reasons for disagreeing with the reviewers' comments

Submission

The author(s) must submit for review:

1. A hard copy of the manuscript to Editors - Soils and Rocks, Av. Prof. Almeida Prado, 532 – IPT, Prédio 54 – DEC/ABMS, 05508-901 - São Paulo, SP, Brazil. The first page of the manuscript should contain the identification of the author(s), or

2. The digital file of the manuscript, omitting the authors' name and any information that eventually could identify them, should be sent to **abms@ipt.br**. The following must be written in the subject of the e-mail message: "*Paper submitted to Soils and Rocks*". The authors' names, academic degrees and affiliations should be mentioned in the e-mail message. The e-mail address from which the digital file of the paper was sent will be the only one used by the editors for communication with the corresponding author.

Follow Up

Authors of manuscripts can assess the status of the review process at the journal website (www.soilsandrocks.com.br) or by contacting the ABMS secretariat.

Volume 34, N. 4, December 2011

Table of Contents